Novel therapeutic strategies for the treatment of pulmonary arterial hypertension

Colin Suen

Thesis submitted to the Faculty of Graduate and Postdoctoral Studies in partial fulfillment of the requirements for a doctoral degree in Cellular and Molecular Medicine

Department of Cellular and Molecular Medicine, Faculty of Medicine, University of Ottawa

Abstract

Pulmonary arterial hypertension (PAH) is a progressive disease that results in increased pulmonary vasculature resistance, causing right ventricular (RV) remodeling, which eventually progresses into right heart failure and mortality. New and emerging therapeutic strategies involve regenerative approaches to repair the underlying vascular pathology using regenerative cell therapy and methods to alleviate RV dysfunction in the setting of fixed RV afterload. In the first section of the thesis, we investigated the role of EPC paracrine mechanisms in the treatment of PAH. We characterized the paracrine function of EPCs by demonstrating that EPC conditioned medium enhances endothelial cell migration, survival and angiogenesis *in vitro*. We further examined the role of secreted extracellular vesicles in the paracrine function of EPCs, which played a minor role in promoting wound healing. However, using the monocrotaline rat model of PAH, we did not demonstrate a consistent benefit on RV pressures or remodeling with EPCs or EPC conditioned medium. The lack of effect may be related to the advanced phenotype observed in our model of PAH.

Survival in severe pulmonary arterial hypertension (PAH) is related to the ability of the right ventricle (RV) to adapt to increased afterload. Therefore, we explored the effect of genetic background on right ventricular adaptation and survival in a rat model of severe (PAH). Compared to the conventional Sprague-Dawley rat strain, we observed high mortality in the Fischer SUHx model of severe PAH. This was related to a strain-dependent failure of RV adaptation, as evidenced by RV dilatation, RV contractile dysfunction, decreased cardiac ouptut and decreased exercise capacity. Further analysis by gene expression microarrays and fluorescence microangiography demonstrate that failure of RV adaptation is due at least in part due to lack of

adequate microvascular angiogenesis in the hypertrophied RV. This work lays the foundation for the section on RV-specific therapy that follows.

Using the Fischer model of maladaptive RV remodeling, we tested whether cardiotrophin-1 (CT-1), a pro-angiogenic and cardioprotective cytokine, could improve RV adaptation. We demonstrated that as a rescue treatment, CT-1 reduced RV dilatation and function without influencing RV afterload, which suggests improved RV adaptation. These changes were associated with an increase in RV capillary density. As an early-stage preventative treatment, in addition to improving RV remodeling, CT-1 also reduced pulmonary pressures. These hemodynamic changes suggest that CT-1 may also have a direct impact on vascular tone or the underlying pulmonary vascular pathology.

Table of Contents

List of Tables

Table of Figures

List of Abbreviations

ANP	atrial natriuretic peptide
BMP	bone morphogenetic protein
BMPR2	bone morphogenetic protein receptor type II
BNP	brain natriuretic peptide
CM	conditioned medium
CO	cardiac output
CI	cardiac index
CT-1	cardiotrophin-1
EC	endothelial cell
EPC	endothelial progenitor cell
eNOS	endothelial nitric oxide synthase
FAC	fractional area change
HUVEC	human umbilical vein endothelial cell
IL	interleukin
ip	intraperitoneal
iv	intravenous
IPAH	idiopathic pulmonary arterial hypertension
LV	left ventricle
LV+S	left ventricle + septum
MCT	monocrotaline
mPAP	mean pulmonary arterial pressure
MRI	magnetic resonance imaging
MSC	mesenchymal stem cell/mesenchymal stromal cell
NK	natural killer
NO	nitric oxide
PH	Pulmonary hypertension
PAH	Pulmonary arterial hypertension
PASMC	pulmonary arterial smooth muscle cell
PBMC	peripheral blood mononuclear cell
PH	Pulmonary hypertension
PVR	pulmonary vascular resistance
RV	Right ventricle
RVH	Right ventricular hypertrophy
RVEF	Right ventricular ejection fraction
RVF	Right ventricular failure
RVSP	right ventricular systolic pressure
sc	subcutaneous
SD	Sprague-Dawley
SMC	smooth muscle cell
SU	SU5416
SUHx	SU5416 + chronic hypoxia
TAPSE	tricuspid annulus planar systolic excursion
VEGF	vascular endothelial growth factor
VEGFR2	vascular endothelial growth factor receptor, type 2

Acknowledgements

This thesis would not have been possible without the help of a number of exceptional individuals at the Ottawa Hospital Research Institute and University of Ottawa. First and foremost, I would like to thank my supervisor, Dr. Duncan Stewart for his mentorship and providing me with the freedom to explore my intellectual curiosity. As well, I am grateful for the support of the members of my PhD thesis advisory committee, Dr. Bernard Thebaud, Dr. David Allan and Dr. Derrick Gibbings.

Thank you to Dr. Yupu Deng, who performed all of the animal surgeries in these studies. Thank you to Anli Yang and Sophie Wen, who also helped tremendously in providing the technical support to carry out these experiments. I would especially like to thank Dr. Ketul Chaudhary for his help in experimental design and for his scientific contributions to our studies which include performing the PCR array. Likewise, I am thankful to have worked with great friends as colleagues such as Mohamad Taha who worked tirelessly to setup the hypoxia chambers for our SUHx model and Will Foster for their eagerness to engage in countless scientific and non-scientific discussions over coffee

I would also like to thank our collaborators, Dr. Lynn Megeney and Mohammad Abdul-Ghani, who generously provided CT-1 as well as scientific and technical support to carry out the cardiotrophin-1 studies. Also, I thank Dr. Gareth Pawlidor for providing on microarray analysis and to Dr. Gregory Cron and Dr. Rebecca Thornhill for carrying out the cardiac MRI.

Finally, I would like to thank CIHR for providing funding support through the Vanier Canada Graduate Scholarships and the Training Program in Regenerative Medicine awards.

I would like to dedicate this thesis to my family. I could not have made it through the last 7 years of the MD/PhD program without the support and patience of my wife, Kaley, my parents, Wilson and May Suen and my brother Brandon. Thank you for encouraging me throughout and helping me become the person I am today.

Chapter 1: Introduction

Contributions: Portions of this manuscript have been published as a review article in the journal *Comprehensive Physiology*

1.1 INTRODUCTION

Pulmonary hypertension (PH) is a progressive disease that results from restricted blood flow through the pulmonary circulation, leading to increased resistance in the pulmonary vasculature and eventually right heart failure. Clinically, PH is defined as an increase of the mean pulmonary arterial pressure to ≥ 25 mmHg at rest assessed by right heart catheterization. Pulmonary hypertension (PH) refers to a group of diseases with similar pathological findings and hemodynamic characteristics. The original classification scheme for PH was first introduced by the World Health Organization (WHO) in 1993 in Geneva, Switzerland[1]. The most recent update from the 5th World Symposium on PH held in Nice in 2014 categorizes pulmonary hypertension into five main groups (Table 1-1) to reflect similarities in pathophysiology, clinical presentation and therapeutic options: (1) pulmonary arterial hypertension (PAH), (1') pulmonary veno-occlusive disease and/or pulmonary capillary hemangiomatosis, (2) PH owing to left heart disease, (3) PH owing to lung diseases and/or hypoxia, (4) chronic thromboembolic pulmonary hypertension (CTEPH) and (5) PH with unclear multifactorial mechanisms[2].

Pulmonary arterial hypertension (PAH) is defined by mean pulmonary arterial pressure (mPAP) ≥ 25 mmHg (at rest); pulmonary capillary wedge pressure (PCWP) ≤15 mmHg, and pulmonary vascular resistance (PVR) > 5 woods units, and is classified as World Health Organization (WHO) Group I pulmonary hypertension[3]. It is a progressive and debilitating lung disorder and the early symptoms of the disease are subtle and include dyspnea, fatigue, syncope, chest pain, and peripheral edema[4]. Unfortunately, PAH is often only diagnosed when the disease has reached its advanced stages, when survival rates are poor. In fact, if the disease is left untreated from the time of first diagnosis, death occurs within three years. The prevalence of PAH is estimated to be approximately 10-15 per million, according to recent reports from the French Registry and the

Registry to Evaluate Early and Long-term Pulmonary Arterial Hypertension Management (REVEAL)[5,6].

PAH represents a group of diseases of various etiologies that are characterized by the same pathological features: narrowing or loss of the small pulmonary arterioles (or resistance vessels) thought to be initiated by endothelial injury/activation with an imbalance of vasoactive mediators (i.e. nitric oxide, endothelin-1, prostacyclin, thromboxane A2, serotonin), leading to vasoconstriction and medial and intimal hyperplasia[7-9]. More recently, lung endothelial cell apoptosis has been recognized as a critical trigger for the development of PAH, resulting in complex arterial remodeling associated with the emergence of apoptosis-resistant vascular smooth muscle and endothelial cells, which together with contribute to obliterative plexiform lesions that represent the hallmark feature of PAH. Currently available PAH-specific therapies consist largely of pharmacological vasodilators that are unable reverse the more profound structural abnormalities and the extensively remodeled pulmonary vasculature that characterize advanced disease[10]. Thus, the development of clinically effective strategies to restore normal structure and function of the distal arteriolar bed in established PAH are urgently needed.

Table 1-1. Clinical Classification of WHO Group 1 Pulmonary Hypertension

1. Pulmonary arterial hypertension (PAH)
1.1 Idiopathic PAH
1.2 Heritable PAH
1.2.1 BMPR2
1.2.2 ALK-1, ENG, SMAD9, CAV1, KCNK3
1.2.3 Unknown
1.3 Drug and toxin induced
1.4 Associated with:
1.4.1 Connective tissue disease
1.4.2 HIV infection
1.4.3 Portal hypertension
1.4.4 Congenital heart disease
1.4.5 Schistosomiasis

1’ Pulmonary veno-occlusive disease and/or pulmonary capillary hemangiomatosis
1’’. Persistent pulmonary hypertension of the newborn (PPHN)

Adapted from Simonneau et al, JACC 2013[2]

1.2 PATHOGENESIS OF PAH

The pathogenesis of PAH is complex and multifactorial. Regardless of the etiology, lungs of patients with advanced (usually end-stage) PAH are characterized by hallmark pathological features in the small peripheral pulmonary arteries, which include intimal hyperplasia, medial hypertrophy, fibrosis, infiltration of inflammatory cells, and in many instances of advanced disease, plexiform lesions[8,11-13]. However, most of our understanding of the pathology of this disease comes from the examination of lungs from patients with very advanced disease. This is a major limitation since extrapolation of the features found in end-stage disease does not necessarily shed light on the mechanisms involved in the initiation of PAH, which may be very different.

1.2.1 EARLY ENDOTHELIAL INJURY AND DYSFUNCTION

The initiating mechanisms underlying the structural changes within the pulmonary vasculature in PAH remains elusive. However, there is a general consensus that PAH is instigated through a perturbation of endothelial cell (EC) homeostasis (Figure 1-1)[12-14]. Under normal conditions, the endothelium in the pulmonary vasculature is considered to be in a “quiescent” state, and functions to regulate vascular tone, permeability, and coagulation. However, injury to pulmonary ECs can result from to direct exposure to insults that are known to induce PAH such as hypoxia, viruses, drugs, toxins, or inflammation, resulting in EC dysfunction[12-14].

One of the first consequences of endothelial dysfunction is a loss of endothelium vasodilators, such as prostacyclin (PGI_2)[15] and nitric oxide[16], and an increase in the release of vasoconstrictors, such as thromboxane[17] and endothelin-1 (ET-1)[18]. Apart from modulating vasomotor tone, these factors control vascular cell growth; PGI_2 and eNOS are known to elicit anti-mitogenic effects on SMCs and ET-1 induces SMC proliferation[19] (Figure 1-2). Moreover, NO has been reported to inhibit the production and release of ET-1[20]. Thus, with endothelial dysfunction and the loss of endogenous inhibitory factors, aberrant proliferation of SMCs results, and leads to further vasoconstriction and remodeling of the pulmonary vasculature[8,13,21,22]. Changes in EC permeability also exposes the sub-endothelial layers to blood-borne cytokines and growth factors, resulting in further SMC dysfunction, and exacerbating the proliferation of cells in the intimal and adventitial layers, leading to the production of extracellular matrix components, fibrosis, and *in situ* thrombosis[8,13,21].

In addition, recent evidence suggests that EC apoptosis at the level of the distal intra-acinar arterioles and may play a prominent role in the early development of PAH[23-27]. At the pre-capillary level, the arteriole consists of one or two ECs with scant matrix support and few if any supporting mural cells (pericytes). Therefore, this arteriolar region is particularly fragile and may be uniquely vulnerable to degeneration upon exposure to relevant PAH stressors[22]. Also, this level of the lung vasculature contributes to the majority of the pulmonary vascular resistance, and therefore small changes in the cross-sectional area of these arterioles can lead to significant elevations of pulmonary arterial pressures[28]. These changes could occur either by a reduction in diameter or by a decrease in the overall number of vessels, both of which would lead to a decrease in the cross-sectional area of the lung circulation[28]. Experimental studies have demonstrated that enhancing expression of EC survival factors such as vascular endothelial growth factor (VEGF)[23], eNOS[27],

or angiopoietin-1 (Ang1)[24] using cell-based gene transfer in rat models of MCT- and hypoxia-induced PAH can protect against the development of severe PAH.

In a seminal report, Taraseviciene-Stewart *et al.* demonstrated that EC apoptosis resulting from a combination of transient exposure to hypoxia and treatment with a VEGF receptor-2 (VEGFR2) inhibitor, SU5416, led to the development of severe PAH in rats[29] (see Section 1.3.2). The authors also demonstrated that EC apoptosis can give rise to hyperproliferative lesions which resemble the intimal proliferative lesions observed in humans, and could lead to the obliteration of microvessels[29]. Moreover, inhibiting the apoptotic process using the caspase-inhibitor Z-ASP completely abrogated the severe PAH phenotype in response to the SU compound[29]. Similarly, Sakao *et al.* demonstrated the emergence of hyperproliferative ECs in response to VEGFR2 inhibition and high fluid shear stress in an artificial capillary system[30]. These hyperproliferative cells were also found to be phenotypically altered, expressing higher levels of the tumour marker survivin and the anti-apoptotic protein Bcl-xl[30]. Furthermore, these cells were also resistant to the induction of apoptosis when challenged with the pro-apoptotic agents TNF-α and cycloheximide or hydrogen peroxide[30]. While these findings potentially provide insight into the genesis of the 'angioproliferative' lesions that often (but not always) characterize advanced human disease, it should be noted that most animal models (and some clinical cases) of severe PAH do not show any evidence of these lesions. Moreover, as will be discussed below, even when plexiform lesions are present, it is unclear to what extent they actually contribute to the increase in pulmonary vascular resistance that is seen in these patients.

1.2.2 VASCULAR REMODELLING

A common histopathological feature observed in the lung sections of PAH patients is the extension of SMCs into the normally non-muscular, peripheral pulmonary arterioles within the respiratory acinus (Figure 1-1)[8,22]. Although the cellular processes leading to the muscularization of the pre-capillary segments of the pulmonary arteries are not completely understood, intermediate cells lying inside the internal elastic lamina have been shown to proliferate and differentiate into SMCs[22]. For example, pericytes have been shown to exhibit considerable plasticity *in vitro*, being capable of differentiating into SMCs, osteoblasts, phagocytes, and adipocytes[22,31]. Furthermore, the most distal vessels which lack an elastic lamina and medial SMCs, become muscularized by the recruitment of interstitial fibroblasts from the surrounding lung parenchyma, which subsequently take on a smooth muscle-like phenotype, thereby contributing to the muscularization process[22].

In addition, in the small peripheral muscular arteries, fibroblast hyperplasia and increased production of extracellular matrix components have been reported[21]. Collagen deposition and elastin synthesis in the adventitial layer culminates in further narrowing of the vascular lumen and contributes to the reduced arterial compliance[21,32]. With respect to a mechanism leading to the excessive vascular muscularization, Rabinovitch *et al.* have demonstrated that EC damage/activation leads to increased vascular permeability, allowing serum factors to stimulate SMC production of serine elastase[33,34]. This increase in elastolytic activity has been shown to liberate matrix-bound SMC mitogens (basic fibroblast growth factor, for example) and activate matrix metalloproteinases (MMPs)[35,36]. MMPs in turn can induce the expression of the ECM glycoprotein, tenascin-C, which leads to further proliferation of SMCs [37].

In the proximal muscular arteries, hypertrophy, and to a lesser extent, hyperplasia of medial SMCs occur upon exposure to a higher intraluminal pressure secondary to the vasoconstriction and

remodelling in the small peripheral vessels[38]. Also, rather than a contractile phenotype, these SMCs take on a more synthetic phenotype. New elastic laminae are deposited between the muscle layers, and increased collagen deposition leads to stiffening of the vessel wall. In addition to these medial wall changes, an increase in adventitial fibroblast proliferation and further collagen deposition occur as well[21,32].

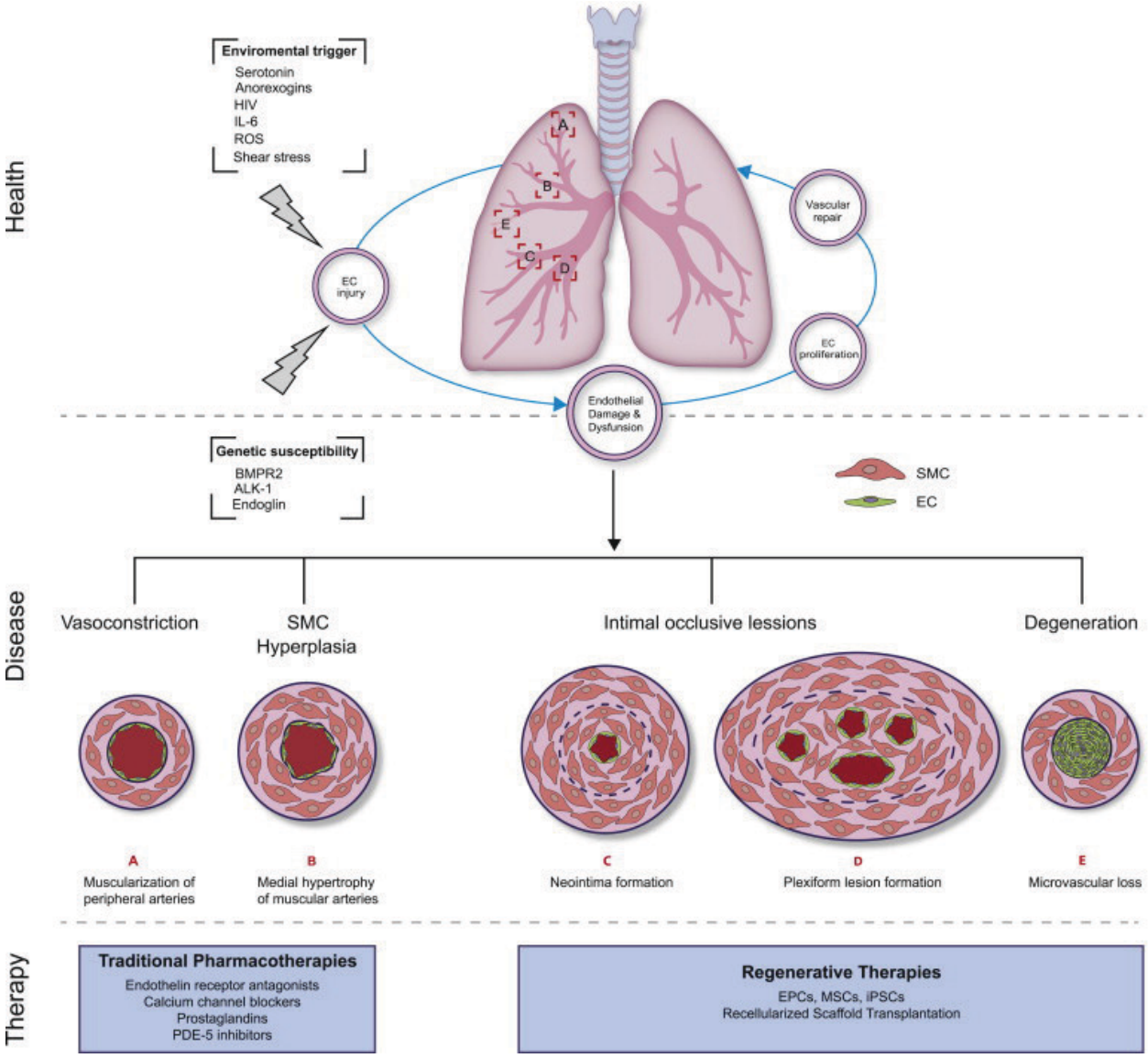

Figure 1-1. Pathophysiological mechanisms of pulmonary arterial hypertension (PAH). Exposure to environmental insults such as increased serotonin levels, anorexigens, viruses, increaseed levels of inflammatory cytokines such as interleukin 6 (IL-6), or sheer stress can contribute to endothelial cell (EC) damage and injury. In healthy individuals, physiological

repair processes restore normal lung function via proliferation of nearby ECs and/or the recruitment of circulating endothelial progenitor cells (EPCs). Alternatively, in individuals with PAH, pulmonary vascular cell damage contributes to the degeneration of microvasculature and/or arteriolar remodelling. In patients with hereditary PAH underlying genetic mutations to the genes encoding for bone morphogenetic protein receptor type 2 (BMPR2), activin-like receptor kinase-1 (ALK-1), and endoglin are associated with increased susceptibility to EC damage and injury. Traditional pharmacotherapies aimed at restoring imbalances in vasoactive factors are presented alongside emerging therapies aimed at regenerating the microvasculature. iPSCs, induced pluripotent stem cells; MSCs, mesenchymal stromal/stem cells; PDE-5, phosphodiesterase type 5; ROS, reactive oxygen species; SMC, smooth muscle cell. *Adapted from Foster et al, Can J Cardiol 2014* [39]

1.2.3 NEOINTIMAL AND PLEXIFORM LESIONS

A hallmark of severe PAH is the formation of a layer of myofibroblasts and extracellular matrix between the endothelium and the internal elastic lamina, termed the neointima[22,40]. These myofibroblasts express SMC markers, such as α-smooth muscle actin and vimentin, but not markers of highly differentiated SMCs, such as smooth muscle myosin, or any EC markers[40,41]. Although the origin of these neointimal cells is unclear, several studies have postulated that they may arise by transdifferentiation of ECs (i.e. endothelial-mesenchymal transition), by migration of "SMC-like cells" from the media, or by migration of adventitial fibroblasts[40,41].

The formation of plexiform lesions in severe PAH has intrigued researchers over the years. They typically occur just distally to the bifurcation sites of the smaller arteries of patients with IPAH (Figure 1)[42,43] . The mechanisms responsible for the disorganized proliferation of ECs have not been elucidated, but it has been hypothesized that these lesions are related to a failed and dysfunctional angiogenic process[44]. Indeed, ECs within these lesions have been found to over-express markers of angiogenesis, such as VEGF and its receptors, and to be supported by a stroma comprised of matrix proteins and α-smooth muscle actin-expressing myofibroblasts[45]. More

recently, it has been suggested that complex arterial lesions may be a consequence of the emergence of apoptosis-resistant and hyperproliferative ECs[30,46,47]. Moreover, in one report ECs within the plexiform lesions in IPAH patients have been found to be monoclonal in origin[48]; however, this finding has not been replicated to our knowledge. Plexiform lesions have also been reported to exhibit reduced expression of prostacyclin synthase[15] and nitric oxide synthase[16], and increased expression of ET-1[18], 5-lipoxygenase and 5-lipoxygenase activating protein, FLAP[49], and contain somatic mutations in apoptosis and proliferation regulating genes, such as Bax and transforming growth factor-beta (TGF-β) type II receptor[50,51]. Together, these alterations may contribute to abnormalities in vascular remodeling*, in situ* thrombosis, as well as the appearance of hyperproliferative, apoptosis-resistant ECs in patients with severe PAH[52].

While neointimal and plexiform lesions are present in severe forms of PAH, these features are not recapitulated in many of the commonly used animal models such as chronic hypoxia or monocrotaline (MCT)-induced PH[53]. However, "two-hit" animal models have been able to reproduce some of these lesions, such as in the variant of the MCT model, whereby rats are treated with MCT and subjected to pneumonectomy[54-56] and more recently, the SU5416/hypoxia model[57]. Also, neointimal lesions were observed in rats deficient in the endothelin-B receptor and treated with MCT[58]. Plexogenic pulmonary vascular lesions have been observed in a few transgenic mouse models, including constitutive over-expression of IL-6 under the lung-specific Clara cell 10-kDa promoter [59], and more recently, endothelial-specific knockout of prolyl-4 hydroxylase 2 (PHD2)[60]. However, in all nearly all mouse models, the hemodynamic and RV remodeling disturbances do not reach the severity of clinical PAH.

1.3 EXPERIMENTAL MODELS OF PAH

A significant challenge in studying PAH is the use of appropriate animal models to reflect human PAH. As described previously, the precise causes of Group I PH, i.e. PAH, are likely multifactorial, involving a combination of genetic and environmental factors that lead to vascular injury and the resultant remodeling of the pulmonary vasculature to a disease state. Thus, the most widely utilized animal models for PAH do not necessarily recapitulate the same pathogenic mechanisms that cause human PAH, but may simulate some of the pathological features of PAH, such as medial remodeling of lung arteries, right ventricular hypertrophy and dysfunction, and vascular inflammation, but not others such as the development of complex obliterative lesions in distal pulmonary arterioles.

A number of PH models have been developed in different animal species such as dogs, rats and mice. Small animal models are particularly advantageous to most researchers because of low cost and accessibility in most institutions. PH is commonly studied in rats and mice and each species offers their own inherent advantages and limitations. Although mice have the advantage of low cost and are amenable to transgenic modifications to knock-out or overexpress candidate genes to study precise molecular mechanisms, they are quite resistant to PH, and fail to respond reliably to the PH-inducing agents that can readily induce severe PH in rats as described below. Perhaps the best murine PH model is the chronic hypoxia model; however, even this fails to reproduce the severity of pulmonary pressure elevation and right ventricular remodeling seen in humans disease[53]. In contrast, rats are highly susceptible to PH, and two different induction methods are most often used, the monocrotaline (MCT) and the combined SU5416/chronic hypoxia (SUHx) models are described below and can produce irreversible pulmonary vascular lesions, severely elevated pulmonary hemodynamics, and right ventricular remodeling[61]. In fact, the SU5416 hypoxia rodent model exhibits complex pulmonary arterial lesions that are very similar to those

seen in severe human PAH. Given the similarities to clinical PAH, the rat MCT and SUHx rat models remain the most widely used models of PAH. However, in cell therapy literature, the rat MCT is the most frequently utilized platform and has become the de facto standard for testing efficacy, despite its flaws (Table 1-3 and Table 1-4.). To date, are no published studies demonstrating the efficacy of cell therapy in the SUHx rat model.

1.3.1 THE RODENT MONOCROTALINE MODEL

Monocrotaline (MCT) is an alkaloid derived from the seeds of the *Crotalaria spectabilis* plant. It was first discovered by Heath *et al.* as a compound that induced PH in rats in 1967[62]. Since then, the monocrotaline model has served as the most widely utilized animal model of PH. MCT requires hepatic bioactivation by the cytochrome P450 enzyme CYP3A4 to form monocrotaline pyrrole (MCTP), the key metabolite responsible for inducing PH[53]. A single administration at a dose of 60-100 mg/kg in rats causes rapid progression to pulmonary hypertension within 3 weeks, which is an earlier onset than in the SUHx model (5-8 weeks)[63]. Another distinct technical advantage of the MCT model is that it does not require the need for specialized equipment to induce chronic hypoxia as in the SUHx model, nor does it require extensive manipulation as in the surgically-induced left-to-right shunt or pulmonary artery banding[61]. MCT and/or its derivatives have been used to induce PAH in a variety of species such as rat, dog, primates, pig, and across multiple animal strains, albeit with considerable variability in response in different strains[53].

Monocrotaline results in injury to the pulmonary endothelium, resulting in endothelial cell apoptosis and endothelial dysfunction. These processes are believed to contribute to the development of PH. MCT induces apoptosis through caspase-3 activation in pulmonary

endothelial cells *in vitro*[64]. This was further illustrated *in vivo* in the rat model, where Jurasz et al. observed a progressive accumulation of apoptotic ECs in the lung from day 3 to 21 after MCT. Furthermore, blockade of caspase-3 using Z-Asp significantly attenuated the response to MCT[58], suggesting that apoptosis through the caspase-3 pathway is an integral process of the MCT-induced PH. When exposed to pulmonary ECs, MCTP forms cross-linkages with DNA, causing inhibition of cell proliferation[65]. Huang et al reported that MCT induces a disruption of endothelial membrane proteins such as caveolin-1, which in turn resulted in loss of eNOS and the subsequent activation of proliferative and anti-apoptotic pathways leading to pulmonary vascular remodeling[66]. MCT has been associated with an inhibition of BMPR2 signaling as well as a decrease in the BMPR2 protein itself in the pulmonary endothelium, which further promotes to EC apoptosis[67]. Similarly, MCT-induced defects in BMPR2 signaling in pulmonary artery smooth muscle cells contribute to apoptosis resistance[68,69]. This model is also characterized by inflammation, particularly with the accumulation of mononuclear cells in the pulmonary adventitia of small intraacinar vessels[70]. Although MCT and its metabolite MCTP are rapidly cleared in less than 24 h from the circulation, there is continued remodeling throughout the 3-week period, presumably due to a partial reservoir of MCTP accumulated in erythrocytes[71]. Following the injury, MCT results in pulmonary vascular changes such as medial hypertrophy in small pulmonary arterioles, and increase in pulmonary arterial pressures (mPAP > 35 mm Hg). By 3 weeks, significant RV hypertrophy and RV dysfunction ensue.

The MCT model has often received criticism as model of clinical PAH. Although medial hypertrophy occurs in the pulmonary vasculature, the MCT model does not reproduce the same pathological changes in patients with severe PAH[53,61,72]. Unlike other models such as the MCT + pneumonectomy[54] and SUHx models[57] which will be discussed below, MCT alone does not result

in the development of the hallmark intimal and obliterative plexiform-like pulmonary vascular lesions that are typically seen in patients. Another important limitation is the toxicity of MCT, which is not confined to the pulmonary vasculature. The MCT model causes damage to the pulmonary parenchyma and results in pulmonary edema, alveolar septal hyperplasia as well as impaired gas exchange[73]. As well, MCT causes myocarditis of both right and left ventricles, which confounds the effect of PH-driven RV dysfunction[74]. Remarkably, a single exposure to MCT has been associated with characteristics of end stage renal disease including glomerular enlargement, mesangial cell loss and tubule hyalinization in rats surviving to 60 days post-MCT[75]. High doses of MCT (60-300 mg/kg) can cause further off-target toxicity to the liver, causing damage to hepatic endothelial cells and parenchymal cells. In fact, MCT has been used to model hepatic veno-occlusive disease[76] and can even cause portal hypertension in dogs[77], which in and of itself is a inciting factor for pulmonary hypertension. These off-target effects contribute to the "monocrotaline syndrome", which confound the effect of PAH on mortality in this model. Mortality is also very high after 3 weeks post-MCT [72], which severely limits the long-term study of new therapies for PAH. Therefore, alternatives to the MCT model have to overcome these distinct disadvantages.

1.3.2 THE RODENT SU5416-HYPOXIA MODEL

The Sugen-5416 (SU5416) compound is a receptor tyrosine kinase inhibitor that antagonizes the vascular endothelial growth factor receptor 2 (VEGFR2), among other receptors, and was originally developed as semaxinib, an anti-angiogenic agent for cancer therapy[61]. The development of the SUHx model confirms the importance of the VEGF signaling pathway to homeostasis and survival of the endothelium. Taravsaveciene-Stewart and colleagues showed in the rodent model that VEGFR2 inhibition with SU5416 led to widespread pulmonary endothelial cell apoptosis with

the appearance of highly proliferative and apoptosis-resistant vascular cells that contributed to obliteration of the precapillary artrerioles[29]. Growth dysregulated ECs in this model are associated with increased expression of survival proteins IGF-1, Bcl-2 and Bcl-X. SU5416 alone produces modest increases in PAP, but when is combined with chronic hypoxia, the result is a severe, irreversible form of PH. The model was first developed by Voelkel and Tuder using three injections of 200 mg/kg subcutaneous injection for three weeks at Denver altitude[29]. It has since been refined and simplified to a single injection of SU5416 at 20 mg/kg followed by 3 weeks of hypoxia (10% O_2) and a return to normoxia for an additional 2-9 weeks[61]. This model exhibits complex vascular lesions, and in many cases the formation of plexiform-like lesions that closely resemble the pathology seen in human patients with PAH[57]. Also, unlike the monocrotaline model, the SU5416+hypoxia (SUHx) model is generally well tolerated depending on the background strain (see below), with low mortality in Sprague-Dawley rats even beyond 12 weeks.

The rodent SUHx model is often compared to MCT model of PAH. SUHx results in higher pulmonary pressures than the MCT, with RVSP often exceeding 90 mm Hg (or mPAP of ~50 vs. ~35 for SUHx and MCT, respectively). The SUHx model also results in marked RV remodeling, including RV hypertrophy and RV enlargement in later stages of the disease. Medial hypertrophy and neointimal proliferation of small pulmonary arteries (<50 μm) begins at around 5-6 weeks[61]. At 8 weeks post SU5416, concentric laminar intimal thickening is observed. Finally, plexiform-like lesions, similar to those in human PAH, appear at approximately 10–12 weeks after SU5416 administration[57].

The SUHx model is currently the most representative model of human PAH, based on its ability to reproduce the most of the salient features of PAH including elevated pulmonary pressures, RV remodeling, and plexiform lesions. Remarkably, the SU5416 compound appears to be selectively

toxic to the lung and not other highly vascular organs such as the liver or kidney[29], possibly due to the uniquely fragile nature of the distal lung arterial bed and the need for VEGF survival signaling to maintain EC homeostasis. Furthermore, since survival is typically good due to the lack of off target toxicity, the SUHx is well suited for the testing of the safety and efficacy of new therapies in long-term studies. One criticism of the model is that there is an absence or low levels of perivascular inflammation[53], which is commonly observed in MCT and in human IPAH[78]. As well, this model is slightly more complex, requiring an apparatus to induce chronic hypoxic, and takes longer to perform an experiment, typically 8 weeks compared to 3 for the MCT model, which incurs significantly greater costs.

Table 1-2 Rodent models of pulmonary hypertension

Animal model	**Advantages**	**Limitations**
Monocrotaline rat (60-100 mg/kg sc or ip)	Short, reproducible induction period No specialized equipment required Long track record as preclinical model of PAH	No plexiform lesions unless combined with pneumonectomy High mortality, likely due to off-target toxicity to heart, kidney, liver and lung parenchyma
Chronic hypoxia rat (10% O_2 x 3-4 weeks)	Extensively studied	Mild PH phenotype with low mortality Reversible upon return normoxia
SU5416 (20 mg/kg sc) + chronix hypoxia rat (10% O2 x 3 weeks)	Severe form of PAH Plexiform lesions Toxicity limited to pulmonary vasculature	Long, complex induction period No evidence of efficacy of cell therapy in this model
Left-to-right shunt	Model of PAH due to congenital heart disease	Surgical model - heterogeneity
Pulmonary arterial banding	Fixed RV afterload Useful for study of RV pressure overload without the effect of pulmonary circulation	Surgical model - heterogeneity RVH is adaptive rather than maladaptive in severe PAH

It should be noted that all preclinical models of PAH, or any disease, are far from ideal representations of human disease. Furthermore, while experimental therapies may demonstrate efficacy in preclinical studies, only a small fraction translate into clinical benefit [53]. A major limitation of preclinical studies is that unlike clinical trials, there is a lack of standards for experimental design and execution, which likely leads to large heterogeneity and likely contributes to poor reproducibility even within a same model. Preclinical studies should incorporate aspects of clinical trials designed to minimize bias in clinical studies such as stating pre-defined hypothesis, statistical power calculations, randomization, blinding of treatment and analysis. In recent years, efforts have been undertaken to improve standards for reporting of animal studies. The ARRIVE (Animal Research: Reporting of *In Vivo* Experiments) guidelines have been developed by a scientific consensus group to provide a checklist of items describing the minimum information that all scientific publications reporting research using animals should include, such as the number and specific characteristics of animals used (including species, strain, sex, and genetic background); details of housing and husbandry; and the experimental, statistical, and analytical methods (including details of methods used to reduce bias such as randomization and blinding)[79]. Many journals (over 300) are beginning to adopt and endorse the ARRIVE guidelines, which may, in the future, facilitate high quality reporting and the ability to conduct critical reviews of preclinical [80]. Taken together, the systematic embracing of these methodologies to minimize bias and improve the quality of the preclinical research and thus increase translational success.

1.4 PHARMACOLOGICAL THERAPIES

Therapeutic agents currently in clinical use for PAH are mainly vasodilators designed to address endothelial dysfunction and an imbalance in vasodilator and vasoconstrictor factors. These include calcium-channel blockers, prostanoids, endothelin receptor antagonists, phosphodiesterase type 5 inhibitors and direct soluble guanylate cyclase stimulators (Figure 2).

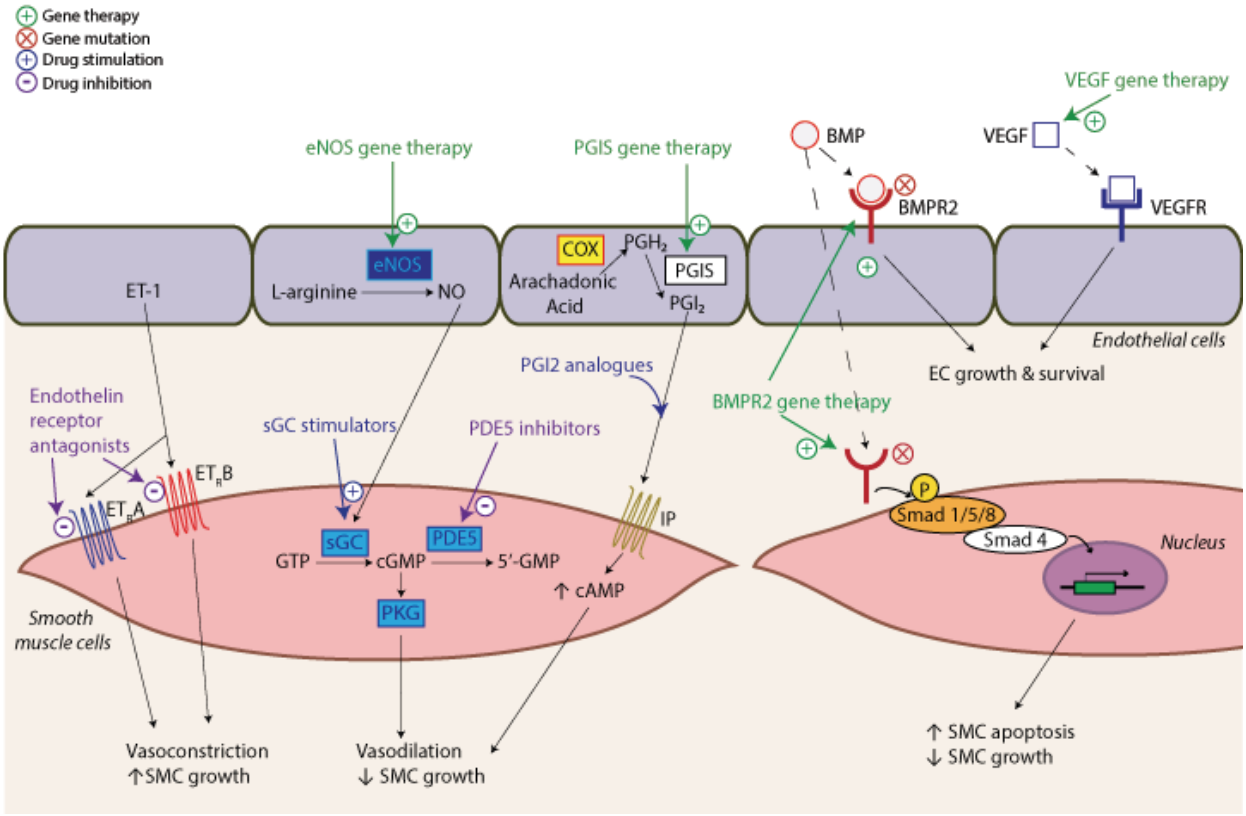

Figure 1-2. Key signaling pathways targeted in PAH therapy.
In PAH, homeostasis is mediated by balance of the release of endothelial cell vasodilatory factors such as NO and PGI_2 and vasoconstrictors such as thromboxane, and ET-1 which act on smooth muscle cells to regulate vascular tone. Furthermore, PGI_2 and eNOS, and BMP are known to exhibit anti-proliferative, pro-apoptotic effects to regulate smooth muscle growth. Impaired signaling through ET-1. NO, PGI_2 and have been implicated in PAH, which have become targets for drug therapy using endothelin receptor antagonists, PDE5 inhibitors, sGC inhibitors and prostacyclin analogs. Experimental gene therapy and cell-based gene therapy studies enhance the expression of eNOS, PGIS and BMPR2. In addition, dysregulation of endothelial growth or apoptosis is associated with the development of PAH and may be ameliorated by gene transfer of BMPR2 or VEGFR. *Adapted and modified from Suen et al, Compr Physiol 2013*[81]

1.4.1 PROSTANOIDS

Prostacyclin is a metabolite of arachidonic acid and promotes vasodilation, while inhibiting smooth muscle cell proliferation and platelet aggregation. Epoprostenol was the first FDA-approved therapy for PAH and was demonstrated to not only produce symptomatic and hemodynamic improvement in IPAH patients, but also associated with improved survival in New York Heart Association (NYHA) functional class III or IV patients[84-86]. However, because of its short half-life (3-6 minutes) and thus, need for an indwelling catheter and portable battery-operated infusion pump, the risk of potentially life-threatening infections exists and acute short-term withdrawal of epoprostenol can lead to fatal rebound effects[84]. Several newer prostacyclin analogs have been introduced with more convenient formulations. Treprostenil is a tricyclic benzidine analog of prostacyclin with a longer half-life compared to epoprostenol, allowing it to be delivered IV or subcutaneously (SC) by a smaller mechanical pump with less demanding storage requirements[87]. This medication has been approved by the FDA for patients with PAH functional class II to IV. Another prostacyclin analog, iloprost, is available as an inhaled mediation administered 6-9 times daily, which was approved in 2004 by the FDA for patients with WHO functional class III or IV symptoms[88]. Similarly, treprostinil has also been available as an inhaled medication since FDA approval in 2009[87].. More recently, selexipag, an oral prostacyclin analog has been approved by the FDA and Health Canada and has demonstrated good efficacy in reducing pulmonary hemodynamics and improving cardiac output[89]. Beraprost is another oral prostacyclin analog that is available in some countries but has not been FDA approved for PAH[88]

1.4.2 ENDOTHELIN-RECEPTOR ANTAGONISTS

Endothelin-1 (ET-1) is a potent vasoconstrictor and smooth muscle cell mitogen[90]. In patients with PAH, ET-1 levels within pulmonary vascular endothelial cells and in plasma are elevated and correlate with disease severity[18,91]. The effects of ET-1 are mediated through two receptor types: ET-A and ET-B. ET-A (Figure 1-2) is expressed primarily on smooth muscle cells and mediates vasoconstriction and proliferation; ET-B, on the other hand, is expressed on the surface of endothelial cells and mediates not only vasoconstriction, but also vasodilation by inducing the release of prostacyclin and nitric oxide, and functions in ET-1 clearance[16]. Although a number of ET-1 receptor antagonists with varying specificity for receptor blockade have been developed, there is no convincing evidence from clinical trials to support either non-specific or specific ET-A receptor blockade as the preferred mode of therapy in PAH. Bosentan, a dual endothelin receptor antagonist, was found to decrease pulmonary vascular resistance and improve exercise capacity in a large-scale clinical trial[92] and is an important part of the treatment algorithm in PAH[10]. Ambrisentan, an ET-A specific receptor antagonist, has also led to improvements in hemodynamics and exercise capacity in PAH patients[93-96] Macitentan is a novel dual ET-A/ET-B antagonist recently approved for the treatment of PAH[97].

1.4.3 PHOSPHODIESTERASE-5 INHIBITORS

Phosphodiesterase-5 (PDE-5) is an enzyme that metabolizes cGMP, an intracellular second messenger that mediates vasodilation via nitric oxide (NO), and which also has anti-proliferative actions on pulmonary arterial smooth muscle cells[98]. Interestingly, high concentrations of PDE-5 have been detected in the pulmonary vasculature and oral administration of the PDE-5 inhibitor, sildenafil, has been shown to produce relatively selective pulmonary vasodilation acutely and

improve both exercise capacity and pulmonary hemodynamics in PAH patients following long-term administration[99,100]. More recently, the longer-acting PDE-5 inhibitor tadalafil, has been introduced for PAH management[100,101].

1.4.4 SOLUBLE GUANYLATE CYCLASE STIMULATORS

Riociguat, a soluble guanylate cyclase (sGC) stimulator, belongs to a novel class of drugs that has recently gained approval in USA, Canada, Europe and Japan for the treatment of PAH and as the first medical therapy for inoperable chronic thromboembolic pulmonary hypertension (CTEPH) or persistently/recurring CTEPH after pulmonary endarterectomy (PEA)[102,103]. Nitric oxide is released by the endothelium and binds with sGC in smooth muscle cells to catalyze the synthesis of the secondary messenger cyclic guanosine monophosphate (cGMP) from guanosine triphosphate (GTP), leading to activation of protein kinase G (PKG) (Figure 1-2)[103]. Smooth muscle cell relaxation and vasodilation is facilitated by PKG-mediated lowering of intracellular calcium. Defects in NO–sGC–cGMP signaling have been implicated in pulmonary vascular derangements such as endothelial dysfunction, smooth muscle cell proliferation, vasoconstriction, platelet aggregation and fibrosis, and pulmonary vascular remodeling[104,105]. While PDE5 inhibitors act by inhibiting the degradation of cGMP, sGC stimulators such as riociguat stabilize NO binding to sGC and also directly stimulate sGC independently of NO, thereby increasing cGMP[103].

Riociguat has been evaluated in two Phase III clinical trials, one in PAH patients (PATENT-1) and another in inoperable CTEPH and/or persistent/recurrent CTEPH after PEA (CHEST-1) [106,107]. The PATENT-1 study was a randomized controlled trial that demonstrated a significant improvement in the primary endpoint, 6MWD and secondary endpoints such as PVR, mPAP, WHO functional class and cardiac output after 12 weeks of riociguat treatment[106]. The 1 year

follow-up extension study, PATENT-2, demonstrated sustained improvements in 6MWD and WHO functional class[108]. The CHEST-1 trial also demonstrated favourable outcomes in patients with inoperable CTEPH or persistent/recurrent CTEPH after PEA, improving 6MWD, PVR, and WHO functional class. In the CHEST-2 long-term extension study, improvements 6MWD and WHO functional class were sustained for 2 years[109,110]. So far, the evidence for riociguat in the treatment of PAH and CTEPH has shown promise in a small number of studies. Future studies will provide more information about the long-term safety profile and effect of sGC inhibitors on prognosis and/or survival in this patients with PAH and CTEPH.

1.4.5 COMBINATION THERAPY FOR PAH

Combination therapy—using 2 or more classes of drugs simultaneously—has been used successfully in the treatment of systemic hypertension [111] and heart failure [112]. PAH may be amenable to this strategy based on the 3 major signaling pathways involved: the prostacyclin pathway, the endothelin pathway, and the NO pathway. The current PAH treatment algorithm, as updated following the 5th World Symposium on Pulmonary Hypertension, recommends targeting at least one of the three main disease pathways [113].

The current treatment algorithm indicating the addition of a second treatment to background therapy may be considered when an inadequate clinical response or deterioration is observed with monotherapy in patients in World Health Organization (WHO) functional class III/IV[113]. Currently, dual combination therapy with a phosphodiesterase-5 inhibitor and an endothelin receptor antagonist is the most widely utilized combination regimen [114]. A recent systematic review and meta-analysis of 18 clinical studies showed that combination therapy using 2 or more pulmonary vasodilators was associated with a reduction in risk of "combined clinical worsening"

(combination of all-cause mortality, admission to hospital, lung transplantation, escalation of treatment by adding another pulmonary vasodilator or increasing prostacyclin dose, and percentage change in 6MW or functional class) compared to monotherapy[115]. As well, while parental prostacyclin therapy had been reserved for patients with severe PAH, the availability of oral prostacyclin analogues now facilitates targeting all three pathways at an earlier disease stage [114]. Evidence from small clinical studies demonstrates that upfront triple therapy that this approach can not only improve 6-minute walk distance and hemodynamics, but also increase survival [116].

Despite the availabilities of these various therapies and the use of combination therapy to target the different pathways involved in PAH pathogenesis, nearly all patients continue to progress[10]. Prognosis remains poor despite introduction of a number of new therapies in the last decade[117]. The most recent estimate of 5-year survival of newly diagnosed PAH is 61.2%[117]. A significant limitation of pharmacotherapy is based in the mechanism of action, which is aimed primarily at restoring pulmonary endothelial function by restoring imbalances in vasoactive factors rather than reversing the primary pathological process of lung arterial remodeling. Thus, it is not surprising that current pharmacotherapy options only provide modest effects on pulmonary hemodynamics at best and are non-curative, thereby warranting the need for more effective treatment strategies. Recent cell and cell-based gene therapy studies in experimental models suggest that this may be the new frontier in PAH medical management.

1.5 CELL-BASED THERAPIES FOR PAH

The pulmonary microcirculation plays a crucial role in cardiopulmonary physiology, by accommodating the entire cardiac output at pressures that are only a slightly higher than venous pressure, thus enabling the efficient oxygenation of the blood. The normal lung has excess microvasculature capacity that can be recruited to accommodate maximal cardiac output during exercise in a healthy individual[39] thereby maintaining low pulmonary arterial pressures even during vigorous exertion. However, the seminal feature of PAH is a functional rarefaction of the lung microcirculation, such that the residual microvascular capacity is not able to accommodate the cardiac output even at rest, thus leading to progressive increase in the pulmonary arterial pressures[39]. The mechanisms underlying the functional loss of lung microcirculation were discussed in detail in previous sections and include both proliferative and degenerative changes. Regardless of the mechanism, the end result is the same with marked reductions in the effective microvascular cross-sectional area, such that any further reduction can result in large changes in hemodynamics and functional status. However, the reverse is also true and even small improvements in microvascular area could produce large functional benefits. Therefore, regenerative therapeutic approaches to restore the lung microvasculature be an effective method for treating this devastating disease.

Recent understanding of the role of adult stem and progenitor cells in the maintenance of vascular homeostasis and repair of injury has stimulated interest in the potential for regenerative cell therapies for PAH (Figure 1-3). The lung offers a unique advantage for cell-based therapies since, in addition to oxygenating the blood, the lung represents the filter of the circulation, removing any small thrombi or other material that does not belong in the blood, such a non-circulating cells. Moreover, this filtration function occurs at the level of the smallest lung arteries, the pre-capillary

arterioles. As has been reviewed above, these arterioles represent the main site of pathology in PAH. Thus, stem or progenitor cells can be delivered directly to the damaged lung microvasculature by intravenous injection[23,75,118].

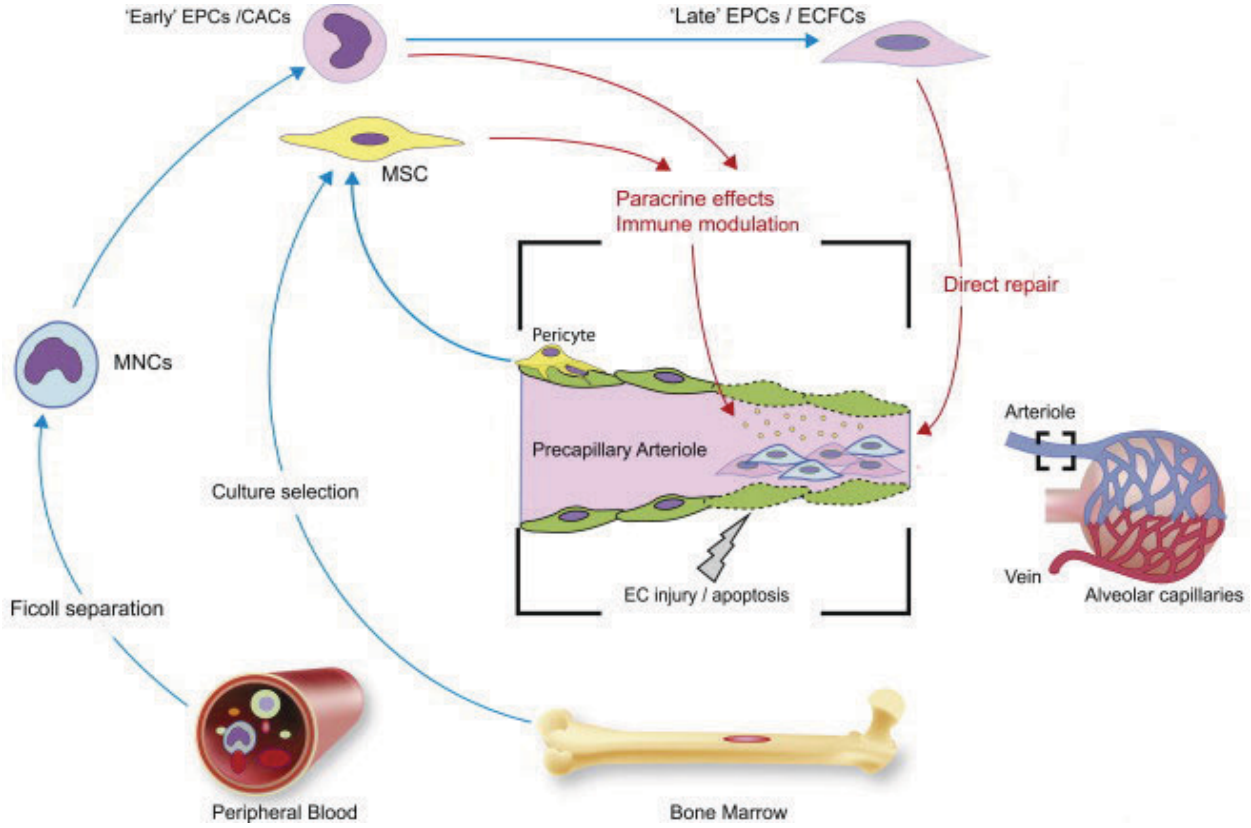

Figure 1-3. Origins, lineages, and functions of endothelial progenitor cells (EPCs) and mesenchymal stromal/stem cells (MSCs) in the context of pulmonary arterial hypertension (PAH).
Blue arrows indicate stem/progenitor cell origins and differentiation pathways from peripheral blood or bone marrow. Solid red arrows and hashed red arrows highlight the known and hypothetical therapeutic mechanisms by which selected cell populations act on areas of pulmonary precapillary arteriole injury/dysfunction, respectively. CACs, circulating angiogenic cells; EC, endothelial cell; ECFCs, endothelial colony forming cells; MNCs, mononuclear cells. *Adapted and modified from Foster et al, Can J Cardiol 2014*[39]**.**

Most of the preclinical studies of cell therapy for PAH have used two cell types in particular, early-outgrowth endothelial progenitor cells (EPCs, also known as circulating angiogenic cells, myeloid

angiogenic cells) and mesenchymal stromal cells (MSCs, also known as mesenchymal stem cells, adult stem cells)[81,119]. EPCs and MSCs have been described as dynamic and responsive cells that can migrate to sites of vascular injury in several *in vivo* animal disease models[120], facilitating neovascularization and reducing inflammation[81]. As treatments for PAH, preclinical studies involving these cell types have demonstrated efficacy in improving key pathological features of PAH such as cardiopulmonary hemodynamics, restoring the degenerated microvascular area, and reducing both right ventricular and pulmonary vascular remodeling [81]

1.5.1 ENDOTHELIAL PROGENITOR CELLS

Endothelial progenitor cells (EPC) were first described by Asahara *et al.* as a population of circulating bone marrow-derived cells that contribute to *in vivo* postnatal vasculogenesis [121]. These $CD34^+$ mononuclear cells were isolated from human peripheral blood and after 7 days in culture, they were able to take on a mature endothelial cell phenotype expressing markers such as CD31 (platelet endothelial cell adhesion molecule-1), Flk-1/KDR (vascular endothelial growth receptor 2), Tie-2, and endothelial nitric oxide synthase (eNOS). Further supporting their endothelial phenotype was their ability to take up acetylated LDL (acLDL), bind *ulex eurpaeus* agglutinin-1 (UEA-1) and form tube-like structures on fibronectin-coated plates. When transplanted, these cells were shown to co-localize with capillary vessels and improve blood flow sites of ischemic injury in rabbit and mouse models of hindlimb ischemia. Taken together, these data were remarkable in pointing out the existence of circulating progenitor cells with signs of endothelial lineage that could migrate to and repair sites of vascular injury.

Since this seminal study, a number of different methods have been used to identify a variety of differing cell populations that have all been referred to as “EPCs”, causing confusion as to what is

a "true" EPC. Two main strategies have been used to identify EPCs based on expression of surface markers or the ability to differentiate under defined cell culture conditions. Regarding the first, there is still a general lack of consensus on what surface markers specifically characterize a circulating EPC. Asahara selected for $CD34^+$ mononuclear cells from peripheral blood using magnetic beads. Since then, a number of cell surface markers have been suggested to identify circulating EPCs, including CD133 (prominin), Tie-2 and eNOS [121-128]. Numerous studies have utilized combinations of CD34, CD133 and/or VEGFR2 to correlate EPCs with disease states, with variable success. Recently it has been suggested that $CD34^+CD133^+VEGFR2^+$ cells are not EPCs, but are in fact hematopoietic progenitors that are do not form vessels in vivo [129,130]. Moreover, bone marrow hematopoietic cells that express the putative endothelial progenitor cell markers retain a monocytic cell, and not an endothelial gene expression pattern [131]. This topic has been recently reviewed in detail by Yoder [132].

The second approach uses culture selection to isolate progenitor cell populations[133]. Mononuclear cells from peripheral blood are plated in fibronectin-coated plates in the presence of endothelial growth factors. After several days, non-adherent cells are removed. The remaining cells express some EC markers, bind to lectins and take up acetylated LDL. Several studies using this definition of early outgrowth EPCs, also termed circulating angiogenic cells (CACs), have shown an inverse correlation with increases in risk factors of coronary artery disease [134]. Early outgrowth EPCs are probably better described as culture modified mononuclear cells, that are highly enriched in monocytes, since other populations such as lymphocytes and platelets do not persist under these conditions. There are two main cell phenotypes that can be observed in mononuclear culture[124,135]. The early outgrowth cells take on a rod-shaped morphology are largely nonproliferative and usually die out after several weeks in culture (Figure 1-4)[124,135]. In contrast, late outgrowth EPCs,

arise from colony-like clusters of cells usually after 2 weeks of culture and are thus commonly referred to in literature as endothelial colony forming cells (ECFC) or blood outgrowth ECs (BOECs) [124,135,136]. They are rapidly proliferative and exhibit a cobblestone-shaped appearance and a strong endothelial phenotype when assessed by surface markers of gene expression microarrays (Figure 1-4)[131]. Late outgrowth EPCs spontaneously form human blood vessels when grown on matrix scaffolds [137-140]. Of note, late outgrowth EPCs can form functional human blood vessels when included into Matrigel plugs implanted into immunodeficient mice, and these were able to anastomose to the murine systemic circulation [141]. Late outgrowth EPCs possess the characteristics, i.e. clonal proliferation, self-renewability, and ability to form new vessels *in vivo* that best fit the definition a progenitor cell population capable of postnatal vasculogenesis [142]. These cells appear to originate in the peripheral blood, belonging to a subset of cells expressing key surface markers which include CD34, CD146, but not CD133[143,144].

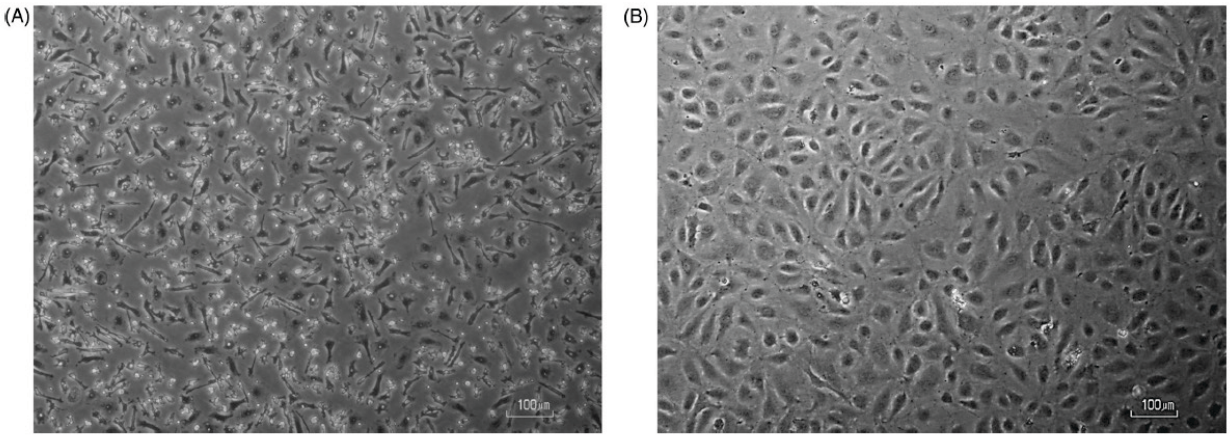

Figure 1-4. Morphology of early and late outgrowth EPCs using light microscopy.
(A) Early outgrowth EPCs with spindle-like morphology. (20X objective) (B) Late outgrowth EPCs with cobblestone morphology and abundant proliferation (20X objective). Scale bars represent 100 μm. Adapted from Suen et al, Compr Physiol 2013[81]

Another approach is the *in vitro* colony forming assays, that have been used mainly to quantify the number of circulating EPCs as a biomarker of vascular health. The first of these assays was described by Hill *et al.*, called the colony forming unit-Hill (CFU-Hill)[122]. Mononuclear cells isolated form peripheral blood are cultured on fibronectin-coated dishes and after 48 hours, non-adherent cells are then re-plated for further culture. These cells are able to form colonies sprouting cells radiating from a central cluster as seen by Asahara *et al.*. Despite a report of an inverse correlation between levels of CFU-Hill and increased cardiovascular risk, these CFU-EPCs fail to form human blood vessels when transplanted into immunodeficient mice[127].

These various populations of EPCs have been shown to be highly angiogenic; however, the mechanism in which they induce neovascularization is not fully understood. Bone-marrow derived EPCs can be mobilized into systemic circulation by chemokines and growth factors released in response to tissue injury, particularly tissue ischemia and vascular damage[145]. Once recruited, EPCs can incorporate into sites of endothelial denudation in order to initiate repair of the vessel wall[146]. In animal models of myocardial infarction, transplanted early outgrowth EPCs significantly improved blood flow, cardiac function and reduced left ventricular scarring[137,138,147]. Similarly, treatment with *ex vivo* isolated EPCs improved neovascularization in nude mouse and rat models of hind limb ischemia[137-140]. Both early and late EPCs show similar potential for *in vivo* neovascularization[135,148,149]; whereas, terminally differentiated mature endothelial cells do not improve neovascularization. This suggests that the undifferentiated state is an important attribute that contributes to their regenerative capacity[135,137,150,151].

The mechanisms by which EPCs contribute to vascular repair and regeneration appear to be complex and dependent on the specific progenitor cell subtype. The rate of incorporation of early outgrowth EPCs into vessels is extremely low (~1%)[152] under normal conditions; however, bone

marrow-derived cell incorporation can be increased in models of ischemia, with reported rates ranging from 0% to 90%[139,152-156]. However, the angiogenic effect of early outgrowth EPCs does not seem to be dependent of cell persistence, and it is has been widely accepted that they induce neovascularization primarily by paracrine mechanisms. Urbich *et al.* demonstrated that human peripheral blood MNC-derived early outgrowth EPCs secrete proangiogenic growth factors such as VEGF, stromal cell-derived factor 1 (SDF-1), insulin-like growth factor-1 (IGF-1), hepatocyte growth factor (HGF) and NO [157]. These factors may exert angiogenesis by stimulating proliferation and migration and survival of nearby mature endothelial cells[151]. In contrast, macrophages, which are known to release similar growth factors[125,158], failed to incorporate into vessel structures when infused into ischemic tissue and did not stimulate neovascularization to the same extent as incorporated EPCs[140]. In contrast to early outgrowth EPCs, Hur et al. observed that secretion of key angiogenic factors, such as IL-8 and VEGF, was markedly lower in late outgrowth versus[135]. Combined with their higher proliferative potential and greater ability to integrate into vessels in various models of angiogenesis, it has been suggested that late outgrowth EPCs promote neovascularization mainly by engraftment and direct transdifferentiation[135,141]. In the MCT model, xenotransplantation of human early outgrowth EPCs into immunodeficient (nude) rats was shown to ameliorate PAH despite low cell persistence, consistent with a paracrine effect;[75,159,160]; whereas late outgrowth EPCs had no beneficial effect [159]. It must be recognized that the nude rat model has intact natural killer cell (NK) activity and both early and later outgrowth EPCs were rapidly cleared from the lung. Indeed, there was a greater persistence of both cell types when residual NK cells were ablated using a specific antibody; however, the beneficial effects of early EPCs were lost, suggesting an immunological mechanism of action in this model[159].

Recent studies have attempted to use circulating EPC levels as a biomarker for PAH. In a number of clinical studies, reduced levels of circulating EPCs (early EPCs) have been correlated with increased risk of cardiovascular events[122,161,162]. In patients with idiopathic PAH, Junhui *et al.* observed reduced $CD133^{+}KDR^{+}$ cell levels, and reduced and dysfunctional early EPCs [163]. Similarly, Diller *et al.* showed low levels of $CD34^{+}KDR^{+}$ cells in patients with either Eisenmenger syndrome or idiopathic PAH[164]. However, another study by Asosingh *et al.* demonstrated increased levels of circulating $CD34^{+}CD133^{+}$ precursor cells in patients with IPAH and that high levels of EPCs may actually contribute to the proliferative processes that take place during pulmonary vascular remodelling [165]. Therefore, further study is necessary to elucidate the role of EPCs in the pathophysiology of PAH and other diseases before using them as surrogate markers of disease.

1.5.2 MESENCHYMAL STEM CELLS

Mesenchymal stem cells (MSCs), also called mesenchymal stromal cells or marrow stromal cells, are adult stem-like cells with many desirable features for cell therapy[166]. In the 1960s and 1970s, Friedenstein *et al.* published several seminal reports on these fibroblast-like cells that had been derived from bone marrow through their plastic attachment property[167]. Evidence from these and later studies subsequently established that MSCs are self-renewing, mostly heterogeneous populations of stem cells with the ability to differentiate into various tissues of mesenchymal lineage, such as bone, muscle, fat and even vascular tissue[168-170]. Unlike EPCs, there are now well validated methods of MSC characterization and/or isolation with a wide array of surface markers to which no specific combination has been agreed upon[171]. According to the position paper published by the International Society for Cellular Therapy in 2006, more than 95% of MSC

population are expected to express surface marker CD105, CD73 and CD90 but lack the expression of CD79a, CD19, HLA class II, or hematopoietic lineage markers such as CD45, CD34, CD14 and CD11b[166]. The most commonly used MSC isolation method to date still utilizes the plastic adherent property of MSCs. Even though the majority of MSCs described in literature have been isolated from bone marrow, isolation of MSCs or MSC-like cells from other tissues, including adipose tissue, umbilical cord, amniotic fluid, lung and other organs, have also been described [172]. Nevertheless, their relative ease of isolation, ability to be expanded to large numbers *ex vivo* and genetic stability make them a robust cell type that can be employed in a variety of applications, including in the treatment of cardiovascular diseases, pulmonary fibrosis, spinal cord injury, bone repair, cartilage repair[173].

Studies have demonstrated that MSCs are able to enter the circulation, home to sites of injury, differentiate into cells of the residing tissue and engraft to these tissue to restore function[168,169] Additionally, MSCs lack class II major histocompatibility complex (MHC) antigens and exhibit little (or no) expression of co-stimulatory molecules; thus, they can be used in allogeneic transplantation with a low risk of immune rejection[174-176]. For autologous cell transplantation, cells have to be harvested from the patient's own tissue or blood (as in the case of EPCs); this process is cumbersome and adds complexity and cost the manufacturing process. Another caveat of using autologous cells is that the therapeutic potential of patient's own cells may be suboptimal due to the patient's existing disease state[133,163,164]. A large number of clinical trials to date have used MSCs in an allogeneic fashion (transplantation of MSCs from donors to unrelated recipients)[177]. Therefore, it is no surprise that MSCs are one of the most widely studied cell types for cell therapy[178], as the therapeutic cell in its own right, as well as a platform for cell-based gene therapy for the treatment of pulmonary arterial hypertension[179-181].

It has been well established that the therapeutic effects of MSCs, particularly in the setting of acute[182,183] or chronic[184] inflammatory diseases, is in large part due to their ability to modulate the host immune system, although the precise mechanisms have not been clearly defined. Soluble factors secreted by MSCs themselves, or by MSC-stimulated immune cells have also been implicated in MSC-mediated immunomodulatory and immunosuppressive effects. Factors involved in inflammation, such as interleukin-10 (IL-10), transforming growth factor (TGF)-β, indoleamine 2,3-dioxygenase (IDO), angiopoietin-1 (ANGPT1) and prostaglandin E2 (PGE2), have been attributed to mediate the immunosuppressive action of MSCs [185]. Furthermore, published evidence also suggests that MSCs can alter the cytokine secretion profile of immune cells, including natural killer cells, dendritic cells, macrophages, and lymphocytes [186]. Given the increasing recognition that immune function and inflammation play major roles in the progression of PAH, the putative immunomodulatory properties of MSC may offer a unique approach for the treatment of PAH in patients.

1.5.3 ENDOTHELIAL PROGENITOR CELL THERAPY FOR PULMONARY ARTERIAL HYPERTENSION

Endothelial dysfunction and EC loss are thought to be key factors in the pathogenesis of PAH[187]. Because of their potential for stimulating neovascularization, EPCs are an attractive cell type for the treatment of PAH by potentially contributing to the repair and regeneration of damaged or lost lung microvessels [121,188]. On their own, transplantation of early outgrowth EPCs has been shown to be beneficial in preventing right ventricular hypertrophy, elevations in RVSP and mPAP, and pulmonary vascular remodeling in rodent models of monocrotaline-induced PAH [75,189,190] (Table 1-3.). Our group has shown that intravenously administered EPCs were able to incorporate into the endothelial lining of distal pulmonary arteries of MCT-injured lungs[75,190] . At the molecular level, EPC transplantation increases eNOS expression in the lung and RV[190-192], possibly due to

the expression of eNOS by the transplanted EPCs themselves. However, since early outgrowth EPCs express very low levels of eNOS compared to mature ECs, it is more likely that they increase the endogenous levels of endothelial eNOS in the lung vasculature indirectly which, in turn, increases production of the vasodilatory and antiproliferative nitric oxide[9,128]. Additionally EPC therapy has been shown to reduce expression of apoptotic proteins such as caspase-3 and Bax, and increase the anti-apoptotic protein Bcl-2, in the RV and lungs of MCT-injured rats, consistent with an anti-apoptotic role[192]. Still, unmodified EPC transplantation has not been able to effectively reverse established experimental PH, which would be a requirement for a curative therapy for PAH

.

1.5.4 MESENCHYMAL STEM CELL THERAPY FOR PULMONARY ARTERIAL HYPERTENSION

One of the main advantages of MSCs over other cell types, including EPCs, is that their immunoprivileged status may allow for allogeneic transplantion. Thus, the use of allogeneic cells derived from young healthy donors avoids the concerns summarized above of using diseased autologous stem/progenitor cells which by definition must be derived from the diseased host. This would also reduce the complexity and delay in processing and administering the product as MSCs isolated from healthy donors can be expanded in culture in large quantities, cryopreserved and stored to be made available on demand, similar to the way some blood products are currently given. Additionally, as indicated above MSCs are immunomodulatory, which may be very relevant for the treatment of PAH since chronic inflammation is increasingly recognized to play a major role in its pathogenesis.

Kanki-Horimoto *et al.* were the first to demonstrate the potential for MSC therapy in preclinical rat models of PH (Table 1-3.). Intravenous delivery of 1 million bone marrow-derived MSCs one

week after the administration of MCT resulted in a modest reduction of RVSP (28%) and RV hypertrophy (22%). Similarly, Baber *et al.* and He *et al.* demonstrated attenuation of PH, as well as RV and arteriolar remodelling using 3 x 10^6 and 5 x 10^6 MSCs, respectively. As well, intratracheal[193] and intravenous[194] administration of allogeneic MSCs 2 weeks after MCT injury partially reduced pulmonary pressures and right ventricular hypertrophy. Additionally, Umar *et al.* demonstrated benefit in using autologous MSC transplantation in MCT-injured rats, which circumvents the issue of donor-recipient immune reactivity should it ever become a concern[194].

Table 1-3. Summary of preclinical studies using cell therapy as a treatment for PH

Cell Type	Model	Key findings
EPC	MCT	Takahashi *et al*, 2004 [189] • Intratracheal injection of EPCs prevented MCT-induced PAH in dogs • Reduction in elevated mPAP, PVR • Improved cardiac output • Increased formation of new vessels
EPC	MCT	Zhao *et al*, 2005 [75] • IV administration of EPCs via central vein 3 days post-MCT injury prevented PAH in rats • Early EPC injection prevented rise in RVSP and RV/LV+S ratio, while skin fibroblasts had no protective effect • EPCs engrafted at small precapillary arterioles, distal arterioles and occasionally regenerating the endothelium of arterioles in pulmonary circulation • Fluorescent microangiography showed restoration of pulmonary capillary perfusion
EPC	MCT	Yip *et al*, 2008 [190] • IV administration of autologous EPCs at 28 weeks post-MCT injury prevented progression of PAH in rats • Reduction of elevated RVSP, RV/LV+S ratio, pulmonary vascular resistance • Protected against decreased mRNA expression of connexin43 and eNOS in lung and RV, protein expression of Bcl-2 • Reduced vessel wall thickness and increased lung vascularization
EPC	MCT	Mirsky *et al*, 2011 [195] • IV administration of EPCs via tail vein did not result in rescue of MCT-induced PAH in rats • No benefit in survival, hemodynamics, right ventricular hypertrophy or vascular remodeling
EPC	MCT	Ormiston *et al*, 2010 • IV administration of human-derived early vs late EPCs in nude athymic rat model of MCT-induced PAH • Prevention of PAH with early but not late outgrowth EPCs: reduced RVSP, RV/LV+S ratio, pulmonary arteriolar remodeling • Early EPC therapy was independent of long-term cell persistence in lung, but dependent on presence of NK and NKT cells
MSC	MCT	Baber *et al*, 2007 [193] • Intratracheal administration of MSCs 2 weeks post-MCT injury reversed PAH in rats • Reduction of elevated mPAP, PVR and RV/LV+S ratio • Improved vasodilator response to acetylcholine • Immunohistochemistry and immunofluorescence revealed MSC engraftment in airways but not in walls of pulmonary vessels, suggesting paracrine function
MSC	MCT	Umar *et al*, 2009 [194] • IV administration of MSCs 2 weeks post-MCT injury attenuated PAH in rats (4 weeks post-MCT) • Reduction of elevated RVSP, RV/LV+S ratio and normalized RV ejection fraction • Reduced pulmonary edema, inhibited thickening of pulmonary arterioles and alveolar septa
MSC	MCT	He et al, 2009 [196] • Delivery of MSCs 22 days post-MCT significantly reduced mPAP, RV hypertrophy, and pulmonary arteriolar thickening • Survival rate was improved from 50% to 90% 49 days post-MCT
MSC	MCT	Luan et al, 2011 [197] • IV administration of MSCs significantly reduced RVSP, mean right ventricular pressure, mPAP, RV/LV+S ratio in MCT-induced PAH in rats • Mean survival increased from 11 to 18 days

1.6 CELL-BASED GENE THERAPY FOR PULMONARY ARTERIAL HYPERTENSION

Cell-based gene delivery to the pulmonary microcirculation for the treatment of PAH has been studied using several somatic cell types such as pulmonary artery smooth muscle cells (PASMCs)[23,26,118] and fibroblasts[27] as the "vectors" for cell-based gene therapy (Table 1-4.). These initial studies demonstrated that intravenous administration of these cells through the left external jugular vein results in some engraftment within the distal pulmonary vessels and transmigration out of the vascular region into perivascular regions. Using a rat model of MCT, significant attenuation in the development of PH was observed after the delivery of $5x10^5$ pulmonary artery smooth muscle cells transfected with plasmid DNA containing eNOS, VEGF, or ANGPT1[23,26,118]. Following 3 weeks of MCT, rats that received the transfected cells had significantly reduced RVSP, RV hypertrophy, and muscularization of distal arterioles compared to MCT-treated controls receiving cells transfected with the null vector.

Several groups have now been able to combine the potential of regenerative cell types such as EPCs and MSCs with gene enhancement using cell-based gene therapy to treat experimental PAH, as summarized in Table 1-4. .

1.6.1 EPC-BASED GENE THERAPY

While autologous cell therapy has the major advantage of avoiding immune mismatch, EPCs derived and expanded from patients with PAH may exhibit reduced regenerative activity based on the effect genetic mutations or host factors associated with this disease. For example, late

outgrowth EPCs derived from patients with BMPR2 mutations demonstrated functional deficits such as decreased cell proliferation, migration and angiogenesis[133]. The function of autologous EPCs from patients with PAH or other cardiovascular disease can be enhanced by overexpression of potential therapeutic genes. Nagaya *et al.* were the first group to demonstrate the potential of this strategy[160] (Table 1-4.). While administration of 1 x 10^6 nontransfected human umbilical cord-derived early EPCs had a modest effect when transplanted into immunodeficient MCT-treated rats, this was greatly improved by transfection to overexpress adrenomedullin, resulting in significant decreases in mPAP, PVR and improved pulmonary arteriolar remodeling and survival. At about the same time, our group reported the efficacy of syngeneic rat EPCs when delivered 3 days after MCT. In this report, 1.5 x 10^6 EPCs nearly completely prevented the development of PAH. In the "treatment" model in which cell therapy was administered 3 weeks after MCT, at a time when PH was fully established, EPCs alone reduced the progression of PH over the subsequent 2 weeks, but failed to significantly reverse established PH[75]. In contrast, administration of EPCs transfected with human eNOS reversed established PH, resulting in with significant reductions in RVSP measured in the same animals at 5 weeks compared to 3 weeks post MCT. Moreover, RV/LV+S ratio, pulmonary perfusion and pulmonary arteriolar muscularization were almost completely restored to normal (pre-MCT) values. Most importantly, eNOS gene-enhanced EPC therapy was associated with a greater improvement in survival compared to non-transfected EPCs. In another report, human early outgrowth EPCs overexpressing calcitonin gene-related peptide (CGRP), a potent inhibitor of smooth muscle proliferation and vasoconstriction, was shown to be more effective compared to unmodified EPCs in ameliorating PH induced by left-to-right shunt operation in immunodeficient rats[198]. More recently, Zhou et al, engineered rat EPCs to overexpress a cyclooxygenase isoform 1-prostacycin synthase (COX1-PGIS) fusion protein to

augment prostacyclin production[199]. The fusion protein couples the activity of both enzymes, where COX1, which a precursor prostaglandin for PGIS to convert into prostacyclin. When compared to unmodified EPCs, COX1-PGIS enhanced EPCs showed improved hemodynamics, pulmonary vascular remodeling and RV hypertrophy in prevention of MCT-induced PH in rat. However, in a reversal model, there were was no additional benefit to COX1-PGIS enhancement in the above parameters.

The ability for cell-based gene therapy to reverse established PH in preclinical models provides the basis for translation of this therapeutic strategy for the treatment of patients with PAH. Based on the success of these preclinical studies, the first clinical trial using autologous EPC-based *eNOS* gene therapy for PAH, the Pulmonary Hypertension and eNOS Cell Therapy Trial (PHACeT), was undertaken in Toronto and Montreal, which established the safety and feasibility of this approach [200], and a larger phase 2 SAPPHIRE trial (Study of Angiogenic cell therapy for Progressive Pulmonary Hypertension: Intervention with Repeat dosing of eNOS-enhanced EPCs) which is planned to begin in early 2017 .

1.6.2 MSC-BASED GENE THERAPY

To date, MSC therapy has shown benefit in some prevention models, but has not been demonstrated to reverse established disease, which is the clinically relevant "treatment" scenario. Some studies using transfected MSCs have shown improvements over unmodified MSCs in reversing experimental PH in rats (Table 1-4.). Cell-based gene therapy for PH has been studied using MSCs overexpressing eNOS, prostacyclin (PGI_2) synthase and heme oxygenase-1 (HO-1)[179-181]. Kanki-Horimoto *et al.* studied the effects of MSCs expressing eNOS in the reversal of

MCT-induced PAH [179]. Rats treated with 1 x 10^6 MSCs or 5 x 10^5 eNOS-MSCs at 3 weeks post-MCT injury had improved pulmonary hemodynamics (lower RVSP) and reduced RV hypertrophy (RV/body weight ratio) compared to controls receiving saline. eNOS-MSC treatment significantly prolonged survival compared to treatment with MSCs alone, suggesting that eNOS gene transfer may confer additional benefits. In fact, Takemiya *et al.*, transplantation of allogeneic MSCs expressing prostacyclin synthase (PGIS) but not unmodified MSCs reversed elevations in RVSP, RV/LV+S ratio and pulmonary arterial thickening over two weeks in the rat MCT model[181]. Cell-based gene therapy using MSCs overexpressing heme oxygenase-1 (HO-1) has also been beneficial in a murine model of chronic hypoxia-induced PH [180]. HO-1 has anti-proliferative and pro-apoptotic effects on vascular smooth muscle cells, which may play a key role in preventing pulmonary vascular remodelling and repair[201]. Intravenous delivery of MSCs overexpressing HO-1 to mice exposed to hypoxia (8-10% O_2) restored RVSP, right ventricular and pulmonary arterial remodelling to normal levels corresponding to mice without hypoxia exposure whereas treatment with unmodified MSCs only resulted in a reduction in RV remodelling (RV/LV+S ratio). The results of these studies suggest that MSCs may serve as a suitable vector for cell-based gene therapy to treat experimental PAH and that the addition of gene therapy can enhance the effectiveness of stem cell therapy.

Table 1-4. Cell-based gene therapy strategies for PAH in animal models

Cell Type	Gene	Model	Key findings
PASMC	eNOS	MCT	Campbell *et al*, 1999 [118] • IV administration of PASMCs transfected with eNOS via internal jugular vein prevented MCT-induced PAH in rats • Cell-based eNOS transfer reduced elevations in RVSP and RV/LV+S ratio • Detected engraftment of fluorescently-labeled PASMCs into pulmonary artery walls with no evidence of immune response
PASMC	VEGF	MCT	Campbell *et al*, 2001 [23] • IV administration of PASMCs transfected with VEGF via internal jugular vein prevented MCT-induced PAH in rats • Cell-based VEGF transfer reduced elevations in RVSP and RV/LV+S ratio • VEGF-PASMC treatment decreased medial thickness of histological sections of pulmonary arteries • Endothelial cell caspase-3 staining was reduced in VEGF-PASMC-treated rats, suggesting reduced endothelial cell apoptosis
PAMSC	Angiopoeitin-1 (Ang-1)	MCT	Zhao *et al*, 2003 [26] • IV administration of PASMCs transfected with Ang-1 via external jugular vein prevented MCT-induced PAH • Elevated RVSP and RV/L+S ratio was reduced by Ang-1 gene transfer • Tie-2 receptor expression was downregulated in rats treated with MCT, but partially restored by Ang-1 gene therapy • 28-day post-MCT mortality rate was improved from 77% to 14% in rats receiving Ang-1 gene therapy
Fibroblast	eNOS, VEGF	MCT	Zhao *et al*, 2007 [27] • IV administration of eNOS-transfected fibroblasts at 3 weeks post-MCT-induced PAH reversed elevated RVSP in rats while VEGF-transfected fibroblast treatment only prevented further increases in RVSP from week 3 to week 5 • eNOS and VEGF transfer reduced elevations in RV/LV+S ratio • Fluorescent microangiography revealed that eNOS gene transfer improved pulmonary microcirculation • eNOS gene transfer but not VEGF gene transfer reduced muscularization of small pulmonary arterioles
EPC	Adrenomedullin	MCT	Nagaya *et al*, 2003 [160] • IV administration of human-derived EPCs transfected with adrenomedullin ameliorated MCT-induced PAH in nude rats • Reduction of elevated mPAP and PVR • Reduction of increased pulmonary artery medial wall thickness • Increased survival rate • Adrenomedullin-expressing EPCs were superior to EPCs alone
EPC	Calcitonin gene-related peptide (CGRP)	Left-to-right shunt	Zhao *et al*, 2007 [198] • IV administration of CGRP-EPCs via jugular vein 10 weeks post-shunt operation reversed PAH in immunodeficient rats • Reduction of elevated mPAP and PVR • Reduction of increased pulmonary wall thickness • Increased survival rate
EPC	eNOS	MCT	Zhao *et al*, 2005 [75] • IV administration of eNOS-EPCs but not EPCs alone via external jugular vein 3 weeks after MCT injury reversed PAH in rats • eNOS-EPC treatment reduced elevations in RVSP and RV/LV+S ratio, but EPCs alone did not significant improve RVSP • eNOS-EPC restored lung circulation by fluorescent microangiography showed restoration of, whereas EPCs alone only showed modest improvements • 35 day post-MCT survival rates were highest in eNOS-EPC group, followed by EPC only group and lowest in saline control group.
MSC	Heme oxygenase 1 (HO-1)	Hypoxia	Liang *et al,* 2011 [180] • IV administration of MSCs constitutively expressing HO-1 via jugular vein reversed MCT-induced PAH

			• Reduction of elevated RVSP and RV/LV+S ratio, pulmonary arteriolar medial wall thickness • MSC transplantation modulated hypoxia-induced lung inflammation
MSC	Prostacyclin synthase (PGIS)	MCT	Takemiya *et al*, 2010 [181] • IV administration of PGIS-MSCs 2 weeks after MCT injury reversed established PAH in rats • Reduction of elevated RVSP and RV/LV+S ratio, and decreased arteriolar wall thickening • MSC engraftment in lung was enhanced in rats with PAH vs non-PAH • PGIS-MSC treatment restored prostacyclin production to 50% of non-PAH rats • 7-week survival rates were highest in PGIS-MSC group (100%), whereas PBS (38%) and GFP-MSC (44%) control groups survival rates were lowest

Abbreviations: pulmonary artery smooth muscle cells = PAMSC, endothelial progenitor cell = EPC, mesenchymal stem cell = MSC, monocrotaline = MCT, intravenous = I

Adapted from Suen et al, Compr Physiol 2013[81]

1.7 THE RIGHT VENTRICLE IN PAH

Studies of patients with PAH have established a strong correlation between right ventricular (RV) function and prognosis, much more so than with the severity of hemodynamic abnormalities, such as pulmonary artery pressures (PAP) or resistance (PVR)[202]. In a cohort study of 110 PAH patients, Van de Veerdonk et al. reported that RV ejection fraction (RVEF) $< 35\%$ was associated with poor 12-month survival ($p=0.001$)[202]. PAH patients with stable or increased RVEF after therapy had better survival rates than patients with decreased RVEF[202]. In fact, these observations have spurred the development of newer composite right heart scoring systems to better predict outcomes in PAH, which illustrate the importance of RV function[203].

Current pharmacotherapies for PAH using first-line vasodilatory agents, such as endothelin receptor antagonists, prostacyclin analogues, and PDE5 inhibitors, are based on reducing pulmonary vascular resistance in pressures, thereby decreasing RV afterload. However, these therapies have only modest effects on hemodynamics, which continue to worsen over time, and do little to correct underlying pulmonary vasculature disease and do not restore lung microcirculation[200]. Interestingly, agents such as PDE5 inhibitors and ET receptor antagonists may also target molecular mechanisms involved in RV dysfunction, and thus it has been suggested that some of the benefits seen may relate to improved RV compensation independent of any effects on the pulmonary circulation, further supporting the importance of the RV in determining patient outcomes[204,205]. The mainstay treatments of LV failure such as beta-blockers, ACE inhibitors and angiotensin receptor blockers have limited (or no) clinical efficacy in treatment of RV failure associated with PH[206,207]. The lack of effective therapies for RV failure highlights a need for a better understanding of the mechanisms behind RV decompensation, in order to design novel effective RV-specific therapies.

The distinction between the LV and RV occurs early on in development, when the heart is patterned into the first heart field, which gives rise to the LV and both atria, and the secondary heart field which gives rise to the RV and outflow tract[208]. Gene patterning of the two chambers is directed by transcription factors such as dHAND and MEF2C in the RV, whereas development of the LV is guided by Nkx2.5 and eHAND[207]. In the developing fetus, maternal-fetal exchange across the placenta provides the sole source of oxygenation and nutrients[209]. Oxygenated blood flows through the umbilical vein and inferior vena cava to the right atrium[209]. The majority of the blood passes through the foramen ovale into the left atrium, which is subsequently ejected by the LV to the aorta to perfuse the upper extremities[209]. Of the blood returning from the upper extremities to the superior vena cava to the right atrium, approximately 2/3 is shunted across the foramen ovale, whereas the remaining 1/3 enters the RV. Blood entering the RV is ejected into the pulmonary trunk which bypasses the pulmonary artery via the ductus arteriosus to the aorta due to the high resistance in the pulmonary circulation of the non-ventilating lung[209]. Respiration beginning in the postnatal period triggers a number changes that lead to a substantial reduction pulmonary vascular resistance (PVR) and the switch from the fetal to the postnatal pulmonary circulation. These include increased lung P_AO_2 and the release of endothelium-dependent vasodilators such as NO and PGI_2 resulting in profound lung vasodilation thereby reducing PVR. As well, the closure of the ductus arteriosus, mediated by lung metabolism of prostaglandins, together with the foramen ovale, which is closed by the sudden decline in right relative to left atrial pressures, interrupts the right to left shunting of the fetal circulation. This is replaced by the separate and parallel pulmonary and systemic circulations of extrauterine life[207]. Therefore, during fetal development and persisting into immediate neonatal life, the RV is exposed to systemic pressures and thus has thick, hypertrophied walls that allow it eject blood at high pressures[210]. As

pulmonary pressures drop RV adapts to this decrease in afterload by transitioning to a thin-walled chamber, since it requires little work to maintain normal cardiac output while pumping against the low pressures of the normal pulmonary bed (~10-15 mm Hg). This is in stark contrast to the high systemic pressures (>100 mm Hg) encountered by the left ventricle (LV)[210]. Considering the distinct origins and environments encountered by each ventricle, unique understanding and therapeutic strategies the must be considered for the RV.

1.7.1 RIGHT VENTRICULAR REMODELING

In PAH, RV afterload is governed by Laplace's law (below), whereby wall stress is proportional to intraventricular pressure and diameter, and inversely related to wall thickness[211]. An increase in wall stress increases myocardial oxygen demand and impedes myocardial perfusion. Thus, the RV adapts to the increased pressure by increasing muscle mass, i.e. hypertrophy, and by adopting a more spherical shape which is more efficient than the crescent shape of the normal "unloaded" RV.

$$\sigma = \frac{P \times r}{h}$$

σ = wall stress, P = intraluminal pressure, r = radius (of the chamber), h = wall thickness

RV hypertrophy (RVH) is achieved by an increase in cardiomyocyte size via increased protein synthesis and the addition of sarcomeres[211]. The addition of sarcomeres in series causes cardiomyocyte lengthening, allowing a greater stroke volume to maintain cardiac output via Frank-Starling mechanisms[212]. Increased afterload results in cardiomyocyte stretch, stimulating the release of autocrine and paracrine growth factors such as insulin growth factor (IGF-1), angiotensin-II, endothelin-1, cardiotrophin-1 (CT-1), and epidermal growth factor (EGF) are

released during stretch[213]. An increase in afterload is sensed by integrins and sarcolemmal proteins such as phospholipase, protein kinase C and ion exchangers (Na^+/H^+ exchanger) in cardiac cells (myocytes, fibroblasts, endothelial cells)[213,214]. Ultimately, mechanical stretch results in the transduction of MAPK and JAK/STAT pathways, triggering increased protein synthesis, extracellular matrix remodeling, and re-expression of fetal genes. In addition, neurohumoral activation of the renin-angiotensin and sympathetic nervous systems contribute to angiotensin II-mediated and adrenergic-mediated cardiac hypertrophy[211].

In order to support the increased myocardial mass and increased diffusion distances in RV hypertrophy, a proportional increase in RV capillary density is needed to maintain adequate perfusion. Myocardial angiogenesis is regulated by secreted angiogenic growth factors, including VEGFs, angiopoietin-1 and -2, fibroblast growth factors, transforming growth factors, and platelet-derived growth factors[215]. Failure to increase capillary density and angiogenesis is associated with pathological hypertrophy and contributes to decompensated heart failure[215]. For example, mice treated with VEGF receptor decoy subjected to pressure overload using transverse aortic constriction develop rarefaction of myocardial capillary density and accelerated transition to decompensated heart failure[216]. Similarly, VEGF treatment improves capillary growth which leads to preservation of contractile function of the heart and prevents apoptosis in aortic banding induced LVH[217]. VEGF is also involved in physiological cardiac hypertrophy. Postnatal heart growth is impaired in *Vegfb*-null mice[218], and mice and rats overexpressing *Vegfb* in the heart developed cardiac hypertrophy with preserved cardiac function[219,220].

RV hypertrophy is associated with the reactivation of the fetal cardiac gene program. Similar to the LV, α-myosin heavy chain expression is decreased in favour of in expression of β-myosin heavy chain, a slower and less active isoform[221]. This isoform switch allows the myocytes to utilize

less energy for a given contractile force, thereby reducing the RV's overall ATP demand. In the postnatal heart, fatty acid oxidation is the predominant source of energy, responsible for 60-90% of ATP production, while glucose contributes 10-40%[222]. Fatty acid oxidation requires 12% more oxygen to generate the same amount of ATP as glucose oxidation[223]. During RV hypertrophy, the myocardium undergoes a metabolic shift, from using fatty acid oxidation to glycolytic pathways as the primary energy source[224]. These changes reflect a response to lower the RV's oxygen demand, but are still insufficient to maintain healthy contractile function[211].

Cardiac hypertrophy is also accompanied by expression of natriuretic peptides such as atrial and brain natriuretic peptide (ANP and BNP, respectively). ANP is synthesized mainly in the atria while BNP is produced by the ventricles[225]. The endocrine function of ANP and BNP causes diuresis, natriuresis, vasodilation, and inhibition of renin-angiotensin system to decrease blood pressure and effective circulating volume[225]. Additionally, these peptides also exert cardioprotective effects by inhibiting cardiac hypertrophy, cardiomyocyte apoptosis, fibrosis, and inflammation by activating natiuretic peptide receptor A (NPR-A) in cardiomyocytes, stimulating the production of cGMP and the activation of PKG[225].

1.7.2 ADAPTIVE VS MALDAPTIVE RV REMODELING IN PAH

Adaptive RV remodeling occurs when the RV is able to maintain normal cardiac output, RV ejection fraction (RVEF), RV filling pressures and exercise capacity despite having to accommodate increased afterload[207]. During adaptive remodeling, the RV undergoes concentric hypertrophy with minimal dilation or fibrosis (Figure 1-5)[207]. Adaptive remodeling of the RV occurs in physiological states such as exercise training and pregnancy, and this is characterized by a proportional increase in capillary density to increasing myocardial mass[226]. Although RV

hypertrophy (RVH) may initially be compensatory, allowing the RV to generate high pressures to accommodate increased afterload, over time the RV can transition to maladaptive or decompensated state, ultimately resulting in RV failure (RVF) and reduced cardiac output [207]. RVF is defined clinically based on signs and symptoms, which include dyspnea, syncope, chest pain, and peripheral edema[207]. Although there is no standard definition of RVF, the decline in RV function is often associated with reduced RV ejection fraction (RVEF) and RV dilatation, which are correlated with poor prognosis. As previously described, 5-year survival has been reported to be above 90% in PAH patients with stable or improving RV function, whereas decreased RV function, independent of changes in PVR, is correlated with higher mortality[202]. As well, increased thickness of the RV wall results in greater oxygen demand and a larger diffusion distance, causing a greater demand for oxygen[207,211]. The precise mechanisms that influence the transition from adaptive to maladaptive RV remodeling are still unclear, but there is increasing evidence that inadequate vascularity of the hypertrophied myocardium is an important contributing mechanism as discussed below.

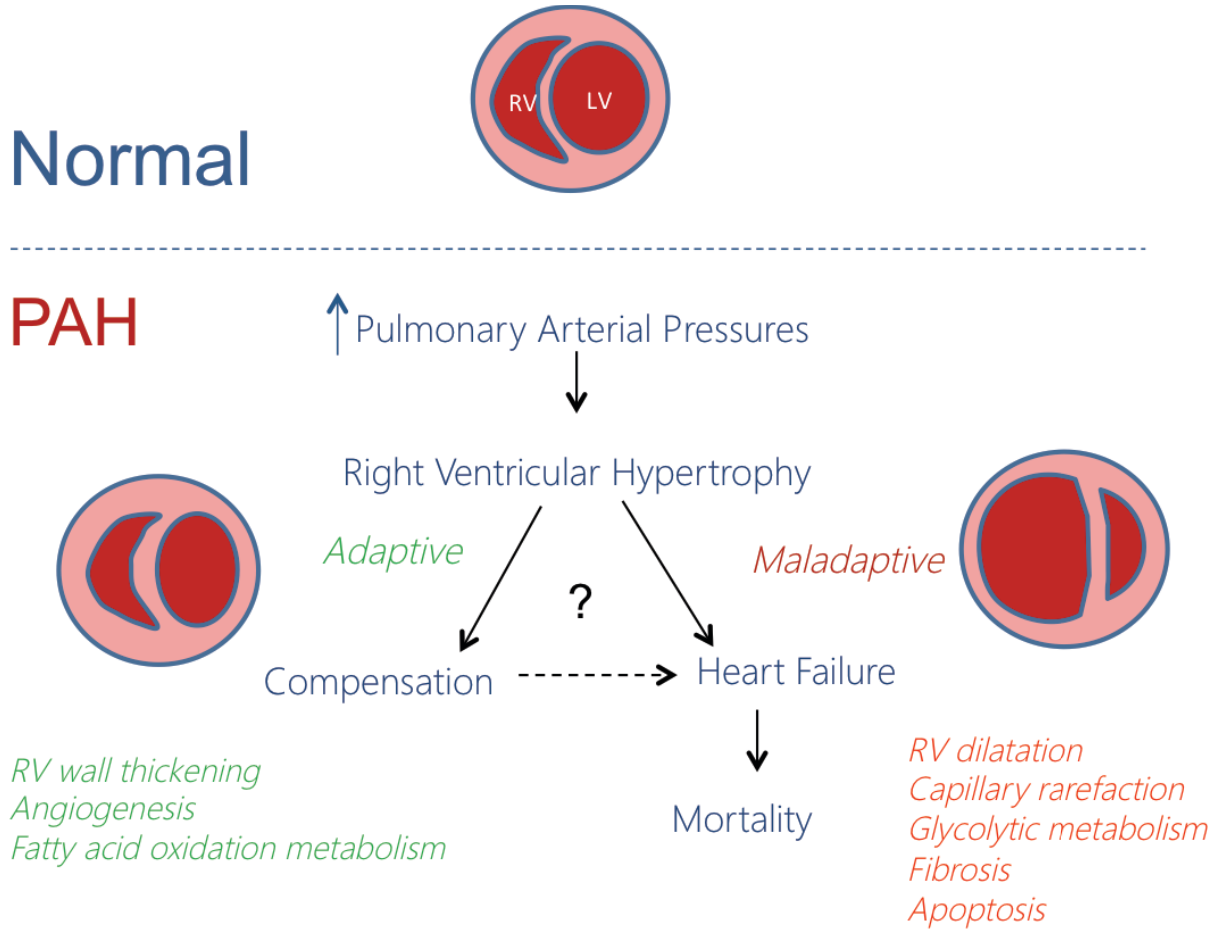

Figure 1-5. Adaptive vs maladaptive RV hypertrophy in PAH.
Increased afterload causes right ventricular hypertrophy. Initially, compensatory and adaptive mechanisms take place, which are characterized by RV wall thickening, concentric hypertrophy and a proportional increase in angiogenesis to match the increased myocardial mass. In contrast, Maladaptive hypertrophy is characterized by dilatation of the RV, capillary rarefaction, fibrosis and apoptosis resulting in RV failure. Due to inadequate O2 supply due to RV ischemia, the RV transitions from fatty acid metabolism as the main source of energy production to a less energy efficient form in glycolytic pathways.

Several lines of evidence suggest that hemodynamic stress alone does not fully account for RV dysfunction in PH. Patients with severe PAH can remain highly functional (NYHA Functional Class I) for many years without developing RV failure[227]. This is illustrated by one case study in which a PAH patient who exhibited adaptive RV remodeling survived 18 years despite little to no

improvement in pulmonary pressures (mPAP > 47, PVR > 6.5 Woods units) with epoprostenol therapy. Moreover, in the rat model, chronic pressure overload generated mechanically by pulmonary artery banding does not reproduce the same degree of RV dysfunction as in PH models, such as the SUHx model[228], despite comparable increase in pressures. Similarly, patients with mechanical stress alone, such as patients with pulmonary valvular stenosis, survive longer than patients with idiopathic or familial PAH[229]. As well, patients with PH due to congenital heart disease with Eisenmenger's syndrome, a state in which persistent left-to-right shunting leads to increased pulmonary flow and pulmonary hypertension, can maintain compensated RV function with concentric hypertrophy for many years, whereas patients with IPAH decompensate within 5 years after diagnosis[230]. To some extent the more favourable prognosis of patients with congenital heart disease and Eisenmenger's syndrome is related to the fact that their RV never fully transitions to the normal thin walled configuration after birth, since it continues to be exposed to near systemic pressures postnatally because of the presence of significant left to right shunts. Therefore, the RV in Eisenmenger's syndrome maintains a more thick-walled ventricular structure typical of the fetal state that is better adapted to higher pressures[231].

1.7.3 MICROVASCULAR CHANGES IN THE MALADAPTIVE RV REMODELING

Several clinical studies have demonstrated deficits in RV perfusion in PAH-associated RVF, including decreased right coronary artery flow[232], decreased coronary reserve in RV of patients with PAH[233], and decreased myocardial perfusion[234]. Data from animal and clinical studies suggest differences in RV microvascular density in maladaptive versus adaptive RV remodeling. RV biopsies of patients with "adaptive" forms of RVH, such as patients with Eisenmenger's syndrome, show greater microvascular density compared to patients with IPAH-associated RV failure[235]. As discussed earlier, although the increase in RV afterload is the same (mPAP), RV adaptation is

worse in the rat SUHx model compared with pulmonary arterial banding[228], which is associated with capillary rarefaction and a decrease in angiogenic genes such as VEGF when compared to pulmonary artery banding[228]. Transcriptomic profiling reveals that RVF (SUHx) is associated downregulation of angiogenic genes such as Ang-1, apelin and VEGF when compared to compensated RVH (hypoxia only)[236]. Sutendra et al. demonstrated that an accumulation of mitochondrial ROS resulted in the suppression of HIF1α-mediated RV angiogenesis in MCT rats[237]. As well, capillary rarefaction in RVF has been seen both in human and experimental PH, associated with downregulation of the angiogenic micrRNA, miR-126, resulting in impaired VEGF signaling and RV endothelial cell dysfunction[235]. Impaired RV angiogenesis may contribute to maladaption by producing RV ischemia and thereby resulting in reduced RV function, which has several important implications for RV metabolism as discussed in the following section.

1.7.4 METABOLIC CHANGES IN MALADAPTIVE RV REMODELING

In the normal healthy adult heart, oxidative metabolism is the primary source of energy, with fatty acid oxidation being the predominant form of energy production, accounting for 50-70% of ATP production, while glucose metabolism accounts for remainder[238]. In the failing RV, metabolism shifts from oxidative metabolism to anaerobic glycolysis which in part be an adaptation to increased O_2 demand caused by wall tension, and decreased supply from processes such as capillary rarefaction[207,236]. Glucose oxidation generates 32 molecules of ATP for each molecule of glucose to glycolysis, while glycolysis generates only 2 molecules of ATP, and therefore glucose uptake is markedly increased [207]. The increase in glucose uptake can be imaged by single photon positron emission tomography computed tomography (PET) using ^{18}F-FDG uptake. At the same time, it has been demonstrated that RV fatty acid metabolism is reduced in RVF in patients with

PAH which can be imaged using ^{123}I-BMIPP[234,239,240]. Fatty acid oxidation requires 12% more oxygen to generate the same amount of ATP as glucose oxidation[238]. Increased RV expression of glycolytic proteins PDK4 (Pyruvate Dehydrogenase Kinase, Isozyme 4) and Glut1 (Glucose Transporter Type 1), which reflect increased glycolysis and consequently glucose uptake, has been observed in PAH patients with early mortality due to RV failure vs long-term survivors[227]. PDK4 is a key inhibitor of pyruvate dehydrogenase, a mitochondrial enzyme that is responsible for converting pyruvate to acetyl-CoA to fuel the Krebs cycle[241]. In animal models of PH, activation of PDK4 inhibits PDH and decreases glucose oxidation in favour of glycolysis which reduces the O_2 demand of the myocardium at the expense of ATP production[241]. Furthermore, glycolysis can be maladaptive as it generates lactate as a byproduct, which can further impair RV contractility.

In animal models of PAH, RVF is associated with a reduction in the master regulator of oxidative metabolism, PGC-1α (peroxisome proliferator-activated gamma coactivator 1-alpha), and its corresponding receptors PPAR-α (peroxisome proliferator-activator alpha) and ERR-α (estrogen-related receptor alpha)[242,243]. PGC-1α is a transcriptional coactivator that plays a key role in coordinating expression of genes involved in fatty acid oxidation[244]. In fact, knockout of PGC-1α is associated with impaired contractile function, reduced mitochondrial activity and reduced ATP, LV dilation, reduced exercise capacity[245]. As well, PGC-1α knockout is associated with maladaptive remodeling in models of left ventricular failure such as transverse aortic constriction[246].

1.7.5 RV FIBROSIS IN MALADAPTIVE RV REMODELING

RV fibrosis is associated with maladaptive remodeling, as excessive fibrosis can cause increases in tissue stiffness, cardiomyocyte atrophy, arrhythmia, and hypoxia [247]. In patients, late gadolinium enhanced on magnetic resonance imaging (MRI) often reveals fibrosis localized to the insertion points of the RV to the interventricular septum, which is correlated with poor prognosis in PAH[248]. When compared to patients adaptive RVH due to Eisenmenger's syndrome, RV specimens from patients with IPAH show increased perivascular and interstitial fibrosis. Animal models such as the SUHx and MCT models also frequently exhibit fibrotic areas in the RV[228]. The maladaptive SUHx model is associated with increased RV fibrosis compared to pulmonary arterial banding, which is considered to be a model of adaptive hypertrophy pressure overload [228]. Maladaptive hypertrophy in animal models is associated with upregulation of TGF-β1, SMAD4 and CTGF, which contribute to myofibroblast differentiation and scar formation [236]. Treatments such as carvedilol that improve RV adaptation and function in experimental PAH are associated with decreased fibrosis [249], but less is known about the progression of RV fibrosis post-treatment in clinical PAH.

1.8 NON-INVASIVE ASSESSMENT OF THE RIGHT VENTRICLE

Pulmonary arterial hypertension results in pressure overload-induced RV hypertrophy. Initially, RVH can be adaptive and it is characterized by a concentric shape with preserved contractile function (Figure 1-5). However, over time the RV progressively enlarges and dilates, resulting in impaired systolic function. These morphometric changes can be progressively tracked using non-invasive imaging modalities such as echocardiography and magnetic resonance imaging (MRI).

1.8.1 ECHOCARDIOGRAPHY

Echocardiography is one of the clinical mainstays in screening PH screening, monitoring progression and RV function for reasons such as low cost, portability and rapid assessment. It can be performed non-invasively at the bedside and provide valuable information about pulmonary hemodynamics, cardiac structure and function within a short period of time.

In small animals, echocardiography is the most practical non-invasive tool to assess outcome. Since it can be performed without surgical techniques in live animals with only minimal stress to the animal due to anesthesia, it can be a powerful modality that provides information about the progression of disease. Several measurements using echo can be used reliably as a surrogate for many of the values obtained using more invasive techniques such as right heart catheterization.

1.8.1.1 PULSED-WAVE DOPPLER ECHOCARDIOGRAPHY

Pulmonary hemodynamics can be assessed using pulsed-wave Doppler at the level of the main pulmonary artery[61,63]. The Doppler tracing shows pulmonary artery flow, which can be dramatically altered in PAH. In PAH, the non-compliant pulmonary vascular bed causes reflection of velocity waves and reverse flow cancellation, which results in partial closing of the pulmonic valve[250]. This causes the characteristic mid-systolic "notching" seen in PAH (Figure 1-6). As a result, the pulmonary arterial acceleration time (PAT), measured by the time elapsed between the initiation of pulmonary flow to peak velocity, is dramatically shortened. Clinical [251] and animal [63] data show that PAT inversely correlates with mPAP, where a shortening of the PAT is associated with poor hemodynamics. In rats, PAT is normally > 30 ms, whereas in PAH, PAT continuously shortens with increasing severity and progression of disease [63]. Additionally, cardiac output can be estimated using this technique, using the pulmonary artery velocity-time integral method described by Urbonne et al. [63]. It is important to note that while mPAP and PA systolic pressure

(PASP) can be estimated by echocardiography in PAH patients, these measurements require a tricuspid regurgitant jet which, in our experience and others, is inconsistently observed in rats [61]. Furthermore, echo-derived mPAP and PASP have not been validated for small animals.

1.8.1.2 M-MODE AND 2-DIMENSIONAL ECHOCARDIOGRAPHY

The greatest utility of echocardiography is the assessment cardiac function and structure. In RV hypertrophy, the RV free wall thickness increases, which can be assessed using 2-dimensional B-mode or M-mode (1-dimensional) echocardiography. In PAH, RV remodeling is also associated with RV enlargement or dilation. This this can be represented as internal diameter of the RV (RVID) in M-mode either in short-axis (Figure 1-6) or parasternal long axis views[252]. This provides a 2-dimensional estimate of RV chamber volume. As well, since a large component of RV contraction occurs longitudinally, a surrogate measurement of RV shortening can be obtained by measuring the distance that the tricuspid annulus moves towards towards the apex from diastole to systole expressed as tricuspid annulus planar systolic excursion (TAPSE)[250]. This can be measured in standard M-mode and 2D B-mode echo. In contrast to the conical LV, where there are formulas available to estimate ejection fraction based on estimated volume, RV ejection fraction is difficult to obtain due to the irregular geometry of the RV. As a surrogate measure, RVEF can be estimated by orienting the RV to an apical 4-chamber view and measuring the 2D fractional area change (FAC%) between diastole and systole [252] (Figure 1-6).

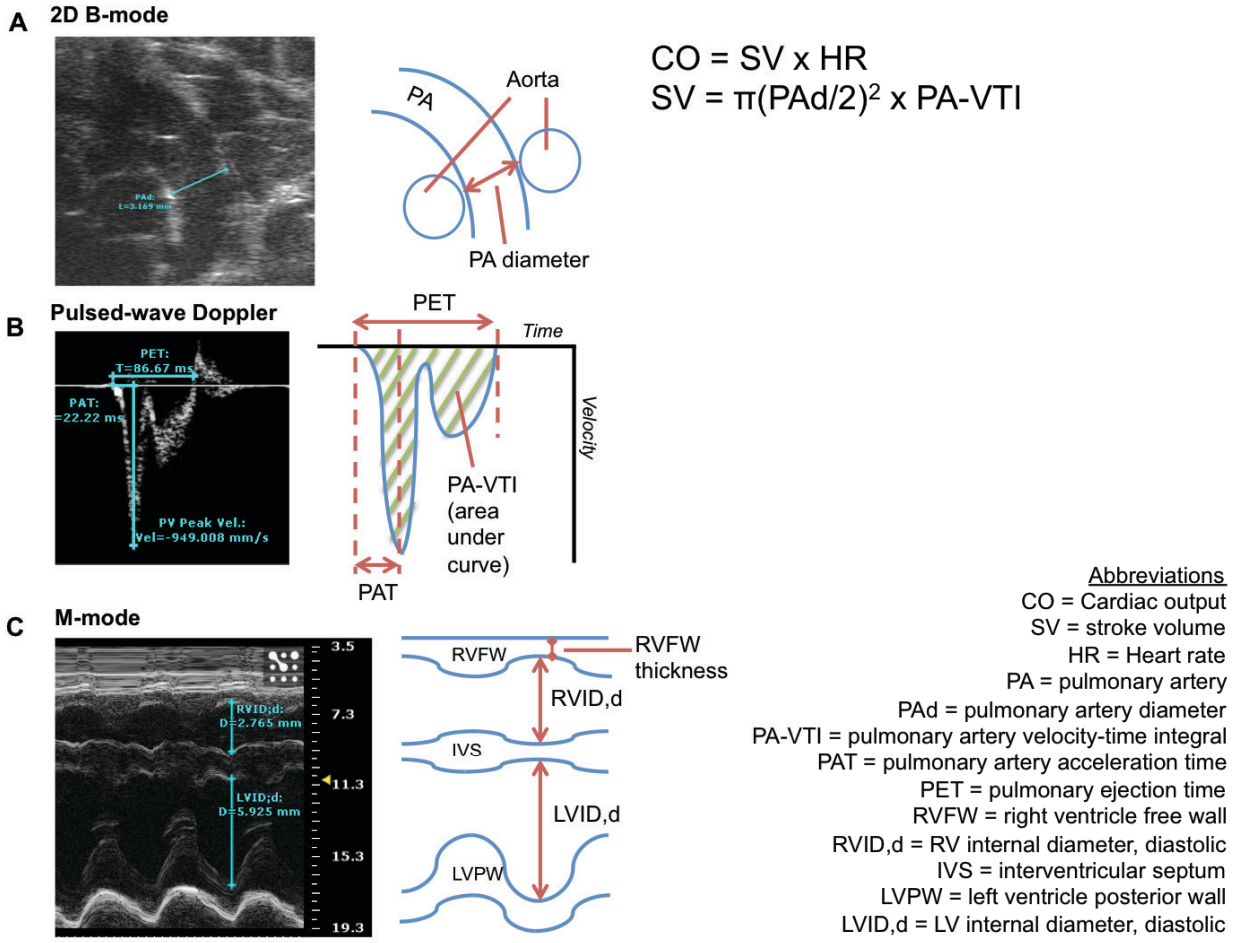

Figure 1-6. Echocardiography measurements in the evaluation of pulmonary hypertension. (A) 2D B-mode view is used to measure pulmonary artery diameter. (B) Pulsed-wave Doppler of pulmonary artery flow can be used to determine pulmonary artery acceleration time (PAT) which is determined by the time to peak flow, and the pulmonary artery velocity time-integral (PA-VTI). Using the formula shown above, cardiac output (CO) can be estimated using PA diameter and PA-VTI, and heart rate. (C) M-mode views are used to determine RV and LV internal diameter to assess RV enlargement in pulmonary hypertension.

1.8.2 CARDIAC MAGNETIC RESONANCE IMAGING

MRI is considered the gold standard imaging modality for assessment of RV size, mass and function. Unlike the left ventricle, the RV has a complex geometry and contractile pattern that is not easily predicted by mathematic models and therefore, RV volumes and ejection fraction are

difficult to evaluate by 2D echocardiography[253]. Conventional two-dimensional views of the RV (i.e. conventional echocardiography) only visualize RV movement and structure in one discrete plane, which may not represent the wall motion or structural abnormalities in other regions. Therefore, a major limitation of techniques such as 2D echocardiography is the inability to assess RV in 3 dimensions. MRI is a useful non-invasive imaging tool that has excellent resolution for soft tissues such as the heart with 3-dimensional imaging capacity[253]. As well, in contrast to other modalities such as echocardiography, which are heavily operator-dependent, MRI also has relatively high reproducibility and accuracy[254]. The interstudy variability has been reported to be 6.2% for end-diastolic volume, 14.1% for end-systolic volume, 8.3% for ejection fraction (EF), and 8.7% for RV mass [254]. Therefore, MRI has become the imaging modality of choice for clinical trials. The series of MRI acquisitions allow for 3-dimensional computational measurements of volume, which is particularly advantageous for assessment of the irregular geometry of the RV. Thus, MRI can be used reliably and accurately to measure stroke volume, ejection fraction and RV dilatation.

Standard MRI sequences can be recorded using ECG-gating to record cinematic images of the complete cardiac cycle. Contiguous slices of fixed thickness can be summated using Simpson's rule to estimate the volume of the atria and ventricles[255]. Therefore, the end-systolic volumes (ESV) and end-diastolic volumes (EDV) can measured and used to calculate the stroke volume (SV; EDV-ESV). From these calculations, ejection fraction (EF) can be obtained using the formula EF = SV/EDV or (EDV-ESV)/EDV and cardiac output using SV x heart rate. RV mass can also be calculated using RV volume multiplied by the myocardial specific gravity (1.05 g/cm^3)[250]. In a prospective study of 64 PAH patients followed up for 32 months, low SV and high RV volume at baseline and further worsening of SV and RV dilation were all strong predictors of mortality and

response to therapy[256]. As well, RV mass has shown good correlation with mPAP ($R=0.75$, $p< 0.003$)[257].

Contrast enhanced-MRI can be utilized to reveal other pertinent findings such as fibrosis. In a study of 25 PAH and CTEPH patients, 23 patients showed areas of late gadolinium enhancement at the insertion points of the RV and intraventricular septum[258]. These areas of delayed contrast enhancement are related to the increased volume of distribution in areas of fibrosis and slower washout kinetics due to relative accumulation of gadolinium in areas of increased extracellular space. Interestingly, the delayed contrast enhancement myocardial mass is inversely correlated to parameters of RV function such as EF and stroke volume[259,260].

Although not routinely used, MRI has been adopted for assessment of RV function in small animal studies of PAH. Urboniene et al. showed MRI-derived cardiac index was found to have a strong correlation with cardiac index obtained by catheter-based thermodilution ($R^2 = 0.851$)[63]. As well, RV mass by MRI correlated well with Fulton's Index (RV/LV+S) on autopsy ($R^2=0.844$). Other studies have utilized cardiac MRI to evaluate RV ejection fraction, which has been shown to be ~40% in the monocrotaline rat compared to healthy controls (70%)[261,262].

Chapter 2: Role of extracellular vesicles and paracrine activity of endothelial progenitor cell therapy for pulmonary arterial hypertension

2.1 INTRODUCTION

Therapies using stem and progenitor cells, including endothelial progenitor cells (EPCs), have been studied in a variety of clinical and preclinical applications for the treatment of cardiovascular and respiratory diseases such as acute myocardial infarction, heart failure, critical limb ischemia, neonatal bronchopulmonary dysplasia (BPD), acute lung injury/acute respiratory distress syndrome (ALI/ARDS), and pulmonary hypertension (PH)[263,75,200,264-267]. As described in section 1.5, EPCs are derived from circulating mononuclear cells and appear to play a role in the repair of vascular injury and postnatal neovascularization[121]. Since endothelial apoptosis leading to microvascular degeneration and remodeling are key factors in the pathogenesis of PAH[187], the regenerative potential of EPCs has made them an attractive cell type for cell-based therapies[121,188].

So far, early EPCs have been studied the most extensively in cell therapy studies[268,269], and have demonstrated therapeutic efficacy in clinical PAH[75,159,160,267]. While it was originally hypothesized that the mechanism of action of EPCs was from incorporation into damaged tissue and transdifferentiation into endothelium, emerging evidence challenges this theory. Cell persistence is extremely low after *in vivo* transplantation in studies in which EPCs have been effective[75,159,160]. Furthermore, the time course of the reparative effects greatly outlast the persistence of transplanted EPCs. This was particularly exemplified in a xenotransplant study by Ormiston *et al* in which human early EPC were undetectable using a sensitive PCR technique in the lung 24 hours after transplantation into immunodeficient nude rats, yet, there was significant protection against the development of PH[159].

It has been postulated that the therapeutic effects of early EPCs are mediated mainly by secretion of paracrine factors rather than direct engraftment and transdifferentiation, giving rise to the so-called “paracrine hypothesis”. Early EPCs secrete a much higher level of angiogenic factors such

as VEGF and interleukin-8 (IL-8) and are able to stimulate angiogenesis indirectly when co-cultured with other mature endothelial types such as human umbilical vein endothelial cells (HUVECs)[135]. Moreover, transcriptomic assessment of gene expressing and proteomic profiling of the EPC secretome have revealed increased secretion of numerous pro-angiogenic factors such as vascular endothelial VEGF, stromal cell-derived factor (SDF-1), insulin-like growth factor-1 (IGF-1), and hepatocyte growth factors (HGF) in comparison to mature endothelial cells[157]. In addition to having angiogenic activity, EPCs possess immunomodulatory properties, which have been demonstrated by the release of anti-inflammatory cytokine IL-10 upon induction by various proinflammatory signals[159]. Further characterization of these cells suggests that EPCs share features similar to alternatively activated M2 macrophages[270] and regulatory dendritic cells[159], immunomodulatory cell types which not act to resolve inflammation but also facilitate angiogenesis concurrently to promote tissue healing[159].

The "paracrine hypothesis" has been tested in a number of studies involving conditioned media from cultured EPCs. Di Santo *et al* generated EPC-conditioned media (EPC-CM) by subjecting early EPCs to 72 hours of hypoxia which stimulated increased production of proangiogenic cytokines such as IL-8, SDF-1, HGF, and VEGF-A compared to normoxic conditions[271]. Interestingly, repeated intramuscular injection of EPC-CM was equivalent to EPC treatment in improving blood flow and neovascularization model of rat hindlimb ischemia. Similarly, Kim *et al.* demonstrated that administration of $CD34^+$ cord blood-derived EPC-CM was therapeutically equivalent to the delivery of $CD34^+$ cord blood-derived EPCs in a model of diabetic wound healing[272]. As well, *in vitro* studies show that that EPC-CM may inhibit endothelial cell apoptosis and smooth muscle cell hyperproliferation that contribute to vascular remodeling in PAH[273,274] .

In addition to growth factors and cytokines, secreted extracellular membrane vesicles (EV) are emerging as key mediators in paracrine signaling. EVs are generally categorized into two groups based on size and mechanism of production. Microvesicles are large vesicles which bud from the plasma membrane with a size of approximately 0.1 – 1 μm and also referred to as microparticles, ectosomes, or exovesicles[275]. Exosomes are another group of vesicles that are typically 40-100 nm in size formed by the inward budding of endosomes which are released as the multivesicular endosome fuses with the plasma membrane. Although the precise function of microvesicles and exosomes is still being investigated, recent developments have shown that they can mediate extracellular mode of transport of mRNA, microRNA or protein between cells [276].

In a recent report, Lee et al. demonstrated that the therapeutic effects of cell therapy could be achieved without cell engraftment in a model of hypoxia-induced pulmonary hypertension in mice[277]. In fact, a high dose of exosome-enriched MSC-conditioned medium was able to fully prevent PH and PH-associated inflammation in this model. EPC-derived exosomes have also be shown to induce re-endotheliazation of balloon-induced systemic arterial injury[278]. Therefore, exosome release may be a novel mechanism by which EPCs exert their paracrine angiogenic and reparative effects and perhaps exosome enrichment may lead to the synthesis of a more potent cell-free therapeutic product.

In this study, we sought to determine the role of paracrine mechanisms of EPCs in an animal model of PAH. For all its limitations as a "true" model of PAH, the majority of cell therapy studies for PAH have been investigated in the monocrotaline model, with a small number of experimental studies tested in the chronic hypoxia and left-to-right shunting and none in the SUHx model [279]. Furthermore, this study builds upon the findings of Ormiston et al [159], which demonstrated efficacy of EPCs in the nude athymic rat model of MCT-induced PAH despite lack of cell persistence.

Therefore, we utilized the nude athymic rat model of PAH to appropriately study the effects of xenotransplntation of human EPCs.

2.2 OBJECTIVES AND HYPOTHESIS

Objective: To determine the role of paracrine mechanisms of EPCs in the prevention and rescue of pulmonary arterial hypertension.

Hypothesis: We hypothesize that since cell persistence/engraftment rates are extremely low in current cell therapy strategies, the therapeutic effects of EPCs in pulmonary arterial hypertension are driven primarily by a paracrine mechanism and therefore, cell-free EPC conditioned media is equivalent to EPC therapy.

Specific Hypothesis:

We hypothesize that the paracrine actions of EPCs are primarily mediated by secreted extracellular vesicles (exosomes), and that enrichment of exosomes can increase therapeutic potency.

2.3 METHODS

2.3.1 ETHICS

All study protocols were approved by the animal ethics and research committee (University of Ottawa, Ontario, Canada) and conducted according to guidelines from the Canadian Council for the Care of on Animal Care (CCAC).

2.3.2 EARLY OUTGROWTH EPC ISOLATION

Human early EPCs were generated from leukapheresis samples obtained from Leuko-Paks purchased from AllCells, inc (Almeda, California, USA) or obtained from healthy donors in accordance with the Ottawa Hospital Research Institute's Research Ethics Board. Mononuclear

cells were enriched on Ficoll-Paque Premium (GE Healthcare, Missisauga, ON) and plated on fibronectin-coated plates in EGM-2MV (Lonza, Burlington ON, Canada) media supplemented with 20% human serum (Wisent, St. Bruno, Quebec, Canada). Plates were changed with fresh media every 48 hours.

2.3.3 PHENOTYPIC CHARACTERIZATION OF EPCS

Day 6 EPCs were washed with PBS and detached using TrypLE (Lonza) for 5 minutes. Cells (250,000 cells) were pelleted and resuspended 100 ul ice-cold flow cytometry buffer containing PBS + 2% FBS + 0.2% sodium azide. Surface antigens were labelled using the mouse monoclonal antibodies: 10 ul of PE-CD14, PE-CD31, PE-CD34, FITC-CD45, FITC-CD144 (BD Biosciences, Missisauga, ON, Canada), 10 ul of FITC-VEGFR2 (R&D), 5 ul of PE-CD68, FITC-CD80, FITC-CD83, and PerCP-e710-CD86 according to manufacturer's protocol. For intracellular staining, cells were permeabilized using 0.5% saponin in flow cytometry buffer, washed with PBS and then stained with PE-CD68 (eBiosciences, San Diego, CA, USA). Cells were then washed and resuspended in 400 ul for analysis using the Attune flow cytometer (Life Technologies, Burlington ON, Canada).

Additionally, fluorescence labelling and staining were performed on EPCs grown on fibronectin-coated culture chamber slides. EPCs were incubated with 2.4 g/mL DiI–labeled acetylated LDL (Dil-Ac-LDL) (Invitrogen), then fixed using 4% PFA in PBS and counterstained with 1:100 FITC-conjugated Ulex Europaeus agglutinin (UEA-1) lectin (Vector Labs, Burlington, ON, Canada) and DAPI (Vector Labs). Immunofluorescence staining was also performed on fixed EPCs in fibronectin-coated chamber slides. 0.2% Triton-X100 in PBS was used to permeabilize cells, followed by staining with 1:100 dilutions of polyclonal rabbit antibody to vWF (Dako, Carpinteria, CA, USA), polyclonal rabbit antibody to VEGFR2 (Cell Signaling Technologies), and rabbit

polyclonal antibody to CD31 (Dako) at 4°C overnight. Afterwards, cells were labelled with 1:10,000 Alexafluor 480-conjugated goat anti-rabbit antibodies (Invitrogen) for 2 hr at room temperature. Prior to imaging, cells were mounted using Vectashield hardset mounting media containing DAPI (Vector labs) and coverslipped. Fluorescence microscopy was performed at 20X magnification to visualize staining, where images were acquired by thresholding to respective isotype controls.

2.3.4 GENERATION OF EPC-CONDITIONED MEDIA

EGM-2MV growth medium from day 5-6 EPCs was removed and cells were washed twice with DPBS. EPCs were then maintained in serum-free endothelial basal medium (EBM-2, Lonza,) for 24 hours and the supernatant was collected. To remove cells, the supernatant was centrifuged at 300 g for 5 minutes. The resultant supernatant was then centrifuged 2000 g x 15 minutes to pellet dead cells and debris. The clarified supernatant was then loaded 3K MWCO centrifugal filtration devices (Millipore, Etobicoke, ON, Canada) and concentrated up to 50X by centrifugation at 4000 g for 45 minutes to obtain concentrated EPC conditioned media (EPC-CM). Control conditioned media was obtained from HUVEC cells (Lonza) using the above method. For subsequent *in vitro* and *in vivo* studies, conditioned media potency was calculated based on number of adherent cells per unit volume.

2.3.5 MATRIGEL TUBE FORMATION ASSAY

24-well plates were coated with 280 µl of Matrigel (BD Biosciences). Approximately 40,000 HUVECs were seeded in to a final volume of 500 µl EBM-2 + 0.5% FBS (control medium) per well. Test conditions were generated by addition of EPC-CM (from 1 x 10^6 cells), HUVEC-CM (from 1x10^6 cells), or 50 ng/ml VEGF (R&D Systems, Minneapolis, MN, USA) to control medium. Inverted phase contrast light microscopy pictures of the networks were taken at 24 h.

Number of cords, nodes, and cord length were quantified using ImageJ with the Angiogenesis analyzer plugin (http://image.bio.methods.free.fr/ImageJ/?Angiogenesis-Analyzer-for-ImageJ). A node was defined as the point of intersection of at least 3 tubules.

2.3.6 EC MIGRATION ASSAY

HUVECs were grown in endothelial growth medium (EGM-2), which is created using EBM-2 plus the addition of 2% FBS, human epidermal growth factor, hydrocortisone, gentamicin, amphotericin-B, VEGF, human fibroblast growth factor, insulin growth factor 1, ascorbic acid, and heparin (Lonza). HUVECs were grown on 24-well plates to confluency and serum-starved 18 hours to arrest proliferation. A "wound" was created by scratching the adherent monolayer using a 10 ul pipette tip and incubated in the presence of EPC-CM (from 200,000 cells), HUVEC-CM (from 200,000 cells), VEGF (50 ng/ml) in EBM-2 + 0.5% or EGM-2. Phase contrast photomicrographs were taken at 10X magnification at baseline and at 24 hours. Analysis of wound area was performed using TScratch software (http://www.cse-lab.ethz.ch/index.php?&option=com_content&view=article&id=363) and expressed as percentage of wound area relative to baseline. All conditions were tested in triplicate wells.

2.3.7 EC SURVIVAL STUDIES

HUVECs were grown on 96-well plates to confluency (approx. 40,000/well). To induce cell death, cells were serum starved in 100 µl control medium (EBM-2) and incubated with 50 ng/ml VEGF, HUVEC-CM, (from 4 x 10^4 cells) or EPC-CM (from 4 x 10^4 cells) or 2% FBS (serum replete) for 48 hours. After 48 hours of serum starvation, cells were washed and incubated in 2 ug/ml Calcein-AM viability dye (Invitrogen) in EBM-2+0.5% FBS for 30 minutes. Fluorescence detection was determined by a fluorescent microplate reader using excitation filter 485 nm, emission 520 nm (Omega PolarStar). All conditions were tested in triplicate wells.

2.3.8 BRDU PROLIFERATION ASSAY

To test the potential for EPC-CM to induce EC proliferation, 20,000 HUVECs were plated onto 96-well plates and maintained in factor free, serum-free EBM-2 for up to 24 hours to induce growth cycle arrest. Afterwards, medium was changed to control medium (EBM-2 + 0.5% FBS) with or without EPC-CM (from $1x10^6$ cells) or HUVEC-CM (from $1x10^6$ cells), VEGF (50 ng/ml) or fully supplemented EGM-2 followed by the addition of bromodeoxyuridine (BrdU) (Millipore). After 24 hours of incubation, cells were fixed and stained using mouse anti-BrdU primary antibody followed by secondary detection using goat anti-mouse IgG-peroxidase conjugate as per manufacturer protocol (Millipore). TMB peroxidase substrate was added and read after 30 mins using the Omega PolarStar spectrophometer to detect the colorimetric change (450 nm/550 nm). Each data point represents a mean from triplicate wells.

2.3.9 LUMINEX ASSAY

Conditioned media was collect and concentrated from HUVECs, EPCs and $CD14^+$ monocytes as previously described. CD14+ monocytes were generated by plating PBMCs isolated from leukapheresis packs after Ficoll separation. PBMCs were then subjected to selection using CD14 MACS cell separation (Miltenyi Biotec, Auburn, CA, USA) and plated onto plastic flasks at $1x10^6$ cells/cm2 in RPMI medium (Lonza). After 24 hours, conditioned media was collected, clarified and concentrated using methods described earlier. From each sample, 25 µl was plated in triplicate with the Milliplex MAP Human Cytokine 41-plex kit reagents and incubated overnight at 4^oC as per manufacturer's protocol (Millipore, Etobicoke, ON, Canada). Analytes were read using BioRad BioPlex system to determine analyte concentrations based on premixed standards supplied by the manufacturer. Analyte concentrations were then normalized to pg produced by 10^4 cells.

2.3.10 EXOSOME ISOLATION

Extracellular vesicles were obtained using a differential ultracentrifugation method adapted from Thery et al.[280]. Conditioned media was collected supernatants of cells grown in serum-free media for 48h. The conditioned media was clarified by a centrifugation at 2000 g for 20 minutes to remove dead cells and debris and 10,000 g for 30 minutes to pellet larger secreted vesicles (microvesicles, MV). Afterwards, the remaining supernatant was centrifuged at 110,000 g for at 70 minutes to 2 hours to pellet the exosome (EXO) fraction. The pellet was washed by in PBS with an additional centrifugation under the same conditions. The remaining pellet was resuspended in small volumes of PBS for downstream analysis or stored at -80^{o}C. Exosome quantification was approximated by lysing the exosome solution in 10X ice cold RIPA buffer (Millipore) followed by sonication and protein quantification using the BCA method.

2.3.11 CHARACTERIZATION OF EXTRACELLULAR VESICLES

Freshly isolated extracellular vesicles were diluted 5-fold in PBS and analyzed nanoparticle tracking analysis using the Nanosight LM10 (Malvern Instruments) instrument with NTA 2.3 software. Protein concentration was determined on EV lysates using BCA assay. EV lysates were also subjected to Western blotting for the exosomal markers CD63, CD81 and ER-marker calnexin (negative in EVs). For some EV samples, intact EVs were captured using magnetic CD63-conjugated Dynabeads (Invitrogen) overnight, washed with PBS and then stained PE-conjugated antibodies to CD9, CD63, or CD81 as well as their respective IgG isotype controls. Surface marker expression was analyzed using flow cytometry as described previously.

2.3.12 RODENT MONOCROTALINE MODEL OF PH

PH was induced in athymic nude rats (Charles River Labs, Montreal, QC, Canada) weighing 150-200 g by a single intraperitoneal injection of MCT (70 mg/kg in ddH_2O), whereas healthy controls received an equivalent volume of sterilized water. Three days after MCT, rats were anesthetized using xylazine (5 mg/kg) and ketamine (30 mg/kg) and the left jugular vein was cannulated for delivery of EPC, EPC-CM or vehicle control (DPBS). For cell injections, cells were detached using TrypLE (Gibco) and counted by Trypan blue exclusion and resuspended in DPBS to deliver a dose of $5x10^6$ cells/kg body weight. Conditioned media was prepared from Day 6 EPCs as previously described. EPC-CM was adjusted to deliver a dose equivalent to the volume of conditioned media from $5x10^6$ adherent EPCs.

On day 24, non-invasive echocardiography (VEVO 2100, Visual Sonics) was be performed on rats anesthetized using 2% isoflurane to assess blood flow (pulmonary artery acceleration time (PAAT), pulmonary ejection time (PET), RV contractility (triscuspid annular plane systolic excursion (TAPSE)) and cardiac structure (RV wall thickness, RV/LV diastolic ratio). Afterwards, rats were anesthetized by an intraperitoneal injection of xylazine (7 mg/kg) and ketamine (35 mg/kg). High-fidelity pressure catheters (Transonic-Scisense Inc., London, ON, Canada) were inserted into the right jugular vein and advanced through the superior vena cava and right atrium into the RV. Hemodynamic parameters were recorded and analyzed using the LabScribe3 software (iWorx, Dover, NH, USA). After data acquisition, animals were euthanized by exsanguination. The heart was excised and the ventricles were dissected from the atria, the aorta and the pulmonary trunk. The right ventricle (RV) and left ventricle (LV) and septum were separated and RV hypertrophy was assessed by evaluating the ratio of RV weight to LV plus septum weight (RV/LV+S).

2.4.1 ISOLATION AND CHARACTERIZATION OF EPCS

Early outgrowth EPCs were positive for expression of surface antigens CD14 (66.7%), CD31 (93.3%), CD45 (82.7%), with moderate CD105 (14.2%) expression, and lacked expression of VEGFR2 (< 1%), CD34 (< 1%) by flow cytometry (Table 2-1). Further confirmation of endothelial phenotype as provided by presence of acetylated LDL uptake, lectin binding, and immunofluorescence staining for intracellular vWF, VEGFR2 and CD31 (Figure 2-1).

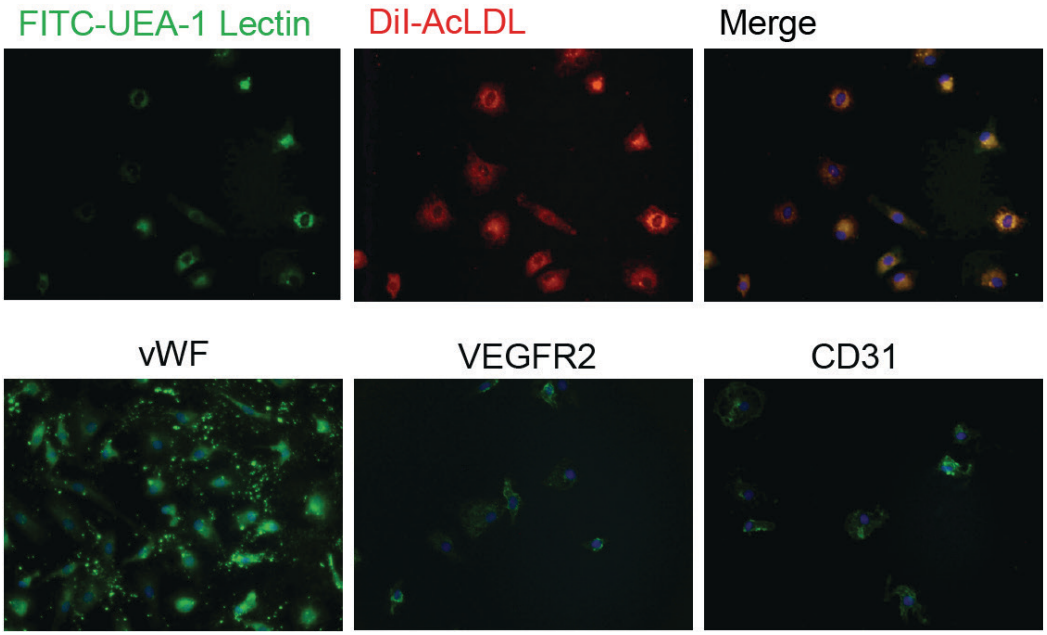

Figure 2-1. Phenotyping of EPCs by fluorescence imaging.
Top: EPCs took up DiI-acetylated-LDL (red) and bound FITC-UEA-1 lectin (green). Bottom: Immunofluorescence demonstrates expression of vWF, VEGFR2 and CD31.

Previous reports have suggested that early outgrowth EPCs have features common to myeloid cells[270] and that they have immunomodulatory properties[159,270] that differ from classical macrophages and dendritic cells. Therefore, in addition to classical EC markers, we demonstrated that our EPCs expressed some antigen presenting cell markers (CD86) such as dendritic cell

(CD11c) and macrophage (CD68) markers, but lacked the T-cell co-stimulatory molecule CD80 (Table 1-1).

Table 2-1. Immunophenotyping of EPCs by flow cytometry

	% positive	Marker specificity
CD11c	6.9 ± 3.3	Dendritic cell
CD14	66.7 ± 0.9	Monocyte
CD31	93.3 ± 4.6	Endothelial
CD34	1.03 ± 0.04	Hematopoetic/vascular
CD45	66.7 ± 4.4	Leukocyte
CD105	14.2 ± 7.1	Endothelial
VEGFR2	1.03 ± 0.39	Endothelial
HLA-DR	83.5 ± 6.5	Antigen presenting cell
CD80	0.164 ± 0.086	Antigen presenting cell
CD83	0.194 ± 0.057	Dendritic cell
CD86	76.9 ± 3.6	Antigen presenting cell
CD68	65.0 ± 8.5	Macrophage

n=8 individual donors, mean ± SEM

2.4.2 EPC-CM ENHANCES ENDOTHELIAL CELL TUBULE FORMATION

In order to test the angiogenic potential of EPC-CM on endothelial cells *in vitro*, we used a Matrigel-based assay to simulate capillary network formation. HUVECs were incubated with EPC-CM versus control medium, VEGF (50 ng/ml) and HUVEC-CM for 24h on growth. Incubation with EPC-CM resulted in an increase in cord formation which was stable for at least 24 hours. We observed a ~50% increase in node formation ($p<0.001$), total number of cords ($p<0.01$) and cord length ($p<0.01$) when compared to control (Figure 2-2). Interestingly, this effect was greater than that of the positive control, VEGF (50 ng/ml) which resulted in modest, significant increases in nodes, number of cords and cord length ($p<0.05$). On the other hand, control conditioned media (HUVEC-CM) did not stimulate network formation.

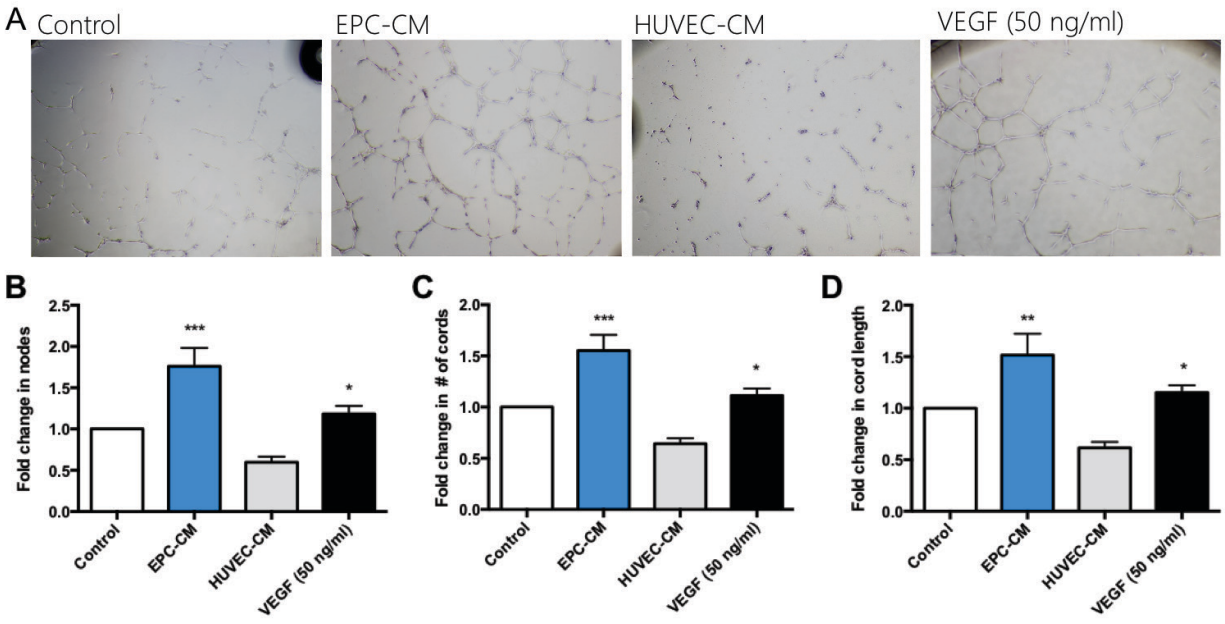

Figure 2-2. EPC-CM improves *in vitro* Matrigel analysis cord formation.
HUVECs treated were treated with EPC-CM, VEGF or HUVEC-CM. (A) Representative images of Matrigel assay under various conditions. Quantification of nodes (B), number of cords (C) and cord length (D). *, **, ***$p < 0.05$, 0.01, 0.001 vs EBM-2+0.5% (Control) using One-way ANOVA with Dunnett's post-hoc test, n=3.

2.4.3 EPC-CM ENHANCES MIGRATION OF ENDOTHELIAL CELLS

EC migration is a crucial step in the initiation of neovascularization and angiogenesis. In order to test EC migration, a scratch wound assay was used to test the capacity to close an artificial wound created by a gap in the confluent EC monolayer. Scratch wound healing, as determined by % of wound area, was significantly improved by EPC-CM compared to control medium (12±4.3% vs 51±4%, $p < 0.05$) (Figure 2-3). The extent of this effect was similar to stimulation with 50 ng/ml VEGF (15±8%). EGM-2 (endothelial growth medium) is a commercially available fully supplemented growth medium that contains 2% serum and growth factors used in cell culture and expansion, as described in the Methods, and therefore was used an additional control in which the

growth cycle was not arrested. Scratch wound healing was greatest in the EGM-2 group, which reflects a combination of migration and cell proliferation.

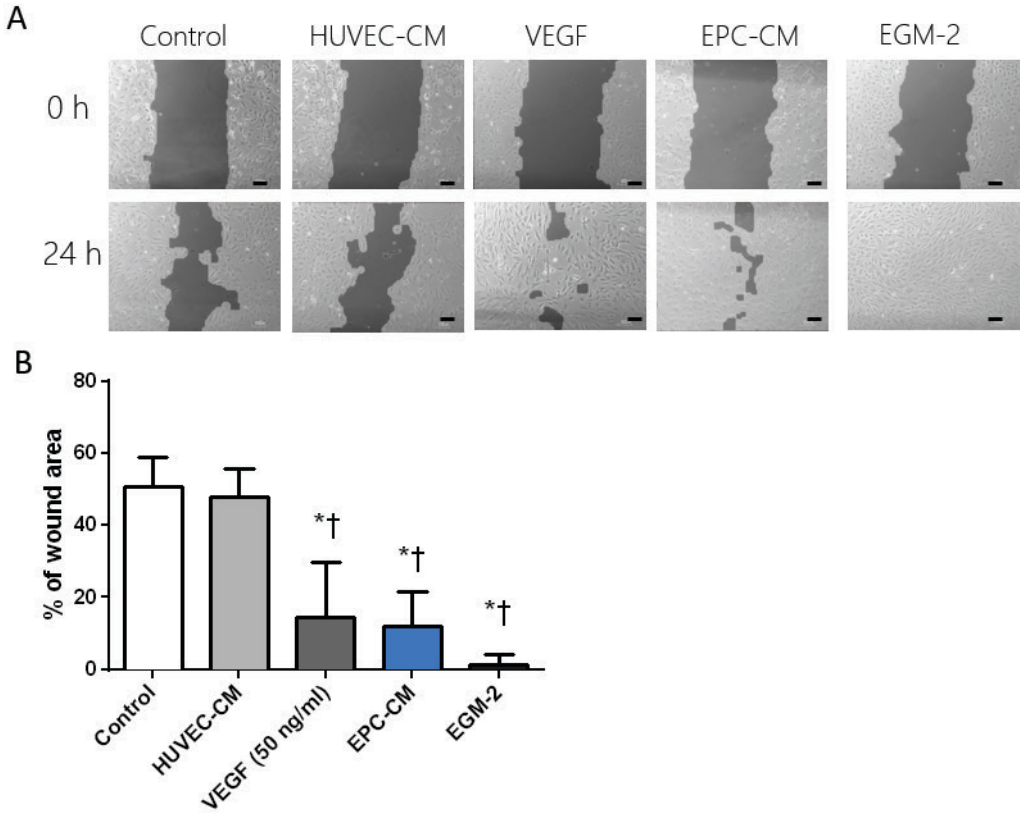

Figure 2-3. EPC-CM improves 24-hour wound healing of HUVECs.
(A) Representative phase contrast microscopy images and (B) quantification of wound healing in HUVECs treated with EPC-CM (n=4/group). Scale bar represents 100 µm. Groups analyzed by ANOVA with Bonferroni's *post-hoc* test. *$p < 0.05$ compared to control medium.

2.4.4 EPC-CM HAS PRO-SURVIVAL EFFECTS BUT DOES NOT INDUCE PROLIFERATION OF ENDOTHELIAL CELLS

HUVECs were exposed to serum starvation for 48 h (control medium containing serum-free EBM) and subsequently stained with the viability dye calcein-AM to determine survival. The re-introduction of 2% FBS to control medium (no growth factors) was used as a positive control for

survival, as indicated by increased calcein-AM vs serum-starved HUVECs (control medium, serum-free). EPC-CM improved calcein-AM staining vs control medium (0.74 ± 0.06 vs 0.22 ± 0.05 relative fluorescence units, $p < 0.05$) (Figure 2-4A).

We also hypothesized that EPC-CM would promote vascular repair by promoting endothelial cell proliferation. BrdU incorporation was measured in HUVECs incubated in control medium (EBM-2+0.5% FBS) with or without the addition of HUVEC-CM, EPC-CM, or VEGF. The positive control, fully supplemented endothelial growth medium 2 (EGM-2) significantly increased BrdU incorporation ($p < 0.05$) (Figure 2-4B). However, neither HUVEC-CM, EPC-CM, nor VEGF significantly affected BrdU incorporation (Figure 2-4B).

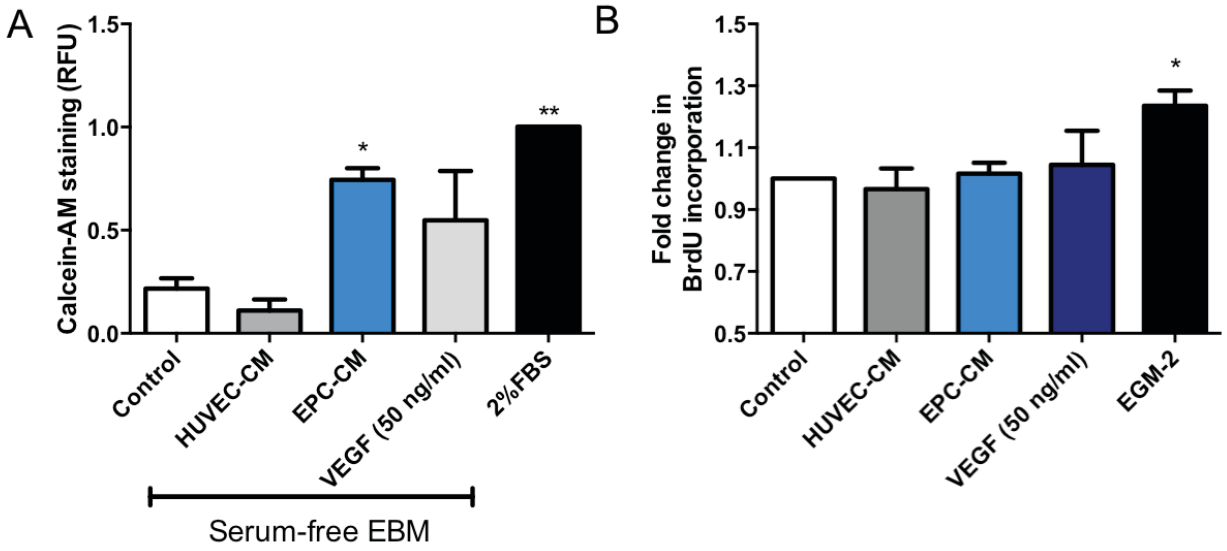

Figure 2-4. Effect of EPC-CM on survival and proliferation.
EPC-CM enhanced EC survival assessed by (A) calcein-AM viability staining. However, EPC-CM did not enhance cell proliferation determined by (B) BrdU incorporation. * , **** $p< 0.05$, 0.0001 vs control medium. ANOVA with Dunnett's post-hoc analysis, n=3/group.

2.4.5 CHARACTERIZATION OF EXTRACELLULAR VESICLES OBTAINED BY DIFFERENTIAL ULTRACENTRIFUGATION

We validated a methodology for isolation of extracellular vesicles by ultracentrifugation from human bone marrow-derived MSC conditioned media. The population of vesicles obtained from 10,000 x g centrifugation was termed "microvesicle" and those obtained at 110,000 x g were termed "exosomes". Indeed, size distribution analysis by nanoparticle tracking (Nanosight) confirmed a peak diameter of 110 nm of the exosome fraction, in agreement with previous reports[281] (Figure 2-5). Both exosomes and microvesicles were enriched in exosome-specific markers such as CD81 and deficient in non-plasma membrane associated markers such as calnexin (Figure 2-5B). Flow cytometry confirmed expression of exosome-associated markers CD9 (83%) and CD63 (94%) on exosomes (Figure 2-5C). Western blotting for CD63 showed enrichment in the exosome fraction vs whole cell lysate (Appendix Figure 2-2)

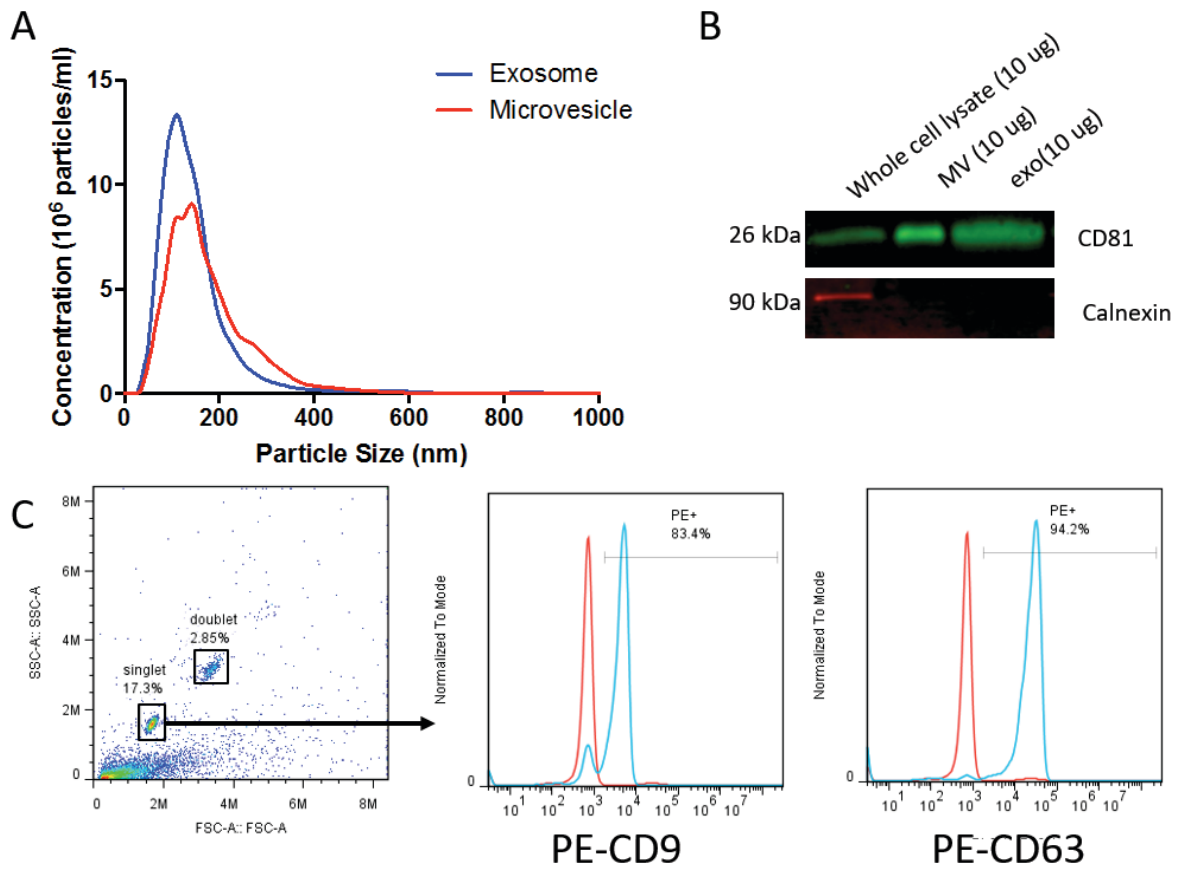

Figure 2-5. Characterization of extracellular vesicles derived from MSCs.
Nanoparticle tracking analysis (A), Western blot of CD81, CD63 and calnexin in exosome fractions, MV and whole cell lysates (B), and (C) flow cytometric data showing expression of CD9 and CD63 on exosomes.

2.4.6 EPC EXTRACELLULAR VESICLES CONTRIBUTE MINIMALLY TO WOUND HEALING

Using the same technique as above, EVs were obtained from early EPC conditioned media and analyzed using nanoparticle tracking analysis. The mode diameter of EPC exosomes was 134 nm, while microvesicles were typically >160 nm (Figure 2-6A-C). The distribution of microvesicles (typically ~200 nm) from EPCs was larger overall than those purified from MSCs, which may be attributable to contaminants such as apoptotic bodies, as early EPCs exhibit higher rates of

apoptosis than MSCs when serum-starved. In our studies, the representative exosome yield was approximately 0.5-1 μg exosomes per 1 million cells; and therefore a dose of 5 ug/ml was approximately equal to a conditioned media potency of 10 to 20 million cells/ml. Both microvesicles (5 μg/ml) and exosomes (5 μg/ml) had minimal effects on wound healing (Figure 2-6D). However, EV-depleted media improved wound healing to a greater extent than either microvesicles or exosomes alone. The effect was greatest when exosomes and microvesicles were added back, suggesting an additive effect when EVs and other components of conditioned media. This suggests that non-EV components such as growth factors and cytokines play a key in EPC-mediated paracrine function. Indeed, EPCs secreted pro-angiogenic cytokines such as VEGF, IL-8, EGF when compared to HUVECs (Appendix Figure 2-1). As well, EPCs secreted high amounts of anti-inflammatory cytokine IL-10, and low amounts of IL-1, IL-6, and TNFα when compared to undifferentiated CD14+ monocytes. Therefore, unfractionated conditioned media was used for subsequent *in vivo* testing of the paracrine effect of EPCs in the treatment of PH.

A

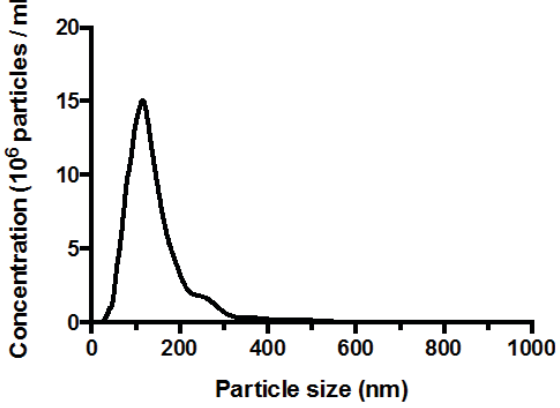

B

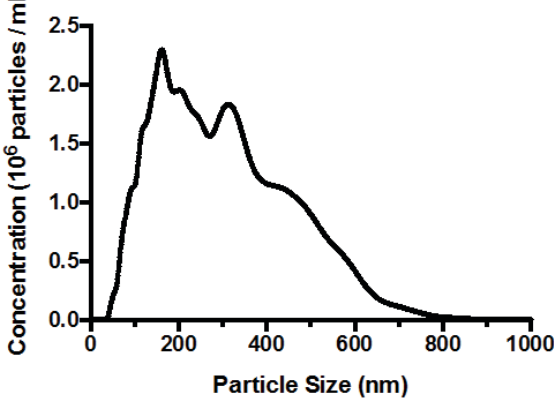

C

Size (nm)	Exosome	Microvesicle
Mode	134	161
Mean	172	306
Standard Deviation	83	148

D

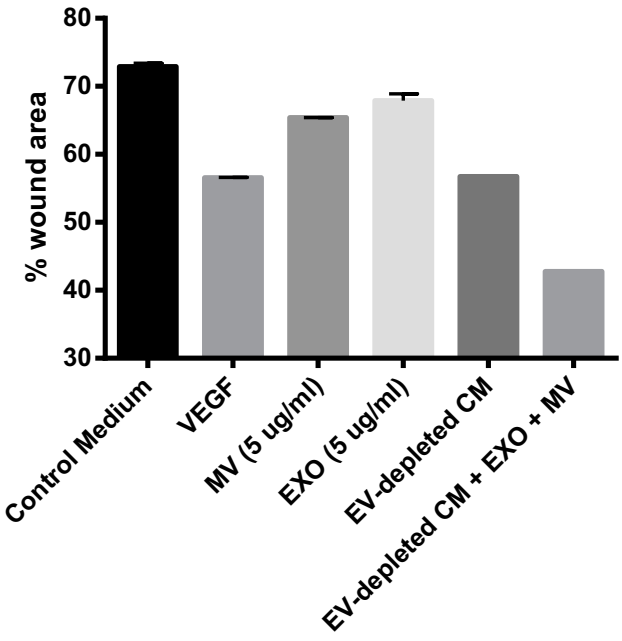

Figure 2-6. EPC-derived exosomes exhibit limited paracrine activity.
Size distribution of (A) EPC-derived exosomes and (B) microvesicle fractions. (C) Descriptive statistics of EPC-derived extracellular vesicle size. (D) Contribution of EPC-secreted extracellular vesicles to wound healing (n=2).

2.4.7 IN VIVO INJECTION OF EPC RESULTED IN MODEST IMPROVEMENTS IN HEMODYNAMICS, BUT NOT RV REMODELLING

Previous reports have demonstrated reduction in pulmonary pressures and RV remodeling after EPC therapy despite minimal cell persistence[159,160]. Therefore, we conducted a pilot study to determine the efficacy of human EPC therapy in the prevention of MCT-induced PH prior to testing paracrine effects using an experimental approach described previously[159]. At 21 days after receiving EPC therapy, mean RVSP was significantly reduced from 78.1 ± 2.1 to 67.7 ± 3.0 mmHg ($p < 0.05$) (Figure 2-7). Pulmonary acceleration time (PAT) was also significantly reduced, however, there were no significant changes in other measures of RV structure and function such

as RV/LV+S ratio, RV/LV diameter ratio, pulmonary ejection time (PET), or tricuspid annular plane systolic excursion (TAPSE).

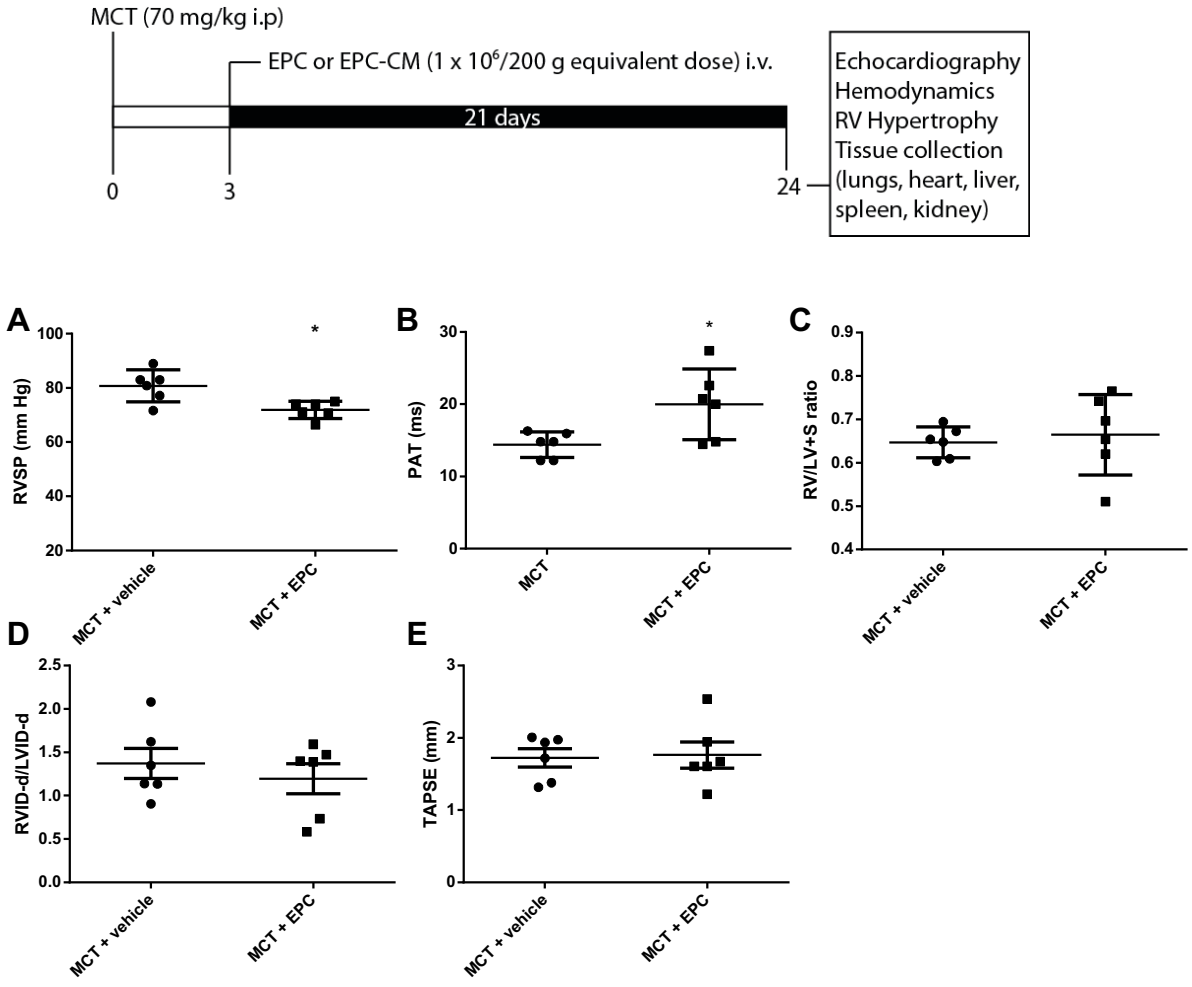

Figure 2-7. EPC therapy reduces pulmonary hemodynamics, but not RV remodeling. Schematic diagram of MCT prevention model (top). Right ventricular systolic pressure (RVSP) (A), RV remodeling (C), RV end diastolic internal diameter/LV end diastolic internal diameter (RVID-d/LVID-d) (D), and tricuspid annuls systolic planar excursion (TAPSE). in nude rats 24 days after MCT injection. Groups were analyzed Student's t-test. *$p < 0.05$, n=6 in each group

2.4.8 PH WAS NOT IMPROVED BY ESCALATING DOSES OF EPC-CM

In separate sets of experiments aimed at directly comparing the relative efficacy of EPCs and EPC-CM, neither EPC-CM nor EPC therapy significantly improved RVSP, PAT, and RV remodeling parameters (Figure 2-8). There was a slight increase in TAPSE in the EPC-CM (2.25 ± 0.18 mm) group when compared to MCT+vehicle (1.52 ± 0.09 mm) which reached statistical significance (p=0.0185), but this was not observed in the EPC group (1.57 ± 0.07 mm). Additionally, there was no added benefit of a 10-fold increased dose of EPC-CM ($5x10^7$ cells/kg equivalent). In fact, high doses of EPC-CM resulted in a trend towards increased RVSP and RV remodeling (Figure 2-9).

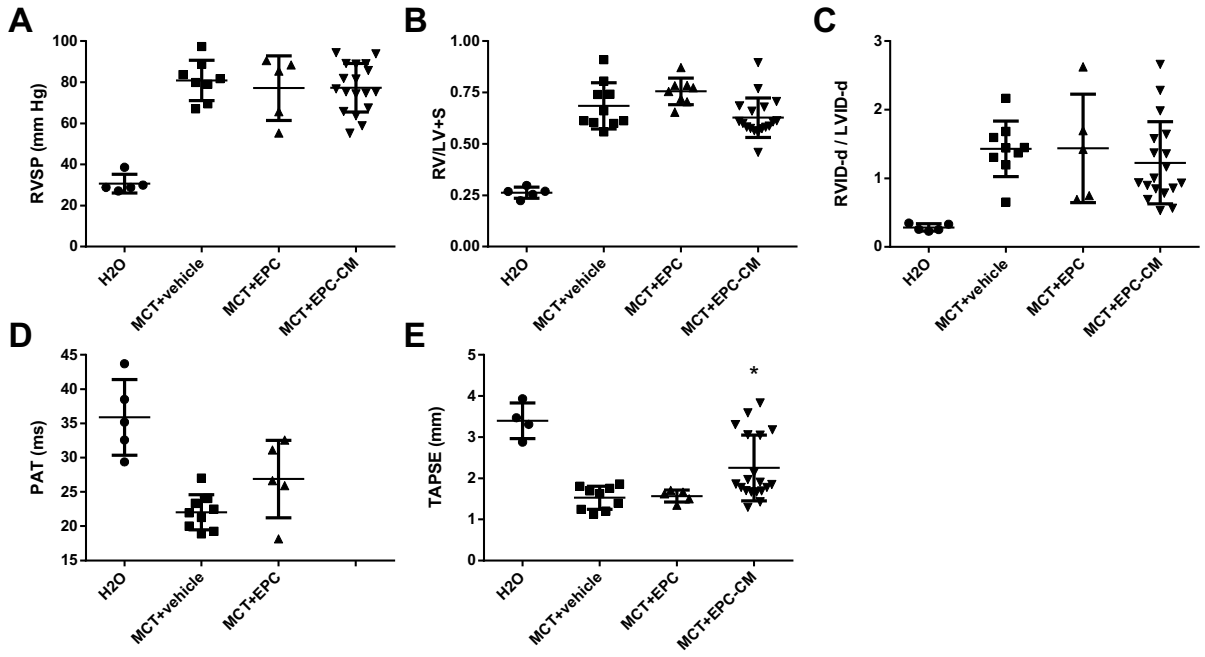

Figure 2-8. EPC and EPC-CM did not prevent pulmonary hypertension.
Right ventricular systolic pressure (RVSP) (A), RV remodeling (B) and echocardiography parameters (C-E) in nude rats 24 days after MCT injection (21 days after cell or conditioned media delivery). Groups analyzed by ANOVA, followed by Dunnett's *post-hoc* analysis. *p < 0.05 vs MCT + vehicle

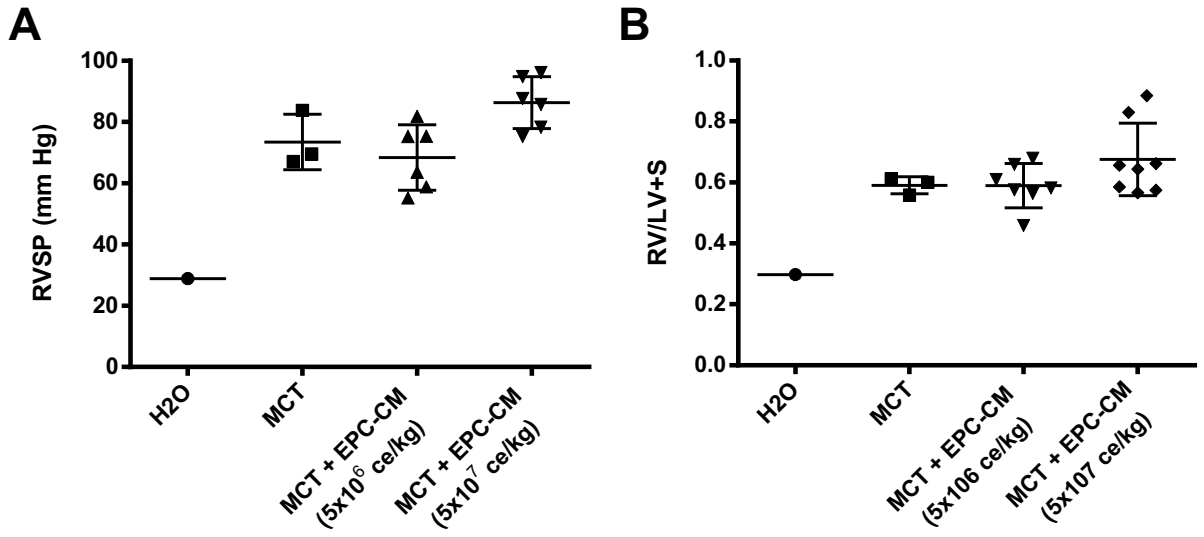

Figure 2-9. RVSP and RV remodeling in a trial of escalating doses of EPC-CM.
Neither standard dose ($5x10^6$ ce/kg) nor high dose ($5x10^6$ ce/kg) of EPC-CM improved RVSP or RV hypertrophy. ce = cell equivalent dose of conditioned medium.

2.5 DISCUSSION

The present study attempts to test the hypothesis that the therapeutic effects of stem/progenitor cell therapy are meditated by paracrine activity rather than the direct participation of tissue repair by long-term engraftment and transdifferentiation. This theory is supported by observations of *in vivo* therapeutic efficacy in models such as bronchopulmonary dysplasia associated pulmonary hypertension and myocardial infarction, where there is typically poor long-term engraftment of stem cells and recapitulation of these effects using their secreted factors, i.e. stem cell conditioned media[282-284]. We provide *in vitro* data that confirmed the importance the paracrine activity in the context of EPC ability to induce angiogenesis and endothelial repair. Overall, we demonstrated that EPC-conditioned media stimulated *in vitro* EC cord formation, EC migration and survival,

which are important pro-angiogenic activities. Interestingly, the effects of EPC-CM on Matrigel cord-formation, wound healing and survival were not observed with HUVEC-CM, suggesting that these paracrine-mediated effects are specific to the progenitor cell type, and may also highlight the regenerative potential of endothelial progenitors in contrast to mature ECs. Similar findings have also been reported by others, such as Dimmeler's group, which demonstrated that EPC-CM stimulated migration of mature ECs whereas HUVEC-CM did not, which was partially mediated by traditional soluble factors/cytokines VEGF and SDF-1[157]. Similarly, Xia *et al.* also demonstrated that early outgrowth EPC conditioned media inhibited shear stress induced EC apoptosis and promotes EC proliferation via VEGF signaling[273].

In our study, EPC-CM did not increase BrdU incorporation, suggesting that EPC-CM does not have a pro-proliferative effect. In fact, stimulating proliferation could potentially exacerbate disease in a state where pulmonary endothelial cells and smooth muscle cells already exhibit a cancer-like hyperproliferative phenotype. As well, these experiments involved maintaining cells under low serum conditions which diminishes proliferative capacity in and of itself. Rather, the rationale for this was to replicate the conditions in scratch wound assay to exclude the cell proliferation as a confounder to migration.

While the present study was conducted using HUVECs as the model for mature ECs, a more appropriate choice for translation to PAH would have been human or rat pulmonary microvascular endothelial cells. Cells from the pulmonary microvascular bed may respond differently to certain stimuli including the factors contained in EPC-CM. As well, there is evidence to suggest that endothelial cells from patients with PAH (BMPR2 mutations) are dysfunctional compared to healthy controls [285]. Taken together, these factors may have contributed to the lack of translation to efficacy in subsequent *in vivo* studies.

A few studies have reported extracellular vesicles are released from $CD34^+$ mononuclear cells, and endothelial colony forming cells (i.e. late outgrowth EPCs)[286-288]. Deregibus *et al.* demonstrated that late outgrowth EPC-derived microvesicles could activate an angiogenic pathway involving PI3K/Akt/eNOS signaling in ECs by horizontal transfer of mRNA[289]. In the present study, we isolated exosome- and microvesicle-enriched fractions of EPC-CM. Our data suggest that exosomes and microvesicles stimulated migration, but only modestly in comparison to the soluble factors in the CM. In contrast to soluble protein factors that are non-membrane bound, the genetic material such as mRNA, microRNA that is transferred by EVs requires further downstream processing which may require extended periods of observation to capture the full extent of their effects. A recent report by Li et al. demonstrated that exosomes from human cord EPCs stimulated EC wound healing using the "scratch" assay[278]. Compared to our study, a 20-fold higher dose of exosomes (100 μg/ml) was necessary to achieve this effect. Based on our yield, this would equate to 10-20 million cells/ml vs. 200-400 million cells/ml, a dose well above feasible cell therapy doses in the other study. Future studies may require that higher concentrations of extracellular vesicles be used to reach peak biological effect in migration assays. Another explanation may be that cord-derived EPCs and exosomes may have an increased therapeutic potency over adult peripheral blood EPCs, [123]. . As well, other EVs may exert more potent effects in other biological processes such as capillary network formation, cell survival and proliferation, which were not tested in this study.

A significant limitation of using ultracentrifugation-based extracellular vesicle isolation is low yield complicated by low sample recovery and long processing times[290,291]. It would be tremendously challenging to scale to *in vivo* experimental studies especially for rodent dosing. In contrast, Lee *et al.* used the chronic hypoxia mouse model of PAH, where mice are much

approximately 10 times smaller than rats and therefore require much less exosomes[277]. Alternative techniques such as ultrafiltration, size exclusion chromatography, and commercially available exosome precipitation reagents (eg. ExoQuick™, Invitrogen Total Exosome Isolation Reagent) may increase extracellular vesicle yield and reduce sample processing to increase the feasibility of large-scale animal studies or clinical trials[292]. Nevertheless, a key initial step in testing stem cell paracrine hypothesis *in vivo* was to evaluate the effect of unfractionated conditioned medium before further subfractionating EVs and other soluble factors.

In the present study, EPC therapy was unable to produce consistent benefits in the nude rat monocrotaline model PAH. In our initial pilot study, we demonstrated a modest attenuation of RVSP with EPC therapy with virtually no benefit to RV remodeling. Subsequent trials of EPC therapy failed to recapitulate the benefits on pulmonary hemodynamics. We did, however, observe a slight improvement in TAPSE with EPC-CM, which suggests that EPC-CM could have direct effect on cardiac contractility. Further studies involving more detailed cardiac parameter measurements such as pressure-volume loops or cardiac output measurement would clarify the effect on cardiac performance. Nevertheless, these cardiac effects may be trivial as neither EPC nor EPC-CM treatment resulted in a survival benefit (not shown) consistent with a clinically meaningful effect. Furthermore, we observed a statistically non-significant trend towards increased RVSP and RV remodeling at escalating doses of EPC-CM, suggesting potential deleterious effects. At these elevated concentrations, the low levels of pro-inflammatory cytokines such as IL-6, IL-1 and TNF-a in EPC-CM may have reached the threshold to activate inflammation and thus exacerbate disease progression. Further histological studies would be needed to elucidate this effect. Nevertheless, this data demonstrates that there is no additional benefit of increasing EPC-CM doses up to 10-fold.

The lack of reproducible efficacy of EPC therapy in the present study may be attributable to xenotransplantation of human cells into an immune deficient nude rat host. While the nude rat lacks a thymus and therefore cannot generate mature T-cells, other components of the immune system, such as natural killer (NK) cells are intact and even enhanced. This could result in very rapid removal of human cells therefore reducing the therapeutic efficacy of cell therapy. However, this is contrast to the results from Ormiston et al., which showed prevention of MCT-induced PH by xenotransplantation of human early outgrowth EPCs into the nude rat model, with reductions in RVSP and RV/LV+S similar to those seen using syngeneic cells transplanted into wild-type rats[159]. On the other hand, reports by Nagaya et al. observed only modest reductions in RVSP but not RV remodeling with human EPC therapy at 7 days post induction of MCT-induced PH[160], while Mirsky et al. showed no effect on RVSP and RV remodeling with EPC therapy administered between at 14 or 21 days post-MCT[195]. Together, these findings highlight the high degree of variability reported in the literature.

Moreover, Miyata et al. reported greater pulmonary vascular inflammation, medial thickening and RV hypertrophy in athymic nude rats vs euthymic littermates, suggestive of a more severe PH phenotype in these immune deficient models,[293] that may be less amenable to therapeutic interventions. Indeed, in our studies we observed mean RVSP exceeding 80 mmHg and RV/LV+S in excess of 60%, which is in contrast to mean RVSPs of 60-65 mmHg and RV/LV+S < 50% in earlier studies by Ormiston et al.[159], Nagaya et al.[160], and Mirsky et al.[195]. The phenotype observed in our model is in keeping with a more severe or advanced form of pulmonary hypertension, which may be inherently more resistant to therapy. The variability in phenotype could be due to differences in the metabolism of MCT or varying degrees of tissue response such as vascular injury/remodeling and inflammation. These findings illustrate the challenges in establishing and

validating the efficacy of a human cell therapy product in preclinical animal models, which may be dependent on factors such as the rapid rate of cell clearance or effects of background on the nature and severity of the animal model of PH. However, xenotransplant models are necessary since there is no equivalent early outgrowth EPC product for rodents. Nevertheless, we were unable to demonstrate the importance of EPC paracrine activity *in vivo*.

In order to overcome the above limitations of xenotransplantation and better test the paracrine hypothesis, future studies could incorporate strategies to enhance the efficacy of cell-based therapy. Gene enhancement, which involves transfection of EPCs using candidate therapeutic genes such as adrenomedullin[160], eNOS[75], prostacyclin synthase[199] and CGRP[198] has been shown to augment the existing therapeutic properties of EPCs, stimulating regeneration of the pulmonary microvasculature and/or alleviating increased pulmonary pressures[81]. In addition to delivering the therapeutic gene of interest, which may have immediate beneficial effects to the pulmonary vascular bed, gene enhancement may also augment EPC survival and long-term retention[75,199]. In fact, in several studies have shown that gene-enhanced EPCs are able to reverse or rescue established PAH[81]. In particular, our group has developed expertise in translating EPC therapy a phase 1 clinical trial in which PAH patients received human eNOS-enhanced EPCs (The Pulmonary Hypertension and Angiogenic Cell Therapy; PPHCeT)[294]. Also, the preclinical animal model does not recapitulate the clinical scenario in which patients are typically on a background therapy consisting of a combination of ET-1 receptor antagonists, PDE5 inhibitors or prostacyclin analogues. It is unclear whether EPC or EPC-CM would yield any additional benefit when measured against the standard of care and is worth investigating for future translational efforts.

Another limitation of the present study was that it focused mainly on the pro-angiogenic activity of EPC-CM, and other processes such as inflammation were not evaluated. Widespread pulmonary

vascular inflammation involving nearly all immune cell types including monocytes, macrophages, lymphocytes, dendritic cells, mast cells has been observed in PAH patients, as well as in the MCT and SU5416/hypoxia animals models of PH[81]. Interestingly, regenerative cell types with even stronger endothelial characteristics and pro-angiogenic function such as late outgrowth EPCs have failed to demonstrate efficacy in a PH model in which early outgrowth EPC therapy was effective[159]. Nonetheless, very similar late EPC type, ECFCs, were able to reduce injury and improve function in a rat model of bronchopulmonary dysplasia [284].

Whether early outgrowth EPCs are indeed true endothelial progenitors has been challenged by Yoder et al. He argues that unlike a true stem or progenitor cell, early outgrowth EPCs do not self-renew, do not exhibit clonal proliferation and do not give rise directly to mature ECs[127,132]. Indeed, the gene expression and proteomic profiles of EPCs share more in common with monocytes than they do with mature ECs[131]. Ormiston *et al.* suggested that EPCs resemble closely regulatory dendritic cells, including the secretion of the anti-inflammatory cytokine IL-10[159]. Medina *et al*. demonstrated that early EPCs expressed markers of M2-macrophages, a subtype of alternatively activated macrophages with anti-inflammatory and trophic effects that aid in resolving acute inflammation and promoting tissue healing[270]. Future studies of the immunomodulatory properties of EPCs may represent an opportunity to better understand the mechanisms and identify strategies to enhance EPC treatment for PH.

Chapter 3: Strain-dependent defect in right ventricular adaptation leads to early heart failure and death in Fischer rats with severe pulmonary arterial hypertension

3.1 INTRODUCTION

Pulmonary hypertension (PH) is a devastating disease characterized by increased pulmonary vascular resistance resulting from complex arterial remodeling and lung microvascular rarefaction.[200] These changes lead to elevated pulmonary pressures and increased right ventricular (RV) afterload resulting in RV hypertrophy which is initially compensatory but ultimately progresses to decompensated RV remodeling, RV dysfunction and right heart failure.[211] However, the degree of hemodynamic abnormality does not necessarily predict the level of RV dysfunction, and it is not uncommon for patients with very similar pulmonary hemodynamic abnormalities to display marked differences in the adequacy, RV compensation and function. Importantly, RV function is predictive of clinical status and prognosis in PH. For example, 5-year survival in patients with pulmonary arterial hypertension (PAH) is highly correlated with RV ejection fraction (RVEF), and less so with pulmonary artery pressures (PAP) or pulmonary arterial resistance (PVR).[202] Therefore, the degree to which the RV can adapt to chronic increases in afterload is believed to be a major determinant of functional capacity and long-term prognosis in patients with PH, independent of the severity of hemodynamic abnormalities.[227]

However, individual patients exhibit remarkable variability in RV adaptation to similar increases in afterload, which is almost certainly influenced by complex genetic determinants. Previously, we have observed important strain-dependent differences in the severe PAH phenotype in rats exposed to a single injection of the VEGFR2 antagonist, SU5416 (SU), combined with a 3-week exposure to chronic hypoxia (SUHx)[295]. In particular, Fischer rats exhibited very high mortality in the SUHx model of severe PAH by 7 weeks, whereas Sprague Dawley (SD) rats showed excellent survival for up to 14 weeks in the same model.[295] As well, Fischer rats showed greater RV dilatation compared to SD rats, despite comparable hemodynamic severity of PAH. Therefore, we

hypothesized that the high mortality in the Fischer rat may be due to maladaptation of the RV to increased afterload in response to severe PAH, unique to this strain, thereby recapitulating the variability in RV remodeling seen in human patients.

In the present study we now show defective RV adaptation in response to severe PAH in Fischer versus SD rat strains, related to a reduced vascularization of the hypertrophied RV, and associated with unique differences in expression of genes involved in angiogenesis, as well metabolic and immunological responses. Therefore, targeting these pathways may provide novel therapeutic opportunities to improve RV adaption and function thereby improving functional status and survival in patients with PH.

3.2 OBJECTIVES AND HYPOTHESES

Objective: To characterize and identify physiological and molecular changes associated with RV adaptation in response to serve pulmonary arterial hypertension using animal models.

Hypothesis: High mortality in the Fischer rat is due to maladaptation of the RV in response to increased afterload SUHx-induced PAH.

3.3 METHODS

3.3.1 ETHICS

All study protocols were approved by the animal ethics and research committee (University of Ottawa, Ontario, Canada) and conducted according to guidelines from the Canadian Council for the Care of on Animal Care (CCAC).

3.3.2 SU5416+CHRONIC HYPOXIA MODEL OF PAH

Male Sprague Dawley (SD, Harlan laboratories, Indianapolis, IND, USA) and Fischer (CDF, Charles River, Montreal, QC, Canada) rats weighing 125-200 g were used for this study. PAH was induced by a single subcutaneous injection of SU5416 (SU:3-(3,5-dimethyl-1H-pyrrol-2-ylmethylene)-1,3-dihydroindol-2-one)) (Tocris, Bristol, United Kingdom) suspended in 0.5% vehicle of CMC (0.5% carboxymethylcellulose sodium, 0.9% sodium chloride, 0.4% Tween 80, 0.9% benzyl alcohol in deionized water) as previously described[29,296]. Immediately after SU injection, rats were exposed to chronic hypoxia (8.5-10% O_2) in hypoxic chamber system using controlled nitrogen gas release (Biospherix, Lacona, NY, USA) for 3 weeks (SU5416-hypoxia; SUHx). Control rats received CMC vehicle and remained at room air (21% O_2) until end study at 4 or 7 weeks.

3.3.3 NON-INVASIVE SERIAL ASSESSMENT BY ECHOCARDIOGRAPHY

In order to account for the exceptionally high mortality between 4-7 weeks in Fischer rats, we used a sample size of n=30 for Fischer-SUHx (F-SUHx) and n=12 Sprague Dawley (S-SUHx) for the 7 week serial measurement cohort, which included some rats from a previous study with results that had not been previously reported[295]. Echocardiography was performed weekly using the Vevo2100 ultrasonography system (VisualSonics, Toronto, ON, Canada). Rats were anesthetized using 2-3% inhaled isoflurane. Survival was determined in a new 7-week cohort where F-SUHx (n=9) and S-SUHx (n=12). Pulsed-wave Doppler mode was used to assess pulmonary artery flow in the parasternal long axis view. Pulmonary artery acceleration time (PAT) was measured as the time elapsed between the onset of systolic flow to peak outflow velocity. Using short-axis M-mode echocardiography, RV chamber size was expressed as the ratio of end-diastolic RV to LV internal diameter (RVID-d/LVID-d) obtained in short-axis M-mode. RV free wall (RVFW) thickness was

measured as the distance between the epicardium and the endocardium of the right ventricular wall. Cardiac output (CO) was calculated using the pulmonary artery velocity time integral PA-VTI method as previously described[63], where pulmonary artery cross section area (PA_{CSA}) = π $(PA_{diameter}/2)^2$, stroke volume (SV) = PA_{CSA} x PA-VTI, and CO = SV x heart rate. Cardiac index was calculated as cardiac output divided by body weight. Tricuspid annulus planar systolic excursion (TAPSE) was assessed in apical 4-chamber view in M-mode.

3.3.4 CARDIAC MAGNETIC RESONANCE IMAGING (MRI)

Cardiac magnetic resonance imaging was performed using the 7T GE/Agilent MRI system at the uOttawa preclinical imaging core. Rats were anesthetized using 2% inhaled isoflurane. Axial, two-chamber, and short-axis localizer scans were first performed, followed by short-axis cine. For the short-axis cine, ECG gating was used with 30 reconstructed cardiac phases and 2 views per segment. The field of view, matrix size, and slice thickness were 7 cm, 256x192, and 1.5 mm, respectively. Using short-axis cine MRI, RV and LV volumes were calculated by summation of the endocardial volume of sequential stacks during diastole or systole using ImageJ. RV ejection fraction was calculated as (end diastolic volume – end systolic volume)/end diastolic volume x 100%.

3.3.5 EXERCISE CAPACITY TESTING

On day 24 post-SU, rats received treadmill training at a speed of 10 m/min (no incline) for 5 minutes. An electrical shock grid is located at the rear of the treadmill belt to deliver stimulate running on the treadmill. On day 31, the endurance test was performed using the following protocol: starting at 10 m/min x 5 minutes, incremented by 5 m/min every 5 minutes to a maximum of speed of 25 m/min (no incline). Fatigue was determined by a blinded assessor when the rat accepted the electrical stimulus 3 times within 10 seconds.

3.3.6 RIGHT HEART CATHETERIZATION AND RV MORPHOMETRY

At end study, rats were anesthetized by an intraperitoneal injection of xylazine (7 mg/kg) and ketamine (35 mg/kg). High-fidelity pressure catheters (Transonic-Scisense Inc., London, ON, Canada) were inserted into the right jugular vein and advanced through the superior vena cava and right atrium into the RV. Hemodynamic parameters were recorded and analyzed using the LabScribe3 software (iWorx, Dover, NH, USA). After data acquisition, animals were euthanized by exsanguination. The heart was excised and the ventricles were dissected from the atria, the aorta and the pulmonary trunk. The right ventricle (RV) and left ventricle (LV) and septum were separated and RV hypertrophy was assessed by evaluating the ratio of RV weight to LV plus septum weight (RV/LV+S).

3.3.7 LUNG AND HEART MORPHOMETRIC AND HISTOLOGICAL MEASUREMENTS

The left lobe of the lung was perfusion fixed with via the trachea with 50:50 OCT/saline solution (Tissue-Tek OCT; Qiagen, Mississauga, ON, Canada) and then removed. The left lobe and whole heart was then sectioned and fixed in 4% paraformaldehyde (PFA) for 48 h, rinsed in PBS and stored in 70% ethanol until the day of paraffin embedding. Tissue blocks were sectioned 5 μm thickness with a microtome (Leica Microsystems, Concord, ON, Canada), placed onto poly-L-lysine-coated slides, dried at 37°C for 16 hours and then dewaxed and dehydrated through graded alcohols. For microscopy and quantitative morphometry of the lung, hematoxylin and eosin (H&E) staining was performed with standard protocols and data was analyzed using the Aperio Imagescope Plus software (Leica, Concord, ON, Canada). Morphology of the heart and cardiomyocytes was assessed using Masson's Trichrome staining using standard protocols. For quantitative assessment of RV cardiomyocyte cross sectional area, the area of each cardiomyocyte was traced from each 3 random cross-sectional fields /animal (20X objective).

3.3.8 IMMUNOHISTOCHEMISTRY

Paraffin heart sections were deparaffinized through graded alcohols. After antigen unmasking specimens were blocked in 2% normal goat serum in PBS-T. Endogenous biotin and avidin were blocked using the Vector Avidin/Biotin blocking kit (Vector Labs, Burlington, ON, Canada). Sections were stained with rabbit polyconal antibody to CD31 (Novus Biologicals, Oakville, ON, Canada) at 1:250 dilution for 1 hour at room temperature, followed by endogenous peroxidase quenching by incubation with 3% H_2O_2 for 15 minutes. Sections were then incubated with biotinylated goat anti-rabbit IgG antibody at 1:66 dilution (Vector Labs, Burlington, ON, Canada), followed by DAB staining using the VECTASTAIN ABC Elite kit (Vector Labs, Burlington, ON, Canada) according to manufacturer's protocol.

3.3.9 FLUORESCENCE MICROANGIOGRAPHY

Following exsanguination, residual blood was flushed using 60 ml of heparanized saline (10 U/ml) via jugular vein. The ascending aorta and pulmonary vein were ligated and an incision was made in the right atrium. A cannula was inserted into the aorta to deliver warm (37^{o}C) flush buffer (10 U/mL heparin, 0.0025 ng/mL sodium nitroprusside) to flush the coronary circulation by retrograde perfusion. Approximately 2 ml of pre-warmed 0.22 μm fluorescent microspheres dissolved in 2% low melting point agarose (Life Technologies, Burlington, ON, Canada) were perfused into the coronary circulation via the aorta. Immediately afterwards, the heart was placed on ice for 5 minutes to cast the fluorescent microspheres, and then fixed in 4% PFA for 48 h. Following a PBS wash, whole hearts were embedded in frozen OCT ((Tissue-Tek OCT; Qiagen, Mississauga, ON, Canada) and sectioned into 50 μm sections using a cryostat (Leica Microsystems, Concord, ON, Canada). Slides were washed in PBS, mounted with Vector Hardset mounting medium (Vector Labs, Burlington, ON, Canada) and coverslipped. The FMA sections were visualized using a laser

confocal microscope (Zeiss LSM510), where 40 z-stacks at 20X objective per slide were acquired using a 1 μm step size. To quantify capillary volume, fluorescent pixels were thresholded based on a uniform pixel intensity to represent filled vessels using ImageJ (threshold=50). For each stack, the thresholded pixel area (capillary area) and total image area was multiplied by the slice thickness to obtain the capillary volume and total image volume. Afterwards the capillary volume and image volume were summated for each stack, where Capillary Volume % = [total capillary volume]/[total image volume] x 100.

3.3.10 PCR ARRAY FOR ANGIOGENIC GENES

RV tissue was snap frozen in liquid nitrogen and stored at -80° C until RNA isolation. Tissue homogenization was achieved using the TissueLyser-II system (Qiagen, Toronto, ON, Canada) at 30 Hz for 5 min followed by RNA isolation lysis using miRCURY RNA isolation kit (Exiqon, Woburn, MA, USA) according to manufacturer's protocol.

cDNA was prepared using RT^2 First Strand Kit (Qiagen, Toronto, ON, Canada) as per manufacturer's instructions. The cDNA was stored at -80° C until used for the RT^2 Profiler PCR array for angiogenic genes (Qiagen, Toronto, ON, Canada). Quantitative RT-PCR was performed using SYBR green qPCR mastermix (Qiagen, Toronto, ON, Canada) as per the manufacturer's instructions.

3.3.11 MICROARRAY GENE EXPRESSION AND ANALYSIS

RNA was isolated as described above and total RNA was assayed using Affymetrix Rat Gene 2.0ST and Affymetrix miRNA 4.0 gene chips. Annotations from Affymetrix (RaGene-2_0-st-v1.na35.rn5.transcript) were used to assign gene symbols. Fold change analyses were performed using the R Bioiconductor limma package, according to gene expression changes in PAH vs

control in SD and F subsets with cutoff values of adjusted p-value < 0.05 and fold-change > 3. Heat maps and hierarchical clustering were also constructed in R Bioiconductor. Fold change analyses used the limma package and PCA analysis used prcomp. For gene-gene ontology enrichment analysis, lists were subdivided into fold-changes common to both, unique to SD and unique to Fischer, and gene ontology was performed on each subset using the DAVID Functional Annotation tool (https://david.ncifcrf.gov/) using the PANTHER database for biological processes.

3.3.12 QUANTITATIVE REAL-TIME PCR

RNA was isolated as described above and converted to cDNA using the Taqman High Capacity cDNA Reverse Transcription kit (Applied Biosystems, Burlington, ON, Canada). Quantitative RT-PCR was performed using Taqman probes for rat α-myosin heavy chain (Myh6, Rn00691721_g1), β-myosin heavy chain (Myh7, Rn01488777_g1), atrial natiuretic peptide (Nppa, Rn00664637_g1), brain natiuretic peptide (Nppb, Rn04219558_g1) and α-actinin-1 (Actn1, Rn00667357_m1) (Applied Biosystems, Burlington, ON, Canada).

3.3.13 ATRIAL NATRIURETIC PEPTIDE ELISA

Atrial natriuretic peptide in the RV homogenate and plasma was measured using ANP (NPPA) rat ELISA kit (Abcam, ON, Canada) as per manufacturer's instructions. Briefly, the RV was weighed and homogenized using 0.1% Trioton-X 100 in PBS (pH 7.4) using the TissueLyser (Qiagen, ON, Canada) two cycles of 25hz for 3 min. The homogenate was centrifuged at 12000xg for 20 min at 4° C and the supernatant was collected. Protein concentration of the supernatant was measured by the DC Protein Assay (Bio-rad, ON, Canada) and 150 μg protein was used per test. For plasma, 50 μL of undiluted plasma was used per test. Samples were analyzed in triplicates.

3.3.14 WESTERN BLOTTING

RV lysates were prepared in CelLytic™ MT Cell Lysis Reagent (Sigma, ON, Canada) using the TissueLyser (Qiagen, ON, Canada) two cycles of 25hz for 3 min. The tissue lysate was then centrifuged at 12000xg for 10 min and supernatant was collected. Protein concentration of the protein extract was determined colorimetrically by the DC Protein Assay kit (Bio-rad, ON, Canada), using bovine serum albumin as standard. SDS-polyacrylamide gel electrophoresis of RV protein extract (50 µg) was performed with NuPAGE® Novex® 4-12% Bis-Tris Protein Gels (ThermoFisher Scientific, ON, Canada). Following transfer of the separated proteins to nitrocellulose membranes (NOVEX iBLOT Gel transfer Stacks, ThermoFisher Scientific, ON, Canada), blots were blocked with 2% BSA in PBS-T (PBS containing 0.1% Tween 20, pH 7.4). After blocking, blots were incubated with primary antibodies to Atrial natriuretic peptide (Abcam, ON, Canada), B-type natriuretic peptide (EMD Millipore, ON, Canada) and β-actin (ThermoFisher Scientific, ON, Canada) for overnight at 4° C. Then the blots were washed for three times for 15 min with PBS-T and incubated with appropriate IRDye® anti-rabbit or anti-mouse secondary antibodies (LI-COR Biotechnology, NE, USA) in 2% BSA/PBS-T. Further the blots were washed for three times for 15 min with PBS-T and imaged with Odyssey® imaging system (LI-COR Biotechnology, NE, USA).

3.3.15 STATISTICAL ANALYSIS

Data are represented as mean ± SEM unless otherwise stated. Statistical analysis was performed using Student's t-test or One-Way ANOVA (> 2 groups) followed by Tukey's multiple comparison test with significance level of $p < 0.05$, unless otherwise stated. Survival curves were compared using the Log-rank Mantel-Cox analysis.

3.4 RESULTS

3.4.1 HIGH MORTALITY IN FISCHER RATS IS NOT DUE TO DIFFERENCES IN RV HEMODYNAMIC AFTERLOAD OR LUNG VASCULAR REMODELING

Median survival of Fischer rats was 34 days (n=9) after induction of severe PAH whereas all of SD rats survived to end-study (56 days) post SU ($p < 0.0002$) (Figure 3-1A). Importantly, this striking discrepancy in survival could not be attributed to differences in RV hemodynamic afterload, as right ventricular systolic pressure (RVSP) and RV hypertrophy (right ventricle/left ventricle + septum mass ratio, RV/LV+S) were similar between SD and Fischer in early (4 weeks post SU) and late PAH (7 weeks post SU) (Figure 3-1B-C). Moreover, histopathological examination of pulmonary arterioles showed no significant differences in the proportion of non-, partially-, or fully-obstructed pulmonary vessels between SD and Fischer receiving SUHx at 4 weeks post-SU (Figure 3-1D-F).

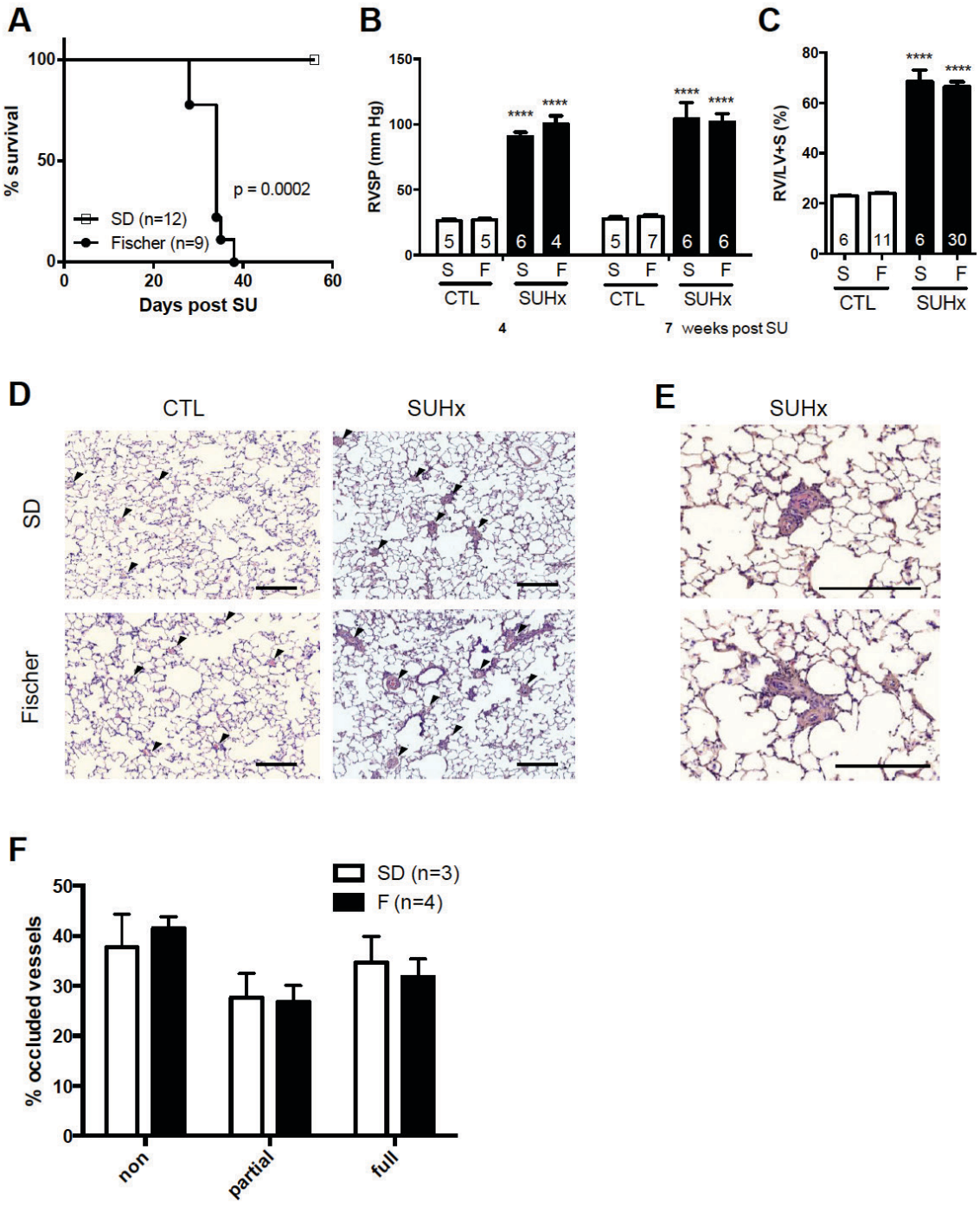

Figure 3-1. Characterization of response to SUHx in SD and Fischer rats

(A) Kaplan Meier Survival analysis of Fischer (F) and SD (S) rats after SUHx (Log rank /Mantel-Cox analysis. Pulmonary hemodynamics, (B) RVSP: right ventricular systolic pressure, and (C) RV/LV+S: RV/left ventricle plus septum weight ratio were similar in both strains after SUHx. Representative hematoxylin and eosin staining of paraffin-embedded lung sections from animals 4-weeks post-SU depicting partially and completely occluded pulmonary vessels in SUHx vs

control lungs at (D) low power and (E) medium power magnification. Black arrows indicate vessels, scale bar = 200 μm. (F) Quantitative analysis of percentage of occluded vessels demonstrates similar extent of pulmonary vascular remodeling between both strains.

3.4.2 FISCHER SUHX MODEL IS CHARACTERIZED POOR RV CONTRACTILITY AND SEVERE DILATATION

Serial echocardiographic analysis of RV function and structure was performed in Fischer (n=30) and SD (n=12) rats at 3, 4 and 7 weeks post SU. The ratio of end-diastolic RV internal diameter/LV internal diameter (RVID/LVID) was similarly increased compared to healthy control rats in both rat strains at 3 weeks post SU, (Figure 3-2A, B). However, Fischer rats showed progressive RV dilatation over time, and RVID/LVID became significantly greater between the Fischer vs. SD rats at 4 weeks (1.06 ± 0.06 vs. 0.74 ± 0.06, $p<0.0001$; Figure 3-2B). As well, right ventricular free wall (RVFW) thickness was reduced at 7 weeks in Fischer rats (Figure 3-2C; $p<0.05$), consistent with myocardial wall thinning due to RV dilation in the Fischer rat. Cardiac output was comparable at baseline in SD and Fischer rats (95±7 and 77±5 mL/min, respectively mL/min, respectively) and similarly reduced at 3 weeks (58±5 and 57±3 mL/min, respectively). Whereas SD rats exhibited a full recovery in cardiac output at 4 and 7 weeks (88±4 and 99±9 mL/min, respectively), Fischer rats showed a persistent reduction in cardiac output at 4 and 7 weeks post SUHx (58±2 and 46±9 ml/min respectively; $p<0.0001$ vs. control, Figure 3-2D) consistent with progressive RV dysfunction.

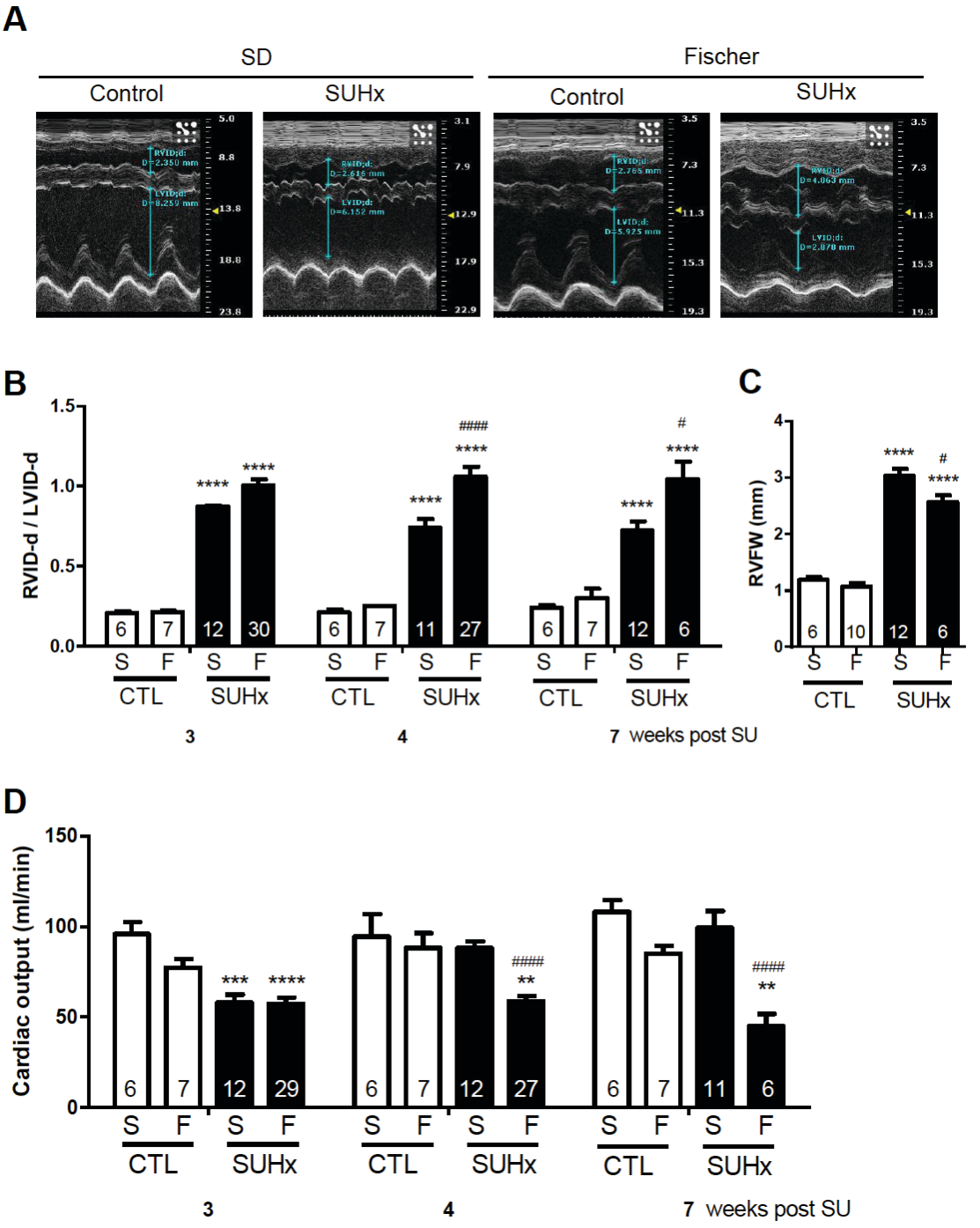

Figure 3-2. Serial assessment of RV function by echo at 3, 4 and 7 weeks post-SU.
(A, B) RVID-d/LVID-d: end diastolic RV/LV internal diameter in M-mode echo; (C) RVFW: RV free wall thickness (M-mode echo); (D) Cardiac output. Data represented as mean +/- SEM. Statistical analysis using One-way ANOVA with Bonferroni's post-hoc test. ** p<0.01, ***, **** p<0.001, 0.0001 vs CTL (matched to strain), #,##,#### p<0.05, 0.01, 0.0001 vs S-SUHx

3.4.3 GREATER RV DILATION AND REDUCED RV EJECTION BY FRACTION CARDIAC MAGNETIC RESONANCE IMAGING (MRI) IN FISCHER RATS WITH SEVERE PAH

Cardiac MRI was used to better define the changes in RV structure and function between the two rat strains in response to severe PAH at 4 weeks post-SU. Again, Fischer rats exhibited evidence of defective RV adaptation (Figure 3-3A,B), with a significantly greater increase in right ventricular/left ventricular end diastolic volume ratio (RVEDV/LVEDV: 2.16±0.24 vs 1.19±0.1, respectively) at 4 weeks of SUHx-induced severe PAH ($p<0.001$; Figure 3-3C). As well, RVEF was significantly decreased in SUHx Fischer rats (39±0.04%, $p<0.0001$ vs. control; Figure 3-3D), whereas no reduction seen in RVEF was seen in the severe PAH model in the SD rats (61.18±0.03%), confirming that RV contractility was better preserved in the SD rat strain ($p < 0.01$; Figure 3-3D).

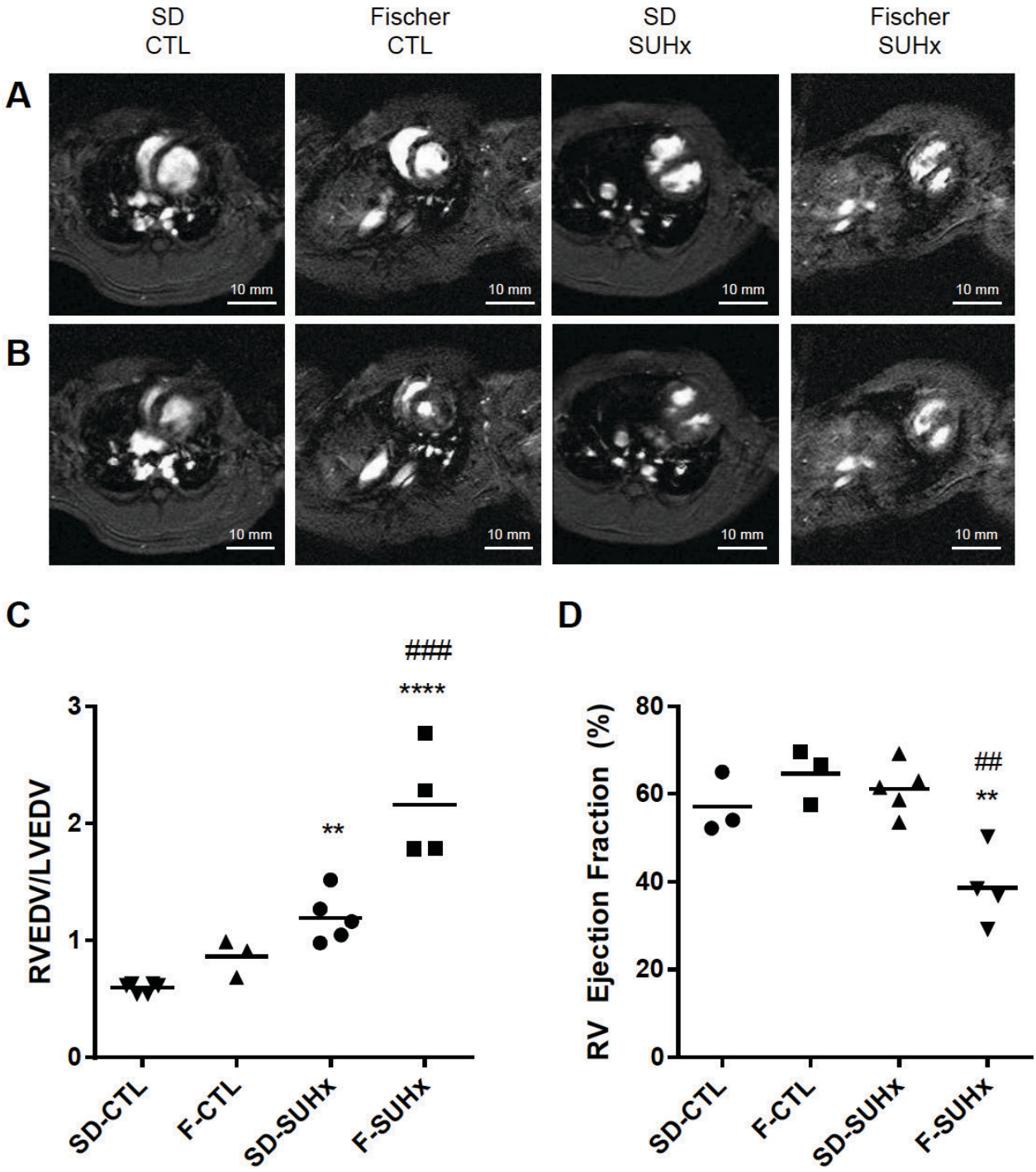

Figure 3-3. Evaluation of RV function by MRI.
Representative short-axis views of RV and LV in (A) end-diastole and (B) end-systole using MRI at 4 weeks post SU5416. (D) End-diastolic RV/LV volumes and (C) RV ejection fraction (%). **, **** $p<0.01$, 0.0001 vs CTL. ## $p<0.01$ vs S-SUHx

3.4.4 EXERCISE CAPACITY IS REDUCED IN THE FISCHER SUHX MODEL

Exercise tolerance was assessed using a standardized treadmill test to better establish the functional importance of abnormalities in cardiac adaptation in PAH at 4.5 weeks (Figure 3-4A). Fischer rats demonstrated significantly reduced exercise capacity vs SD measured by both treadmill distance (59 ± 29 vs 210 ± 52 m, $p < 0.05$) and treadmill time (4.9 ± 2.1 vs 13.8 ± 2.3, $p < 0.05$) (Figure 3-4B).

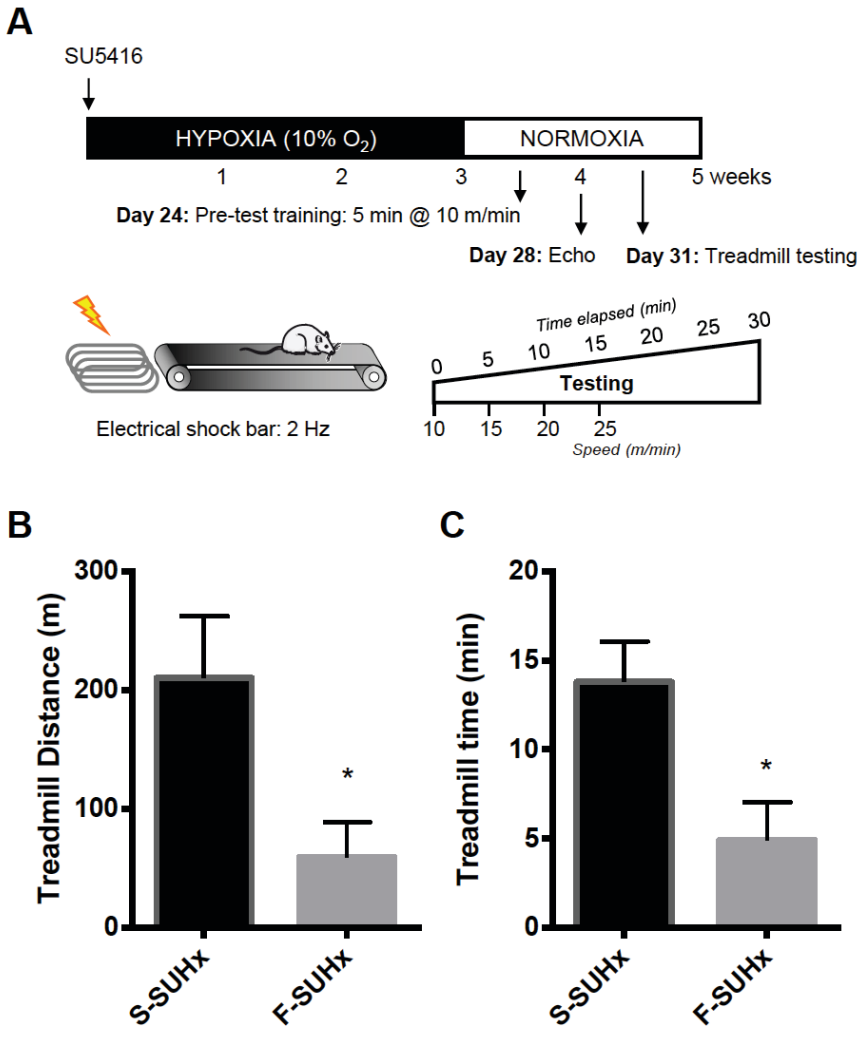

Figure 3-4. Exercise tolerance testing at 4 weeks post SU.
(A) Timeline of treadmill exercise testing and echocardiography. Training is performed 7 days prior to treadmill testing (top). Schematic of treadmill configuration with electric stimulus at the rear of the treadmill belt (bottom left). Treadmill testing protocol (bottom right) begins at a speed

of 5 m/min, after which the speed is increased by 5 m/min every 5 min until a maximum speed of 25 m/min is reached. Exercise capacity in Fischer vs SD SUHx rats as determined by treadmill (C) distance and (D) time. *p<0.05 by Student's t-test.

3.4.5 EVIDENCE OF REDUCED RV VASCULARIZATION DESPITE SIMILAR MYOCYTE HYPERTROPHY FISCHER RATS WITH SEVERE PAH AT 4 WEEKS

At 4 weeks post-SU, Masson's Trichrome staining showed no significant differences in right ventricular myocyte cross sectional between Fischer and SD rats in the SUHx model of severe PAH (Figure 3-5 A, B and E). While immunohistochemical staining for endothelial cell-specific CD31 revealed a reduction in capillary density in RV cross sections in both strains in the SUHx model at 4 weeks vs. strain-matched controls (Figure 3-5C, F), loss of capillary density was significantly greater in Fischer vs SD ($p < 0.05$). Functional RV microcirculation was imaged by fluorescence microangiography, to better demonstrate the 3-dimensional architecture of perfused microvessels (Figure 3-5D).[297] This revealed a rarefaction of the RV capillary network in SUHx treated rats of both strains compared to their respective controls, although once again more marked in the Fischer rats. The size of the capillary bed was quantified by measuring capillary volume expressed as a % of the total volume imaged by optical sectioning, revealing a significant reduction in the severe PAH model, though again this was more marked in between F-SUHx and S-SUHx groups ($12\pm1\%$ vs $17\pm2\%$, $p < 0.01$) (Figure 3-5G).

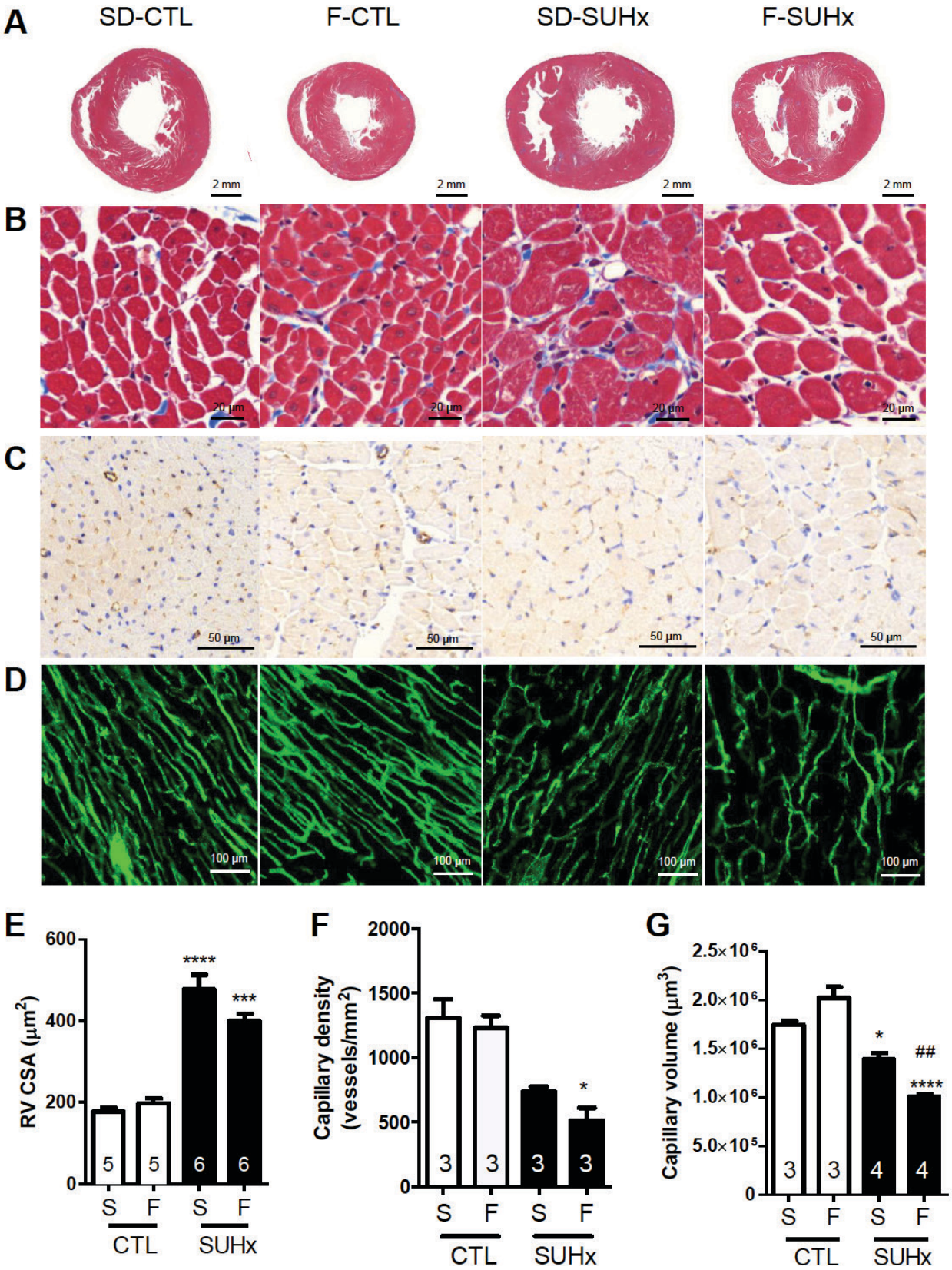
A
SD-CTL
F-CTL
SD-SUHx
F-SUHx
2 mm
B
20 µm
C
50 µm
D
100 µm
E
RV CSA (µm²)
600
400
200
0
****
***
5
5
6
6
S
F
S
F
CTL
SUHx
F
Capillary density (vessels/mm²)
2000
1500
1000
500
0
*
3
3
3
3
S
F
S
F
CTL
SUHx
G
Capillary volume (µm³)
2.5×10⁶
2.0×10⁶
1.5×10⁶
1.0×10⁶
5.0×10⁵
0
*
##
****
3
3
4
4
S
F
S
F
CTL
SUHx

Figure 3-5. Microscopy of heart tissue sections reveals cardiomyocyte hypertrophy and capillary rarefaction in response to SUHx-induced PAH at 4 weeks following SU.
(A) Macroscopic images of Masson's Trichrome stained heart sections shown to same scale. (B) Microscopic images of RV cross-sections (5 μm) illustrating cardiomyocyte fibre thickness and (E) quantification of cardiomyocyte cross sectional area. (C) Immunohistochemistry staining for CD31 reveals a reduction in capillary density after SUHx in both strains and (F) quantification of capillary density. (D) Single slice confocal microscopy images of RV after fluorescence microangiography. (G) 3D capillaryvolume rendering from FMA stacks was expressed as capillary volume %. One-way ANOVA with Tukey's multiple comparisons test where *,**,***,**** $p<0.05$, 0.01, 0.001, 0.0001 vs CTL; #,## $p<0.05$, 0.01 vs SD-SUHx

3.4.6 SUHX-INDUCED PAH IS ASSOCIATED WITH REACTIVATION OF RV FETAL GENE PROGRAM AND ALTERED EXPRESSION OF ANGIOGENIC GENES

SUHx was associated with reduction of α-MHC expression and up-regulation of β-MHC, ANP and BNP, assessed by quantitative RT-PCR (Appendix Figure 3-1). No significant differences in expression of these four genes were observed between SD and Fischer rats in the SUHx model of severe PAH. A greater relative increase in ANP expression in Fischer SUHx was attributable almost entirely to the low basal expression in the control Fischer rats; however, protein levels of ANP and BNP were similar in Fischer and SD RV both at baseline and in response to SUHx (Appendix Figure 3-2).

A focused PCR array was performed to evaluate alterations in 84 key genes involved in modulating the biological processes of angiogenesis in the RV of Fischer and SD rats. There were significant differences in gene expression at baseline, with higher expression of 11 genes, and lower expression of 5 genes, in Fischer rats as compared to SD rats (Appendix Table 3-1). In response to SUHx, 14 genes were differentially expressed between the two strains relative to their respective baseline controls (Figure 3-6 and Appendix Table 3-2). These included prostaglandin endoperoxidase synthase 1 (Ptgs1) and endothelin 1 (Edn1), which were uniquely increased in the RV of Fischer rats, while tumor necrosis factor (Tnf), chemokine (C-C motif) ligand 2 (Ccl2),

vascular endothelial growth factor C (Vegfc), angiopoeitin 1 (Angpt1) and V-akt murine thymoma viral oncogene homolog 1 (Akt1) were decreased in response to SUHx (Figure 3-6). Overall, a relative down-regulation of angiogenic genes was observed in the RV of Fischer rats as compared to SD rats, consistent with the decreased RV capillary density in Fischer rat RV.

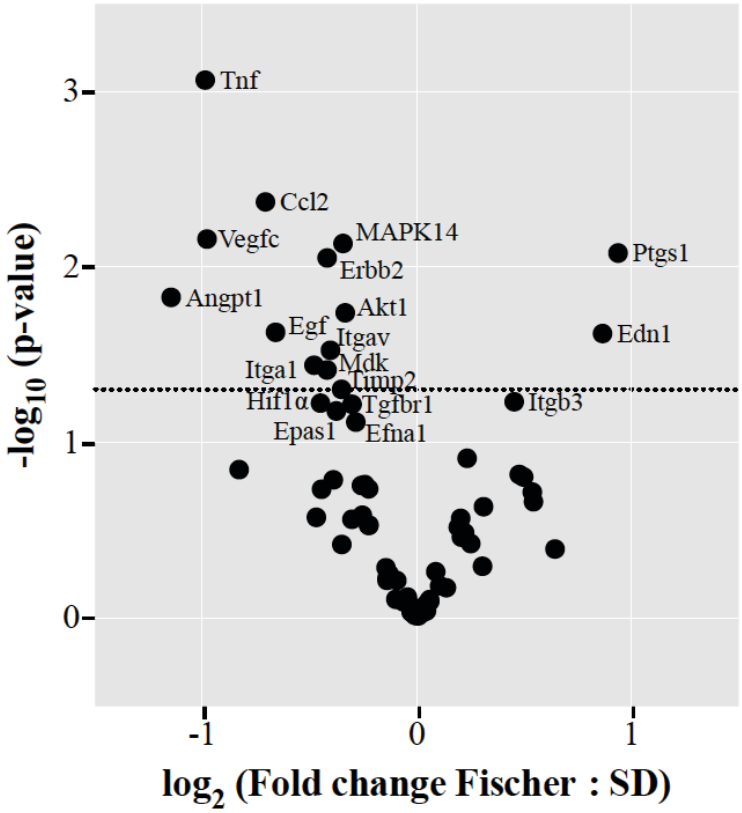

Figure 3-6. Volcano Plot graph of PCR-array of angiogenic genes in right ventricles.
The graph shows Log 2 of the ratio of fold change in each gene's expression in Fischer rats to SD rats. The fold change for each gene's expression in SUHx group was calculated relative to control group. P-values were derived from the t-test. The dashed line indicates $p<0.05$.

3.4.7 GLOBAL EXPRESSION PROFILING REVEALS UNIQUELY REGULATED RV GENES RELATED TO CIRCULATION PROCESSES IN FISCHER RATS

Unbiased, global transcriptional profiling was performed to compare changes in RV gene in the SUHx model of severe PAH in Fischer and SD rats. As expected, principle component analysis

(PCA) revealed substantial differences in RV gene expression between control and PAH rats, which were greater than the differences observed between the two rat strains under the two conditions (Figure 3-7A). However, based on unbiased hierarchical clustering, Fischer and SD rats were seen to exhibit distinct transcriptional profiles (Figure 3-7B). Moreover, a plot showing the relative changes in Fischer and SD rats in transcriptional activity induced by severe PAH at 4 weeks post SUHx showed that ~400 genes were significantly differentially regulated (Figure 3-7C). Of the 20,000 genes studied, 318 were found to be uniquely regulated in Fischer rats whereas only 41 genes were uniquely regulated in SD rats, and 82 genes were similarly regulated in both rat strains (Appendix Tables 3-3). Gene ontology (GO) analysis revealed that unique changes in expression of genes in the Fischer rats were associated mainly with biological processes such as innate immunity, fatty acid metabolism, immunity and defense, and regulation of vasoconstriction and vasodilation (Table 1-1). These included genes that corresponded to GO terms related to vasoconstriction and blood circulation included EDNRB (endothelin receptor type B), PTGIS (prostacyclin synthase), CORIN (Atrial Natriuretic Peptide-Converting Enzyme), EDN1 (endothelin-1), CCR2 (Chemokine (C-C Motif) Receptor 2) and NPPA (Atrial natriuretic peptide, ANP). Down-regulated genes in Fischer rats with severe PAH included those related to natural killer (NK)-cells (KLRC3, KLRK1, KLRB1C, KLRD1, KLRB1A), fatty acid metabolism, as well as PGC1α (Peroxisome Proliferator-Activated Receptor Gamma, Co-activator 1 Alpha; PPARGC1A), a master regulator of mitochondrial activity.

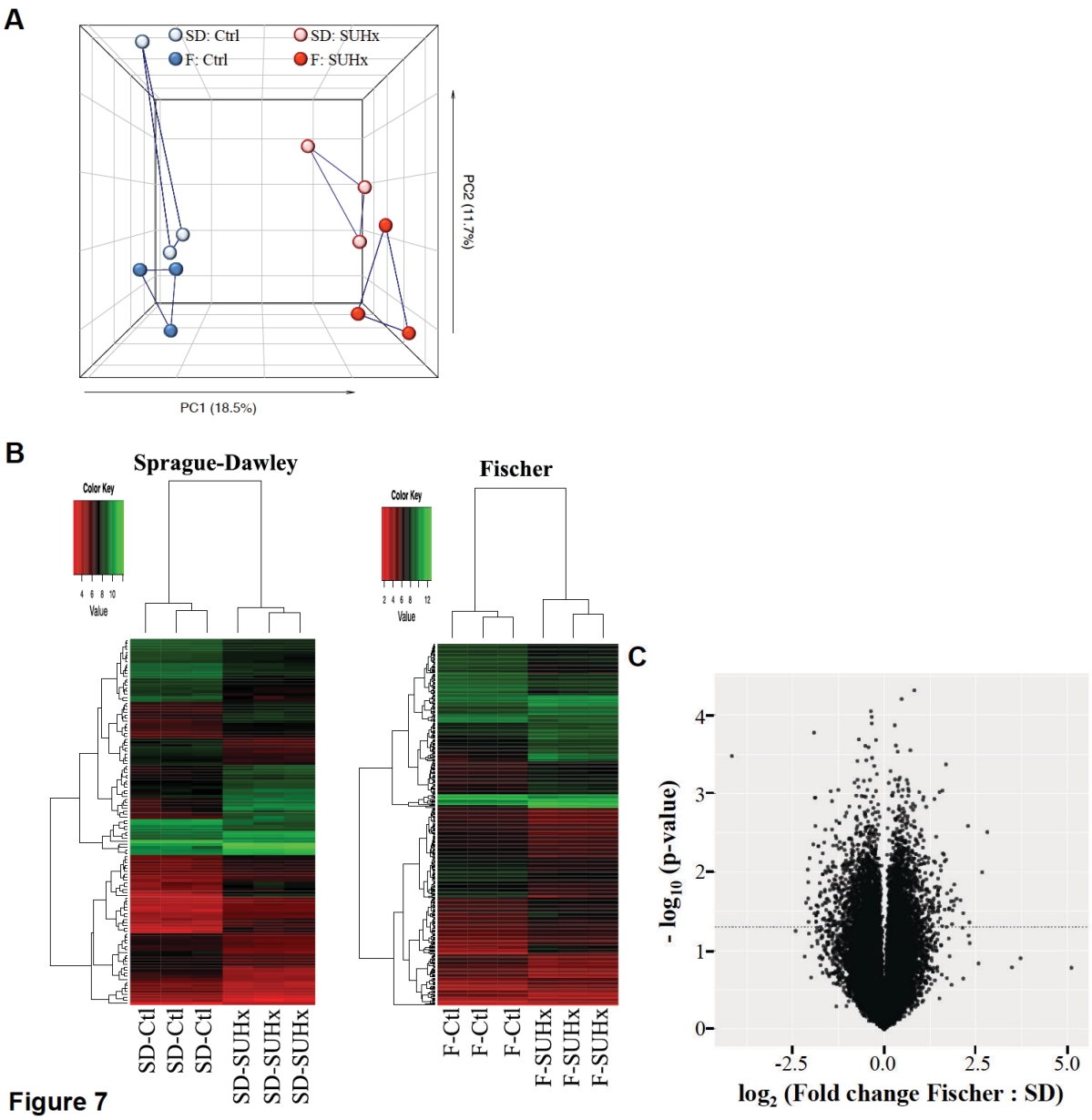

Figure 3-7. Microarray analysis of gene expression in the right ventricle at 4 weeks post SU.

(A) Principal component analysis of RV gene expression changes in Sprague-Dawley and Fischer CDF rats treated with/without SUHx. (B) Heatmap of differentially expressed genes in Sprague-Dawley and Fischer RVs in control and SUHx-induced PAH. Genes with significant fold changes were filtered at a threshold of $p < 0.05$, > 3-fold change. (C) Volcano plot of RV gene expression changes in Sprague-Dawley and Fischer CDF rats treated with SUHx relative to control.

Table 3-1. GO term analysis by biological processes unique to PAH in Fischer

Rank	GO term	P-value	Genes
1	Natural killer cell mediated immunity	0.002086119	KLRC3, FCGR1A, KLRK1, KLRB1C, KLRD1, KLRB1A
2	Fatty acid metabolism	0.002151395	SLC27A1, ACADSB, PTGIS, ACSL1, DECR1, CYP2E1, HPGDS, LIPE, HADHA, CYP4B1
3	Immunity and defense	0.002800724	CTHRC1, IL1R1, CCL2, KLRC3, LITAF, KLRK1, CD1D1, C1QC, HSPA2, CD69, FCGR1A, CD2, GSTZ1, KLRD1, HPGDS, PLAT, C5AR1, LGALS3, SLAMF9, IL1RN, SLAMF8, C1QA, C1QB, CD86, CD55, CCR2, COQ10B, SEMA4D, HSPB3, KLRB1C, GADD45A, F2R, IQUB, KLRB1A
4	Cell communication	0.003307644	RP1, KLRC3, FGF7, CCL2, THRB, GABRB2, EDN1, CD151, FOXS1, SPHKAP, LAMB3, CD2, SEMA3D, KLRD1, PTPRD, IL1RN, PCDH7, ARHGAP26, FOXP2, TNFAIP6, CDH13, MAGIX, CD86, ADAM1A, LAMA5, GRN, CCR2, ADAMTS1, SEMA4D
5	Regulation of vasoconstriction, dilation	0.004281473	EDNRB, PTGIS, EDN1, CCR2, NPPA
6	Blood circulation and gas exchange	0.007987292	EDNRB, PTGIS, CORIN, EDN1, CCR2, NPPA
7	Complement-mediated immunity	0.008314347	C1QA, C1QB, CTHRC1, CD55, C1QC
8	Lipid, fatty acid and steroid metabolism	0.017330542	SLC27A1, CYP2J4, ACADSB, SPTLC2, CORIN, OSBPL6, CYP2E1, DECR1, CYB5B, CDS1, ANXA5, PPARGC1A, HADHA, CYP4B1, ACSL1, PTGIS, INPP5J, SULT1A1, HPGDS, LIPE
9	Other homeostasis activities	0.030329365	CCR2, CLIC1, RGD1566189, PPARGC1A, NPPA
10	Homeostasis	0.033749417	ISCU, EDN1, CCR2, SLC30A3, CLIC1, RGD1566189, PPARGC1A, NPPA
11	B-cell- and antibody-mediated immunity	0.038297877	SLAMF9, CD69, FCGR1A, IL1RN, SLAMF8
12	Cell adhesion	0.040097918	PTPRD, KLRC3, LGALS3, SLAMF9, KLRK1, PCDH7, MCAM, CD151, HMCN2, ITGA9, CDH13, LAMB3, CD2, LOXL1, KLRD1
13	Cell adhesion-mediated signaling	0.041487794	CDH13, PTPRD, LAMB3, KLRC3, LAMA5, CD2, ADAMTS1, PCDH7, CD151, KLRD1, ARHGAP26
14	Cell proliferation and differentiation	0.046212612	FGF7, ERBB4, EDN1, SLAMF8, PCDH7, MEIS1, TGFB1, JUNB, FOXS1, FOXP2, EPHA3, EDNRB, CD86, CCND1, EPHA7, PLK2, NDRG4, RGD1566399, TFDP2, EMP1
15	Extracellular matrix protein-mediated signaling	0.050271633	TNFAIP6, LAMB3, LAMA5, ADAMTS1
16	Muscle contraction	0.050789496	EDNRB, CNN3, PHKG1, TAGLN2, HPGDS, TPM3, CKB
17	Oogenesis	0.059665763	LDLR, ERBB4, PIWIL2, LOC691325

3.5 DISCUSSION

We have previously shown substantial variability among rat strains in the SUHx model of severe PAH[295]. In particular, we have demonstrated a profound difference in survival between Fischer and SD rats, despite similar changes in pulmonary hemodynamics and vascular remodeling at 7-8 weeks. High mortality in the Fischer strain has also reported by others[298]; however, the mechanisms underling the high mortality in the Fischer rat strain in the severe PAH model have not been previously elucidated.

Unlike the SD rats which exhibited only moderate RV enlargement in response to severe PAH, Fischer rats showed more pronounced increases in RV diameter and volumes, as early as 4 weeks after exposure to SUHx and associated with a progressive decline in RV function, as evidenced by reduced cardiac output and RVEF, measured by two independent modalities (ultrasound and MRI). Moreover, these changes in RV adaptation were associated with a markedly diminished exercise capacity in Fischer rats, consistent with a phenotype of RV maladaptation in the Fischer rat.

The SUHx model of severe PAH represents a significant advance by not only by better reproducing the severity of pulmonary hemodynamic changes (i.e. RVSP > 90 mm Hg), but also exhibiting predictable development of the complex, obliterative vascular remodeling reminiscent of plexiform lesions characteristic of the human disease[29,57]. Previous studies using the SD rat have demonstrated excellent long-term survival in this model[57,295], another substantial advantage over the MCT model that has very high mortality in large part due to off-target toxicity to the lung parenchyma, liver[72] and kidney[75]. However, we now show that long-term survival in the SUHx model in the Fischer and SD rat strains is dependent on the degree of RV adaptation to the marked increases in afterload, and the ability of the RV to compensate varies markedly in two commonly used background strains of rat.

Recently, RV decompensation in PAH has been attributed to capillary rarefaction resulting in relative myocardial ischemia within the markedly hypertrophied RV.[207,232,234] Consistent with this, decreased coronary flow reserve has been described in RV of patients with PAH,[233] and decreased capillary density has been reported to be a distinguishing feature between decompensated and compensated RV remodeling in PAH patients.[235] Interestingly, endothelial cells isolated from the RV of patients with right heart failure demonstrated reduced in vitro angiogenic activity,[235] suggesting that differences in the neovascularization of the hypertrophied myocardium may be critical for adequate RV adaptation. In our study, we also demonstrated a marked reduction in RV capillary density in the severe PAH model, which was more marked in Fischer compared with SD rats. This was associated with a decrease in expression of angiogenic genes in the RV of Fischer rats compared to SD rats, again consistent with the emerging concept that microvascular angiogenesis is critical for adaptive RV remodeling in response to marked increases in afterload associated with severe PAH.

It is now well established that RV function is a far better predictor of prognosis in PAH than pulmonary hemodynamics[202,299] and thus elucidating the mechanisms that contribute to adaptive RV remodeling may have important clinical implications. The reproducible and consistent differences in RV adaptation in the SUHx model between Fischer and SD rats are likely due in large part to differences in genetic backgrounds between the SD and Fischer rat strains, reflected in differences in patterns of gene expression in response to progressive increases RV afterload. Microarrray analysis revealed a number of differentially regulated pathways in the Fischer vs. SD rats which may offer further insights in to mechanisms underlying adaptive vs. maladaptive remodeling. These pathways include innate immunity, fatty acid metabolism and vascular homeostasis, many of which have been previously implicated in myocardial remodeling[237,300].

Although myocardial inflammation has been strongly implicated left-sided heart failure[301], less is known about the role of inflammation in RV remodeling. Interestingly, we observed a marked down-regulation of natural killer (NK) cell related genes by global gene profiling in the RV of Fischer during PAH. Natural killer cells are known not only for their role in innate immunity and host defense, but can also contribute to angiogenesis. Decidual NK cells have been long recognized to promote role placental vascularization by modulating complex vascular remodeling of the spiral arteries during pregnancy, in part by secreting angiogenic factors[302]. Moreover, NOD-SCID mice exhibit poor recovery and revascularization following myocardial infarction compared to immune-competent mice, which can be rescued by adoptive transfer of IL-2 stimulated NK cells, in part by stimulating cardiac endothelial cell proliferation[300]. NK cells have also been implicated in the pathobiology of PAH.[159] The therapeutic effect of endothelial progenitor cells the MCT model of PH was shown to be in part dependent of NK cell activity, and impaired NK cell function was found in patients with PAH [303].Therefore, failure of NK cell activation may be another mechanism contributing to the reduced RV vascularity in Fischer rats in the severe PAH model.

The transcriptomic analysis also revealed down-regulation in genes regulating fatty acid metabolism in Fischer rats in response to severe PAH including several enzymes important for the synthesis and metabolism of acyl-CoA such as acyl-CoA dehydrogenase, as well as peroxisome proliferator-activated receptor gamma coactivator 1-alpha (PGC-1α), the master regulator of oxidative metabolism.[243] It is well established that metabolic changes play an important role in the development of both left and right heart failure[240,304,305]. Increased RV glucose uptake and impaired RV fatty acid metabolism have been observed in patients with PAH using ^{18}F-FDG and ^{123}I-BMIPP single photon emission computed tomography[234,239,240]. Since fatty acid oxidation requires 12% more oxygen to generate the same amount of ATP as glucose oxidation, this shift in

metabolism may aggravate the state of relative RV ischemia caused by impaired angiogenesis in maladaptive remodeling[207]. Indeed, fatty acid oxidation inhibitors such as trimetazidine and ranolazine shift metabolism towards glucose oxidation, improving RV function[306]. In fact, therapies targeting cardiac metabolism are in now development for the treatment of PAH. Dichloroacetate, an inhibitor of pyruvate dehydrogenase kinase 4 (PDK4), has shown promise in preclinical studies by reversing changes in RV metabolism caused by upregulation of PDK4 in PAH, resulting in an increase in glucose oxidation[241,307]. Dichloroacetate is now being investigated in a Phase I clinical trial. [306]

Interestingly, both PGC-1α and genes encoding the acyl-CoA dehydrogenases have been previously shown to be reduced in the RV of SD rats exhibiting RV dysfunction in a similar model of severe PAH[308]. However, in this report SD rats were kept in hypoxic conditions for 4 weeks, rather than 3 weeks, and gene expression was studied at 6, rather than 4 weeks, which likely explains the presence of RV decompensation. Of note, no reduction in metabolic gene expression or RV decompensation was seen after pulmonary artery banding in this report, despite similar increases in RVSP.[308] This suggests that increased RV afterload alone is not sufficient, and additional inflammatory, and other signals associated with PH biology, are required for RV dysfunction to be manifested.

In conclusion, we have demonstrated that Fischer rats develop maladaptive RV remodeling in the SUHx model of severe PAH which leads to early mortality. This was associated with impairment in the RV angiogenesis and differential expression in a number of gene families associated with vascular homeostasis, inflammation and cardiac metabolism. Our findings suggest that Fischer rats may be uniquely suited for the study of RV decompensation in response to severe PAH, and

provide an ideal model for the further exploration of molecular mechanisms underlying maladaptive remodeling, as well as for the study of novel RV-targeted therapies.

Chapter 4: Role of cardiotrophin-1 in right ventricular adaptation in severe pulmonary arterial hypertension in Fischer rats

4.1 INTRODUCTION

The ability of the RV to adapt is a major determinant of survival in PAH, yet there are few effective pharmacological therapies for the treatment of RV failure[202]. Even with the introduction of new PAH-specific pharmacotherapy, most patients experience only modest improvement pulmonary arterial pressures (PAP) and therefore little change in RV afterload[202]. Moreover, while parenteral prostanoids, which still represent the gold standard for PAH therapy, often result in substantial improvements in pulmonary vascular resistance, this can be attributed mainly to increased cardiac output, with only modest decreases in mPAP[202]. Interestingly, it has been suggested that some of the benefits agents of existing pharmacological agents such as PDE5 inhibitors and ET receptor antagonists may relate to improved RV compensation independent of any effects on the pulmonary circulation, further supporting the importance of the RV in determining patient outcomes[204,205]. The mainstay treatments of LV failure such as beta-blockers, ACE inhibitors and ARBs have limited or no clinical efficacy in treatment of RV failure associated with PH[206,207]. Therefore, there is an urgent need for the development of effective RV-specific therapies.

Previously (Chapter 3), we showed a strain-dependent failure of RV adaptation in the SUHx model of PAH, characterized by severe decompensation of the RV systolic function, RV dilatation, poor exercise tolerance and high mortality beginning at 4 weeks post SU5416 in Fischer rats. The rapid decline in RV function in Fischer rats contrasts sharply with the response to SUHx in SD rats, which demonstrated excellent long-term survival (100% at 13 weeks) and mild RV dysfunction[295]. Therefore, the severe RV phenotype in the Fischer rat is uniquely suited as a model to address the need for the treatment or PAH patients with severe RVF.

Cardiotrophin-1 (CT-1) is a cytokine member of IL-6 family expressed by cardiomyocytes and other tissues such as liver, lung, kidney and blood[309]. In cardiomoyocytes, CT-1 has hypertrophic

and cardioprotective effects[310-312]. CT-1 exerts its effects by binding to the extracellular leukemia inhibitory factor (LIF) receptor/glycoprotein 130 (gp130) complex, which is well established as a critical pathway in cardiac development and in protecting against myocardial apoptosis and dilated cardiomyopathy[313,314]. As a potent inducer of cardiomyocyte hypertrophy, CT-1 signaling is mediated through the JAK/STAT pathway, resulting in the addition of sarcomeres in series rather than in parallel as well as an increase in myocyte length[312]. CT-1 has also been shown to exert cytoprotective effects by activating survival pathways such as PI3K/Akt-mediated phosphorylation inactivating BAD, and the MAPK/MEK1 pathway[315,316] in response to stimuli such as serum deprivation or ischemia[317]. As well, CT-1 has been shown to upregulate angiogenic genes in cardiomyocytes such as VEGF in order to match vascular supply to the hypertrophied ventricle[318].

In the normal heart, CT-1 is expressed abundantly, but can be further induced by stimuli such as hypoxia, ischemia or mechanical stress in pathophysiological states. CT-1 expression is elevated in the heart in experimental models of cardiovascular disease such as myocardial infarction, spontaneously-hypertensive rats, pressure overload induced heart failure, pacing-induced heart failure and Chagas' disease cardiomyopathy[319-323]. In humans, CT-1 has been studied as cardiovascular disease biomarker. Elevating circulating levels of CT-1 have been observed in unstable angina[324], acute myocardial infarction [325] and heart failure [326] and tend to be negatively correlated with LV systolic function[325,326]. Despite the tendency to attribute CT-1 to pathological cardiac disease states, CT-1 upregulation may suggest a compensatory response, similar to the manner in which the cardioprotective peptide BNP is induced. In fact, chronic CT-1 administration *in vivo* in normal rats results in physiological (reversible) ventricular hypertrophy and increased cardiac output, and provides protection against myocardial ischemia[311,318,327].

The role of CT-1 in pulmonary arterial hypertension is still undetermined. In one study, CT-1 was effective as a pretreatment for chronic hypoxia-induced PAH in rats by reducing pulmonary pressures and RV remodeling through nitric oxide-mediated pulmonary vasodilation[328]. Interestingly, although increased expression of CT-1 is associated with diseases of left ventricular dysfunction[319-323], here, we show for the first time that CT-1 expression is downregulated in the RV in SUHx-induced pulmonary arterial hypertension. We postulate that decreased CT-1 signaling in the myocardium in PAH results in pathological remodeling of the RV. This study is unique in that it tests the effect of CT-1 in severe right heart failure in the Fischer rat SUHx model of PH. Given the potential for cardioprotective and vasodilatory effects, we hypothesize that restoration of CT-1 signaling by exogenous administration of CT-1 would be beneficial in maintaining RV function.

4.2 OBJECTIVES AND HYPOTHESIS

Objective: To test the efficacy of cardiotrophin-1 (CT-1) in severe right heart failure due to PAH.

Hypothesis: We hypothesize that cardiotrophin-1 will be effective in PAH by promoting adaptive remodeling to increased afterload and thereby improving RV structure and function, and as a result, improve survival in Fischer rats in the severe PAH model.

4.3 METHODS

4.3.1 ETHICS

All study protocols were approved by the animal ethics and research committee (University of Ottawa, Ontario, Canada) and conducted according to guidelines from the Canadian Council for the Care of on Animal Care (CCAC).

4.3.2 ANIMAL MODEL OF PAH

Male Fischer rats (Charles River, Montreal, QC, Canada) rats weighing 125-200 g were used for this study. PAH was induced by a single subcutaneous injection of SU5416 (SU:3-(3,5-dimethyl-1H-pyrrol-2-ylmethylene)-1,3-dihydroindol-2-one)) (Tocris, Bristol United Kingdom) suspended in 0.5% vehicle of CMC (0.5% carboxymethylcellulose sodium, 0.9% sodium chloride, 0.4% Tween 80, 0.9% benzyl alcohol in deionized water) as previously described [29,296]. Immediately after SU injection, rats were exposed to chronic hypoxia (8.5-10% O_2) in hypoxic chamber system using controlled nitrogen gas release (Biospherix, Lacona, NY, USA) for 3 weeks.

4.3.3 CARDIOTROPHIN-1 ADMINISTRATION AND TIMING OF LATE "RESCUE" INTERVENTION

CT-1 was administered as a rescue treatment for established PAH at 3 weeks post SU. Osmotic Minipumps (Model 2ML4, Alzet®; Durect) were used to infuse the cardiogenic growth factor Cardiotrophin-1 (CT-1) which was kindly provided by Fate Therapeutics, Inc. (San Diego, California). Phosphate-buffered saline (PBS) was infused for the control rat groups. CT-1 was diluted accordingly in PBS based on the average body weight per group to give a final infusion dose of 6 μg/kg/hr. All prepared Minipumps (PBS and CT-1) were pre-equilibrated in Normal Saline, 0.9% NaCl (Baxter Corporation; Mississauga, Ontario) overnight at 37°C in order to reach the steady state pumping rate of 2.5 μL/hr at the time of subcutaneous implantation. Prior to pump implantation, rats were anesthetized by an intraperitoneal injection of xylazine (7 mg/kg) and ketamine (35 mg/kg) and baseline RVSP was measured (as previously decribed in Methods). The minipump was inserted subcutaneously in the dorsum of the rat for a duration of 4 weeks (7 weeks post-SU).

4.3.4 CT-1 ADMINISTRATION AND TIMING OF EARLY INTERVENTION

CT-1 was administered at an earlier time point to demonstrate its utility as a preventative treatment. Osmotic minipumps were prepared as described above. On day 7 post SU, rats were anesthetized using 2-3% isoflurane and the pump was implanted subcutaneously in the dorsum of the rat. End study occurred at week 5 post-SU.

4.3.5 RIGHT HEART CATHETERIZATION AND RV MORPHOMETRY

At end study, rats were anesthetized by an intraperitoneal injection of xylazine (7 mg/kg) and ketamine (35 mg/kg). High-fidelity pressure catheters (Transonic-Scisense Inc., London, ON, Canada) were inserted into the right jugular vein and advanced through the superior vena cava and right atrium into the RV. Hemodynamic parameters were recorded and analyzed using the LabScribe3 software (iWorx, Dover, NH, USA). After data acquisition, animals were euthanized by exsanguination. The heart was excised and the ventricles were dissected from the atria, the aorta and the pulmonary trunk. The right ventricle (RV) and left ventricle (LV) and septum were separated and RV hypertrophy was assessed by evaluating the ratio of RV weight to LV plus septum weight (RV/LV+S).

4.3.6 LUNG AND HEART MORPHOMETRIC AND HISTOLOGICAL MEASUREMENTS

The left lobe of the lung was perfusion fixed with via the trachea with 50:50 OCT/saline solution (Tissue-Tek OCT; Qiagen, Mississauga, ON, Canada) and then removed. The left lobe and whole heart was then sectioned and fixed in 4% paraformaldehyde (PFA) for 48 h, rinsed in PBS and stored in 70% ethanol until the day of paraffin embedding. Tissue blocks were sectioned 5 μm thickness with a microtome (Leica Microsystems, Concord, ON, Canada), placed onto poly-L-lysine-coated slides, dried at 37°C for 16 hours and then dewaxed and dehydrated through graded alcohols. For microscopy and quantitative morphometry of the lung, hematoxylin and eosin

(H&E) staining was performed with standard protocols and data was analyzed using the Aperio Imagescope Plus software (Leica, Concord, ON, Canada). Morphology of the heart and cardiomyocytes was assessed using Masson's Trichrome staining using standard protocols. For quantitative assessment of RV cardiomyocyte cross sectional area, area of each cardiomyocyte was traced from each 3 random cross-sectional fields /animal (20X objective).

4.3.7 IMMUNOHISTOCHEMISTRY

Paraffin heart sections were deparaffinized through graded alcohols. After antigen unmasking specimens were blocked in 2% normal goat serum in PBS-T. Endogenous biotin and avidin were blocked using the Vector Avidin/Biotin blocking kit (Vector Labs, Burlington, ON, Canada). Sections were stained with rabbit polyconal antibody to CD31 (Novus Biologicals) at 1:250 dilution for 1 hour at room temperature, followed by endogenous peroxidase quenching by incubation with 3% H_2O_2 for 15 minutes. Sections were then incubated with biotinylated goat anti-rabbit IgG antibody at 1:66 dilution (Vector Labs, Burlington, ON, Canada), followed by DAB staining using the VECTASTAIN ABC Elite kit (Vector Labs, Burlington, ON, Canada) according to manufacturer's protocol.

4.3.8 GENE EXPRESSION

RV tissue was stored in RNA Later stabilizing solution (ThermoFisher). at -80°C until RNA isolation. Tissue homogenization was achieved using the TissueLyser-II system (Qiagen, Toronto, ON, Canada) at 30 Hz for 5 min followed by RNA isolation lysis using the miRCURY RNA isolation kit (Exiqon, Woburn, MA, USA) according to manufacturer's protocol. RNA was converted to cDNA using the Taqman High Capacity cDNA Reverse Transcription kit (Applied Biosystems, Burlington, ON, Canada). Quantitative RT-PCR was performed on 30 ng of cDNA

using Taqman probes for rat cardiotrophin (Ctf1, Rn00567503_m1) and α-actinin-1 (Actn1, Rn00667357_m1) (Applied Biosystems, Burlington, ON, Canada) as per manufacturer's protocol using the BioRad CFX96 RT-PCR system (BioRad).

4.3.9 WESTERN BLOTTING

RV lysates were prepared as described in Chapter 3 from animals treated with SUHx for 4 weeks as described in Chapter 3. Western blotting was performed using the Novex and iBlot system as described in Chapter 3. Blots were blocked with 2% BSA in PBS-T (PBS containing 0.1% Treen 20, pH 7.4). After blocking, blots were incubated with mouse monoclonal primary antibodies to dilution of cardiotrophin-1 (Abcam, ON, Canada; 1:1000 dilution) overnight at 4° C, then probed with goat anti-mouse HRP-conjugates secondary antibody, washed 3 times with PBS-T. Protein expression was detected using the ECL detection kit (GE Healthcare). As a loading control, blots were probed with β-actin (ThermoFisher Scientific, ON, Canada) and incubated with appropriate IRDye® anti-rabbit or anti-mouse secondary antibodies (LI-COR Biotechnology, NE, USA) in 2% BSA/PBS-T. Further the blots were washed for three times for 15 min with PBS-T and imaged with Odyssey® imaging system (LI-COR Biotechnology, NE, USA).

4.4 RESULTS

4.4.1 CARDIOTROPHIN-1 EXPRESSION IN THE RV IS REDUCED IN EXPERIMENTAL PAH

Rats were exposed to SU5416 plus 3 weeks of chronic hypoxia. At 4 weeks post-SU5416, using qRT-PCR, we detected a reduction in CT-1 mRNA in the RV in animals with SUHx-induced PAH ($p < 0.01$), which corresponded with a ~30% reduction at the protein level by Western blotting (p

< 0.05) (Figure 4-1). This suggests that increased RV afterload in PAH results in a decrease in RV expression of the cardiogenic factor CT-1.

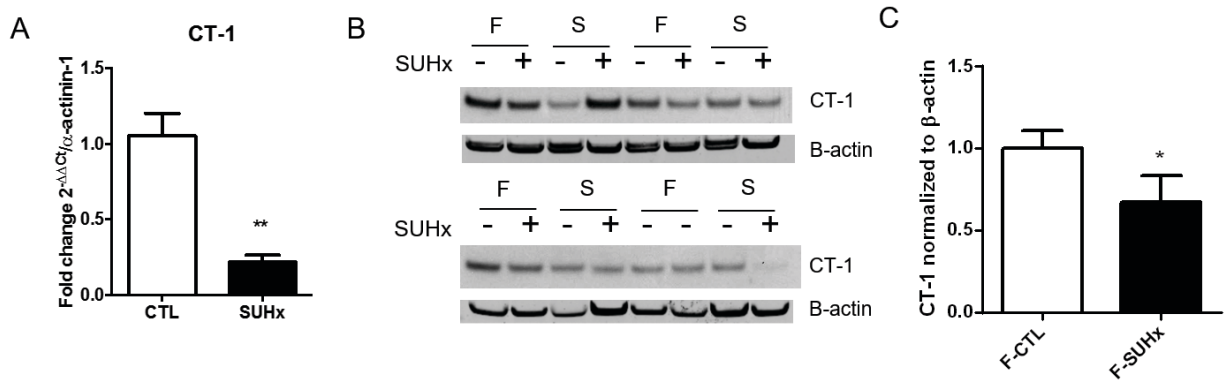

Figure 4-1. RV expression of CT-1 is decreased in Fischer rats in SUHx-induced PAH determined by quantitative RT-PCR.
(A) q-RT-PCR shows decreased mRNA levels in Fischer rat RVs after SUHx. (B) Representative Western Blots and quantification show decreased CT-protein levels in the Fischer rat after SUHx. *,**p < 0.05, 0.01 SUHx vs Control, t-test. S = Sprague Dawley, F = Fischer, where n=3-5 per group.

4.4.2 LATE ADMINISTRATION OF CARDIOTROPHIN-1 REDUCES RV DILATION, IMPROVES RV FUNCTION AND CONTRACTILITY

In the SUHx model, pulmonary hypertension was already established by 3 weeks post SU (Figure 4A), at which time animals were returned to normoxia. The RV was characterized by marked and progressive dilatation from week 3-6 post-SU as illustrated in **Figure** 4-2, and summary data are presented in Figure 4-3. The increase in RV dimensions was accompanied by a reduction in cardiac output ($p<0.0001$), fractional area change % ($p<0.0001$) and TAPSE ($p<0.0001$), and an increase in RV free wall thickness ($p<0.0001$) compared to healthy controls (No SUHx) starting at 3 weeks which persisted throughout the remainder of the study (Figure 4-3A-E). In contrast, CT-1 treatment significantly reduced RV dilation as early as 1 week after the initiation of therapy (i.e. 4 weeks post-SU) ($p <0.001$) (Figure 4-3A), and resulted in progressive improvement until at least week 6

(SU+CT-1 vs SU+PBS, $p < 0.0001$). Fractional area change at 4 ($p<0.001$), 5 ($p<0.0001$) and 6 ($p<0.0001$) weeks post-SU (Figure 4-3A-E) was also markedly improved with CT-1. As well, CT-1 therapy significantly improved cardiac output, TAPSE and reduced RVFW thickness assessed 6 weeks post-SU ($p<0.01$) (Figure 4-3B-E).

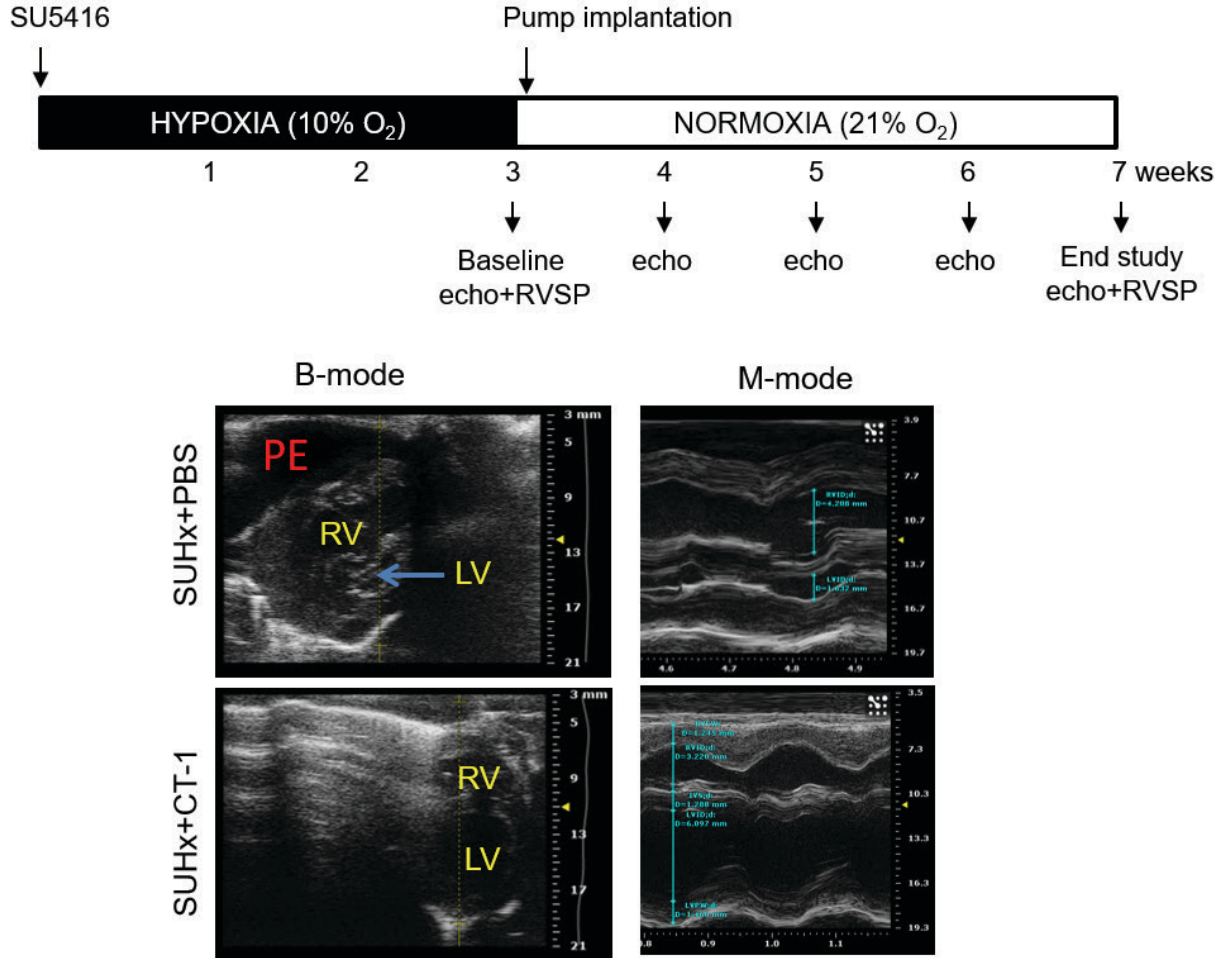

Figure 4-2. Timeline of late administration of CT-1 and weekly serial echocardiography (top). Representative B-mode and M-mode echo images depicting RV and LV chamber sizes in end diastole. Pericardial effusion (PE) was observed in some animals in the SU+PBS group.

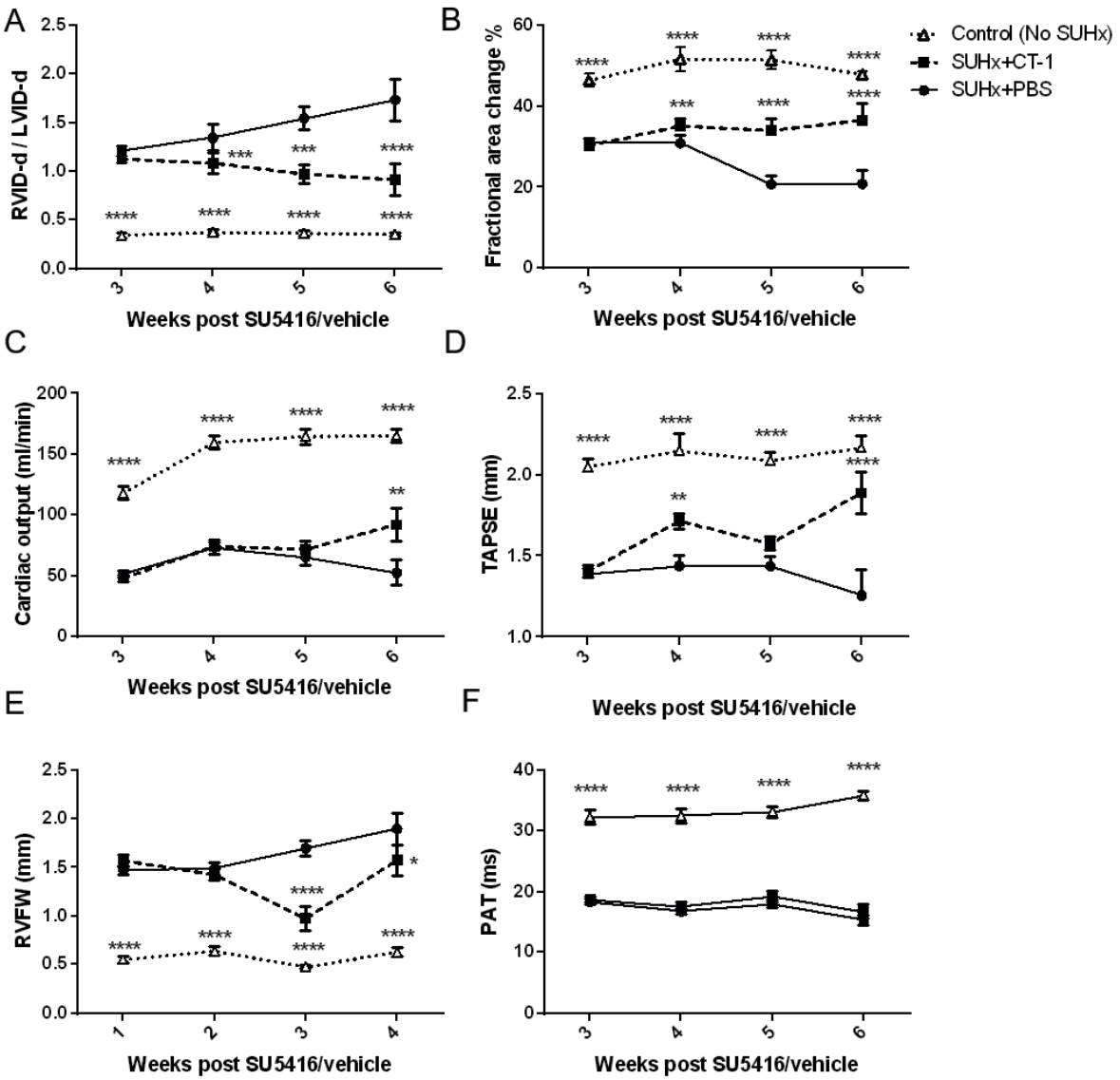

Figure 4-3. Effects of late administration of CT-1 on RV structure and function over time. Comparison of echocardiographic parameters (A) RV/LV end-diastolic ratio (RVID-d/LVID-d), (B) fractional area change, (C) cardiac output and (D) TAPSE, (E) RV free wall thickness and (F) pulmonary acceleration time. Two-way ANOVA with Dunnett's post hoc test. *,**,***,**** $p<0.05$, 0.01, 0.001, 0.0001 vs. SUHx+PBS, respectively.

4.4.3 LACK OF PULMONARY HEMODYNAMIC BENEFIT OF LATE ADMINISTRATION OF CT-1

At baseline (3 weeks post-SU) prior to treatment, there were no significant differences in RVSP between SUHx+PBS and SUHx+CT-1 groups (**Figure** 4-4A). At week 7, late administration of CT-1 was not associated with improvement in pulmonary hemodynamics, as determined by pulmonary acceleration time (Figure 4-3F) and RVSP (**Figure** 4-4A). However, because of the previously described high mortality in Fischer rats in this model, RVSP could only be obtained in the 2 surviving SU+PBS rats. While no statistical analysis could be performed on such a low sample size, these values were within the range seen in the 5 surviving CT-1 treated animals, and the mean RVSP in SU+CT-1 was similar to previous pressures obtained at 7 weeks post-SU data (historic control). As well, RV hypertrophy by RV/LV+S was not changed (**Figure** 4-4C). Interestingly, RVEDP was elevated in the two SUHx+PBS vs control, which would be consistent with RV failure.

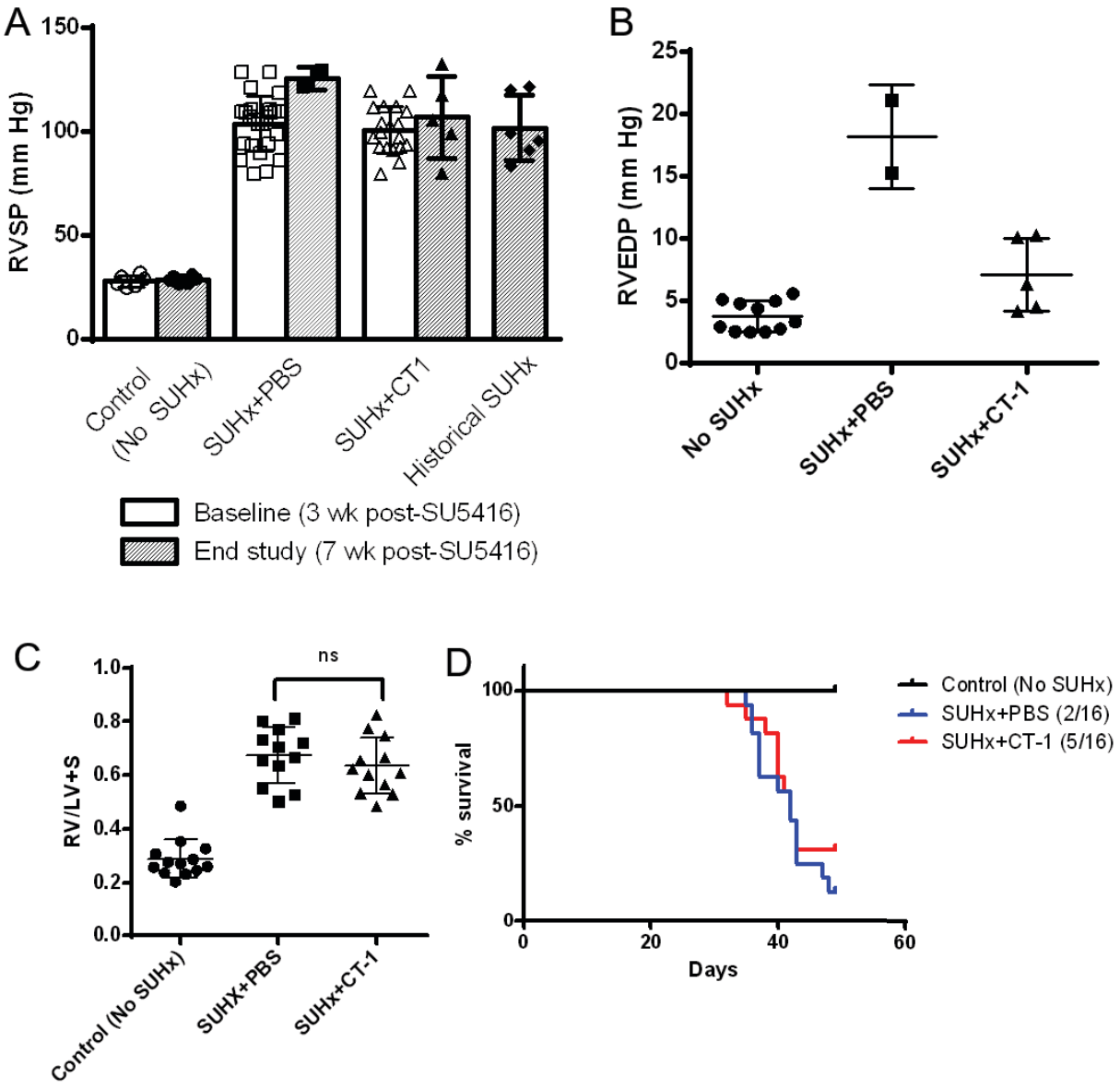

Figure 4-4. Effects of late administration of CT-1 on pulmonary hemodynamics and survival.
(A) Right ventricular systolic pressure at baseline (3 weeks post-SU) and end study (7 weeks). Historical SUHx controls are shown to provide a comparison of expected RVSP in this model. (B) Right ventricular end diastolic pressure at end study. (C) RV hypertrophy measured by RV/LV+S at end study. (D) Kaplan-Meier survival curves in rats receiving CT-1 vs PBS.

4.4.4 SURVIVAL AFTER CT-1 THERAPY

We observed a 2.5-fold improvement in the number of survivors from 2/16 (12.5%) in PBS vs 5/16 (31.25%) in CT-1 groups. However, Kaplan-Meier analysis showed no significant difference in survival between SU+CT-1 vs SU+PBS (**Figure** 4-4D).

4.4.5 LATE CT-1 THERAPY IMPROVES RV CAPILLARY DENSITY

Mean RV cardiomyocyte cross-sectional area was significantly increased from SU+PBS (555.1±54.1) and SU+CT-1 (466.2±71.7) vs control (Figure 4-5A,C). However, no significant difference was observed between SU+CT-1 and SU+PBS groups ($p=0.147$). Endothelial-specific CD31 immunohistochemical staining revealed decreased RV capillary density in SU+PBS vs Control (no SU) ($p<0.01$). In contrast, CT-1 treatment increased RV capillary density compared to SU+PBS ($p<0.05$). There was no significant difference in capillary density between SU+CT-1 vs control groups (Figure 4-5B, D).

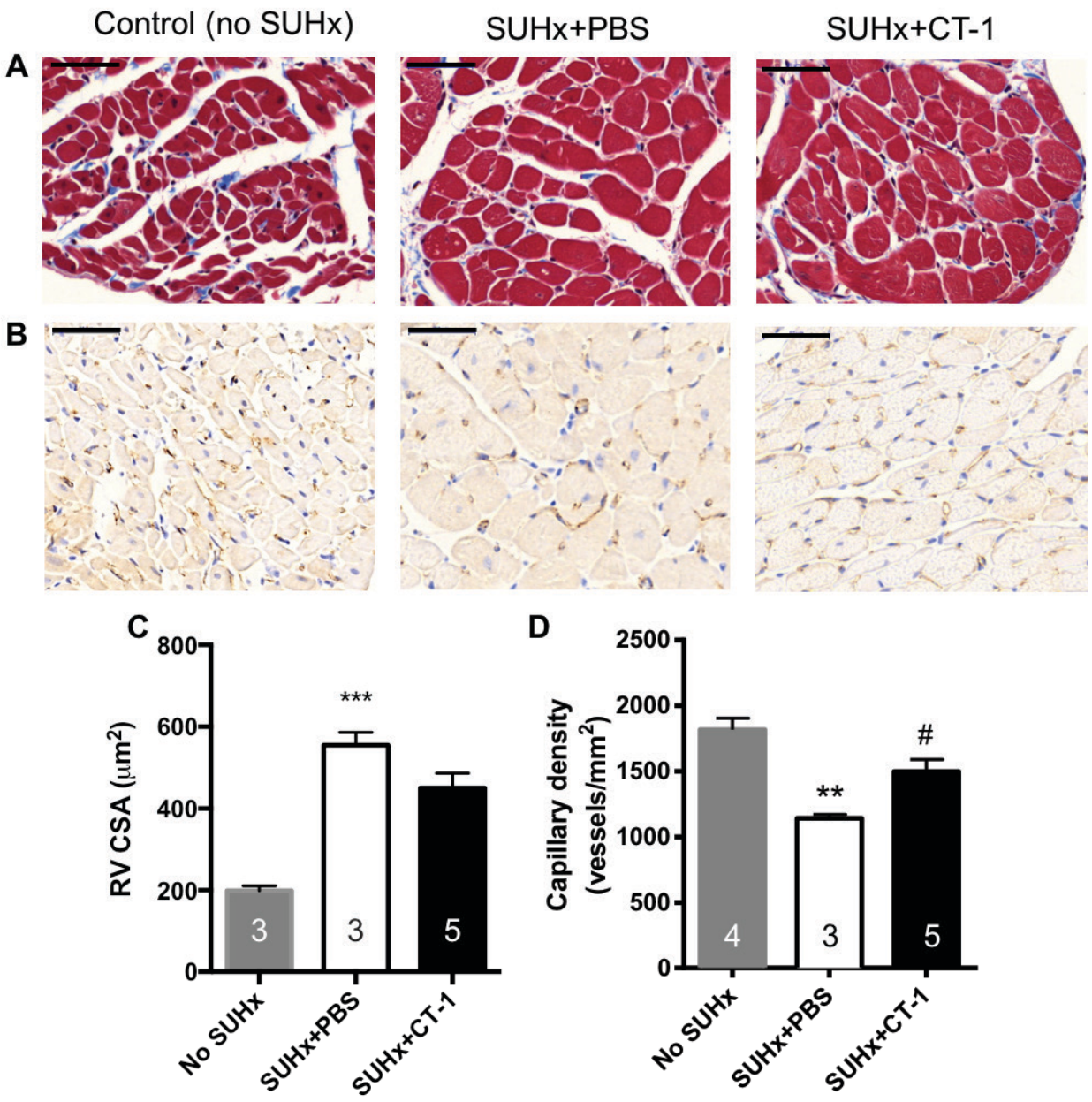

Figure 4-5. Tissue analysis of RVs after late administration of CT1.
(A) Masson's Trichrome staining of RV cross section illustrating cardiomyocyte hypertrophy. (C) Cross sectional area was not significantly reduced by CT-1. (B) Immunohistochemistry staining for CD31-positive capillaries in RV cross-sections show (D) improved capillary density with CT-1 treatment. **,*** $p < 0.01$, 0.001 vs Control (no SUHx); # $p < 0.05$ vs SUHx+PBS using One-way ANOVA with Tukey's multiple comparison test. Scale bars represent 50 μm.

4.4.6 EARLY CT-1 THERAPY IMPROVES SEVERITY OF PAH AND SUBSEQUENT RV REMODELING

In a separate set of experiments, we tested whether CT-1 therapy administered at an earlier time in the RV remodeling process (1 week post SU) would yield survival benefits. Indeed, RVID/LVID, fractional area change, cardiac output, and RV/LV+S were significantly improved by CT-1 treatment from weeks 3-5 post SU (Figure 4-6B-E). Surprisingly, early CT-1 therapy also resulted in significant hemodynamic improvements in reducing RVSP and improving PAT (Figure 4-6). Early CT-1 therapy was effective in reducing RV afterload, possibly by a direct effect on the pulmonary vasculature.

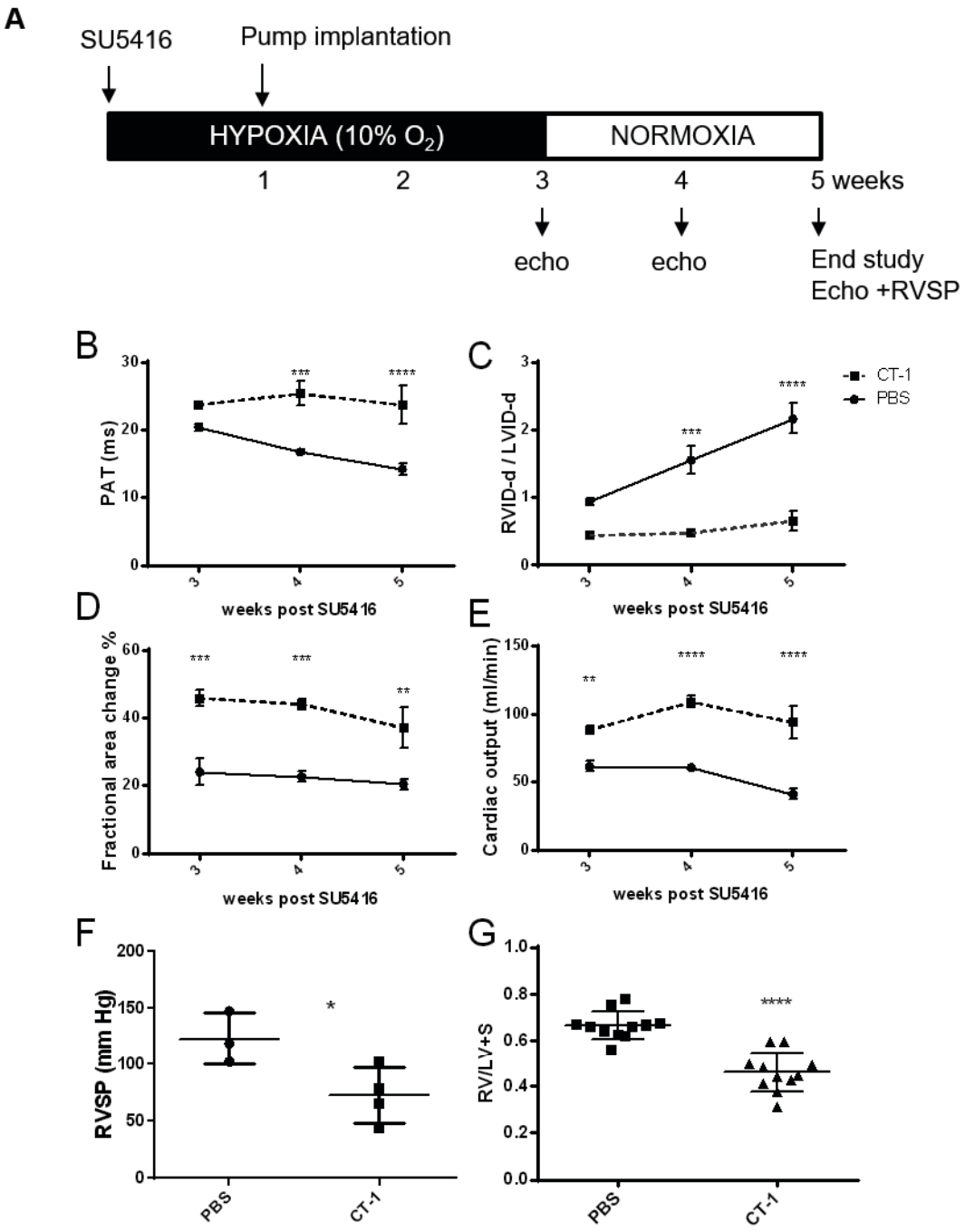

Figure 4-6. Early administration of CT-1 significantly improved pulmonary hemodynamics as well as RV remodeling.

(A) Timeline of early administration. Serial assessment of (B) PAT, (C) RVID/LVID, (D) fractional area change and (E) cardiac output. **, ***, ****, $p < 0.05$, 0.01, 0.001, 0.0001 vs PBS using Two-way ANOVA with Tukey's multiple corrections test. At end study, we observed

improvement in (F) RVSP and decreased (G) RV hypertrophy (RV/LV+S), where *,****p < 0.05, 0.0001 vs PBS using t-test.

In 6/12 CT-1 treated rats, a collection of adverse effects associated with clinical deterioration was observed from week 3-4 that appeared to be independent of PAH. These included ascites, pleural effusion, hematuria and chylomicronemia (based on milky white appearance of plasma) in 5 rats, which resulted in humane sacrifice according to CCAC humane endpoints (Appendix Figure 4-1A). Despite these findings, terminal echocardiography (3 weeks) revealed no significant differences in RV dimensions, RV function or pulmonary hemodynamics compared to CT-1 treated animals that did not develop these complications. In both CT-1 groups, significant and similar improvements were seen in PAT, FAC, RVID/LVID compared to control (Appendix Figure 4-1C), suggesting that these adverse events were caused by either an off target effect of CT-1 or a possible contaminant. Given that these unusual findings were not observed in any previous or subsequent trials involving CT-1, these observations appear to be isolated to one specific batch of CT-1. Due to these confounding adverse effects, we were unable to determine whether CT-1 had any survival benefits when administered early.

4.5 DISCUSSION

In this study, we report that CT-1 therapy exerted context-dependent effects in SUHx-induced PAH. Systemic administration of CT-1 was effective as rescue treatment by improving RV remodeling and function in established PAH (late; 3 weeks post SU). Overall, mortality was very high in this PAH model as previously reported[295], and CT-1 treatment appeared to be associated

with a modest, but statistically insignificant survival benefit. Notably, CT-1 did not affect RV afterload, consistent with the assertion that CT-1 has a direct effect on the RV. In contrast, when CT-1 was administered as a preventative treatment (early; 1 week post SU), we observed an improvement in pulmonary hemodynamics, in addition to drastic and beneficial changes in RV remodeling, function and contractility. The marked improvement in pulmonary hemodynamics with early CT-1 administration is consistent with partial prevention of pulmonary hypertension and consequently, a reduction in RV afterload. The finding that early treatment with CT-1 had a profound effect on the development of severe PAH in this model is of great interest. Since CT-1 has been shown to have important pro-angiogenic and vasodilator effects[318,328], it may inhibit endothelial cell apoptosis which is a critical driver of the early stages of PAH in this model. Nonetheless, with early CT-1 treatment it is difficult to determine the extent to which the benefits on RV structure and function were driven by direct effects on RV adaptation versus afterload reduction. Therefore, future experiments should utilize the pulmonary arterial banding model of pulmonary hypertension to eliminate the confounding pulmonary vasodilator effect of CT-1 by providing a fixed elevated afterload to isolate the RV adaptive effects of CT-1[61].

CT-1 is a member of the interleukin-6 cytokine family, of which its members (IL-6, LIF, CT-1) have demonstrated important cardioprotective effects by activating of gp130 signaling[329]. Conditional cardiac-specific gp130 knockout studies have illustrated that gp130 is necessary for adaptive LV hypertrophy from transverse aortic constriction (TAC)-induced pressure overload[313]. Its main downstream effector is the transcription factor signal transducer and activator of transcription 3 (STAT3) which provides protection against ischemia-reperfusion injury and facilitates myocardial vascularization[330] via paracrine release of VEGF[331]. Among other IL-6 family members, this property appears unique to CT-1. VEGF expression in rat cardiomyocytes is

stimulated by CT-1 in a dose-dependent manner, but not by IL-6[332]. CT-1 is known to be a potent inducer of cardiac hypertrophy via gp130-JAK/STAT3 signaling, promoting a form of hypertrophy involving myocyte lengthening accompanied by the addition of sarcomeres added in series without a concomitant increase in cell width[333]. The impact of this morphological change on cardiac remodeling is unclear, although the results of the present study would suggest that CT-1 does not promote RV dilation and improves contractility. Interestingly, STAT3 activation occurs in adaptive concentric hypertrophy in states of physiological hypertrophy such as pregnancy[332,334]. However, STAT3 activation in the pulmonary vascular bed is associated with growth dysregulation and apoptosis resistance, which suggests a pathological role and the potential detrimental effects in disease progression of PAH [335]. Further histological studies may clarify whether the CT-1 mediated STAT3 activation is detrimental in pulmonary vascular remodeling. Furthermore, the cardioprotective role of CT-1 has been highlighted in several studies demonstrating the role of CT-1 as an inhibitor of cardiomyocyte apoptosis via gp130-mediated activation of JAK/STAT, MEK1/2-ERK1/2 and PI3K/Akt pathways and by upregulating hsp70 and hsp90[315,317,329,336].

In the present study, we show for the first time that CT-1 expression is decreased in the failing RV in the Fischer SUHx model of PAH. In contrast to our study, Samillan et al. reported increased levels of circulating CT-1 after 5 weeks of hypoxic exposure[337]. However, unlike our study timeline, the sampling took place immediately after hypoxia, and therefore could be confounded the direct effects of hypoxia inducing CT-1 via the HIF-1 axis[338]. Circulating levels of CT-1 have been negatively correlated with various forms of cardiac dysfunction[325,326,339,340]. Indeed, pressure overload of the LV has been to be a stimulus for CT-1 expression[341]. However, less is known about the physiological effects of chronic exposure to CT-1, let alone as a therapy for cardiovascular

disease. Although chronic administration of exogenous CT-1 (25-100 μg/kg) to healthy mice for 14 days results in a dose-dependent increase in ventricular mass, it is unclear whether this is remodeling is beneficial[311]. The results of this study suggest that CT-1 is deficient in the failing RV, which is rescued upon supplementation with exogenous administration of CT-1. Although the regulation of CT-1 was opposite of LV failure states, the role of CT-1 in the RV in PAH may be distinct from disease of the left-heart.

Some studies have demonstrated that CT-1 exerts pulmonary vasodilator effects mediated by nitric oxide which are beneficial in chronic-hypoxia induced PH and endotoxin-induced acute lung injury (ALI)[328,342]. This increase in nitric oxide is mediated by induction of iNOS within 60 minutes of systemic administration of CT-1[343]. As well, CT-1 possesses anti-inflammatory effects which attenuate endotoxin-induced ALI, which may also modify vascular inflammation in PAH[342]. In our study, we did not observe changes in pulmonary hemodynamics when CT-1 was administered as a rescue therapy in estalbshed PAH. On the other hand, we did observe a significant reduction in pulmonary pressures when CT-1 administered at an early time point post SU (1 week), which suggests that CT-1 may have an effect on the development of PAH in this model. As mentioned above, CT-1 has several vasodilator and pro-angiogenic effects that could moderate function and structural changes caused by SU5416[318,328]. These include possibly reducing endothelial cell apoptosis induced by VEGFR2 inhibition by direct opposition of VEGF2 blockade and/or induction of NO which has important vasodilator and beneficial remodeling effects in the lung vasculature[328]. Additionally, when administered at this stage in the disease, the anti-inflammatory effects of CT-1 may interfere with hypoxia-induced inflammation that normally occurs during the induction phase of the SUHx model[342]. Further histological studies of lung tissue would be necessary to evaluate the effect of CT-1 pulmonary vascular remodeling and/or

restoration of the microvasculature possibly by inducing VEGF. Nonetheless, our data strongly suggest that pulmonary circulation is unaffected in established severe PAH, and thus the effects on RV structure and function in the "treatment" model can be attributed solely to its direct effect of the RV.

In one of our experiments, we observed a toxicity profile (chylomicronemia, ascites, pleural effusion) associated with CT-1. These adverse effects have not been previously reported, even in studies using higher doses (100 μg/kg/d) similar to our study (120 μg/kg/d)[311]. Although, in addition to the heart, CT-1 has been documented to cause organomegaly of the liver, kidney and spleen[311], it has been reported to exert prosurvival effects and provide hepatoprotection[309,344] and renal protection[345] in *in vivo* animal models. More importantly, in prior and repeat studies using other preparations of CT-1, we did not observe any of these adverse effects. It is likely that this observation was an isolated incident perhaps caused by a contaminant present in the recombinant protein preparation. Nevertheless, further investigation to determine safety profile of CT-1 prior to translational study is warranted.

In summary, we show that CT-1 improves RV adaptation in established PAH which has important implications in the treatment of RV failure associated with PAH. We demonstrate in addition to improving RV contractility, CT-1 restores RV capillary density and results in a more favourable ratio of microvascularity to increased RV mass, consistent with adaptive hypertrophy[226]. When administered early in the disease process, CT-1 has pulmonary hemodynamic benefits, which may reflect correction of the underlying PH disease pathology itself. Our findings have important implications for the treatment of PAH, in which RV function, more than any hemodynamic parameter, drives prognosis[202]. Indeed, RV failure in PAH is associated with relative ischemia due to inadequate angiogenesis to supply the hypertrophied RV[235]. This study paves the way for studies

to test whether novel therapeutic agents which stimulate RV angiogenesis are beneficial treating RV failure in PH. As well, these experiments may impact the treatment of more prevalent cardiovascular diseases that also present with right-sided heart failure such as heart failure with preserved ejection fraction (HFpEF)[346].

Chapter 5: Perspective

5.1 SUMMARY

The investigations described in Chapter 2 through 4 comprise three independent, but related studies that contribute to understanding of pathogenesis and treatment of PAH.

5.1.1 CLARIFYING THE ROLE OF THE PARACRINE EFFECT IN EPC THERAPY

In Chapter 2, we set out to test the paracrine hypothesis of endothelial progenitor cell therapy. We characterized the paracrine activity of EPCs, which is defined by stimulation of angiogenesis, endothelial cell migration and survival. These processes highlight important mechanisms of action that could potentially repair and restore the microvascular loss and endothelial dysfunction in PAH. However, due to several technical limitations resulting in suboptimal EPC therapeutic efficacy, the extent of paracrine versus cell-to-cell mechanisms contribute to the beneficial effects of these progenitor cells could not be fully assessed. The following future studies will help to achieve our original objective:

1. **Optimization of EPC therapy using cell-based gene enhancement**. We have recently reviewed the literature regarding cell-based gene therapy versus cell-based therapy, which show that enhancement of EPCs with transgenes such as eNOS, prostacyclin synthase and adrenomedullin[81,199]. So far, eNOS-enhanced EPCs have shown the greatest efficacy, with the potential to reverse pulmonary hypertension and RV remodeling in animal models[75]. This technique has been developed in our laboratory and has been scaled to GMP-grade for therapeutic use in the PhACeT clinical trial. In future studies, we may test eNOS-EPCs and their conditioned medium to determine test the paracrine hypothesis.
2. **Selecting the optimal cell product for PAH.** Along the same rationale as above, we anticipate that a consistently therapeutically active product will allow us to form a comparison to conditioned medium. Indeed, other cell types such as MSCs, and other

enhancement strategies such as small molecule priming/preconditioning have been tested in PAH. In order to address this issue, I have begun to conduct a systematic review of preclinical studies of cell therapy in PAH which will incorporate meta-analysis and subgroup analysis by cell type, enhancement method as well as timing and mode of delivery[279]. This data will inform the selection of the optimal cell product and delivery strategy upon which to test our hypothesis.

3. **Limitations of the MCT nude rat model of PAH.**

   The athymic nude rat used for the MCT model in this study is only partially immunodeficient (lacks T-cells). Consequently, residual innate immune cells are able to participate in the rapid clearance of human EPCs that has been observed by Ormiston et al[159]. Unfortunately, it is the same innate immune system (particularly NK-cells) which is necessary to induce the pathogenesis of PAH, thereby limiting the types of models for xenotransplantation. One strategy to combat the issue of immune-mediated cell clearance could involve the use of alternative models of increasing immunodeficiency, such as the severe combined immunodeficiency models (SCID) which lacks both T- and B-cells. Alternatively, future studies could utilize syngeneic EPCs, although efforts to isolate an equivalent to human using rat cells remain elusive.

Although previous studies have demonstrated the efficacy of EPCs in the nude rat model of PAH, we observed a more advanced and severe phenotype of PAH that may be less amenable repair. In order to test this hypothesis, we can validate whether proven pharmacological therapies such as prostacyclins, PDE5 inhibitors or endothelin receptor antagonist have efficacy in our model. Resistance to pharmacotherapy would be consistent

with a phenotype that is worse than human PAH, and would necessitate a strategy to decrease the severity. One possible method could be by decreasing the dose of MCT to lessen the pulmonary insult. Alternatively, a different model, such as the SU5416 model which is considered to be more clinically representative, could be used to investigate the effects of EPCs and conditioned media[347].

5.1.2 FAILURE OF RV ADAPTATION IN THE FICHER SUHX MODEL OF PAH

In Chapter 3, we demonstrated that high mortality in the Fischer model of SUHx-induced hypoxia is associated with poor RV adaptation. This is characterized by decreased RV function, decreased exercise capacity, and capillary rarefaction in comparison to SD rats which experience no mortality and exhibit preserved RV function. These findings are consistent with clinical PAH-associated RVF. Furthermore, molecular screening in this study has the potential to determining a genetic basis for RV maladaptation, and identification of candidates for developing novel RV-specific therapies.

Future studies will be useful in extending these novel observations and to better understand the mechanisms of exaggerated RV failure in this background:

1. **Validation of differences in RV adaptation in the pulmonary artery banding model.** We determined that there were no differences in RVSP at week 4 and week 7 post SU5416 between SD and Fischer rats, which is consistent with equivalent afterload. As well, in the Fischer rat, RVSP remained elevated with a corresponding decrease in cardiac output, which may suggest an increase in pulmonary vascular resistance compared to SD rats. Since this study only utilized measurements of right ventricular systolic pressure and noninvasive cardiac output measurements by echocardiography, PVR cannot be accurately

determined. Future studies should utilize direct measurement of cardiac output as well as pulmonary artery and left heart catheterization to accurately determine whether there are indeed differences in the pulmonary vascular resistance. As well, an important limitation of our study is that we cannot exclude the direct effects of chronic VEGFR inhibition the RV. Indeed, paracrine and autocrine VEGF signaling is important in myocardial angiogenesis and hypertrophy[215]. Differences in VEGF signaling between the strains due to variability in the pharmacokinetics and pharmacodynamics of SU5416 could potentially confound our observations. These above issues could be addressed in the pulmonary artery banding model to provide equivalent pressure overload. However, this model has been characterized as a mild phenotype of PH with improved RV adaptation, improved RV microcirculation compared to more clinically representative models such as SUHx[228].

2. **Clinical validation of molecular targets.** Our study implicates several molecular pathways and candidates associated fatty acid metabolism, angiogenesis, and NK-cell mediated immunity in RV failure. Future proteomic and metabolomics studies can validate whether these targets occur in clinical RV samples, and whether they are associated with adaptive vs maladaptive hypertrophy.
3. **The Fischer SUHx model as a platform to test new RV-specific therapies.** A real clinical problem in the treatment of PAH is that some patients exhibit severe and progressive RV failure despite having hemodynamic abnormalities that are no worse and sometime much less than other PAH patients that maintain RV compensation. Moreover, some patients may respond hemodynamically to pharmacotherapy, but continue to experience worsening of RV function and high mortality[202]. Thus, it is now well accepted that RV adaptation and function is far more predictive of functional capacity and prognosis

than the pulmonary hemodynamics. Yet, most preclinical endpoints are primarily focused on reduction of pulmonary pressures in animals that show good overall survival such as the SD rat in the SUHx model. The Fischer rat model of severe PAH that exhibits a severe maladaptive RV phenotype provides a unique opportunity to study the efficacy RV-specific therapies of RV structure and function and survival in future studies. Indeed, in the final chapter we have taken advantage of this attribute to study the potential efficacy of a molecule that has been shown to induce physiological myocyte growth, CT-1.

5.1.3 CARDIOTROPHIN-1 AS AN RV-SPECIFIC THERAPY FOR PAH

In Chapter 3, we used the Fischer SUHx model of PAH, which exhibits a defect in RV adaptation, to test whether a strategy to enhance RV compensatory remodeling using CT-1 could improve RV structure and function, as well as survival. Together with rapid onset RV dilatation and dysfunction, we identified capillary rarefaction a feature of this phenotype. Using our validated SUHx model, we demonstrated that cardioprotective cytokine cardiotrophin-1 (CT-1) improved RV adaptation and unexpectedly, could also improve afterload if administered earlier on in the disease process. We collaborated with Dr. Lynn Megeney's group, who showed through microarray screening that CT-1 could upregulate pro-angiogenic factors in cardiomyocytes that could affect microvascularization in a paracrine manner[318]. Indeed, we observed preserved capillary density with CT-1 therapy, which suggests that RV adaptation may be improved by an angiogenic therapy. These novel findings could have important implications for the treatment of RV failure in response to any form of PH, not just group 1 (i.e. PAH). Indeed, group 2 (PH associated with elevated left heart filling pressures) represents the largest proportion of PH patients in the developed world, and is becoming an increasing clinical challenge due to the growing

number of patients heart failure and preserved ejection fraction (HFpEF), in whom symptoms and survival are all dependent of RV adaption and function[346].

Future studies will be useful in addressing limitations of this study and to better understand the role of CT-1:

1. **Validation of RV benefits of CT-1 in the pulmonary artery banding model.** A limitation of the SUHx model in our study is the confounding contribution of the pulmonary arterial system. Since we observed a potential hemodynamic effect with CT-1 therapy, reduction of hemodynamic afterload cannot be completely excluded as a confounder of RV adaptation. Pulmonary artery banding will be useful in excluding the hemodynamic factor by introducing a fixed pressure overload, and allowing us to examine the direct effect of CT-1 on the RV.
2. **Mechanistic insight into the role of CT-1 in PAH.** In our study, we demonstrated decreased RV expression of CT-1 in SUHx-induced PAH. We postulated that downregulation of the pro-angiogenic and cardioprotective factor CT-1 could be maladaptive in PAH. Further study is necessary to identify the signal transduction pathways affected by CT-1 such as the downstream effectors JAK/STAT and MAPK. Conversely, studies to antagonize CT-1 via genetic deletion (CT-1 knockout), RNA silencing, or chemical inhibition will be instrumental in elucidating the consequences of deficient CT-1 signaling.
3. **Clinical validation of CT-1 expression in PAH.** Clinically, CT-1 has not been linked to PAH. Interestingly, in our study, we demonstrated decreased RV expression of CT-1 in PAH, and that exogenously administered CT-1 ameliorated RV failure. CT-1 could be a useful biomarker of RV function in PAH in determining whether plasma levels are

associated with hemodynamic changes or clinical picture, which would require clinical validation in either RV biopsies of patients with adaptive vs maladaptive RVH. Alternatively, CT-1 plasma levels are easily obtainable and readily detectable by commercially available assays.

5.2 CONCLUSIONS

In conclusion, this thesis addresses two main pathological processes that are of crucial importance in PAH. Starting with the diseased pulmonary vasculature, we examined alternative methods to treat PAH using cell therapy. We examined the paracrine activity of EPCs, which showed the potential to secrete factors to promote endothelial integrity and homeostasis *in vitro*. Through these experiments, we also highlight the complexity and limitations of animal models of PAH and cell therapy, as well as the challenges associated with a regenerative approach. In some ways analogous to patients with PAH, while we search for a cure for PAH the immediate problem determining clinical outcomes is RV function. In this thesis, we also sought out to determine mechanisms responsible for the strain-dependent exaggeration in RV dysfunction in the Fischer SUHx model. We characterized this phenotype through detailed cardiac function testing, and a molecular signature associated with decreased fatty acid oxidation, innate immunity activity, and vascular homeostasis. Finally, we showed that cardiotrophin-1, a pro-angiogenic and cardioprotective cytokine, was effective in improving RV function and restoring capillary density despite unaltered afterload. Furthermore, we showed potential for CT-1 to improve pulmonary hemodynamics when administered early, which suggests a direct hemodynamic effect in the prevention of PAH. This work presented in this thesis has important clinical implications that contribute to our understanding of the disease process and treatment of PAH.

Chapter 6: Appendix

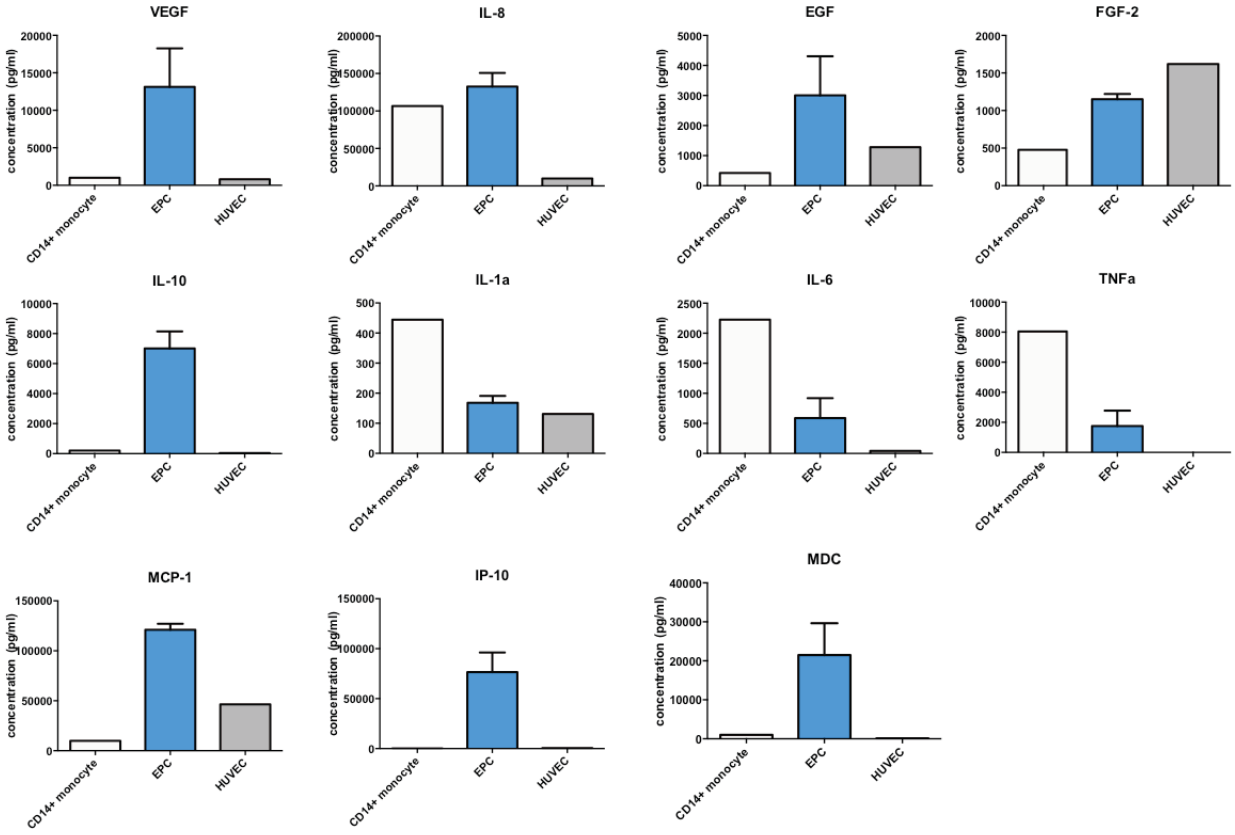

Appendix Figure 2-1. Luminex screening shows that a number of key growth factors and cytokines are secreted in EPCs (n=4) compared to monocytes (n=1) and HUVECs (n=1).

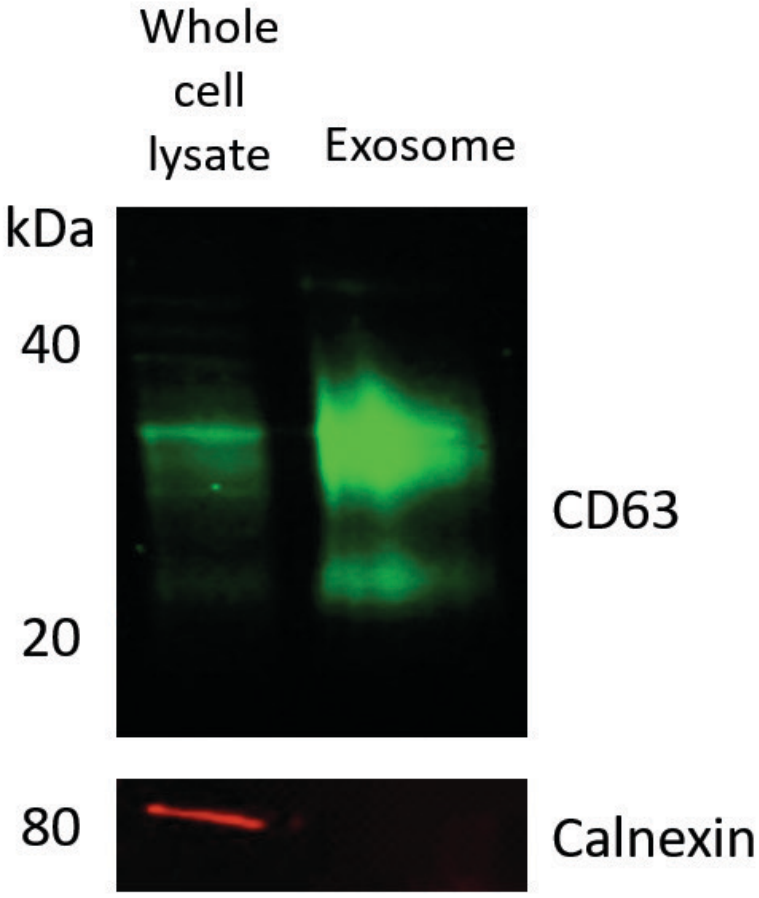

Appendix Figure 2-2. Western blot demonstrating that exosome fractions are enriched in the tetraspannin CD63 (exosome-associated marker) and negative for calnexin (endoplasmic reticulum marker).

Appendix Table 3-1. Baseline angiogenic gene expression in RV of Fischer vs SD rats.

Genes	Gene name	Fold Change	p-value
Up-regulated genes			
Cxcl9	Chemokine (C-X-C motif) ligand 9	2.7403	0.0007
Tymp	Thymidine phosphorylase	1.5117	0.0108
Ccl2	Chemokine (C-C motif) ligand 2	2.1864	0.0235
Angpt1	Angiopoietin 1	1.9241	0.0274
Timp2	metallopeptidase inhibitor 2	1.2288	0.0279
Fgf2	Fibroblast growth factor 2	1.6755	0.0308
Egf	Epidermal growth factor	1.9414	0.0351
Id1	Inhibitor of DNA binding 1	1.3386	0.0398
Vegfc	Vascular endothelial growth factor C	1.3973	0.0407
Fn1	Fibronectin 1	1.3312	0.0435
Tnf	Tumor necrosis factor (TNF superfamily, member 2)	2.3042	0.0457
Serpin1	Serpin peptidase inhibitor, clade E (nexin, plasminogen activator inhibitor type 1), member 1	1.6995	0.0552
Itgav	Integrin, alpha V	1.2264	0.0702
Pecam1	Platelet/endothelial cell adhesion molecule 1	1.2259	0.1365
F3	Coagulation factor III (thromboplastin, tissue factor)	1.3163	0.1598
Plau	Plasminogen activator, urokinase	1.5155	0.1610
Itga1	Integrin, alpha 5 (fibronectin receptor, alpha polypeptide)	1.2771	0.1981
Pdgfb	Platelet-derived growth factor beta polypeptide (simian sarcoma viral (v-sis) oncogene homolog)	1.1683	0.2119
Mapk14	Mitogen activated protein kinase 14	1.2602	0.2158
Pdgfa	Platelet-derived growth factor alpha polypeptide	1.1631	0.2281
Vegfa	Vascular endothelial growth factor A	1.2601	0.2295
Hif1a	Hypoxia-inducible factor 1, alpha subunit (basic helix-loop-helix transcription factor)	1.3209	0.2305
Epas1	Endothelial PAS domain protein 1	1.1778	0.2465
Pgf	Placental growth factor	1.2320	0.2751
Efna1	Ephrin A1	1.2069	0.2819
Vegfb	Vascular endothelial growth factor B	1.2003	0.3225
Erbb2	V-erb-b2 erythroblastic leukemia viral oncogene homolog 2, neuro/glioblastoma derived oncogene homolog (avian)	1.2253	0.3232
Il1b	Interleukin 1 beta	1.5163	0.3928
Eng	Endoglin	1.1375	0.4442
Mdk	Midkine	1.1446	0.4494
Flt1	Fms-related tyrosine kinase 1	1.1094	0.4499
Timp1	metallopeptidase inhibitor 1	1.1329	0.4741
Tgfb1	Transforming growth factor, beta receptor 1	1.1096	0.4790
Thbs1	Thrombospondin 1	1.1433	0.5190
Fgf1	Fibroblast growth factor 1	1.1487	0.5246
Jag1	Jagged 1	1.0542	0.6990
Hgf	Hepatocyte growth factor	1.0584	0.7390
Sphk1	Sphingosine kinase 1	1.1245	0.8130
Nrp1	Neuropilin 1	1.0383	0.8598
Plg	Plasminogen	1.0185	0.9625
Mmp2	Matrix metallopeptidase 2	1.0087	0.9782
Down-regulated genes			
Edn1	Endothelin 1	0.5029	0.0120
Tgfb3	Transforming growth factor, beta receptor 3	0.7895	0.0135
Cdh5	Cadherin 5	0.7139	0.0198
Timp3	metallopeptidase inhibitor 3	0.8594	0.0265
Figf	C-fos induced growth factor	0.5192	0.0429
Ptgs1	Prostaglandin-endoperoxide synthase 1	0.6824	0.1048
Igf1	Insulin-like growth factor 1	0.7624	0.1057
Nrp2	Neuropilin 2	0.8206	0.1836
Anpep	Alanyl (membrane) aminopeptidase	0.8957	0.2219
Serpinf1	Serpin peptidase inhibitor, clade F (alpha-2 antiplasmin, pigment epithelium derived factor), member 1	0.8987	0.2346

Akt1	V-akt murine thymoma viral oncogene homolog 1	0.8554	0.3300
Nos3	Nitric oxide synthase 3, endothelial cell	0.8973	0.3898
Ang1	Angiogenin, ribonuclease, RNase A family, 5	0.8150	0.4004
Tie1	Tyrosine kinase with immunoglobulin-like and EGF-like domains 1	0.8983	0.4228
Mmp14	Matrix metallopeptidase 14 (membrane-inserted)	0.9256	0.4289
Col4a3	Collagen, type IV, alpha 3	0.9116	0.4470
Tgfb2	Transforming growth factor, beta receptor 2	0.9213	0.5209
Ctgf	Connective tissue growth factor	0.9400	0.6147
Mmp19	Matrix metallopeptidase 19	0.9536	0.6477
Fgfr3	Fibroblast growth factor receptor 3	0.9511	0.6717
Kdr	Kinase insert domain receptor	0.9581	0.7085
Itgb3	Integrin, beta 3	0.9644	0.7314
S1pr1	Sphingosine-1-phosphate receptor 1	0.9683	0.7653
Col18a1	Collagen, type XVIII, alpha 1	0.9663	0.7660
Ptk2	protein tyrosine kinase 2	0.9980	0.9235
Tek	tyrosine kinase, endothelial	0.9955	0.9367
Angpt2	Angiopoietin 2	0.9970	0.9384
Tgfbr1	Transforming growth factor, beta receptor 1	0.9982	0.9684
Adgrb1	Brain-specific angiogenesis inhibitor 1	UD	
Cxcl1	Chemokine (C-X-C motif) ligand 1 (melanoma growth stimulating activity, alpha)	UD	
Cxcl2	Chemokine (C-X-C motif) ligand 2	UD	
F2	Coagulation factor II (thrombin)	UD	
Fgf6	Fibroblast growth factor 6	UD	
Ifna1	Interferon-alpha 1	UD	
Ifnb1	Interferon beta 1, fibroblast	UD	
Ifng	Interferon gamma	UD	
Il6	Interleukin 6	UD	
Lect1	Leukocyte cell derived chemotaxin 1	UD	
Lep	Leptin	UD	
Mmp3	Matrix metallopeptidase 3	UD	
Mmp9	Matrix metallopeptidase 9	UD	
Serpinb5	Serpin peptidase inhibitor, clade B (ovalbumin), member 5	UD	
Tgfa	Transforming growth factor alpha	UD	

Note: UD- Undetectable, Cq>35.

Fold change in baseline angiogenic genes expression in the RV of Fischer and SD rats measured by quantitative RT-PCR. N=4 per group using beta-actin as housekeeping gene.

Appendix Table 3-2. Fold change in angiogenic gene expression in RV of both rat strains compared to vehicle.

Gene	Gene name	Fischer		SD	
		Fold change	p-value	Fold change	p-value
Differently regulated genes in either strain					
Vegfc	Vascular endothelial growth factor C	0.5038	0.0045	0.9919	0.9086
Ptgs1	Prostaglandin-endoperoxide synthase 1	1.8385	0.0056	0.9588	0.7228
Fn1	Fibronectin 1	1.8559	0.0071	1.5590	0.0718
Edn1	Endothelin 1	2.2538	0.0199	1.2359	0.1722
Mmp14	Matrix metallopeptidase 14 (membrane-inserted)	0.6985	0.0274	0.8150	0.0823
Tgfbr1	Transforming growth factor, beta receptor 1	0.7141	0.0298	0.8800	0.1027
Tnf	Tumor necrosis factor (TNF superfamily, member 2)	0.4590	0.0427	0.9092	0.3677
Vegfa	Vascular endothelial growth factor A	0.5956	0.0510	0.6065	0.0040
Pecam1	Platelet/endothelial cell adhesion molecule 1	0.6923	0.0546	0.6640	0.0020
Ang1	Angiogenin, ribonuclease, RNase A family, 5	0.5470	0.0705	0.4783	0.0294
Tymp	Thymidine phosphorylase	0.7453	0.0944	0.7541	0.0153
Fgf1	Fibroblast growth factor 1	0.6604	0.0965	0.6406	0.0050
Nos3	Nitric oxide synthase 3, endothelial cell	0.7472	0.1027	0.6469	0.0059
Pdgfb	Platelet-derived growth factor beta polypeptide (simian sarcoma viral (v-sis) oncogene homolog)	0.7532	0.1230	0.6071	0.0001
Figf	C-fos induced growth factor	1.4159	0.1646	1.7456	0.0285
Serpin1	Serpin peptidase inhibitor, clade E (nexin, plasminogen activator inhibitor type1), member 1	1.6212	0.1668	2.2051	0.0019
Angpt2	Angiopoietin 2	1.0225	0.9287	0.7238	0.0040
Up-regulated genes in both strains					
Thbs1	Thrombospondin 1	4.5011	0.0006	3.2311	0.0103
Timp1	metallopeptidase inhibitor 1	2.9759	0.0016	2.9892	0.0000
Tgfb2	Transforming growth factor, beta receptor 2	6.1616	0.0089	4.2252	0.0003
Ctgf	Connective tissue growth factor	7.6548	0.0155	6.1891	0.0003
Ccl2	Chemokine (C-C motif) ligand 2	1.6799	0.0164	2.7391	0.0011
Serpinf1	Serpin peptidase inhibitor, clade F (alpha-2 antiplasmin, pigment epithelium derived factor), member 1	1.9996	0.0166	1.8559	0.0002
Sphk1	Sphingosine kinase 1	4.0936	0.0260	2.8188	0.0003
Tgfb1	Transforming growth factor, beta receptor 1	1.4564	0.0352	1.3692	0.0094
Eng	Endoglin	1.3109	0.1426	1.1139	0.1590
Itgb3	Integrin, beta 3	1.2237	0.2329	0.8932	0.3257
Col18a1	Collagen, type XVIII, alpha 1	1.2452	0.3091	1.2161	0.3751
Tgfb3	Transforming growth factor, beta receptor 3	1.2035	0.6953	0.7700	0.0815
S1pr1	Sphingosine-1-phosphate receptor 1	1.0559	0.8415	0.9048	0.2170
Down-regulated genes in both strains					
Angpt1	Angiopoietin 1	0.0675	0.0004	0.1493	0.0025
Epas1	Endothelial PAS domain protein 1	0.3536	0.0008	0.4584	0.0003
Mapk14	Mitogen activated protein kinase 14	0.4547	0.0028	0.5769	0.0070
Pdgfa	Platelet-derived growth factor alpha polypeptide	0.4841	0.0028	0.5653	0.0001
F3	Coagulation factor III (thromboplastin, tissue factor)	0.3796	0.0067	0.4835	0.0025
Erbb2	V-erb-b2 erythroblastic leukemia viral oncogene homolog 2, neuro/glioblastoma derived oncogene homolog (avian)	0.4532	0.0068	0.6054	0.0077
Vegfb	Vascular endothelial growth factor B	0.4437	0.0071	0.5246	0.0009
Efna1	Ephrin A1	0.4483	0.0074	0.5457	0.0001
Egf	Epidermal growth factor	0.3910	0.0087	0.6171	0.0410
Anpep	Alanyl (membrane) aminopeptidase	0.6472	0.0133	0.7150	0.0111
Akt1	V-akt murine thymoma viral oncogene homolog 1	0.4791	0.0133	0.6037	0.0004
Ptk2	protein tyrosine kinase 2	0.6770	0.0137	0.6929	0.0108
Timp3	metallopeptidase inhibitor 3	0.7475	0.0164	0.6485	0.0011
Tek	tyrosine kinase, endothelial	0.5565	0.0175	0.5643	0.0020
Flt1	Fms-related tyrosine kinase 1	0.5934	0.0186	0.6933	0.0039

Cdh5	Cadherin 5	0.5988	0.0186	0.6593	0.0056
Jag1	Jagged 1	0.5006	0.0284	0.6925	0.0056
Hif1a	Hypoxia-inducible factor 1, alpha subunit (basic helix-loop-helix transcription factor)	0.5127	0.0288	0.6997	0.0148
Col4a3	Collagen, type IV, alpha 3	0.6726	0.0332	0.6696	0.0249
Pgf	Placental growth factor	0.5984	0.0459	0.5437	0.0054
Timp2	metallopeptidase inhibitor 2	0.8105	0.0503	1.0329	0.7315
Cxcl9	Chemokine (C-X-C motif) ligand 9	0.6016	0.0544	0.5832	0.0601
Igf1	Insulin-like growth factor 1	0.7577	0.0665	0.7807	0.1014
Itgav	Integrin, alpha V	0.7660	0.0793	1.0125	0.8125
Hgf	Hepatocyte growth factor	0.7324	0.0834	0.8754	0.2322
Fgfr3	Fibroblast growth factor receptor 3	0.7204	0.0902	0.7682	0.1406
Id1	Inhibitor of DNA binding 1	0.7664	0.1110	0.9136	0.3198
Fgf2	Fibroblast growth factor 2	0.7227	0.1486	0.9463	0.5781
Tie1	Tyrosine kinase with immunoglobulin-like and EGF-like domains 1	0.7721	0.1668	0.8051	0.1008
Nrp1	Neuropilin 1	0.8036	0.2355	0.8088	0.0651
Itga1	Integrin, alpha 5 (fibronectin receptor, alpha polypeptide)	0.8088	0.2444	1.1269	0.2325
Mmp2	Matrix metallopeptidase 2	0.8606	0.2745	0.9404	0.5291
Plg	Plasminogen	0.8329	0.3869	0.9165	0.5298
Kdr	Kinase insert domain receptor	0.8347	0.4109	0.8211	0.0842
Il1b	Interleukin 1 beta	0.8706	0.4468	1.5450	0.4679
Nrp2	Neuropilin 2	0.9238	0.5872	0.8856	0.2934
Mdk	Midkine	0.9712	0.7165	1.2978	0.1503
Mmp19	Matrix metallopeptidase 19	0.9778	0.7918	0.9715	0.7299
Plau	Plasminogen activator, urokinase	0.9835	0.8094	1.0521	0.8072
Adgrb1	Brain-specific angiogenesis inhibitor 1	UD		UD	
Cxcl1	Chemokine (C-X-C motif) ligand 1 (melanoma growth stimulating activity, alpha)	UD		0.7147	0.3784
Cxcl2	Chemokine (C-X-C motif) ligand 2	UD		UD	
F2	Coagulation factor II (thrombin)	UD		UD	
Fgf6	Fibroblast growth factor 6	UD		UD	
Ifna1	Interferon-alpha 1	UD		UD	
Ifnb1	Interferon beta 1, fibroblast	UD		UD	
Il6	Interleukin 6	UD		UD	
Lect1	Leukocyte cell derived chemotaxin 1	UD		UD	
Lep	Leptin	UD		UD	
Mmp3	Matrix metallopeptidase 3	UD		UD	
Mmp9	Matrix metallopeptidase 9	UD		UD	
Serpinb5	Serpin peptidase inhibitor, clade B (ovalbumin), member 5	UD		UD	
Tgfa	Transforming growth factor alpha	UD		3.3091	0.0998
Ifng	Interferon gamma	0.4063	0.0216	UD	

Note: UD- Undetectable, Cq>35.

Fold change in angiogenic genes expression in the RV of SUHx Fischer and SD rats relative to vehicle control of respective group. Gene expression was measured by quantitative RT-PCR, N=4 per group using beta-actin as housekeeping gene.

Appendix Table 3-3: Summary of differentially regulated genes in microarray analysis of RV in PAH vs control

		Fischer		SD	
Gene	Gene name	Fold change	adj p-value	Fold change	adj p-value
Differentially regulated in either strain					
Nppb	natriuretic peptide B	12.6193	0.0065	5.9746	0.0833
Nppa	natriuretic peptide A	47.5618	0.0092	6.7470	0.4638
Hmox1	heme oxygenase 1	3.5358	0.0092	1.9637	0.2000
Crlf1	cytokine receptor like factor 1	4.4842	0.0154	2.5757	0.0500
Tnik	TRAF2 and NCK interacting kinase	0.3021	0.0154	0.5338	0.1472
Cyp2e1	cytochrome P450 family 2 subfamily E member 1	0.2938	0.0154	0.3305	0.0509
Gabrb2	gamma-aminobutyric acid type A receptor beta2 subunit	0.2310	0.0169	0.1897	0.0579
Nadk2	NAD kinase 2, mitochondrial	0.4095	0.0169	0.5344	0.1124
Epha7	EPH receptor A7	0.3951	0.0169	0.5941	0.3616
Lsmem1	leucine rich single-pass membrane protein 1	0.3975	0.0169	0.5851	0.2130
Abhd2	abhydrolase domain containing 2	2.5801	0.0169	1.8580	0.0581
Mir490	microRNA 490	0.2575	0.0169	0.3999	0.0880
Slc16a10	solute carrier family 16 member 10	0.4209	0.0172	0.4799	0.0541
Vwa8	von Willebrand factor A domain containing 8	0.4270	0.0172	0.5089	0.0581
Gpnmb	glycoprotein nmb	2.5486	0.0185	2.3586	0.0881
Gnao1	G protein subunit alpha o1	3.1942	0.0185	3.3488	0.1210
Syt14	synaptotagmin 14	0.4589	0.0187	0.5841	0.1266
Cd68	CD68 molecule	2.0678	0.0198	1.8196	0.1210
Ppm1k	protein phosphatase, Mg2+/Mn2+ dependent 1K	0.4623	0.0210	0.6887	0.1593
Nckap5	NCK associated protein 5	0.3588	0.0210	0.5747	0.0866
Stab1	stabilin 1	2.1801	0.0216	1.7006	0.1554
Acadsb	acyl-CoA dehydrogenase, short/branched chain	0.4789	0.0219	0.6194	0.0994
LOC100359438		0.4617	0.0219	0.7546	0.4779
Cd1d1		0.4610	0.0219	0.4295	0.1039
Isoc1	isochorismatase domain containing 1	0.4949	0.0225	0.6075	0.0637
Rimbp2	RIMS binding protein 2	0.4639	0.0232	0.6058	0.1310
Gpcpd1	glycerophosphocholine phosphodiesterase 1	0.3461	0.0233	0.4911	0.0541
Klrc3	killer cell lectin like receptor C3	0.4980	0.0250	0.5679	0.6643
Lgals3	galectin 3	2.2049	0.0257	1.7769	0.1168
Mcam	melanoma cell adhesion molecule	2.3836	0.0265	1.8103	0.0922
Ppp1r3a	protein phosphatase 1 regulatory subunit 3A	0.5093	0.0265	0.6923	0.2686
Klrd1	killer cell lectin like receptor D1	0.4406	0.0272	0.7043	0.3498
Gprin3	GPRIN family member 3	0.4687	0.0272	0.6638	0.1266
F2r	coagulation factor II thrombin receptor	2.1555	0.0272	1.5522	0.0848
Cds1	CDP-diacylglycerol synthase 1	0.3765	0.0272	0.5248	0.2057
Thrb	thyroid hormone receptor beta	0.5263	0.0280	0.6391	0.2081
Tgfb1i1	transforming growth factor beta 1 induced transcript 1	2.7864	0.0286	2.6509	0.0564
Decr1	2,4-dienoyl-CoA reductase 1	0.4151	0.0286	0.4458	0.0553
Mum1l1	MUM1 like 1	0.5212	0.0286	0.5951	0.1807
P2ry1	purinergic receptor P2Y1	0.5258	0.0286	0.6437	0.3664
Corin	corin, serine peptidase	0.5101	0.0286	0.4859	0.1185
Trabd2b	TraB domain containing 2B	0.5147	0.0288	0.7094	0.1954
Clic1	chloride intracellular channel 1	1.9957	0.0288	1.6340	0.0777
LOC102547230		0.4341	0.0291	0.6784	0.1614
Col6a6	collagen type VI alpha 6 chain	0.3902	0.0291	0.5727	0.1808
Erbb4	erb-b2 receptor tyrosine kinase 4	0.4365	0.0291	0.6410	0.1083
Pfkp	phosphofructokinase, platelet	2.5779	0.0291	2.1292	0.0507
Gadd45a	growth arrest and DNA damage inducible alpha	2.2398	0.0291	2.1031	0.0529
Grid1	glutamate ionotropic receptor delta type subunit 1	0.3503	0.0291	0.3708	0.0610
Tmem196	transmembrane protein 196	0.5239	0.0291	0.7424	0.2265
Kif20b	kinesin family member 20B	2.1659	0.0291	2.0602	0.2748
C1qc	complement C1q C chain	1.9959	0.0291	1.9067	0.1132
LOC498276		1.9087	0.0291	1.1401	0.7588
Ccl2	C-C motif chemokine ligand 2	2.4230	0.0291	2.6266	0.0627
Ednrb	endothelin receptor type B	1.9439	0.0292	1.7535	0.0564
Adamts1	ADAM metallopeptidase with thrombospondin type 1 motif 1	2.0433	0.0292	1.5864	0.1343
Tgfb1	transforming growth factor beta 1	1.9433	0.0292	1.7548	0.0564
Anxa2	annexin A2	2.2868	0.0292	1.8147	0.1086
Ptprd	protein tyrosine phosphatase, receptor type D	0.4680	0.0292	0.5454	0.0591
Gcnt1	glucosaminyl (N-acetyl) transferase 1, core 2	0.4588	0.0292	0.5844	0.1008
Piwil2	piwi like RNA-mediated gene silencing 2	0.4213	0.0292	0.4310	0.0686
Anxa5	annexin A5	2.0730	0.0292	1.7473	0.0690

		Fischer		SD	
Gene	Gene name	Fold change	adj p-value	Fold change	adj p-value
Emc9	ER membrane protein complex subunit 9	0.5078	0.0292	0.6090	0.1168
Eng	endoglin	1.8556	0.0292	1.2453	0.4290
Ftl1		1.9465	0.0292	1.4752	0.3036
Arhgap26	Rho GTPase activating protein 26	0.4501	0.0292	0.5790	0.1266
Flrt2	fibronectin leucine rich transmembrane protein 2	3.1795	0.0292	1.9982	0.0553
Klhl38	kelch like family member 38	0.3990	0.0292	0.5813	0.1953
Sptlc2	serine palmitoyltransferase long chain base subunit 2	2.0422	0.0293	1.7637	0.0534
Osbpl6	oxysterol binding protein like 6	0.3474	0.0293	0.4955	0.1953
Pank1	pantothenate kinase 1	0.5387	0.0293	0.6471	0.2363
Slc16a7	solute carrier family 16 member 7	0.4054	0.0293	0.6193	0.0880
Sphkap	SPHK1 interactor, AKAP domain containing	0.5516	0.0293	1.1640	0.8203
Ank2	ankyrin 2	0.5531	0.0293	0.6038	0.0882
Ms4a7	membrane spanning 4-domains A7	2.1003	0.0294	1.8086	0.2073
Slc22a5	solute carrier family 22 member 5	0.5633	0.0301	0.5655	0.0509
Cthrc1	collagen triple helix repeat containing 1	2.4018	0.0301	2.3199	0.0580
Loxl1	lysyl oxidase like 1	3.0915	0.0301	2.7693	0.0541
Sqle	squalene epoxidase	2.1549	0.0301	1.5470	0.2766
Klrb1c		0.3473	0.0301	0.4938	0.0813
Fam13a	family with sequence similarity 13 member A	0.5732	0.0304	0.6874	0.2592
Rp1	RP1, axonemal microtubule associated	0.4705	0.0305	0.5643	0.1986
Amd1	adenosylmethionine decarboxylase 1	0.5261	0.0305	0.5684	0.0650
Emp1	epithelial membrane protein 1	2.4771	0.0305	1.8590	0.1283
Myoc	myocilin	0.4173	0.0320	0.4500	0.1593
Rai14	retinoic acid induced 14	1.7871	0.0322	1.3930	0.1457
Ppm1l	protein phosphatase, Mg2+/Mn2+ dependent 1L	0.5750	0.0322	0.5991	0.0848
Mpeg1	macrophage expressed 1	1.9393	0.0322	1.9467	0.0564
Tgm2	transglutaminase 2	2.6232	0.0322	1.9559	0.0564
Hook1	hook microtubule tethering protein 1	0.4693	0.0322	0.5573	0.0637
Baz1a	bromodomain adjacent to zinc finger domain 1A	1.7083	0.0322	1.3791	0.2085
Ghr	growth hormone receptor	0.5459	0.0322	0.6841	0.1492
Hsdl2	hydroxysteroid dehydrogenase like 2	0.5144	0.0323	0.5890	0.1100
Ccr2	C-C motif chemokine receptor 2	0.2631	0.0323	0.8702	0.7665
LOC367515		0.4163	0.0323	0.4570	0.2091
Lama5	laminin subunit alpha 5	2.0897	0.0323	1.5082	0.1123
Lxn	latexin	2.0314	0.0323	1.5483	0.0922
C5ar1	complement C5a receptor 1	1.7979	0.0323	1.7283	0.1853
Tox	thymocyte selection associated high mobility group box	0.4667	0.0327	0.6375	0.1135
Dynap	dynactin associated protein	0.1679	0.0327	0.4446	0.1644
Map2k6	mitogen-activated protein kinase kinase 6	0.4174	0.0327	0.4613	0.1277
Il1r1	interleukin 1 receptor type 1	2.1224	0.0327	2.0167	0.0507
Perp	PERP, TP53 apoptosis effector	0.3210	0.0327	0.5573	0.0564
LOC681266		1.8653	0.0327	1.5956	0.1155
Sat1	spermidine/spermine N1-acetyltransferase 1	1.7843	0.0327	1.2346	0.3859
Ndrg4	NDRG family member 4	1.8221	0.0327	1.7620	0.1100
Cyp4b1	cytochrome P450 family 4 subfamily B member 1	0.4816	0.0327	0.6240	0.1791
Pcnt	pericentrin	0.4805	0.0329	0.5088	0.0762
Foxs1	forkhead box S1	1.8334	0.0330	1.0405	0.9181
Cd86	CD86 molecule	2.1621	0.0331	2.2042	0.0749
Hpgds	hematopoietic prostaglandin D synthase	2.0509	0.0341	1.8519	0.4206
Fign	fidgetin, microtubule severing factor	0.4712	0.0346	0.7347	0.3627
Ecm1	extracellular matrix protein 1	2.2444	0.0349	1.7361	0.2583
Eno2	enolase 2	2.0413	0.0349	1.1961	0.7852
Asb15	ankyrin repeat and SOCS box containing 15	0.4252	0.0351	0.5054	0.0512
RragB	Ras related GTP binding B	0.5592	0.0356	0.7563	0.3097
Acot2	acyl-CoA thioesterase 2	0.4934	0.0361	0.5096	0.0994
RGD1561161		0.5498	0.0361	0.7491	0.2429
Oxr1	oxidation resistance 1	0.5818	0.0361	0.7129	0.1464
Cidea	cell death-inducing DFFA-like effector a	0.5688	0.0361	0.6675	0.1449
Iqub	IQ motif and ubiquitin domain containing	0.4598	0.0361	0.5597	0.2132
Odc1	ornithine decarboxylase 1	1.7727	0.0361	1.2598	0.2845
Prodh	proline dehydrogenase 1	0.2257	0.0361	0.3272	0.0570
Ptgis	prostaglandin I2 synthase	2.0164	0.0362	1.6421	0.1423
Bche	butyrylcholinesterase	0.5872	0.0362	0.6227	0.0690
Ppp1r3d	protein phosphatase 1 regulatory subunit 3D	0.4800	0.0362	0.5668	0.0690
Cdh13	cadherin 13	1.9121	0.0362	1.6179	0.1875
Hspb3	heat shock protein family B (small) member 3	2.2230	0.0362	2.1580	0.0564
Fam46c	family with sequence similarity 46 member C	2.5381	0.0362	1.5855	0.1667

		Fischer		SD	
Gene	Gene name	Fold change	adj p-value	Fold change	adj p-value
Phkg1	phosphorylase kinase catalytic subunit gamma 1	0.4477	0.0362	0.3786	0.1932
Lmcd1	LIM and cysteine rich domains 1	1.9741	0.0362	1.5145	0.1604
Tmem65	transmembrane protein 65	0.5401	0.0362	0.6660	0.1083
Klrk1	killer cell lectin like receptor K1	0.4881	0.0362	0.9005	0.7189
Ppfibp2	PPFIA binding protein 2	0.5066	0.0362	0.6690	0.2821
Islr	immunoglobulin superfamily containing leucine rich repeat	3.1070	0.0362	2.8632	0.0849
LOC100362543		1.8105	0.0362	1.0076	0.9909
C1qa	complement C1q A chain	1.7697	0.0364	1.6708	0.2643
Sesn1	sestrin 1	0.5471	0.0364	0.6208	0.0762
LOC102552996		0.3779	0.0364	0.4230	0.0677
Unc5b	unc-5 netrin receptor B	2.4247	0.0366	1.7126	0.2323
Meis1	Meis homeobox 1	0.5786	0.0370	0.6180	0.0847
Clec7a	C-type lectin domain family 7 member A	1.9574	0.0370	2.0257	0.0709
As3mt	arsenite methyltransferase	0.5786	0.0371	0.7430	0.2741
Coq10b	coenzyme Q10B	1.6322	0.0371	1.6419	0.1133
Tbc1d4	TBC1 domain family member 4	0.5570	0.0374	0.6745	0.1114
Junb	JunB proto-oncogene, AP-1 transcription factor subunit	2.0690	0.0379	1.4858	0.4009
Avpi1	arginine vasopressin induced 1	2.1510	0.0380	1.9527	0.0963
LOC102547145		0.5260	0.0391	0.4740	0.0690
Srpx2	sushi repeat containing protein, X-linked 2	1.9295	0.0393	2.1069	0.0708
Ly86	lymphocyte antigen 86	2.1621	0.0394	1.8611	0.0564
Itga9	integrin subunit alpha 9	2.1157	0.0400	1.9086	0.0677
Ccdc28a	coiled-coil domain containing 28A	0.5700	0.0400	0.6854	0.3192
Iqgap2	IQ motif containing GTPase activating protein 2	0.5428	0.0400	0.4149	0.0599
Cers4	ceramide synthase 4	0.5569	0.0400	0.6403	0.1100
Sult1a1	sulfotransferase family 1A member 1	0.4401	0.0400	0.3987	0.0534
Slc27a1	solute carrier family 27 member 1	0.5628	0.0400	0.6002	0.0815
Efcab6	EF-hand calcium binding domain 6	2.0039	0.0400	2.1749	0.1911
Tagln2	transgelin 2	1.8354	0.0400	1.3734	0.2813
Ldlr	low density lipoprotein receptor	1.8171	0.0400	1.6550	0.2305
B3galt2	beta-1,3-galactosyltransferase 2	1.9858	0.0400	1.8765	0.2581
Sema3d	semaphorin 3D	1.9688	0.0400	1.4336	0.2150
Usp2	ubiquitin specific peptidase 2	0.5857	0.0400	0.7713	0.2813
Fzd2	frizzled class receptor 2	1.8169	0.0404	1.3394	0.2313
Plat	plasminogen activator, tissue type	2.0445	0.0404	1.1778	0.6730
Depdc1	DEP domain containing 1	2.2562	0.0408	1.4354	0.2718
Cd2	CD2 molecule	0.4858	0.0408	0.5881	0.2021
LOC102555672		0.5237	0.0408	0.6845	0.2256
Vash2	vasohibin 2	2.2300	0.0408	1.8462	0.0587
LOC691325		0.4863	0.0408	0.6113	0.5106
Gamt	guanidinoacetate N-methyltransferase	0.5395	0.0408	0.4704	0.0507
LOC685505		0.5202	0.0409	0.8508	0.7242
Acsl1	acyl-CoA synthetase long-chain family member 1	0.5407	0.0409	0.5964	0.0583
Herc3	HECT and RLD domain containing E3 ubiquitin protein ligase 3	0.5818	0.0409	0.6338	0.0708
RGD1311756		0.5685	0.0411	0.6728	0.1979
Ftl1l1		1.8416	0.0411	1.4486	0.3458
Mir32	microRNA 32	0.5535	0.0420	0.6622	0.3126
Tnfaip6	TNF alpha induced protein 6	2.0238	0.0426	1.1497	0.6728
Rhoq	ras homolog family member Q	2.2006	0.0426	1.9639	0.0762
Chi3l1	chitinase 3 like 1	3.6964	0.0427	2.5238	0.1078
Zfpm2	zinc finger protein, FOG family member 2	0.6203	0.0430	0.7231	0.2148
C1qb	complement C1q B chain	1.9006	0.0430	2.2538	0.1182
Ccnd1	cyclin D1	2.0780	0.0430	1.5976	0.1453
Hspa2	heat shock protein family A (Hsp70) member 2	1.7197	0.0430	1.1436	0.8045
Cnst	consortin, connexin sorting protein	0.5511	0.0430	0.6398	0.1283
Gcsam	germinal center associated signaling and motility	0.4676	0.0430	0.7320	0.2544
Gba3	glucosylceramidase beta 3 (gene/pseudogene)	3.2596	0.0430	2.4416	0.0599
Kcnd3	potassium voltage-gated channel subfamily D member 3	0.6145	0.0430	0.8157	0.4720
Cd55	CD55 molecule (Cromer blood group)	2.1780	0.0430	2.2225	0.0509
Il1rn	interleukin 1 receptor antagonist	1.8775	0.0430	1.9872	0.0690
Adamtsl2	ADAMTS like 2	1.9368	0.0430	1.7726	0.1660
Trpc6	transient receptor potential cation channel subfamily C member 6	2.4916	0.0430	2.0454	0.0902
Ankrd1	ankyrin repeat domain 1	1.7234	0.0430	1.4945	0.1008
Alk	anaplastic lymphoma receptor tyrosine kinase	1.6514	0.0430	0.8994	0.7564
Dip2c	disco interacting protein 2 homolog C	0.5769	0.0430	0.5966	0.1011
Mical2	microtubule associated monooxygenase, calponin and LIM domain containing 2	1.7775	0.0430	1.6038	0.0916
Pik3ip1	phosphoinositide-3-kinase interacting protein 1	0.5748	0.0430	0.8054	0.5728

		Fischer		SD	
Gene	Gene name	Fold change	adj p-value	Fold change	adj p-value
Stx11	syntaxin 11	2.5853	0.0430	2.5679	0.0583
Dcxr	dicarbonyl and L-xylulose reductase	0.5728	0.0430	0.5156	0.1644
Id4	inhibitor of DNA binding 4, HLH protein	1.6095	0.0430	1.2531	0.6149
RGD1563400		1.8654	0.0431	1.5826	0.0849
RGD1566399		0.5795	0.0431	0.7189	0.1729
Ttk	TTK protein kinase	2.0962	0.0431	1.7726	0.3890
Pde3a	phosphodiesterase 3A	0.5911	0.0431	0.6059	0.0690
Tax1bp3	Tax1 binding protein 3	1.6857	0.0431	1.3386	0.3984
Hadhb	hydroxyacyl-CoA dehydrogenase/3-ketoacyl-CoA thiolase/enoyl-CoA hydratase (trifunctional protein), beta subunit	0.5156	0.0431	0.5896	0.1100
Ywhag	tyrosine 3-monooxygenase/tryptophan 5-monooxygenase activation protein gamma	1.6019	0.0431	1.5089	0.1372
Pcmtd2	protein-L-isoaspartate (D-aspartate) O-methyltransferase domain containing 2	0.6111	0.0431	0.6668	0.1593
Adam1a	ADAM metallopeptidase domain 1A (pseudogene)	0.5637	0.0431	0.6560	0.1147
Idi1	isopentenyl-diphosphate delta isomerase 1	1.8086	0.0432	1.5498	0.1054
Smim19	small integral membrane protein 19	0.6286	0.0432	0.7805	0.2465
Fhl1	four and a half LIM domains 1	1.8109	0.0432	1.8584	0.0826
Scn3b	sodium voltage-gated channel beta subunit 3	4.9263	0.0432	4.0952	0.0564
Ucp3	uncoupling protein 3	0.5402	0.0432	0.4852	0.1986
LOC100360507		0.3470	0.0432	0.4618	0.0595
Cecr2	CECR2, histone acetyl-lysine reader	0.5280	0.0432	0.8546	0.4706
Maoa	monoamine oxidase A	2.7086	0.0432	2.6604	0.1266
Inpp4b	inositol polyphosphate-4-phosphatase type II B	0.5832	0.0432	0.6497	0.1283
Slc30a3	solute carrier family 30 member 3	1.7877	0.0432	1.1824	0.5721
Mfap5	microfibrillar associated protein 5	2.5310	0.0432	1.8905	0.1822
Cyb5b	cytochrome b5 type B	0.5977	0.0432	0.6025	0.0745
Mkx	mohawk homeobox	0.3716	0.0432	0.5581	0.1724
Hpd	4-hydroxyphenylpyruvate dioxygenase	0.5097	0.0432	0.7040	0.3932
Inpp5j	inositol polyphosphate-5-phosphatase J	1.7940	0.0432	1.4286	0.2618
Cd151	CD151 molecule (Raph blood group)	1.7044	0.0433	1.3413	0.2778
Tfdp2	transcription factor Dp-2	0.5909	0.0433	0.6689	0.1135
Ckb	creatine kinase B	2.0692	0.0433	1.3041	0.4051
Hist2h2bb	histone cluster 2 H2B family member b (pseudogene)	1.6798	0.0433	1.2991	0.4878
Zc3h6	zinc finger CCCH-type containing 6	0.5810	0.0433	0.6929	0.2595
Fbp2	fructose-bisphosphatase 2	0.5185	0.0433	0.6454	0.3914
Car4	carbonic anhydrase 4	0.5373	0.0433	0.7146	0.2939
Cnn3	calponin 3	1.6463	0.0433	1.4083	0.1745
Cep70	centrosomal protein 70	0.5513	0.0433	0.7431	0.3629
Rps6ka5	ribosomal protein S6 kinase A5	0.5553	0.0433	0.7109	0.3237
Edn1	endothelin 1	2.2115	0.0433	1.3092	0.3475
Uck2	uridine-cytidine kinase 2	1.6499	0.0433	1.2368	0.4720
Foxp2	forkhead box P2	0.5641	0.0433	0.6718	0.2570
Plk2	polo like kinase 2	2.2053	0.0437	1.8946	0.0690
Dirc2	disrupted in renal carcinoma 2	0.6000	0.0438	0.6392	0.0787
Thap4	THAP domain containing 4	0.5781	0.0443	0.6867	0.1701
Tet1	tet methylcytosine dioxygenase 1	0.5569	0.0445	0.7292	0.2845
Gfpt2	glutamine-fructose-6-phosphate transaminase 2	2.0138	0.0445	1.7986	0.1100
Tecrl	trans-2,3-enoyl-CoA reductase-like	0.5453	0.0446	0.6602	0.1370
Acot11	acyl-CoA thioesterase 11	0.6083	0.0446	0.7376	0.1946
Ube2q2l	ubiquitin conjugating enzyme E2 Q2 like	1.6740	0.0446	1.5306	0.2268
Pcp4l1	Purkinje cell protein 4 like 1	0.6121	0.0446	0.7912	0.4170
Fgf7	fibroblast growth factor 7	0.4164	0.0446	1.1174	0.8840
Bcat2	branched chain amino acid transaminase 2	0.5283	0.0447	0.4722	0.0627
Gem	GTP binding protein overexpressed in skeletal muscle	2.0273	0.0447	1.3833	0.3096
Epha3	EPH receptor A3	0.4144	0.0447	0.6100	0.1384
Ctsz	cathepsin Z	1.7250	0.0449	1.4547	0.2012
Dnajb5	DnaJ heat shock protein family (Hsp40) member B5	1.6924	0.0449	1.3241	0.2623
Mitf	melanogenesis associated transcription factor	0.6244	0.0449	0.7452	0.1821
Sh3pxd2b	SH3 and PX domains 2B	2.0287	0.0449	1.4692	0.1132
Fundc1	FUN14 domain containing 1	0.5994	0.0449	0.6424	0.1038
Gramd1b	GRAM domain containing 1B	0.6237	0.0449	0.8246	0.4929
LOC102551257		0.5839	0.0453	0.9896	0.9919
Erc1	ELKS/RAB6-interacting/CAST family member 1	0.6294	0.0453	0.6861	0.1923
Pls3	plastin 3	1.7026	0.0456	1.4876	0.1147
Fam81a	family with sequence similarity 81 member A	0.5034	0.0456	0.5230	0.1464
Fibin	fin bud initiation factor homolog (zebrafish)	4.4079	0.0456	2.9882	0.0971
Slc25a34	solute carrier family 25 member 34	0.5640	0.0456	0.6949	0.1302

		Fischer		SD	
Gene	Gene name	Fold change	adj p-value	Fold change	adj p-value
Lamb3	laminin subunit beta 3	2.3516	0.0456	1.6636	0.1132
Ctsa	cathepsin A	1.6322	0.0456	1.3181	0.3022
Lpcat3	lysophosphatidylcholine acyltransferase 3	0.5549	0.0456	0.5883	0.0541
Slamf8	SLAM family member 8	1.7277	0.0456	1.4198	0.4202
Tpm3	tropomyosin 3	1.5621	0.0456	1.3975	0.2813
Litaf	lipopolysaccharide induced TNF factor	1.7941	0.0458	1.4420	0.2030
Ccdc28b	coiled-coil domain containing 28B	0.6025	0.0458	0.6698	0.0838
Pnp	purine nucleoside phosphorylase	1.8572	0.0458	1.5731	0.1986
Gstz1	glutathione S-transferase zeta 1	0.3416	0.0458	0.3193	0.0529
Dcaf11	DDB1 and CUL4 associated factor 11	0.6299	0.0462	0.6825	0.1152
Klrb1a		0.4479	0.0464	0.5254	0.1231
Cdkal1	CDK5 regulatory subunit associated protein 1 like 1	0.5920	0.0464	0.8218	0.6087
RGD1305184		0.3534	0.0464	0.3026	0.0813
Ccdc85a	coiled-coil domain containing 85A	0.5072	0.0464	0.5855	0.1548
Il7r	interleukin 7 receptor	1.8120	0.0464	1.7763	0.0690
Baalc	brain and acute leukemia, cytoplasmic	0.4976	0.0464	0.7791	0.3012
Magix	MAGI family member, X-linked	0.5074	0.0464	0.5478	0.0595
Flnc	filamin C	1.6929	0.0472	1.7886	0.0553
Sema4d	semaphorin 4D	0.5060	0.0472	0.6202	0.0833
RGD1562667		0.5004	0.0472	0.8776	0.6924
Csf2rb	colony stimulating factor 2 receptor beta common subunit	1.6623	0.0472	1.1842	0.6920
RGD1566189		1.8958	0.0472	1.5528	0.2848
Slitrk1	SLIT and NTRK like family member 1	0.5715	0.0474	0.7519	0.5645
Ctsc	cathepsin C	0.5919	0.0474	0.6528	0.1006
Aldh6a1	aldehyde dehydrogenase 6 family member A1	0.6127	0.0474	0.6792	0.1155
Med21	mediator complex subunit 21	1.5595	0.0475	1.6007	0.0748
Egln3	egl-9 family hypoxia inducible factor 3	1.6414	0.0475	1.5696	0.1372
Disp1	dispatched RND transporter family member 1	0.6090	0.0477	0.8011	0.3892
Hmcn2	hemicentin 2	1.9314	0.0477	1.6644	0.1086
Fads3	fatty acid desaturase 3	1.6264	0.0477	1.3444	0.2649
Hadha	hydroxyacyl-CoA dehydrogenase/3-ketoacyl-CoA thiolase/enoyl-CoA hydratase (trifunctional protein), alpha subunit	0.5781	0.0477	0.5877	0.0570
Fcgr1a	Fc fragment of IgG receptor Ia	1.9368	0.0477	1.8465	0.1369
Iscu	iron-sulfur cluster assembly enzyme	1.6353	0.0477	1.5050	0.1622
Lipe	lipase E, hormone sensitive type	0.5737	0.0477	0.6316	0.1302
Adcy6	adenylate cyclase 6	0.6064	0.0477	0.6092	0.0591
Grn	granulin precursor	1.6460	0.0477	1.4517	0.3914
RGD1311251		0.5574	0.0477	0.9958	0.9923
Adcy1	adenylate cyclase 1	0.4542	0.0477	0.4073	0.0690
Pcdh7	protocadherin 7	0.6001	0.0477	0.6518	0.2091
Vom1r47		1.6251	0.0477	0.8817	0.7573
Gria1	glutamate ionotropic receptor AMPA type subunit 1	0.5874	0.0477	0.8105	0.6507
LOC102555217		0.6386	0.0478	1.0296	0.9724
Cyp2j4		0.5471	0.0482	0.6544	0.1468
Lancl1	LanC like 1	0.6091	0.0483	0.7195	0.1604
Slamf9	SLAM family member 9	2.0779	0.0484	1.8273	0.2232
Cd69	CD69 molecule	0.4899	0.0484	0.6739	0.2848
LOC100360205		0.5781	0.0484	0.9881	0.9754
Fxyd6	FXYD domain containing ion transport regulator 6	2.1596	0.0484	1.7110	0.0749
Ctsl	cathepsin L	1.5508	0.0486	1.4783	0.1529
Dlgap1	DLG associated protein 1	0.6011	0.0486	0.6854	0.2683
Htatip2	HIV-1 Tat interactive protein 2	1.5989	0.0489	1.2813	0.3142
Atg10	autophagy related 10	0.6463	0.0489	0.7319	0.1576
Ncapg	non-SMC condensin I complex subunit G	2.0647	0.0489	1.4956	0.4178
Ppargc1a	PPARG coactivator 1 alpha	0.5387	0.0495	0.6473	0.0847
Sh3bgrl3	SH3 domain binding glutamate rich protein like 3	1.6459	0.0496	1.2880	0.4354
Clnk	cytokine dependent hematopoietic cell linker	0.5944	0.0496	0.7224	0.3428
Fcer1g	Fc fragment of IgE receptor Ig	1.6729	0.0498	1.9070	0.0623
Hfe2	hemochromatosis type 2 (juvenile)	0.4598	0.0564	0.4152	0.0214
Lsamp	limbic system-associated membrane protein	0.2445	0.0569	0.2545	0.0058
Abca5	ATP binding cassette subfamily A member 5	3.0678	0.0582	2.6446	0.0321
Plod2	procollagen-lysine,2-oxoglutarate 5-dioxygenase 2	2.7881	0.0607	3.3632	0.0236
Rxrg	retinoid X receptor gamma	0.4570	0.0610	0.4502	0.0277
Klrc1	killer cell lectin like receptor C1	0.5227	0.0616	0.4838	0.0443
Kcna2	potassium voltage-gated channel subfamily A member 2	0.3121	0.0652	0.4640	0.0456
Ephx2	epoxide hydrolase 2	0.6024	0.0652	0.4348	0.0443
Crat	carnitine O-acetyltransferase	0.5657	0.0652	0.5435	0.0443

		Fischer		SD	
Gene	**Gene name**	**Fold change**	**adj p-value**	**Fold change**	**adj p-value**
Asb4	ankyrin repeat and SOCS box containing 4	0.4474	0.0675	0.4280	0.0371
Aqp7	aquaporin 7	0.2366	0.0696	0.1947	0.0455
Fitm1	fat storage inducing transmembrane protein 1	0.5480	0.0696	0.4984	0.0321
Pi16	peptidase inhibitor 16	2.4583	0.0698	2.7178	0.0472
Fkbp4	FK506 binding protein 4	0.4960	0.0702	0.4556	0.0236
Hadh	hydroxyacyl-CoA dehydrogenase	0.4212	0.0750	0.4196	0.0277
Mybl1	MYB proto-oncogene like 1	2.3660	0.0752	3.1589	0.0419
Tmod4	tropomodulin 4	0.3977	0.0758	0.3910	0.0236
Dhrs7c	dehydrogenase/reductase 7C	0.2363	0.0768	0.2433	0.0122
Macrod1	MACRO domain containing 1	0.4885	0.0824	0.4411	0.0277
Uap1	UDP-N-acetylglucosamine pyrophosphorylase 1	2.2610	0.0824	2.0719	0.0491
Kcnd2	potassium voltage-gated channel subfamily D member 2	0.3095	0.0845	0.3031	0.0122
Clcn4	chloride voltage-gated channel 4	0.5265	0.0845	0.4822	0.0258
Fap	fibroblast activation protein alpha	2.3651	0.0877	2.8794	0.0122
Cxcr4	C-X-C motif chemokine receptor 4	2.3851	0.0902	2.0009	0.0410
Clec5a	C-type lectin domain family 5 member A	1.8990	0.0939	2.8644	0.0277
Art1	ADP-ribosyltransferase 1	0.3555	0.1077	0.2052	0.0132
Fitm2	fat storage inducing transmembrane protein 2	0.5290	0.1101	0.4200	0.0491
Tnfsf18	tumor necrosis factor superfamily member 18	2.1695	0.1174	2.3636	0.0323
Fam111a	family with sequence similarity 111 member A	2.0780	0.1226	2.6403	0.0277
Foxo1	forkhead box O1	0.6902	0.1385	0.5417	0.0491
Hhatl	hedgehog acyltransferase-like	0.5383	0.1387	0.4082	0.0142
Sbsn	suprabasin	2.6016	0.1445	3.0569	0.0277
Pfkm	phosphofructokinase, muscle	0.5536	0.1451	0.5077	0.0410
Depdc7	DEP domain containing 7	2.0160	0.1554	2.7717	0.0319
Rpl3l	ribosomal protein L3 like	0.4694	0.1722	0.5327	0.0320
Xpr1	xenotropic and polytropic retrovirus receptor 1	1.9265	0.1931	1.9420	0.0319
Fndc5	fibronectin type III domain containing 5	0.6285	0.2257	0.4931	0.0296
Aoah	acyloxyacyl hydrolase	1.2598	0.4124	2.0271	0.0410
LOC102554467		0.7951	0.5535	0.3352	0.0258
Zim1		0.8618	0.7738	0.4213	0.0277
Fam110c	family with sequence similarity 110 member C	1.0046	0.9916	2.4596	0.0154

Upregulated in both strains

Gene	Gene name	Fold change	adj p-value	Fold change	adj p-value
Cyp1a1	cytochrome P450 family 1 subfamily A member 1	18.5171	0.0007	19.9919	0.0014
Tceal7	transcription elongation factor A like 7	11.1439	0.0007	9.0831	0.0115
Rcan1	regulator of calcineurin 1	3.1554	0.0092	2.4327	0.0258
Tnfrsf12a	TNF receptor superfamily member 12A	4.0118	0.0092	3.2911	0.0154
Mest	mesoderm specific transcript	3.0619	0.0092	2.4075	0.0410
Acta1	actin, alpha 1, skeletal muscle	11.1305	0.0097	5.5002	0.0455
Amica1	junction adhesion molecule like	3.4190	0.0097	2.4180	0.0258
Akip1	A-kinase interacting protein 1	6.5008	0.0154	6.5742	0.0036
Ankrd23	ankyrin repeat domain 23	7.9228	0.0159	10.4485	0.0122
Bex1	brain expressed X-linked 1	6.6050	0.0172	7.3223	0.0122
Myot	myotilin	2.5365	0.0174	2.9235	0.0277
Fxyd5	FXYD domain containing ion transport regulator 5	3.0398	0.0174	2.5173	0.0190
Tlr5	toll like receptor 5	2.2476	0.0187	2.3341	0.0456
Ncam1	neural cell adhesion molecule 1	6.9153	0.0187	7.4160	0.0190
Tgfb2	transforming growth factor beta 2	6.2014	0.0209	4.7572	0.0400
Ccnd2	cyclin D2	2.2115	0.0219	2.2701	0.0367
Cyp1b1	cytochrome P450 family 1 subfamily B member 1	5.8359	0.0219	4.2054	0.0256
Tsc22d1	TSC22 domain family member 1	2.7726	0.0225	2.5858	0.0132
Osmr	oncostatin M receptor	2.2309	0.0232	2.1514	0.0296
Thbs1	thrombospondin 1	5.0405	0.0232	3.1856	0.0442
Ahrr	aryl-hydrocarbon receptor repressor	2.7523	0.0272	2.3674	0.0410
Fgf23	fibroblast growth factor 23	9.1111	0.0272	4.5384	0.0277
Ifitm1	interferon induced transmembrane protein 1	2.6934	0.0272	2.0651	0.0320
Rnd1	Rho family GTPase 1	4.9707	0.0272	4.2722	0.0230
RGD1559864		2.7574	0.0274	2.1238	0.0410
Gclc	glutamate-cysteine ligase catalytic subunit	2.0524	0.0291	2.0330	0.0491
Postn	periostin	8.8373	0.0291	7.0604	0.0491
Enah	enabled homolog (Drosophila)	2.7077	0.0291	2.4483	0.0277
LOC100910669		2.1784	0.0292	2.5888	0.0443
Ctgf	connective tissue growth factor	4.8038	0.0292	3.5118	0.0367
Tmem100	transmembrane protein 100	3.3493	0.0312	3.6365	0.0236

		Fischer		SD	
Gene	**Gene name**	**Fold change**	**adj p-value**	**Fold change**	**adj p-value**
Col8a1	collagen type VIII alpha 1 chain	6.1455	0.0318	6.4619	0.0251
C3	complement C3	2.1784	0.0322	1.9973	0.0410
Timp1	TIMP metallopeptidase inhibitor 1	3.1414	0.0327	3.2529	0.0122
Olr1	oxidized low density lipoprotein receptor 1	5.4220	0.0338	8.2207	0.0122
Wbp5	transcription elongation factor A like 9	1.9770	0.0361	1.9143	0.0320
RGD1311744		4.5079	0.0361	3.5994	0.0277
Thbs4	thrombospondin 4	16.5124	0.0362	10.1139	0.0125
Prss23	protease, serine 23	2.3515	0.0420	2.5018	0.0431
Cx3cr1	C-X3-C motif chemokine receptor 1	2.3420	0.0430	2.4459	0.0376
Xirp2	xin actin binding repeat containing 2	2.6386	0.0431	3.0736	0.0151
Cilp	cartilage intermediate layer protein	6.6490	0.0444	6.7025	0.0132
Ltbp2	latent transforming growth factor beta binding protein 2	7.4955	0.0446	6.1763	0.0368
Loxl2	lysyl oxidase like 2	2.5768	0.0449	2.3845	0.0304
MGC105649		2.5626	0.0456	2.6759	0.0258
Cxcl16	C-X-C motif chemokine ligand 16	2.2244	0.0456	2.5248	0.0154
Sorbs2	sorbin and SH3 domain containing 2	1.7747	0.0472	1.9178	0.0367
Serpine2	serpin family E member 2	3.7100	0.0477	3.4697	0.0236
Nupr1	nuclear protein 1, transcriptional regulator	3.6261	0.0484	2.6827	0.0277
Downregulated in both strains					
Gene	Gene name	Fold change	adj p-value	Fold change	adj p-value
Cacng6	calcium voltage-gated channel auxiliary subunit gamma 6	0.2624	0.0092	0.3896	0.0258
Kir3dl1	killer cell immunoglobulin like receptor, three Ig domains and long cytoplasmic tail 1	0.2832	0.0092	0.4109	0.0258
Ddit4l	DNA damage inducible transcript 4 like	0.2523	0.0154	0.1839	0.0036
Klhl33	kelch like family member 33	0.3387	0.0169	0.2926	0.0122
Gpam	glycerol-3-phosphate acyltransferase, mitochondrial	0.3731	0.0169	0.4247	0.0435
Angpt1	angiopoietin 1	0.1475	0.0169	0.2580	0.0266
Ros1	ROS proto-oncogene 1, receptor tyrosine kinase	0.3535	0.0288	0.4413	0.0407
Kcnk2	potassium two pore domain channel subfamily K member 2	0.2946	0.0288	0.2547	0.0189
Scn4b	sodium voltage-gated channel beta subunit 4	0.2675	0.0291	0.2761	0.0218
Deptor	DEP domain containing MTOR interacting protein	0.5285	0.0291	0.5071	0.0312
Atp6ap1l	ATPase H+ transporting accessory protein 1 like	0.1626	0.0292	0.2850	0.0236
Stc2	stanniocalcin 2	0.4889	0.0292	0.4642	0.0277
Pcdh11x	protocadherin 11 X-linked	0.3645	0.0292	0.4130	0.0154
Nudt4	nudix hydrolase 4	0.4203	0.0293	0.3905	0.0277
Slc25a42	solute carrier family 25 member 42	0.5063	0.0322	0.4913	0.0320
Cxadr	coxsackie virus and adenovirus receptor	0.4989	0.0323	0.4568	0.0277
Acacb	acetyl-CoA carboxylase beta	0.4314	0.0327	0.5231	0.0367
Tmem116	transmembrane protein 116	0.5546	0.0356	0.5792	0.0491
Atp1a2	ATPase Na+/K+ transporting subunit alpha 2	0.3742	0.0362	0.3195	0.0320
Myo16	myosin XVI	0.2895	0.0362	0.5090	0.0407
Eci1	enoyl-CoA delta isomerase 1	0.4324	0.0362	0.4091	0.0420
Myo10	myosin X	0.5215	0.0362	0.5310	0.0320
Acsf2	acyl-CoA synthetase family member 2	0.4230	0.0387	0.5071	0.0456
Mlycd	malonyl-CoA decarboxylase	0.5195	0.0430	0.5251	0.0457
Ech1	enoyl-CoA hydratase 1	0.3300	0.0431	0.3291	0.0400
Ano5	anoctamin 5	0.4978	0.0433	0.1547	0.0058
Il2rb	interleukin 2 receptor subunit beta	0.4767	0.0437	0.3749	0.0132
Selenbp1	selenium binding protein 1	0.4853	0.0443	0.4630	0.0420
Adra1b	adrenoceptor alpha 1B	0.4688	0.0456	0.5236	0.0320
Rbfox1	RNA binding protein, fox-1 homolog 1	0.3527	0.0458	0.4154	0.0265
Lpin1	lipin 1	0.5031	0.0469	0.4324	0.0320
Cdnf	cerebral dopamine neurotrophic factor	0.4915	0.0472	0.4990	0.0457

Appendix Table 3-4. GO Term enrichment analysis for SD subset

GO term	Count	P-Value Genes
Embryogenesis	3	0.032027262 XPR1, FOXO1, HHATL

Appendix Table 3-5. GO Term enrichment analysis for both strains subset

GO term	Count	P-Value	Genes
Fatty acid metabolism	5	0.00725223	ECH1, CYP1B1, CYP1A1, ACACB, ACSF2
Cell communication	10	0.03060527	NCAM1, AHRR, LTBP2, CTGF, PCDH11X, FGF23, ANGPT1, COL8A1, AMICA1, KIR3DL1
Lipid, fatty acid and steroid metabolism	8	0.031723598	ECH1, CYP1B1, NUDT4, CYP1A1, ACACB, GPAM, LPIN1, ACSF2
Immunity and defense	11	0.04201403	IL2RB, AHRR, IFITM1, C3, CXCL16, CX3CR1, SELENBP1, THBS1, CXADR, KIR3DL1, THBS4
Receptor protein tyrosine kinase signaling pathway	4	0.047277736	CTGF, FGF23, ANGPT1, ROS1
Developmental processes	14	0.058482062	LTBP2, PCDH11X, RCAN1, POSTN, TLR5, LPIN1, TGFB2, TIMP1, NCAM1, ADRA1B, ANGPT1, THBS1, ROS1, THBS4
Cytokine and chemokine mediated signaling pathway	4	0.061125532	IL2RB, OSMR, CX3CR1, TLR5
Other developmental process	3	0.062572317	THBS1, TIMP1, THBS4

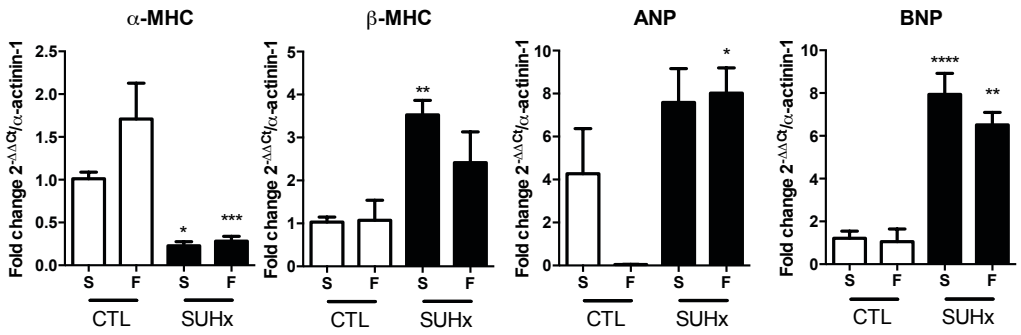

Appendix Figure 3-1. Right ventricular expression of genes involved in cardiac remodeling in Fischer and SD rats +/- SUHx measured by quantitative RT-PCR.
*,**,***,**** $p<0.05$, 0.01, 0.001, 0.0001 vs control. n = 3-6 per group using alpha-actinin-1 as housekeeping gene

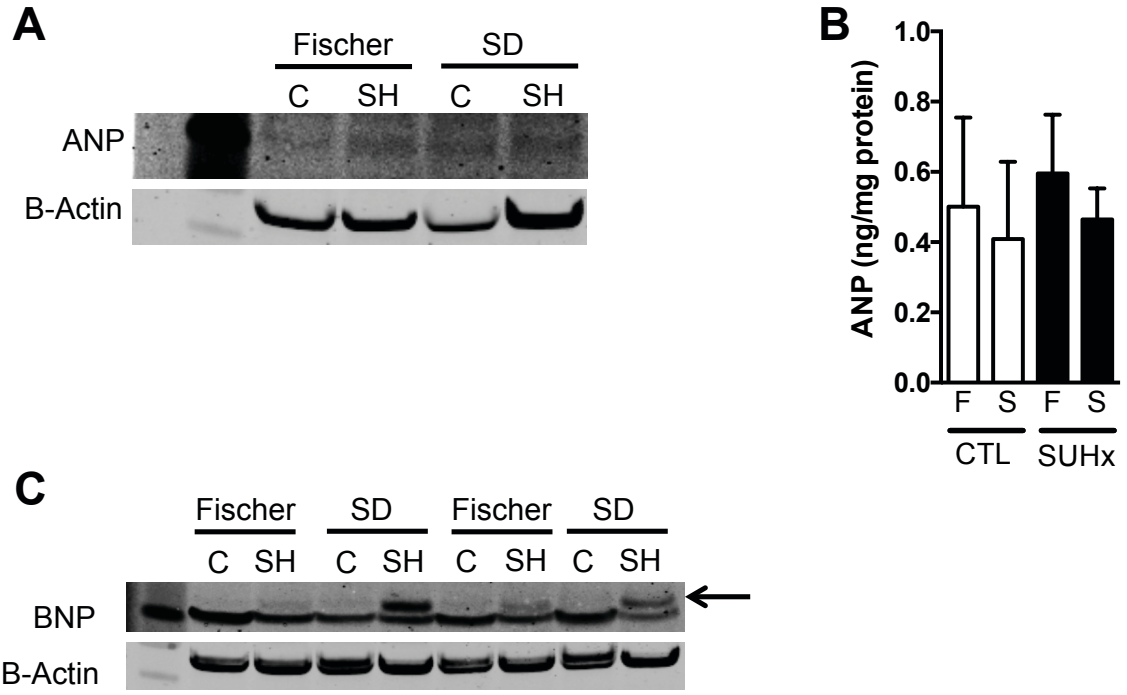

Appendix Figure 3-2. Natriuretic peptide expression in RV. A. Representative image of a western-blot demonstrating ANP protein expression in RV of SD and Fischer +/- SUHx; n=3-4 per group. B. ANP levels in the RV (n=3-5 per group) of SD and Fischer +/- SUHx. C. Representative image of a western-blot showing BNP protein expression in RV of SD and Fischer +/- SUHx; n=3-4 per group.

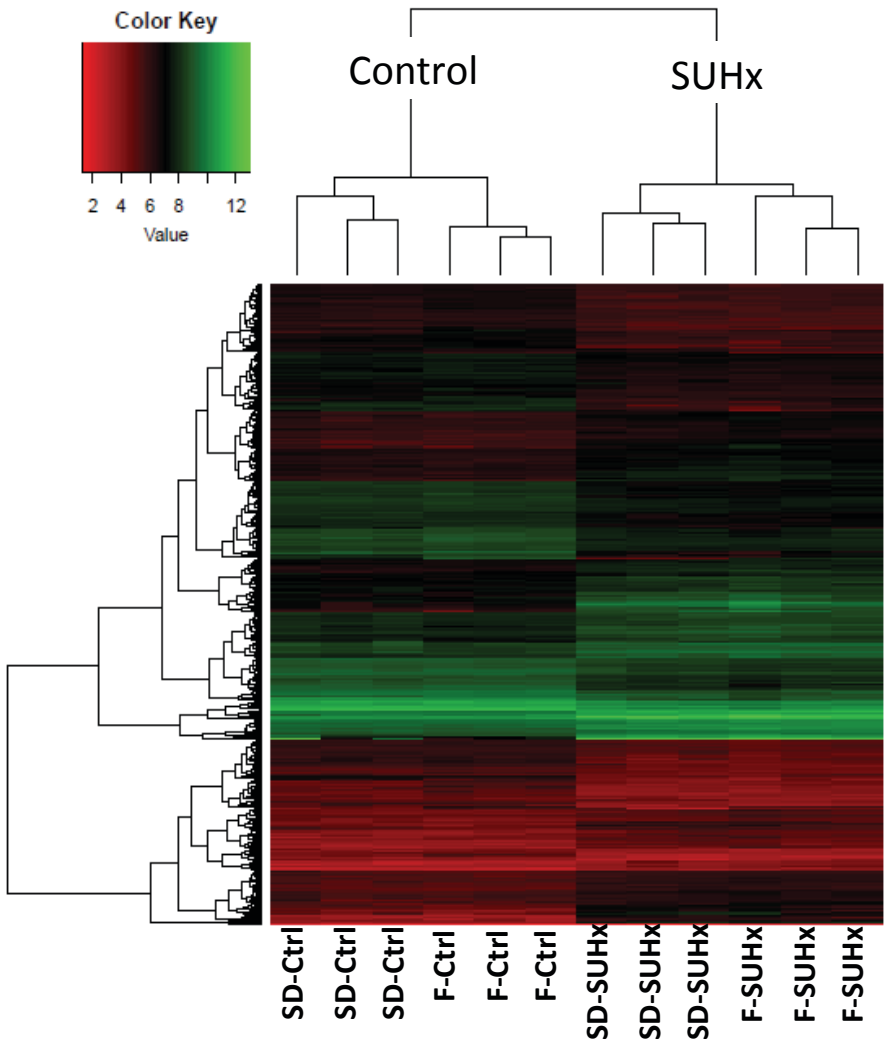

Appendix Figure 3-3. Heatmap demonstrating differentially expressed genes in RV of SUHx Sprague-Dawley or Fischer CDF rats compared to respective controls.

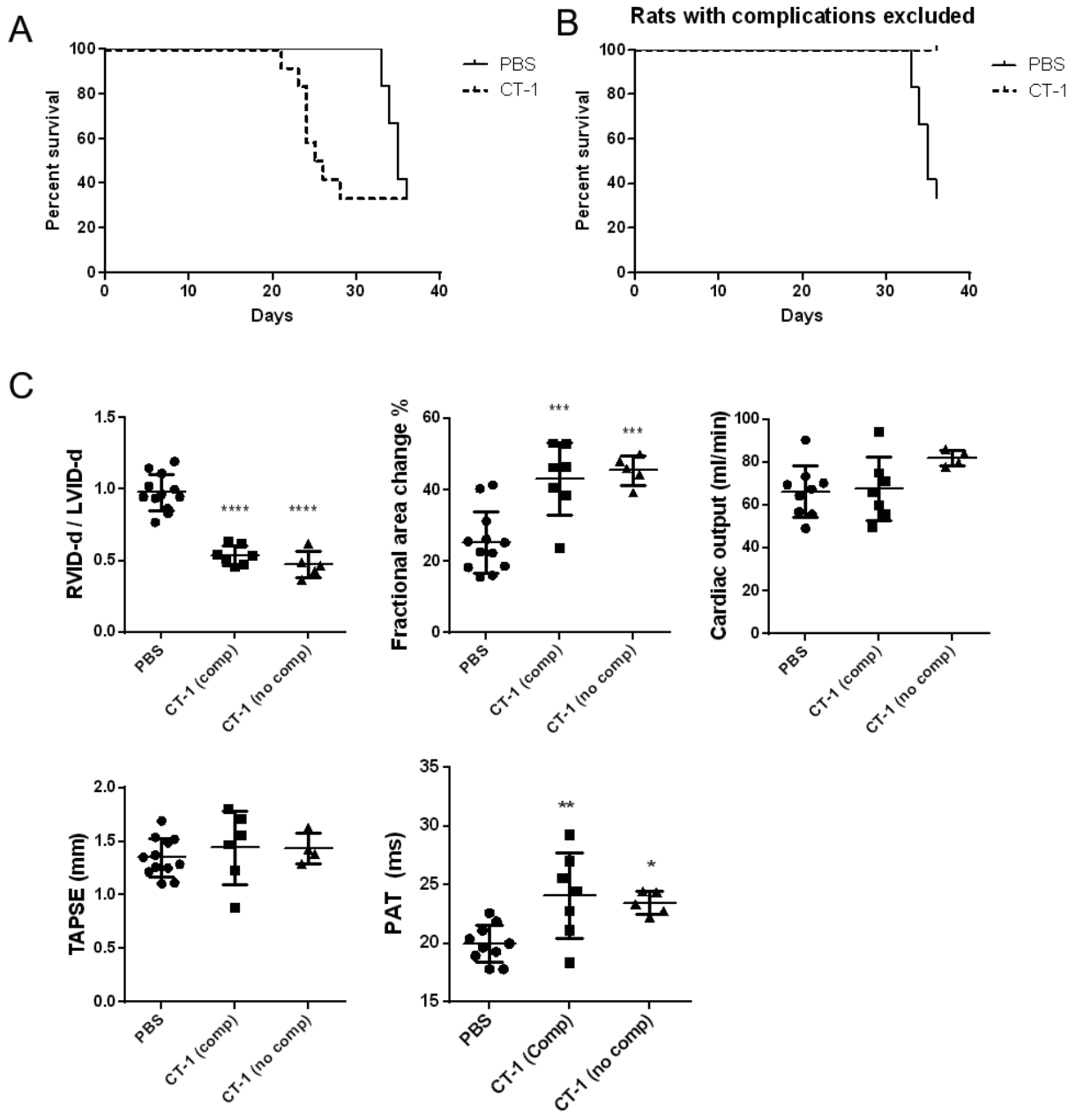

Appendix Fig 4-1. Terminal analysis of CT-1-treated rats with and without complications. (A) Percent survival in all rats compared to (B) rats with complications excluded. (C) RVID-d/LVID-d, FAC, CO, TAPSE, PAT were similar with complications and without. *, **, ***, *** $p < 0.05, 0.01, 0.001, 0.0001$ vs control (One-way ANOVA with Tukey's)

References

1. Simonneau, G.*, et al.* Clinical classification of pulmonary hypertension. *Journal of the American College of Cardiology* **43**, 5S-12S (2004).
2. Simonneau, G.*, et al.* Updated clinical classification of pulmonary hypertension. *Journal of the American College of Cardiology* **62**, D34-41 (2013).
3. Simonneau, G.*, et al.* Updated clinical classification of pulmonary hypertension. *Journal of the American College of Cardiology* **54**, S43-54 (2009).
4. Gaine, S. Pulmonary hypertension. *JAMA* **284**, 3160-3168 (2000).
5. Humbert, M.*, et al.* Pulmonary arterial hypertension in France: results from a national registry. *Am J Respir Crit Care Med* **173**, 1023-1030 (2006).
6. Frost, A.E.*, et al.* The changing picture of patients with pulmonary arterial hypertension in the United States: how REVEAL differs from historic and non-US Contemporary Registries. *Chest* **139**, 128-137 (2011).
7. McLaughlin, V.V.*, et al.* ACCF/AHA 2009 expert consensus document on pulmonary hypertension: a report of the American College of Cardiology Foundation Task Force on Expert Consensus Documents and the American Heart Association: developed in collaboration with the American College of Chest Physicians, American Thoracic Society, Inc., and the Pulmonary Hypertension Association. *Circulation* **119**, 2250-2294 (2009).
8. Humbert, M.*, et al.* Cellular and molecular pathobiology of pulmonary arterial hypertension. *Journal of the American College of Cardiology* **43**, 13S-24S (2004).
9. Schermuly, R.T., Ghofrani, H.A., Wilkins, M.R. & Grimminger, F. Mechanisms of disease: pulmonary arterial hypertension. *Nat Rev Cardiol* (2011).
10. Humbert, M., Sitbon, O. & Simonneau, G. Treatment of pulmonary arterial hypertension. *The New England journal of medicine* **351**, 1425-1436 (2004).
11. Stacher, E.*, et al.* Modern age pathology of pulmonary arterial hypertension. *Am J Respir Crit Care Med* **186**, 261-272 (2012).
12. Budhiraja, R., Tuder, R.M. & Hassoun, P.M. Endothelial dysfunction in pulmonary hypertension. *Circulation* **109**, 159-165 (2004).
13. Tuder, R.M.*, et al.* The pathobiology of pulmonary hypertension. Endothelium. *Clin Chest Med* **22**, 405-418 (2001).
14. Nicod, L.P. The endothelium and genetics in pulmonary arterial hypertension. *Swiss Med Wkly* **137**, 437-442 (2007).
15. Tuder, R.M.*, et al.* Prostacyclin synthase expression is decreased in lungs from patients with severe pulmonary hypertension. *Am J Respir Crit Care Med* **159**, 1925-1932 (1999).
16. Giaid, A. & Saleh, D. Reduced expression of endothelial nitric oxide synthase in the lungs of patients with pulmonary hypertension. *The New England journal of medicine* **333**, 214-221 (1995).
17. Christman, B.W.*, et al.* An imbalance between the excretion of thromboxane and prostacyclin metabolites in pulmonary hypertension. *The New England journal of medicine* **327**, 70-75 (1992).
18. Giaid, A.*, et al.* Expression of endothelin-1 in the lungs of patients with pulmonary hypertension. *The New England journal of medicine* **328**, 1732-1739 (1993).

19. Wedgwood, S., Dettman, R.W. & Black, S.M. ET-1 stimulates pulmonary arterial smooth muscle cell proliferation via induction of reactive oxygen species. *Am J Physiol Lung Cell Mol Physiol* **281**, L1058-1067 (2001).
20. Cardillo, C., Kilcoyne, C.M., Cannon, R.O., 3rd & Panza, J.A. Interactions between nitric oxide and endothelin in the regulation of vascular tone of human resistance vessels in vivo. *Hypertension* **35**, 1237-1241 (2000).
21. Stenmark, K.R. & Mecham, R.P. Cellular and molecular mechanisms of pulmonary vascular remodeling. *Annu Rev Physiol* **59**, 89-144 (1997).
22. Jeffery, T.K. & Morrell, N.W. Molecular and cellular basis of pulmonary vascular remodeling in pulmonary hypertension. *Prog Cardiovasc Dis* **45**, 173-202 (2002).
23. Campbell, A.I., Zhao, Y., Sandhu, R. & Stewart, D.J. Cell-based gene transfer of vascular endothelial growth factor attenuates monocrotaline-induced pulmonary hypertension. *Circulation* **104**, 2242-2248 (2001).
24. Kugathasan, L.*, et al.* Role of angiopoietin-1 in experimental and human pulmonary arterial hypertension. *Chest* **128**, 633S-642S (2005).
25. Michelakis, E.D. Spatio-temporal diversity of apoptosis within the vascular wall in pulmonary arterial hypertension: heterogeneous BMP signaling may have therapeutic implications. *Circ Res* **98**, 172-175 (2006).
26. Zhao, Y.D., Campbell, A.I., Robb, M., Ng, D. & Stewart, D.J. Protective role of angiopoietin-1 in experimental pulmonary hypertension. *Circ Res* **92**, 984-991 (2003).
27. Zhao, Y.D.*, et al.* Microvascular regeneration in established pulmonary hypertension by angiogenic gene transfer. *Am J Respir Cell Mol Biol* **35**, 182-189 (2006).
28. Farber, H.W. Pathophysiology of Pulmonary Arterial Hypertension. in *Pulmonary Hypertension* (eds. Hill, N.S. & Farber, H.W.) 51-72 (Humana Press, Totowa, NJ, 2008).
29. Taraseviciene-Stewart, L.*, et al.* Inhibition of the VEGF receptor 2 combined with chronic hypoxia causes cell death-dependent pulmonary endothelial cell proliferation and severe pulmonary hypertension. *FASEB J* **15**, 427-438 (2001).
30. Sakao, S.*, et al.* Initial apoptosis is followed by increased proliferation of apoptosis-resistant endothelial cells. *FASEB J* **19**, 1178-1180 (2005).
31. Hirschi, K.K. & D'Amore, P.A. Pericytes in the microvasculature. *Cardiovasc Res* **32**, 687-698 (1996).
32. Tozzi, C.A., Christiansen, D.L., Poiani, G.J. & Riley, D.J. Excess collagen in hypertensive pulmonary arteries decreases vascular distensibility. *Am J Respir Crit Care Med* **149**, 1317-1326 (1994).
33. Todorovich-Hunter, L.*, et al.* Increased pulmonary artery elastolytic activity in adult rats with monocrotaline-induced progressive hypertensive pulmonary vascular disease compared with infant rats with nonprogressive disease. *Am Rev Respir Dis* **146**, 213-223 (1992).
34. Zhu, L.*, et al.* The endogenous vascular elastase that governs development and progression of monocrotaline-induced pulmonary hypertension in rats is a novel enzyme related to the serine proteinase adipsin. *J Clin Invest* **94**, 1163-1171 (1994).
35. Thompson, M.M. & Squire, I.B. Matrix metalloproteinase-9 expression after myocardial infarction: physiological or pathological? *Cardiovasc Res* **54**, 495-498 (2002).
36. Okada, Y. & Nakanishi, I. Activation of matrix metalloproteinase 3 (stromelysin) and matrix metalloproteinase 2 ('gelatinase') by human neutrophil elastase and cathepsin G. *FEBS Lett* **249**, 353-356 (1989).
37. Jones, P.L. & Rabinovitch, M. Tenascin-C is induced with progressive pulmonary vascular disease in rats and is functionally related to increased smooth muscle cell proliferation. *Circ Res* **79**, 1131-1142 (1996).

38. Meyrick, B. & Reid, L. Hypoxia and incorporation of 3H-thymidine by cells of the rat pulmonary arteries and alveolar wall. *Am J Pathol* **96**, 51-70 (1979).
39. Foster, W.S., Suen, C.M. & Stewart, D.J. Regenerative Cell and Tissue-based Therapies for Pulmonary Arterial Hypertension. *Canadian Journal of Cardiology* **30**, 1350-1360 (2014).
40. Frid, M.G., Kale, V.A. & Stenmark, K.R. Mature vascular endothelium can give rise to smooth muscle cells via endothelial-mesenchymal transdifferentiation: in vitro analysis. *Circ Res* **90**, 1189-1196 (2002).
41. Short, M., Nemenoff, R.A., Zawada, W.M., Stenmark, K.R. & Das, M. Hypoxia induces differentiation of pulmonary artery adventitial fibroblasts into myofibroblasts. *Am J Physiol Cell Physiol* **286**, C416-425 (2004).
42. Atkinson, C*., et al.* Primary pulmonary hypertension is associated with reduced pulmonary vascular expression of type II bone morphogenetic protein receptor. *Circulation* **105**, 1672-1678 (2002).
43. Yi, E.S*., et al.* Distribution of obstructive intimal lesions and their cellular phenotypes in chronic pulmonary hypertension. A morphometric and immunohistochemical study. *Am J Respir Crit Care Med* **162**, 1577-1586 (2000).
44. Michelakis, E.D., Wilkins, M.R. & Rabinovitch, M. Emerging concepts and translational priorities in pulmonary arterial hypertension. *Circulation* **118**, 1486-1495 (2008).
45. Cool, C.D., Groshong, S.D., Oakey, J. & Voelkel, N.F. Pulmonary hypertension: cellular and molecular mechanisms. *Chest* **128**, 565S-571S (2005).
46. Masri, F.A*., et al.* Hyperproliferative apoptosis-resistant endothelial cells in idiopathic pulmonary arterial hypertension. *Am J Physiol Lung Cell Mol Physiol* **293**, L548-554 (2007).
47. Tuder, R.M., Groves, B., Badesch, D.B. & Voelkel, N.F. Exuberant endothelial cell growth and elements of inflammation are present in plexiform lesions of pulmonary hypertension. *Am J Pathol* **144**, 275-285 (1994).
48. Lee, S.D*., et al.* Monoclonal endothelial cell proliferation is present in primary but not secondary pulmonary hypertension. *J Clin Invest* **101**, 927-934 (1998).
49. Wright, L*., et al.* 5-Lipoxygenase and 5-lipoxygenase activating protein (FLAP) immunoreactivity in lungs from patients with primary pulmonary hypertension. *Am J Respir Crit Care Med* **157**, 219-229 (1998).
50. Richter, A*., et al.* Impaired transforming growth factor-beta signaling in idiopathic pulmonary arterial hypertension. *Am J Respir Crit Care Med* **170**, 1340-1348 (2004).
51. Yeager, M.E., Golpon, H.A., Voelkel, N.F. & Tuder, R.M. Microsatellite mutational analysis of endothelial cells within plexiform lesions from patients with familial, pediatric, and sporadic pulmonary hypertension. *Chest* **121**, 61S (2002).
52. Cool, C.D*., et al.* Three-dimensional reconstruction of pulmonary arteries in plexiform pulmonary hypertension using cell-specific markers. Evidence for a dynamic and heterogeneous process of pulmonary endothelial cell growth. *Am J Pathol* **155**, 411-419 (1999).
53. Stenmark, K.R., Meyrick, B., Galie, N., Mooi, W.J. & McMurtry, I.F. Animal models of pulmonary arterial hypertension: the hope for etiological discovery and pharmacological cure. *Am J Physiol Lung Cell Mol Physiol* **297**, L1013-1032 (2009).
54. White, R.J*., et al.* Plexiform-like lesions and increased tissue factor expression in a rat model of severe pulmonary arterial hypertension. *Am J Physiol Lung Cell Mol Physiol* **293**, L583-590 (2007).
55. Nishimura, T*., et al.* Simvastatin rescues rats from fatal pulmonary hypertension by inducing apoptosis of neointimal smooth muscle cells. *Circulation* **108**, 1640-1645 (2003).

56. Okada, K., Bernstein, M.L., Zhang, W., Schuster, D.P. & Botney, M.D. Angiotensin-converting enzyme inhibition delays pulmonary vascular neointimal formation. *Am J Respir Crit Care Med* **158**, 939-950 (1998).
57. Abe, K.*, et al.* Formation of plexiform lesions in experimental severe pulmonary arterial hypertension. *Circulation* **121**, 2747-2754 (2010).
58. Ivy, D.D.*, et al.* Development of occlusive neointimal lesions in distal pulmonary arteries of endothelin B receptor-deficient rats: a new model of severe pulmonary arterial hypertension. *Circulation* **111**, 2988-2996 (2005).
59. Steiner, M.K.*, et al.* Interleukin-6 overexpression induces pulmonary hypertension. *Circ Res* **104**, 236-244, 228p following 244 (2009).
60. Dai, Z., Li, M., Wharton, J., Zhu, M.M. & Zhao, Y.Y. Prolyl-4 Hydroxylase 2 (PHD2) Deficiency in Endothelial Cells and Hematopoietic Cells Induces Obliterative Vascular Remodeling and Severe Pulmonary Arterial Hypertension in Mice and Humans Through Hypoxia-Inducible Factor-2alpha. *Circulation* **133**, 2447-2458 (2016).
61. Ryan, J.J., Marsboom, G. & Archer, S.L. Rodent models of group 1 pulmonary hypertension. *Handbook of experimental pharmacology* **218**, 105-149 (2013).
62. Kay, J.M., Harris, P. & Heath, D. Pulmonary hypertension produced in rats by ingestion of Crotalaria spectabilis seeds. *Thorax* **22**, 176-179 (1967).
63. Urboniene, D., Haber, I., Fang, Y.H., Thenappan, T. & Archer, S.L. Validation of high-resolution echocardiography and magnetic resonance imaging vs. high-fidelity catheterization in experimental pulmonary hypertension. *Am J Physiol Lung Cell Mol Physiol* **299**, L401-412 (2010).
64. Nakayama Wong, L.S., Lame, M.W., Jones, A.D. & Wilson, D.W. Differential cellular responses to protein adducts of naphthoquinone and monocrotaline pyrrole. *Chemical research in toxicology* **23**, 1504-1513 (2010).
65. Wagner, J.G., Petry, T.W. & Roth, R.A. Characterization of monocrotaline pyrrole-induced DNA cross-linking in pulmonary artery endothelium. *The American journal of physiology* **264**, L517-522 (1993).
66. Huang, J., Wolk, J.H., Gewitz, M.H. & Mathew, R. Progressive endothelial cell damage in an inflammatory model of pulmonary hypertension. *Experimental lung research* **36**, 57-66 (2010).
67. Ramos, M., Lame, M.W., Segall, H.J. & Wilson, D.W. Monocrotaline pyrrole induces Smad nuclear accumulation and altered signaling expression in human pulmonary arterial endothelial cells. *Vascular pharmacology* **46**, 439-448 (2007).
68. Long, L.*, et al.* Altered bone morphogenetic protein and transforming growth factor-beta signaling in rat models of pulmonary hypertension: potential for activin receptor-like kinase-5 inhibition in prevention and progression of disease. *Circulation* **119**, 566-576 (2009).
69. Morty, R.E.*, et al.* Dysregulated bone morphogenetic protein signaling in monocrotaline-induced pulmonary arterial hypertension. *Arterioscler Thromb Vasc Biol* **27**, 1072-1078 (2007).
70. Wilson, D.W., Segall, H.J., Pan, L.C. & Dunston, S.K. Progressive inflammatory and structural changes in the pulmonary vasculature of monocrotaline-treated rats. *Microvascular research* **38**, 57-80 (1989).
71. Pan, L.C., Lame, M.W., Morin, D., Wilson, D.W. & Segall, H.J. Red blood cells augment transport of reactive metabolites of monocrotaline from liver to lung in isolated and tandem liver and lung preparations. *Toxicology and applied pharmacology* **110**, 336-346 (1991).
72. Gomez-Arroyo, J.G.*, et al.* The monocrotaline model of pulmonary hypertension in perspective. *Am J Physiol Lung Cell Mol Physiol* **302**, L363-369 (2012).
73. Woods, L.W., Wilson, D.W. & Segall, H.J. Manipulation of injury and repair of the alveolar epithelium using two pneumotoxicants: 3-methylindole and monocrotaline. *Experimental lung research* **25**, 165-181 (1999).

74. Gomez-Arroyo, J.*, et al.* A brief overview of mouse models of pulmonary arterial hypertension: problems and prospects. *Am J Physiol Lung Cell Mol Physiol* **302**, L977-991 (2012).
75. Zhao, Y.D.*, et al.* Rescue of monocrotaline-induced pulmonary arterial hypertension using bone marrow-derived endothelial-like progenitor cells: efficacy of combined cell and eNOS gene therapy in established disease. *Circ Res* **96**, 442-450 (2005).
76. DeLeve, L.D.*, et al.* Characterization of a reproducible rat model of hepatic veno-occlusive disease. *Hepatology (Baltimore, Md.)* **29**, 1779-1791 (1999).
77. Epstein, R.B., Min, K.W., Anderson, S.L. & Syzek, L. A canine model for hepatic venoocclusive disease. *Transplantation* **54**, 12-16 (1992).
78. Savai, R.*, et al.* Immune and inflammatory cell involvement in the pathology of idiopathic pulmonary arterial hypertension. *Am J Respir Crit Care Med* **186**, 897-908 (2012).
79. Kilkenny, C., Browne, W.J., Cuthill, I.C., Emerson, M. & Altman, D.G. Improving Bioscience Research Reporting: The ARRIVE Guidelines for Reporting Animal Research. *PLOS Biology* **8**, e1000412 (2010).
80. Baker, D., Lidster, K., Sottomayor, A. & Amor, S. Two Years Later: Journals Are Not Yet Enforcing the ARRIVE Guidelines on Reporting Standards for Pre-Clinical Animal Studies. *PLOS Biology* **12**, e1001756 (2014).
81. Suen, C.M., Mei, S.H., Kugathasan, L. & Stewart, D.J. Targeted delivery of genes to endothelial cells and cell- and gene-based therapy in pulmonary vascular diseases. *Comprehensive Physiology* **3**, 1749-1779 (2013).
82. Sitbon, O.*, et al.* Long-term response to calcium channel blockers in idiopathic pulmonary arterial hypertension. *Circulation* **111**, 3105-3111 (2005).
83. Rich, S., Kaufmann, E. & Levy, P.S. The effect of high doses of calcium-channel blockers on survival in primary pulmonary hypertension. *The New England journal of medicine* **327**, 76-81 (1992).
84. Nagaya, N. Drug therapy of primary pulmonary hypertension. *Am J Cardiovasc Drugs* **4**, 75-85 (2004).
85. Barst, R.J.*, et al.* Survival in primary pulmonary hypertension with long-term continuous intravenous prostacyclin. *Ann Intern Med* **121**, 409-415 (1994).
86. Barst, R.J.*, et al.* A comparison of continuous intravenous epoprostenol (prostacyclin) with conventional therapy for primary pulmonary hypertension. The Primary Pulmonary Hypertension Study Group. *The New England journal of medicine* **334**, 296-302 (1996).
87. Skoro-Sajer, N. & Lang, I. Treprostinil for the treatment of pulmonary hypertension. *Expert opinion on pharmacotherapy* **9**, 1415-1420 (2008).
88. Mubarak, K.K. A review of prostaglandin analogs in the management of patients with pulmonary arterial hypertension. *Respiratory medicine* **104**, 9-21 (2010).
89. Sitbon, O.*, et al.* Selexipag for the Treatment of Pulmonary Arterial Hypertension. *The New England journal of medicine* **373**, 2522-2533 (2015).
90. Yanagisawa, M.*, et al.* A novel potent vasoconstrictor peptide produced by vascular endothelial cells. *Nature* **332**, 411-415 (1988).
91. Stewart, D.J., Levy, R.D., Cernacek, P. & Langleben, D. Increased plasma endothelin-1 in pulmonary hypertension: marker or mediator of disease? *Ann Intern Med* **114**, 464-469 (1991).
92. Channick, R.N.*, et al.* Effects of the dual endothelin-receptor antagonist bosentan in patients with pulmonary hypertension: a randomised placebo-controlled study. *Lancet* **358**, 1119-1123 (2001).
93. Barst, R.J.*, et al.* Treatment of pulmonary arterial hypertension with the selective endothelin-A receptor antagonist sitaxsentan. *Journal of the American College of Cardiology* **47**, 2049-2056 (2006).

94. Galie, N.*, et al.* Ambrisentan therapy for pulmonary arterial hypertension. *Journal of the American College of Cardiology* **46**, 529-535 (2005).
95. Galie, N.*, et al.* Ambrisentan for the treatment of pulmonary arterial hypertension: results of the ambrisentan in pulmonary arterial hypertension, randomized, double-blind, placebo-controlled, multicenter, efficacy (ARIES) study 1 and 2. *Circulation* **117**, 3010-3019 (2008).
96. Oudiz, R.J.*, et al.* Long-term ambrisentan therapy for the treatment of pulmonary arterial hypertension. *Journal of the American College of Cardiology* **54**, 1971-1981 (2009).
97. Iglarz, M.*, et al.* Pharmacology of macitentan, an orally active tissue-targeting dual endothelin receptor antagonist. *The Journal of pharmacology and experimental therapeutics* **327**, 736-745 (2008).
98. Wharton, J.*, et al.* Antiproliferative effects of phosphodiesterase type 5 inhibition in human pulmonary artery cells. *Am J Respir Crit Care Med* **172**, 105-113 (2005).
99. Michelakis, E.D.*, et al.* Long-term treatment with oral sildenafil is safe and improves functional capacity and hemodynamics in patients with pulmonary arterial hypertension. *Circulation* **108**, 2066-2069 (2003).
100. Galie, N.*, et al.* Tadalafil therapy for pulmonary arterial hypertension. *Circulation* **119**, 2894-2903 (2009).
101. Cerinic Matucci, M.*, et al.* Therapeutic challenges for systemic sclerosis: facts and future targets. *Ann N Y Acad Sci* **1110**, 448-454 (2007).
102. Conole, D. & Scott, L.J. Riociguat: first global approval. *Drugs* **73**, 1967-1975 (2013).
103. Ghofrani, H.A.*, et al.* Riociguat: Mode of action and clinical development in pulmonary hypertension. *Chest* (2016).
104. Stasch, J.P. & Evgenov, O.V. Soluble guanylate cyclase stimulators in pulmonary hypertension. *Handbook of experimental pharmacology* **218**, 279-313 (2013).
105. Klinger, J.R., Abman, S.H. & Gladwin, M.T. Nitric oxide deficiency and endothelial dysfunction in pulmonary arterial hypertension. *Am J Respir Crit Care Med* **188**, 639-646 (2013).
106. Ghofrani, H.A.*, et al.* Riociguat for the treatment of pulmonary arterial hypertension. *The New England journal of medicine* **369**, 330-340 (2013).
107. Ghofrani, H.A.*, et al.* Riociguat for the treatment of chronic thromboembolic pulmonary hypertension. *The New England journal of medicine* **369**, 319-329 (2013).
108. Rubin, L.J.*, et al.* Riociguat for the treatment of pulmonary arterial hypertension: a long-term extension study (PATENT-2). *Eur Respir J* **45**, 1303-1313 (2015).
109. Simonneau, G.*, et al.* Riociguat for the treatment of chronic thromboembolic pulmonary hypertension: a long-term extension study (CHEST-2). *Eur Respir J* **45**, 1293-1302 (2015).
110. Simonneau, G.*, et al.* Predictors of long-term outcomes in patients treated with riociguat for chronic thromboembolic pulmonary hypertension: data from the CHEST-2 open-label, randomised, long-term extension trial. *The Lancet. Respiratory medicine* **4**, 372-380 (2016).
111. Wright, J.T., Jr.*, et al.* A Randomized Trial of Intensive versus Standard Blood-Pressure Control. *The New England journal of medicine* **373**, 2103-2116 (2015).
112. Cole, G.D.*, et al.* "Triple Therapy" of Heart Failure With Angiotensin-Converting Enzyme Inhibitor, Beta-Blocker, and Aldosterone Antagonist May Triple Survival Time. *Shouldn't We Tell Patients?* **2**, 545-548 (2014).
113. Galiè, N.*, et al.* Updated Treatment Algorithm of Pulmonary Arterial Hypertension. *Journal of the American College of Cardiology* **62**, D60-D72 (2013).
114. Sitbon, O. & Gaine, S. Beyond a single pathway: combination therapy in pulmonary arterial hypertension. *European Respiratory Review* **25**, 408-417 (2016).

115. Fox, B.D., Shtraichman, O., Langleben, D., Shimony, A. & Kramer, M.R. Combination Therapy for Pulmonary Arterial Hypertension: A Systematic Review and Meta-analysis. *Canadian Journal of Cardiology* **32**, 1520-1530 (2016).
116. Sitbon, O.*, et al.* Upfront triple combination therapy in pulmonary arterial hypertension: a pilot study. *European Respiratory Journal* **43**, 1691-1697 (2014).
117. Farber, H.W.*, et al.* Five-Year outcomes of patients enrolled in the REVEAL Registry. *Chest* **148**, 1043-1054 (2015).
118. Campbell, A.I., Kuliszewski, M.A. & Stewart, D.J. Cell-based gene transfer to the pulmonary vasculature: Endothelial nitric oxide synthase overexpression inhibits monocrotaline-induced pulmonary hypertension. *Am J Respir Cell Mol Biol* **21**, 567-575 (1999).
119. Foster, W.S., Suen, C.M. & Stewart, D.J. Cell and Tissue-based Regenerative Therapies for Pulmonary Arterial Hypertension. *Canadian Journal of Cardiology*.
120. Takahashi, T.*, et al.* Ischemia- and cytokine-induced mobilization of bone marrow-derived endothelial progenitor cells for neovascularization. *Nature medicine* **5**, 434-438 (1999).
121. Asahara, T.*, et al.* Isolation of putative progenitor endothelial cells for angiogenesis. *Science (New York, N.Y.)* **275**, 964-967 (1997).
122. Hill, J.M.*, et al.* Circulating endothelial progenitor cells, vascular function, and cardiovascular risk. *The New England journal of medicine* **348**, 593-600 (2003).
123. Ingram, D.A.*, et al.* Identification of a novel hierarchy of endothelial progenitor cells using human peripheral and umbilical cord blood. *Blood* **104**, 2752-2760 (2004).
124. Lin, Y., Weisdorf, D.J., Solovey, A. & Hebbel, R.P. Origins of circulating endothelial cells and endothelial outgrowth from blood. *J Clin Invest* **105**, 71-77 (2000).
125. Peichev, M.*, et al.* Expression of VEGFR-2 and AC133 by circulating human CD34(+) cells identifies a population of functional endothelial precursors. *Blood* **95**, 952-958 (2000).
126. Rohde, E.*, et al.* Immune cells mimic the morphology of endothelial progenitor colonies in vitro. *Stem Cells* **25**, 1746-1752 (2007).
127. Yoder, M.C.*, et al.* Redefining endothelial progenitor cells via clonal analysis and hematopoietic stem/progenitor cell principals. *Blood* **109**, 1801-1809 (2007).
128. Schatteman, G.C., Dunnwald, M. & Jiao, C. Biology of bone marrow-derived endothelial cell precursors. *Am J Physiol Heart Circ Physiol* **292**, H1-18 (2007).
129. Case, J.*, et al.* Human CD34+AC133+VEGFR-2+ cells are not endothelial progenitor cells but distinct, primitive hematopoietic progenitors. *Experimental hematology* **35**, 1109-1118 (2007).
130. Timmermans, F.*, et al.* Endothelial outgrowth cells are not derived from CD133+ cells or CD45+ hematopoietic precursors. *Arterioscler Thromb Vasc Biol* **27**, 1572-1579 (2007).
131. Medina, R.J.*, et al.* Molecular analysis of endothelial progenitor cell (EPC) subtypes reveals two distinct cell populations with different identities. *BMC medical genomics* **3**, 18 (2010).
132. Yoder, M.C. Human endothelial progenitor cells. *Cold Spring Harbor perspectives in medicine* **2**, a006692 (2012).
133. Toshner, M.*, et al.* Evidence of dysfunction of endothelial progenitors in pulmonary arterial hypertension. *Am J Respir Crit Care Med* **180**, 780-787 (2009).
134. Vasa, M.*, et al.* Number and migratory activity of circulating endothelial progenitor cells inversely correlate with risk factors for coronary artery disease. *Circ Res* **89**, E1-7 (2001).
135. Hur, J.*, et al.* Characterization of two types of endothelial progenitor cells and their different contributions to neovasculogenesis. *Arterioscler Thromb Vasc Biol* **24**, 288-293 (2004).
136. Gulati, R.*, et al.* Diverse origin and function of cells with endothelial phenotype obtained from adult human blood. *Circ Res* **93**, 1023-1025 (2003).
137. Kalka, C.*, et al.* Transplantation of ex vivo expanded endothelial progenitor cells for therapeutic neovascularization. *Proc Natl Acad Sci U S A* **97**, 3422-3427 (2000).

138. Kawamoto, A.*, et al.* Therapeutic potential of ex vivo expanded endothelial progenitor cells for myocardial ischemia. *Circulation* **103**, 634-637 (2001).
139. Murohara, T.*, et al.* Transplanted cord blood-derived endothelial precursor cells augment postnatal neovascularization. *J Clin Invest* **105**, 1527-1536 (2000).
140. Urbich, C.*, et al.* Relevance of monocytic features for neovascularization capacity of circulating endothelial progenitor cells. *Circulation* **108**, 2511-2516 (2003).
141. Yoon, C.H.*, et al.* Synergistic neovascularization by mixed transplantation of early endothelial progenitor cells and late outgrowth endothelial cells: the role of angiogenic cytokines and matrix metalloproteinases. *Circulation* **112**, 1618-1627 (2005).
142. Richardson, M.R. & Yoder, M.C. Endothelial progenitor cells: quo vadis? *J Mol Cell Cardiol* **50**, 266-272 (2011).
143. Mund, J.A., Estes, M.L., Yoder, M.C., Ingram, D.A., Jr. & Case, J. Flow cytometric identification and functional characterization of immature and mature circulating endothelial cells. *Arterioscler Thromb Vasc Biol* **32**, 1045-1053 (2012).
144. Tura, O.*, et al.* Late outgrowth endothelial cells resemble mature endothelial cells and are not derived from bone marrow. *Stem Cells* **31**, 338-348 (2013).
145. Fadini, G.P., Avogaro, A., Ferraccioli, G. & Agostini, C. Endothelial progenitors in pulmonary hypertension: new pathophysiology and therapeutic implications. *Eur Respir J* **35**, 418-425 (2010).
146. Rosenzweig, A. Endothelial progenitor cells. *The New England journal of medicine* **348**, 581-582 (2003).
147. Itescu, S., Kocher, A.A. & Schuster, M.D. Myocardial neovascularization by adult bone marrow-derived angioblasts: strategies for improvement of cardiomyocyte function. *Ann Hematol* **81 Suppl 2**, S21-25 (2002).
148. Gulati, R.*, et al.* Autologous culture-modified mononuclear cells confer vascular protection after arterial injury. *Circulation* **108**, 1520-1526 (2003).
149. Rehman, J., Li, J., Orschell, C.M. & March, K.L. Peripheral blood "endothelial progenitor cells" are derived from monocyte/macrophages and secrete angiogenic growth factors. *Circulation* **107**, 1164-1169 (2003).
150. Kocher, A.A.*, et al.* Neovascularization of ischemic myocardium by human bone-marrow-derived angioblasts prevents cardiomyocyte apoptosis, reduces remodeling and improves cardiac function. *Nat Med* **7**, 430-436 (2001).
151. Urbich, C. & Dimmeler, S. Endothelial progenitor cells: characterization and role in vascular biology. *Circ Res* **95**, 343-353 (2004).
152. Crosby, J.R.*, et al.* Endothelial cells of hematopoietic origin make a significant contribution to adult blood vessel formation. *Circ Res* **87**, 728-730 (2000).
153. De Palma, M., Venneri, M.A., Roca, C. & Naldini, L. Targeting exogenous genes to tumor angiogenesis by transplantation of genetically modified hematopoietic stem cells. *Nat Med* **9**, 789-795 (2003).
154. Garcia-Barros, M.*, et al.* Tumor response to radiotherapy regulated by endothelial cell apoptosis. *Science (New York, N.Y.)* **300**, 1155-1159 (2003).
155. Jackson, K.A.*, et al.* Regeneration of ischemic cardiac muscle and vascular endothelium by adult stem cells. *J Clin Invest* **107**, 1395-1402 (2001).
156. Llevadot, J.*, et al.* HMG-CoA reductase inhibitor mobilizes bone marrow--derived endothelial progenitor cells. *J Clin Invest* **108**, 399-405 (2001).
157. Urbich, C.*, et al.* Soluble factors released by endothelial progenitor cells promote migration of endothelial cells and cardiac resident progenitor cells. *J Mol Cell Cardiol* **39**, 733-742 (2005).

158. Berse, B., Brown, L.F., Van de Water, L., Dvorak, H.F. & Senger, D.R. Vascular permeability factor (vascular endothelial growth factor) gene is expressed differentially in normal tissues, macrophages, and tumors. *Mol Biol Cell* **3**, 211-220 (1992).
159. Ormiston, M.L., Deng, Y., Stewart, D.J. & Courtman, D.W. Innate immunity in the therapeutic actions of endothelial progenitor cells in pulmonary hypertension. *Am J Respir Cell Mol Biol* **43**, 546-554 (2010).
160. Nagaya, N.*, et al.* Hybrid cell-gene therapy for pulmonary hypertension based on phagocytosing action of endothelial progenitor cells. *Circulation* **108**, 889-895 (2003).
161. Schmidt-Lucke, C.*, et al.* Reduced number of circulating endothelial progenitor cells predicts future cardiovascular events: proof of concept for the clinical importance of endogenous vascular repair. *Circulation* **111**, 2981-2987 (2005).
162. Werner, N.*, et al.* Circulating endothelial progenitor cells and cardiovascular outcomes. *The New England journal of medicine* **353**, 999-1007 (2005).
163. Junhui, Z.*, et al.* Reduced number and activity of circulating endothelial progenitor cells in patients with idiopathic pulmonary arterial hypertension. *Respiratory medicine* **102**, 1073-1079 (2008).
164. Diller, G.P.*, et al.* Circulating endothelial progenitor cells in patients with Eisenmenger syndrome and idiopathic pulmonary arterial hypertension. *Circulation* **117**, 3020-3030 (2008).
165. Asosingh, K.*, et al.* Circulating angiogenic precursors in idiopathic pulmonary arterial hypertension. *Am J Pathol* **172**, 615-627 (2008).
166. Dominici, M.*, et al.* Minimal criteria for defining multipotent mesenchymal stromal cells. The International Society for Cellular Therapy position statement. *Cytotherapy* **8**, 315-317 (2006).
167. Freidenstein, A.J. *Osteogenic stem cells in bone marrow*, (Elsevier, Amsterdam, 1990).
168. Abedin, M., Tintut, Y. & Demer, L.L. Mesenchymal stem cells and the artery wall. *Circ Res* **95**, 671-676 (2004).
169. Baksh, D., Song, L. & Tuan, R.S. Adult mesenchymal stem cells: characterization, differentiation, and application in cell and gene therapy. *J Cell Mol Med* **8**, 301-316 (2004).
170. Pittenger, M.F.*, et al.* Multilineage potential of adult human mesenchymal stem cells. *Science (New York, N.Y.)* **284**, 143-147 (1999).
171. Herzog, E.L., Chai, L. & Krause, D.S. Plasticity of marrow-derived stem cells. *Blood* **102**, 3483-3493 (2003).
172. Phinney, D.G. & Prockop, D.J. Concise review: mesenchymal stem/multipotent stromal cells: the state of transdifferentiation and modes of tissue repair--current views. *Stem Cells* **25**, 2896-2902 (2007).
173. Barry, F.P. & Murphy, J.M. Mesenchymal stem cells: clinical applications and biological characterization. *Int J Biochem Cell Biol* **36**, 568-584 (2004).
174. Ryan, J.M., Barry, F.P., Murphy, J.M. & Mahon, B.P. Mesenchymal stem cells avoid allogeneic rejection. *J Inflamm (Lond)* **2**, 8 (2005).
175. Devine, S.M. & Hoffman, R. Role of mesenchymal stem cells in hematopoietic stem cell transplantation. *Curr Opin Hematol* **7**, 358-363 (2000).
176. Gotherstrom, C.*, et al.* Immunologic properties of human fetal mesenchymal stem cells. *Am J Obstet Gynecol* **190**, 239-245 (2004).
177. Sueblinvong, V. & Weiss, D.J. Cell therapy approaches for lung diseases: current status. *Current opinion in pharmacology* **9**, 268-273 (2009).
178. Prockop, D.J., Gregory, C.A. & Spees, J.L. One strategy for cell and gene therapy: harnessing the power of adult stem cells to repair tissues. *Proc Natl Acad Sci U S A* **100 Suppl 1**, 11917-11923 (2003).

179. Kanki-Horimoto, S.*, et al.* Implantation of mesenchymal stem cells overexpressing endothelial nitric oxide synthase improves right ventricular impairments caused by pulmonary hypertension. *Circulation* **114**, I181-185 (2006).
180. Liang, O.D.*, et al.* Mesenchymal stromal cells expressing heme oxygenase-1 reverse pulmonary hypertension. *Stem Cells* **29**, 99-107 (2011).
181. Takemiya, K.*, et al.* Mesenchymal stem cell-based prostacyclin synthase gene therapy for pulmonary hypertension rats. *Basic Res Cardiol* **105**, 409-417 (2010).
182. Nemeth, K.*, et al.* Bone marrow stromal cells attenuate sepsis via prostaglandin E(2)-dependent reprogramming of host macrophages to increase their interleukin-10 production. *Nat Med* **15**, 42-49 (2009).
183. Mei, S.H.*, et al.* Mesenchymal stem cells reduce inflammation while enhancing bacterial clearance and improving survival in sepsis. *Am J Respir Crit Care Med* **182**, 1047-1057 (2010).
184. Gonzalez, M.A., Gonzalez-Rey, E., Rico, L., Buscher, D. & Delgado, M. Adipose-derived mesenchymal stem cells alleviate experimental colitis by inhibiting inflammatory and autoimmune responses. *Gastroenterology* **136**, 978-989 (2009).
185. Gebler, A., Zabel, O. & Seliger, B. The immunomodulatory capacity of mesenchymal stem cells. *Trends in molecular medicine* **18**, 128-134 (2012).
186. Nauta, A.J. & Fibbe, W.E. Immunomodulatory properties of mesenchymal stromal cells. *Blood* **110**, 3499-3506 (2007).
187. Tuder, R.M., Marecki, J.C., Richter, A., Fijalkowska, I. & Flores, S. Pathology of pulmonary hypertension. *Clin Chest Med* **28**, 23-42, vii (2007).
188. Rafii, S. & Lyden, D. Therapeutic stem and progenitor cell transplantation for organ vascularization and regeneration. *Nat Med* **9**, 702-712 (2003).
189. Takahashi, M.*, et al.* Transplantation of endothelial progenitor cells into the lung to alleviate pulmonary hypertension in dogs. *Tissue Eng* **10**, 771-779 (2004).
190. Yip, H.K.*, et al.* Autologous transplantation of bone marrow-derived endothelial progenitor cells attenuates monocrotaline-induced pulmonary arterial hypertension in rats. *Crit Care Med* **36**, 873-880 (2008).
191. Sun, C.K.*, et al.* Early combined treatment with cilostazol and bone marrow-derived endothelial progenitor cells markedly attenuates pulmonary arterial hypertension in rats. *The Journal of pharmacology and experimental therapeutics* **330**, 718-726 (2009).
192. Sun, C.K.*, et al.* Enhanced protection against pulmonary hypertension with sildenafil and endothelial progenitor cell in rats. *Int J Cardiol* (2011).
193. Baber, S.R.*, et al.* Intratracheal mesenchymal stem cell administration attenuates monocrotaline-induced pulmonary hypertension and endothelial dysfunction. *Am J Physiol Heart Circ Physiol* **292**, H1120-1128 (2007).
194. Umar, S.*, et al.* Allogenic stem cell therapy improves right ventricular function by improving lung pathology in rats with pulmonary hypertension. *Am J Physiol Heart Circ Physiol* **297**, H1606-1616 (2009).
195. Mirsky, R.*, et al.* Treatment of pulmonary arterial hypertension with circulating angiogenic cells. *Am J Physiol Lung Cell Mol Physiol* **301**, L12-19 (2011).
196. Datta, P.K., Chytil, A., Gorska, A.E. & Moses, H.L. Identification of STRAP, a novel WD domain protein in transforming growth factor-beta signaling. *The Journal of biological chemistry* **273**, 34671-34674 (1998).
197. Luan, Y.*, et al.* Implantation of mesenchymal stem cells improves right ventricular impairments caused by experimental pulmonary hypertension. *Am J Med Sci* **343**, 402-406 (2012).
198. Zhao, Q.*, et al.* Effect of prepro-calcitonin gene-related peptide-expressing endothelial progenitor cells on pulmonary hypertension. *Ann Thorac Surg* **84**, 544-552 (2007).

199. Zhou, L.*, et al.* Endothelial-like progenitor cells engineered to produce prostacyclin rescue monocrotaline-induced pulmonary arterial hypertension and provide right ventricle benefits. *Circulation* **128**, 982-994 (2013).
200. Jurasz, P., Courtman, D., Babaie, S. & Stewart, D.J. Role of apoptosis in pulmonary hypertension: from experimental models to clinical trials. *Pharmacology & therapeutics* **126**, 1-8 (2010).
201. Morse, D. & Choi, A.M. Heme oxygenase-1: from bench to bedside. *Am J Respir Crit Care Med* **172**, 660-670 (2005).
202. van de Veerdonk, M.C.*, et al.* Progressive right ventricular dysfunction in patients with pulmonary arterial hypertension responding to therapy. *Journal of the American College of Cardiology* **58**, 2511-2519 (2011).
203. Haddad, F.*, et al.* Right Heart Score for Predicting Outcome in Idiopathic, Familial, or Drug- and Toxin-Associated Pulmonary Arterial Hypertension. *JACC. Cardiovascular imaging* **8**, 627-638 (2015).
204. Nagendran, J.*, et al.* Phosphodiesterase type 5 is highly expressed in the hypertrophied human right ventricle, and acute inhibition of phosphodiesterase type 5 improves contractility. *Circulation* **116**, 238-248 (2007).
205. Archer, S.L. & Michelakis, E.D. Phosphodiesterase type 5 inhibitors for pulmonary arterial hypertension. *The New England journal of medicine* **361**, 1864-1871 (2009).
206. Poole-Wilson, P.A.*, et al.* Comparison of carvedilol and metoprolol on clinical outcomes in patients with chronic heart failure in the Carvedilol Or Metoprolol European Trial (COMET): randomised controlled trial. *Lancet* **362**, 7-13 (2003).
207. Ryan, J.J. & Archer, S.L. The right ventricle in pulmonary arterial hypertension: disorders of metabolism, angiogenesis and adrenergic signaling in right ventricular failure. *Circulation research* **115**, 176-188 (2014).
208. Zaffran, S., Kelly, R.G., Meilhac, S.M., Buckingham, M.E. & Brown, N.A. Right ventricular myocardium derives from the anterior heart field. *Circ Res* **95**, 261-268 (2004).
209. Finnemore, A. & Groves, A. Physiology of the fetal and transitional circulation. *Seminars in Fetal and Neonatal Medicine* **20**, 210-216 (2015).
210. Firpo, C., Hoffman, J.I. & Silverman, N.H. Evaluation of fetal heart dimensions from 12 weeks to term. *The American journal of cardiology* **87**, 594-600 (2001).
211. Bogaard, H.J., Abe, K., Vonk Noordegraaf, A. & Voelkel, N.F. The right ventricle under pressure: Cellular and molecular mechanisms of right-heart failure in pulmonary hypertension. *Chest* **135**, 794-804 (2009).
212. Poels, E.M., da Costa Martins, P.A. & van Empel, V.P.M. *Adaptive capacity of the right ventricle: why does it fail?*, (2015).
213. Mann, D.L. Left ventricular size and shape: determinants of mechanical signal transduction pathways. *Heart failure reviews* **10**, 95-100 (2005).
214. Mann, D.L. Basic mechanisms of left ventricular remodeling: the contribution of wall stress. *Journal of cardiac failure* **10**, S202-206 (2004).
215. Oka, T., Akazawa, H., Naito, A.T. & Komuro, I. Angiogenesis and Cardiac Hypertrophy: Maintenance of Cardiac Function and Causative Roles in Heart Failure. *Circulation Research* **114**, 565-571 (2014).
216. Izumiya, Y.*, et al.* Vascular Endothelial Growth Factor Blockade Promotes the Transition From Compensatory Cardiac Hypertrophy to Failure in Response to Pressure Overload. *Hypertension* **47**, 887-893 (2006).
217. Friehs, I.*, et al.* Vascular endothelial growth factor prevents apoptosis and preserves contractile function in hypertrophied infant heart. *Circulation* **114**, I290-295 (2006).

218. Bellomo, D*., et al.* Mice lacking the vascular endothelial growth factor-B gene (Vegfb) have smaller hearts, dysfunctional coronary vasculature, and impaired recovery from cardiac ischemia. *Circ Res* **86**, E29-35 (2000).
219. Karpanen, T*., et al.* Overexpression of vascular endothelial growth factor-B in mouse heart alters cardiac lipid metabolism and induces myocardial hypertrophy. *Circ Res* **103**, 1018-1026 (2008).
220. Bry, M*., et al.* Vascular endothelial growth factor-B acts as a coronary growth factor in transgenic rats without inducing angiogenesis, vascular leak, or inflammation. *Circulation* **122**, 1725-1733 (2010).
221. Lowes, B.D*., et al.* Changes in gene expression in the intact human heart. Downregulation of alpha-myosin heavy chain in hypertrophied, failing ventricular myocardium. *J Clin Invest* **100**, 2315-2324 (1997).
222. Neely, J.R. & Morgan, H.E. Relationship between carbohydrate and lipid metabolism and the energy balance of heart muscle. *Annu Rev Physiol* **36**, 413-459 (1974).
223. Abozguia, K., Clarke, K., Lee, L. & Frenneaux, M. Modification of myocardial substrate use as a therapy for heart failure. *Nature clinical practice. Cardiovascular medicine* **3**, 490-498 (2006).
224. Nagendran, J*., et al.* A dynamic and chamber-specific mitochondrial remodeling in right ventricular hypertrophy can be therapeutically targeted. *The Journal of thoracic and cardiovascular surgery* **136**, 168-178, 178.e161-163 (2008).
225. Nishikimi, T., Maeda, N. & Matsuoka, H. The role of natriuretic peptides in cardioprotection. *Cardiovascular Research* **69**, 318-328 (2006).
226. Anversa, P., Levicky, V., Beghi, C., McDonald, S.L. & Kikkawa, Y. Morphometry of exercise-induced right ventricular hypertrophy in the rat. *Circulation Research* **52**, 57-64 (1983).
227. Rich, S*., et al.* Long-term effects of epoprostenol on the pulmonary vasculature in idiopathic pulmonary arterial hypertension. *Chest* **138**, 1234-1239 (2010).
228. Bogaard, H.J*., et al.* Chronic pulmonary artery pressure elevation is insufficient to explain right heart failure. *Circulation* **120**, 1951-1960 (2009).
229. Gudausky, T.M. & Beekman, R.H., 3rd. Current options, and long-term results for interventional treatment of pulmonary valvar stenosis. *Cardiology in the young* **16**, 418-427 (2006).
230. Hopkins, W.E., Ochoa, L.L., Richardson, G.W. & Trulock, E.P. Comparison of the hemodynamics and survival of adults with severe primary pulmonary hypertension or Eisenmenger syndrome. *The Journal of heart and lung transplantation : the official publication of the International Society for Heart Transplantation* **15**, 100-105 (1996).
231. Poels, E.M., da Costa Martins, P.A. & van Empel, V.P.M. Adaptive capacity of the right ventricle: why does it fail? *American Journal of Physiology - Heart and Circulatory Physiology* **308**, H803-H813 (2015).
232. van Wolferen, S.A*., et al.* Right coronary artery flow impairment in patients with pulmonary hypertension. *European heart journal* **29**, 120-127 (2008).
233. Vogel-Claussen, J*., et al.* Right and left ventricular myocardial perfusion reserves correlate with right ventricular function and pulmonary hemodynamics in patients with pulmonary arterial hypertension. *Radiology* **258**, 119-127 (2011).
234. Gomez, A*., et al.* Right ventricular ischemia in patients with primary pulmonary hypertension. *Journal of the American College of Cardiology* **38**, 1137-1142 (2001).
235. Potus, F*., et al.* Downregulation of MicroRNA-126 Contributes to the Failing Right Ventricle in Pulmonary Arterial Hypertension. *Circulation* **132**, 932-943 (2015).
236. Drake, J.I*., et al.* Molecular signature of a right heart failure program in chronic severe pulmonary hypertension. *Am J Respir Cell Mol Biol* **45**, 1239-1247 (2011).

237. Sutendra, G.*, et al.* A metabolic remodeling in right ventricular hypertrophy is associated with decreased angiogenesis and a transition from a compensated to a decompensated state in pulmonary hypertension. *Journal of molecular medicine (Berlin, Germany)* **91**, 1315-1327 (2013).
238. Lopaschuk, G.D., Ussher, J.R., Folmes, C.D.L., Jaswal, J.S. & Stanley, W.C. Myocardial Fatty Acid Metabolism in Health and Disease. *Physiological Reviews* **90**, 207-258 (2010).
239. Kim, Y.*, et al.* Detection of impaired fatty acid metabolism in right ventricular hypertrophy: assessment by I-123 beta-methyl iodophenyl pentadecanoic acid (BMIPP) myocardial single-photon emission computed tomography. *Annals of nuclear medicine* **11**, 207-212 (1997).
240. Nagaya, N.*, et al.* Impaired regional fatty acid uptake and systolic dysfunction in hypertrophied right ventricle. *Journal of nuclear medicine : official publication, Society of Nuclear Medicine* **39**, 1676-1680 (1998).
241. Piao, L.*, et al.* The inhibition of pyruvate dehydrogenase kinase improves impaired cardiac function and electrical remodeling in two models of right ventricular hypertrophy: resuscitating the hibernating right ventricle. *Journal of molecular medicine (Berlin, Germany)* **88**, 47-60 (2010).
242. Gomez-Arroyo, J.*, et al.* Metabolic gene remodeling and mitochondrial dysfunction in failing right ventricular hypertrophy secondary to pulmonary arterial hypertension. *Circulation. Heart failure* **6**, 136-144 (2013).
243. Handschin, C. & Spiegelman, B.M. Peroxisome proliferator-activated receptor gamma coactivator 1 coactivators, energy homeostasis, and metabolism. *Endocrine reviews* **27**, 728-735 (2006).
244. Handschin, C. & Spiegelman, B.M. Peroxisome Proliferator-Activated Receptor γ Coactivator 1 Coactivators, Energy Homeostasis, and Metabolism. *Endocrine reviews* **27**, 728-735 (2006).
245. Arany, Z.*, et al.* Transcriptional coactivator PGC-1 alpha controls the energy state and contractile function of cardiac muscle. *Cell metabolism* **1**, 259-271 (2005).
246. Arany, Z.*, et al.* Transverse aortic constriction leads to accelerated heart failure in mice lacking PPAR-gamma coactivator 1alpha. *Proc Natl Acad Sci U S A* **103**, 10086-10091 (2006).
247. Leask, A. Getting to the heart of the matter: new insights into cardiac fibrosis. *Circ Res* **116**, 1269-1276 (2015).
248. Shehata, M.L.*, et al.* Myocardial delayed enhancement in pulmonary hypertension: pulmonary hemodynamics, right ventricular function, and remodeling. *AJR. American journal of roentgenology* **196**, 87-94 (2011).
249. Bogaard, H.J.*, et al.* Adrenergic receptor blockade reverses right heart remodeling and dysfunction in pulmonary hypertensive rats. *Am J Respir Crit Care Med* **182**, 652-660 (2010).
250. Champion, H.C., Michelakis, E.D. & Hassoun, P.M. Comprehensive invasive and noninvasive approach to the right ventricle-pulmonary circulation unit: state of the art and clinical and research implications. *Circulation* **120**, 992-1007 (2009).
251. Dabestani, A.*, et al.* Evaluation of pulmonary artery pressure and resistance by pulsed Doppler echocardiography. *The American journal of cardiology* **59**, 662-668 (1987).
252. Rudski, L.G.*, et al.* Guidelines for the echocardiographic assessment of the right heart in adults: a report from the American Society of Echocardiography endorsed by the European Association of Echocardiography, a registered branch of the European Society of Cardiology, and the Canadian Society of Echocardiography. *Journal of the American Society of Echocardiography : official publication of the American Society of Echocardiography* **23**, 685-713; quiz 786-688 (2010).
253. Benza, R., Biederman, R., Murali, S. & Gupta, H. Role of cardiac magnetic resonance imaging in the management of patients with pulmonary arterial hypertension. *Journal of the American College of Cardiology* **52**, 1683-1692 (2008).

254. Grothues, F.*, et al.* Interstudy reproducibility of right ventricular volumes, function, and mass with cardiovascular magnetic resonance. *American heart journal* **147**, 218-223 (2004).
255. Chin, B.B.*, et al.* Right and left ventricular volume and ejection fraction by tomographic gated blood-pool scintigraphy. *Journal of nuclear medicine : official publication, Society of Nuclear Medicine* **38**, 942-948 (1997).
256. van Wolferen, S.A.*, et al.* Prognostic value of right ventricular mass, volume, and function in idiopathic pulmonary arterial hypertension. *European heart journal* **28**, 1250-1257 (2007).
257. Katz, J., Whang, J., Boxt, L.M. & Barst, R.J. Estimation of right ventricular mass in normal subjects and in patients with primary pulmonary hypertension by nuclear magnetic resonance imaging. *Journal of the American College of Cardiology* **21**, 1475-1481 (1993).
258. Blyth, K.G.*, et al.* Contrast enhanced-cardiovascular magnetic resonance imaging in patients with pulmonary hypertension. *European heart journal* **26**, 1993-1999 (2005).
259. McCann, G.P.*, et al.* Extent of MRI delayed enhancement of myocardial mass is related to right ventricular dysfunction in pulmonary artery hypertension. *AJR. American journal of roentgenology* **188**, 349-355 (2007).
260. Sanz, J.*, et al.* Prevalence and correlates of septal delayed contrast enhancement in patients with pulmonary hypertension. *The American journal of cardiology* **100**, 731-735 (2007).
261. Vildbrad, M.D.*, et al.* Acute effects of levosimendan in experimental models of right ventricular hypertrophy and failure. *Pulmonary circulation* **4**, 511-519 (2014).
262. Holmboe, S.*, et al.* Iloprost improves ventricular function in the hypertrophic and functionally impaired right heart by direct stimulation. *Pulmonary circulation* **3**, 870-879 (2013).
263. Taljaard, M.*, et al.* Rationale and design of Enhanced Angiogenic Cell Therapy in Acute Myocardial Infarction (ENACT-AMI): the first randomized placebo-controlled trial of enhanced progenitor cell therapy for acute myocardial infarction. *American heart journal* **159**, 354-360 (2010).
264. Pierro, M.*, et al.* Short-term, long-term and paracrine effect of human umbilical cord-derived stem cells in lung injury prevention and repair in experimental bronchopulmonary dysplasia. *Thorax* (2012).
265. Hansmann, G.*, et al.* Mesenchymal stem cell-mediated reversal of bronchopulmonary dysplasia and associated pulmonary hypertension. *Pulmonary circulation* **2**, 170-181 (2012).
266. Mei, S.H.*, et al.* Prevention of LPS-induced acute lung injury in mice by mesenchymal stem cells overexpressing angiopoietin 1. *PLoS Med* **4**, e269 (2007).
267. Wang, X.X.*, et al.* Transplantation of autologous endothelial progenitor cells may be beneficial in patients with idiopathic pulmonary arterial hypertension: a pilot randomized controlled trial. *Journal of the American College of Cardiology* **49**, 1566-1571 (2007).
268. Assmus, B.*, et al.* Transplantation of Progenitor Cells and Regeneration Enhancement in Acute Myocardial Infarction (TOPCARE-AMI). *Circulation* **106**, 3009-3017 (2002).
269. Phillips, J.A., 3rd*, et al.* Synergistic heterozygosity for TGFbeta1 SNPs and BMPR2 mutations modulates the age at diagnosis and penetrance of familial pulmonary arterial hypertension. *Genetics in medicine : official journal of the American College of Medical Genetics* **10**, 359-365 (2008).
270. Medina, R.J.*, et al.* Myeloid angiogenic cells act as alternative M2 macrophages and modulate angiogenesis through interleukin-8. *Molecular medicine* **17**, 1045-1055 (2011).
271. Di Santo, S.*, et al.* Novel cell-free strategy for therapeutic angiogenesis: in vitro generated conditioned medium can replace progenitor cell transplantation. *PloS one* **4**, e5643 (2009).
272. Kim, J.Y.*, et al.* Human cord blood-derived endothelial progenitor cells and their conditioned media exhibit therapeutic equivalence for diabetic wound healing. *Cell transplantation* **19**, 1635-1644 (2010).

273. Xia, L., Fu, G.S., Yang, J.X., Zhang, F.R. & Wang, X.X. Endothelial progenitor cells may inhibit apoptosis of pulmonary microvascular endothelial cells: new insights into cell therapy for pulmonary arterial hypertension. *Cytotherapy* **11**, 492-502 (2009).
274. Fang, L.*, et al.* Calcitonin gene-related peptide released from endothelial progenitor cells inhibits the proliferation of rat vascular smooth muscle cells induced by angiotensin II. *Molecular and cellular biochemistry* **355**, 99-108 (2011).
275. Thebaud, B. & Stewart, D.J. Exosomes: cell garbage can, therapeutic carrier, or trojan horse? *Circulation* **126**, 2553-2555 (2012).
276. Valadi, H.*, et al.* Exosome-mediated transfer of mRNAs and microRNAs is a novel mechanism of genetic exchange between cells. *Nat Cell Biol* **9**, 654-659 (2007).
277. Lee, C.*, et al.* Exosomes mediate the cytoprotective action of mesenchymal stromal cells on hypoxia-induced pulmonary hypertension. *Circulation* **126**, 2601-2611 (2012).
278. Li, X.*, et al.* Exosomes derived from endothelial progenitor cells attenuate vascular repair and accelerate reendothelialization by enhancing endothelial function. *Cytotherapy* **18**, 253-262 (2016).
279. Suen, C.M.*, et al.* Efficacy and safety of regenerative cell therapy for pulmonary arterial hypertension in animal models: a preclinical systematic review protocol. *Systematic reviews* **5**, 89 (2016).
280. Lisk, R.*, et al.* Geriatrician input into nursing homes reduces emergency hospital admissions. *Archives of gerontology and geriatrics* **55**, 331-337 (2012).
281. Thery, C., Amigorena, S., Raposo, G. & Clayton, A. Isolation and characterization of exosomes from cell culture supernatants and biological fluids. *Current protocols in cell biology / editorial board, Juan S. Bonifacino ... [et al.]* **Chapter 3**, Unit 3.22 (2006).
282. Gnecchi, M., Zhang, Z., Ni, A. & Dzau, V.J. Paracrine Mechanisms in Adult Stem Cell Signaling and Therapy. *Circulation Research* **103**, 1204-1219 (2008).
283. Gnecchi, M.*, et al.* Evidence supporting paracrine hypothesis for Akt-modified mesenchymal stem cell-mediated cardiac protection and functional improvement. *The FASEB Journal* **20**, 661-669 (2006).
284. Alphonse, R.S.*, et al.* Existence, functional impairment, and lung repair potential of endothelial colony-forming cells in oxygen-induced arrested alveolar growth. *Circulation* **129**, 2144-2157 (2014).
285. Lavoie, J.R.*, et al.* Proteomic analysis implicates translationally controlled tumor protein as a novel mediator of occlusive vascular remodeling in pulmonary arterial hypertension. *Circulation* **129**, 2125-2135 (2014).
286. Sahoo, S.*, et al.* Exosomes from human CD34(+) stem cells mediate their proangiogenic paracrine activity. *Circ Res* **109**, 724-728 (2011).
287. Sokolova, V.*, et al.* Characterisation of exosomes derived from human cells by nanoparticle tracking analysis and scanning electron microscopy. *Colloids Surf B Biointerfaces* **87**, 146-150 (2011).
288. Sharpe, R.*, et al.* The war against error: a 15 year experience of completion angioscopy following carotid endarterectomy. *European journal of vascular and endovascular surgery : the official journal of the European Society for Vascular Surgery* **43**, 139-145 (2012).
289. Deregibus, M.C.*, et al.* Endothelial progenitor cell derived microvesicles activate an angiogenic program in endothelial cells by a horizontal transfer of mRNA. *Blood* **110**, 2440-2448 (2007).
290. Lamparski, H.G.*, et al.* Production and characterization of clinical grade exosomes derived from dendritic cells. *Journal of immunological methods* **270**, 211-226 (2002).

291. Alvarez, M.L., Khosroheidari, M., Kanchi Ravi, R. & DiStefano, J.K. Comparison of protein, microRNA, and mRNA yields using different methods of urinary exosome isolation for the discovery of kidney disease biomarkers. *Kidney international* **82**, 1024-1032 (2012).
292. Raimondo, F., Morosi, L., Chinello, C., Magni, F. & Pitto, M. Advances in membranous vesicle and exosome proteomics improving biological understanding and biomarker discovery. *Proteomics* **11**, 709-720 (2011).
293. Miyata, M.*, et al.* Athymic nude rats develop severe pulmonary hypertension following monocrotaline administration. *International archives of allergy and immunology* **121**, 246-252 (2000).
294. Granton, J.*, et al.* Endothelial NO-Synthase Gene-Enhanced Progenitor Cell Therapy for Pulmonary Arterial Hypertension: The PHACeT Trial. *Circ Res* **117**, 645-654 (2015).
295. Jiang, B.*, et al.* Marked Strain-specific Differences in the SU5416 Rat Model of Severe Pulmonary Arterial Hypertension. *Am J Respir Cell Mol Biol* (2015).
296. Kotoda, N.*, et al.* Molecular characterization of FLOWERING LOCUS T-like genes of apple (Malus x domestica Borkh.). *Plant & cell physiology* **51**, 561-575 (2010).
297. Dutly, A.E.*, et al.* Fluorescent microangiography (FMA): an improved tool to visualize the pulmonary microvasculature. *Laboratory investigation; a journal of technical methods and pathology* **86**, 409-416 (2006).
298. Alzoubi, A.*, et al.* TRPC4 inactivation confers a survival benefit in severe pulmonary arterial hypertension. *The American journal of pathology* **183**, 1779-1788 (2013).
299. D'Alonzo, G.E.*, et al.* Survival in patients with primary pulmonary hypertension. Results from a national prospective registry. *Ann Intern Med* **115**, 343-349 (1991).
300. Bouchentouf, M.*, et al.* Induction of Cardiac Angiogenesis Requires Killer Cell Lectin-Like Receptor 1 and α4β7 Integrin Expression by NK Cells. *The Journal of Immunology* **185**, 7014-7025 (2010).
301. Mann, D.L. Innate immunity and the failing heart: the cytokine hypothesis revisited. *Circulation research* **116**, 1254-1268 (2015).
302. Hanna, J.*, et al.* Decidual NK cells regulate key developmental processes at the human fetal-maternal interface. *Nat Med* **12**, 1065-1074 (2006).
303. Ormiston, M.L.*, et al.* Impaired natural killer cell phenotype and function in idiopathic and heritable pulmonary arterial hypertension. *Circulation* **126**, 1099-1109 (2012).
304. Talati, M. & Hemnes, A. Fatty acid metabolism in pulmonary arterial hypertension: role in right ventricular dysfunction and hypertrophy. *Pulmonary circulation* **5**, 269-278 (2015).
305. Sankaralingam, S. & Lopaschuk, G.D. Cardiac energy metabolic alterations in pressure overload-induced left and right heart failure (2013 Grover Conference Series). *Pulmonary circulation* **5**, 15-28 (2015).
306. Fang, Y.H.*, et al.* Therapeutic inhibition of fatty acid oxidation in right ventricular hypertrophy: exploiting Randle's cycle. *Journal of molecular medicine (Berlin, Germany)* **90**, 31-43 (2012).
307. Piao, L.*, et al.* FOXO1-mediated upregulation of pyruvate dehydrogenase kinase-4 (PDK4) decreases glucose oxidation and impairs right ventricular function in pulmonary hypertension: therapeutic benefits of dichloroacetate. *Journal of molecular medicine (Berlin, Germany)* **91**, 333-346 (2013).
308. Gomez-Arroyo, J.*, et al.* Metabolic Gene Remodeling and Mitochondrial Dysfunction in Failing Right Ventricular Hypertrophy Secondary to Pulmonary Arterial Hypertension. *Circulation: Heart Failure* **6**, 136-144 (2013).
309. Calabro, P.*, et al.* Novel insights into the role of cardiotrophin-1 in cardiovascular diseases. *J Mol Cell Cardiol* **46**, 142-148 (2009).

310. Ghosh, S., Ng, L.L., Talwar, S., Squire, I.B. & Galinanes, M. Cardiotrophin-1 protects the human myocardium from ischemic injury. Comparison with the first and second window of protection by ischemic preconditioning. *Cardiovasc Res* **48**, 440-447 (2000).
311. Jin, H.*, et al.* In vivo effects of cardiotrophin-1. *Cytokine* **8**, 920-926 (1996).
312. Wollert, K.C.*, et al.* Cardiotrophin-1 activates a distinct form of cardiac muscle cell hypertrophy. Assembly of sarcomeric units in series VIA gp130/leukemia inhibitory factor receptor-dependent pathways. *The Journal of biological chemistry* **271**, 9535-9545 (1996).
313. Hirota, H.*, et al.* Loss of a gp130 cardiac muscle cell survival pathway is a critical event in the onset of heart failure during biomechanical stress. *Cell* **97**, 189-198 (1999).
314. Yoshida, K.*, et al.* Targeted disruption of gp130, a common signal transducer for the interleukin 6 family of cytokines, leads to myocardial and hematological disorders. *Proc Natl Acad Sci U S A* **93**, 407-411 (1996).
315. Sheng, Z.*, et al.* Cardiotrophin 1 (CT-1) inhibition of cardiac myocyte apoptosis via a mitogen-activated protein kinase-dependent pathway. Divergence from downstream CT-1 signals for myocardial cell hypertrophy. *The Journal of biological chemistry* **272**, 5783-5791 (1997).
316. Kuwahara, K.*, et al.* Cardiotrophin-1 phosphorylates akt and BAD, and prolongs cell survival via a PI3K-dependent pathway in cardiac myocytes. *J Mol Cell Cardiol* **32**, 1385-1394 (2000).
317. Brar, B.K.*, et al.* Cardiotrophin-1 can protect cardiac myocytes from injury when added both prior to simulated ischaemia and at reoxygenation. *Cardiovasc Res* **51**, 265-274 (2001).
318. Megeney, L.A., Abdul-Ghani, M., Suen, C. & Stewart, D.J. Abstract 196: Cardiotrophin-1 Promotes Physiologic Cardiac Hypertrophy. *Circulation Research* **117**, A196 (2015).
319. Pan, J.*, et al.* Involvement of gp130-mediated signaling in pressure overload-induced activation of the JAK/STAT pathway in rodent heart. *Heart and vessels* **13**, 199-208 (1998).
320. Aoyama, T.*, et al.* Augmented expression of cardiotrophin-1 and its receptor component, gp130, in both left and right ventricles after myocardial infarction in the rat. *J Mol Cell Cardiol* **32**, 1821-1830 (2000).
321. Chandrasekar, B., Melby, P.C., Pennica, D. & Freeman, G.L. Overexpression of cardiotrophin-1 and gp130 during experimental acute Chagasic cardiomyopathy. *Immunology letters* **61**, 89-95 (1998).
322. Ishikawa, M.*, et al.* cDNA cloning of rat cardiotrophin-1 (CT-1): augmented expression of CT-1 gene in ventricle of genetically hypertensive rats. *Biochemical and biophysical research communications* **219**, 377-381 (1996).
323. Jougasaki, M.*, et al.* Augmented cardiac cardiotrophin-1 in experimental congestive heart failure. *Circulation* **101**, 14-17 (2000).
324. Talwar, S., Squire, I.B., Downie, P.F., Davies, J.E. & Ng, L.L. Plasma N terminal pro-brain natriuretic peptide and cardiotrophin 1 are raised in unstable angina. *Heart (British Cardiac Society)* **84**, 421-424 (2000).
325. Talwar, S.*, et al.* Plasma cardiotrophin-1 following acute myocardial infarction: relationship with left ventricular systolic dysfunction. *Clinical science (London, England : 1979)* **102**, 9-14 (2002).
326. Talwar, S.*, et al.* Elevated circulating cardiotrophin-1 in heart failure: relationship with parameters of left ventricular systolic dysfunction. *Clinical science (London, England : 1979)* **99**, 83-88 (2000).
327. Jin, H.*, et al.* Effects of cardiotrophin-1 on haemodynamics and cardiac function in conscious rats. *Cytokine* **10**, 19-25 (1998).
328. Nomura, N.*, et al.* Cardiotrophin-1 is a prophylactic against the development of chronic hypoxic pulmonary hypertension in rats. *Ann Thorac Surg* **76**, 237-243 (2003).
329. Latchman, D.S. Cardiotrophin-1: a novel cytokine and its effects in the heart and other tissues. *Pharmacology & therapeutics* **85**, 29-37 (2000).

330. Hilfiker-Kleiner, D.*, et al.* Signal transducer and activator of transcription 3 is required for myocardial capillary growth, control of interstitial matrix deposition, and heart protection from ischemic injury. *Circ Res* **95**, 187-195 (2004).
331. Giordano, F.J.*, et al.* A cardiac myocyte vascular endothelial growth factor paracrine pathway is required to maintain cardiac function. *Proceedings of the National Academy of Sciences* **98**, 5780-5785 (2001).
332. Funamoto, M.*, et al.* Signal Transducer and Activator of Transcription 3 Is Required for Glycoprotein 130-mediated Induction of Vascular Endothelial Growth Factor in Cardiac Myocytes. *Journal of Biological Chemistry* **275**, 10561-10566 (2000).
333. Pennica, D.*, et al.* Expression cloning of cardiotrophin 1, a cytokine that induces cardiac myocyte hypertrophy. *Proc Natl Acad Sci U S A* **92**, 1142-1146 (1995).
334. Osugi, T.*, et al.* Cardiac-specific Activation of Signal Transducer and Activator of Transcription 3 Promotes Vascular Formation in the Heart. *Journal of Biological Chemistry* **277**, 6676-6681 (2002).
335. Paulin, R.*, et al.* Signal transducers and activators of transcription-3/pim1 axis plays a critical role in the pathogenesis of human pulmonary arterial hypertension. *Circulation* **123**, 1205-1215 (2011).
336. Railson, J.E.*, et al.* Cardiotrophin-1 and urocortin cause protection by the same pathway and hypertrophy via distinct pathways in cardiac myocytes. *Cytokine* **17**, 243-253 (2002).
337. Samillan, V.*, et al.* Combination of erythropoietin and sildenafil can effectively attenuate hypoxia-induced pulmonary hypertension in mice. *Pulmonary circulation* **3**, 898-907 (2013).
338. Robador, P.A.*, et al.* HIF-1-mediated up-regulation of cardiotrophin-1 is involved in the survival response of cardiomyocytes to hypoxia. *Cardiovasc Res* **92**, 247-255 (2011).
339. Celik, A.*, et al.* Cardiotrophin-1 plasma levels are increased in patients with diastolic heart failure. *Medical science monitor : international medical journal of experimental and clinical research* **18**, Cr25-31 (2012).
340. Song, K.*, et al.* Plasma cardiotrophin-1 levels are associated with hypertensive heart disease: a meta-analysis. *Journal of clinical hypertension (Greenwich, Conn.)* **16**, 686-692 (2014).
341. Pemberton, C.J., Raudsepp, S.D., Yandle, T.G., Cameron, V.A. & Richards, A.M. Plasma cardiotrophin-1 is elevated in human hypertension and stimulated by ventricular stretch. *Cardiovasc Res* **68**, 109-117 (2005).
342. Pulido, E.J.*, et al.* Cardiotrophin-1 attenuates endotoxin-induced acute lung injury. *The Journal of surgical research* **84**, 240-246 (1999).
343. Hamanaka, I.*, et al.* Effects of cardiotrophin-1 on hemodynamics and endocrine function of the heart. *Am J Physiol Heart Circ Physiol* **279**, H388-396 (2000).
344. Marques, J.M.*, et al.* Cardiotrophin-1 is an essential factor in the natural defense of the liver against apoptosis. *Hepatology (Baltimore, Md.)* **45**, 639-648 (2007).
345. Quiros, Y., Sanchez-Gonzalez, P.D., Lopez-Hernandez, F.J., Morales, A.I. & Lopez-Novoa, J.M. Cardiotrophin-1 administration prevents the renal toxicity of iodinated contrast media in rats. *Toxicological sciences : an official journal of the Society of Toxicology* **132**, 493-501 (2013).
346. Thenappan, T., Prins, K.W., Cogswell, R. & Shah, S.J. Pulmonary hypertension secondary to heart failure with preserved ejection fraction. *The Canadian journal of cardiology* **31**, 430-439 (2015).
347. Taraseviciene-Stewart, L.*, et al.* Absence of T cells confers increased pulmonary arterial hypertension and vascular remodeling. *Am J Respir Crit Care Med* **175**, 1280-1289 (2007).